Bauhaus-Universität Weimar
Fakultät Bauingenieurwesen
F.A. Finger-Institut für Baustoffkunde

Dissertation
zur Erlangung des akademischen Grades
Doktor Ingenieur
(Dr.-Ing.)

Hydration of multi-component cements containing clinker, slag, type-V fly ash and limestone

vorgelegt von
Axel Schöler, M.Eng.
aus
Hof/Saale

2015

1. Gutachter:	Prof. Dr.-Ing. Horst-Michael Ludwig F.A. Finger-Institut für Baustoffkunde Bauhaus-Universität Weimar, Weimar, DE
2. Gutachter:	Dr. sc. nat. Barbara Lothenbach Abteilung Beton und Bauchemie Empa - Eidgenössische Materialprüfungs- und Forschungsanstalt Dübendorf, CH
3. Gutachter:	Prof. Yuanzheng Yue, PhD Department of Chemistry and Bioscience Section for Chemistry Aalborg University, Aalborg, DK

Tag der Einreichung:	01.12.2015
Tag der öffentlichen Disputation:	20.06.2016

Meinen Eltern
Friedrich und Inghild Schöler

Ehrenwörtliche Erklärung

Ich erkläre hiermit ehrenwörtlich, dass ich die vorliegende Arbeit ohne unzulässige Hilfe Dritter und ohne Benutzung anderer als der angegebenen Hilfsmittel angefertigt habe. Die aus anderen Quellen direkt oder indirekt übernommenen Daten und Konzepte sind unter Angabe der Quelle gekennzeichnet.

Bei der Auswahl und Auswertung folgenden Materials haben mir die nachstehend aufgeführten Personen in der jeweils beschriebenen Weise entgeltlich/unentgeltlich geholfen:

1. Die Messungen zur Ermittlung der verschiedenen Sulfatspezies in Zementporenlösungen, wie in Kapitel 8 und Anhang 2 beschrieben, wurden an der Abteilung *Advanced Analytical Technologies* der Empa Dübendorf unter Leitung von Herrn Renato Figi durchgeführt. Die Kosten hierbei beliefen sich auf 1000 Schweizer Franken.

2. Die Messungen an Porenlösungen mittels ICP-OES und Ionenchromatographie, wie in Kapitel 4 diskutiert, wurden am HTC Leimen unter Anleitung von Herrn Dr. Mohsen BenHaha durchgeführt.

3. Die Messungen der Porenlösung mittels Ionenchromatographie, wie in Kapitel 8 diskutiert, wurden an der Abteilung *Concrete/Construction Chemistry* der Empa Dübendorf von Herrn Luigi Brunetti durchgeführt.

Weitere Personen waren an der inhaltlich-materiellen Erstellung der vorliegenden Arbeit nicht beteiligt. Insbesondere habe ich hierfür nicht die entgeltliche Hilfe von Vermittlungs- bzw. Beratungsdiensten (Promotionsberater oder anderer Personen) in Anspruch genommen. Niemand hat von mir unmittelbar oder mittelbar geldwerte Leistungen für Arbeiten erhalten, die im Zusammenhang mit dem Inhalt der vorgelegten Dissertation stehen. Die Arbeit wurde bisher weder im In- noch im Ausland in gleicher oder ähnlicher Form einer anderen Prüfungsbehörde vorgelegt.

Ich versichere ehrenwörtlich, dass ich nach bestem Wissen die reine Wahrheit gesagt und nichts verschwiegen habe.

Hof, 01.12.2015

Acknowledgements

The work presented in this thesis was carried out at the Laboratory for Concrete and Construction Chemistry at the Swiss Federal Laboratories for Science and Technology (Empa) in cooperation with HeidelbergCement AG and the F.A. Finger-Institut für Baustoffkunde, Chair of Werkstoffe des Bauens at the Bauhaus-Universität Weimar. HeidelbergCement AG is acknowledged for financial and analytical support. The acknowledgment is expanded to all members and supporters of the project for their participation, contributions and ideas as well as for helpful discussions.

In the following I would like to take advantage of the opportunity to thank the main contributors by name:

First, I would like to express my profound gratitude to my supervisors at Empa, Dr. Barbara Lothenbach and Dr. Frank Winnefeld for their support and guidance as well as for sharing their wealth of experience and expertise with me. I also thank you for your encouraging, always positive outlook on life.

Additionally, I sincerely thank Prof. Horst-Michael Ludwig for accepting me as an external PhD candidate and for his helpful discussions and support of my doctoral research.

My sincere thanks are extended to Dr. Mohsen Ben Haha, Dr. Maciej Zajac and Dr. Frank Bellmann as well as to my Empa fellows Dr. Salaheddine Alahrache, Dr. Lukas Martin and Dr. Florian Deschner.

Furthermore I want to thank all employees of the Laboratory for Concrete and Construction Chemistry, in particular Luigi Brunetti and Boris Ingold who never hesitated to lend me a helping hand whenever I was in need of assistance.

Special Thanks are due to the Trindler Family, especially to Walti, for magnificent accommodation and motivation.

Finally I want to say thank you to my Family and to my dearest love Veronika for her care, companion and unrestricted support especially as the last three years were far from ideal from a relationship point of view.

Danke!

Kurzfassung

Problemstellung und Zielsetzung

1. Die Herstellung von Portlandzementklinker trägt zu etwa 5 bis 8 % zur jährlichen Emissionsmenge an menschlich generiertem CO_2 bei. Dies ist begründet in der Verwendung von fossilen Brennstoffen (ca. 40 % des gesamten CO_2) und in der Entsäuerung des stark kalksteinhaltigen Rohmehls (ca. 60 % des gesamten CO_2).
2. Verschiedene Strategien zur Verringerung des Ausstoßes an CO_2 werden angewandt. Dies sind insbesondere die Optimierung der Prozessführung bei der Klinkerherstellung, die Verwendung alternativer Brennstoffe und die teilweise Substitution des Klinkeranteils in Zementen mit mehreren Hauptbestandteilen durch Zementersatzstoffe, sogenannte SCM (supplementary cementitious materials), wobei Hüttensand, Flugasche und Kalksteinmehl die meist verwendeten Materialien darstellen.
3. Durch die Reduktion des Klinkeranteils können quaternäre Systeme nicht nur einen Beitrag zur Reduzierung von CO_2-Emissionen leisten. Ebenfalls ist es mit derartigen Systemen möglich Hüttensande und Flugaschen möglichst ökonomisch einzusetzen und gegebenenfalls auf Engpässe bei deren Verfügbarkeit zu reagieren.
4. Hüttensande und Flugaschen zeigen Ähnlichkeiten in ihrer prinzipiellen chemischen Zusammensetzung, so dass ähnliche Hydratphasen während ihrer Reaktion in Anwesenheit von Portlandzement gebildet werden können. Im Vergleich zu ternären Systemen, die neben Kalkstein auch Hüttensand oder Flugasche enthalten, kann bei quaternären Zementen, die neben Kalkstein sowohl Hüttensand als auch Flugasche enthalten, eine ähnliche Phasenentwicklung und damit auch ähnliche Festigkeitsentwicklung erwartet werden.
5. Die Verwendung von SCM als Zementersatzstoff ist durch die im Vergleich zu Portlandzement deutlich langsamere Reaktion und die dadurch bedingte ebenfalls langsamere Festigkeitsentwicklung begrenzt. Dies betrifft insbesondere die Entwicklung innerhalb der ersten 28 Tage. Dementsprechend ist es unerlässlich die Reaktivität von SCM wie Hüttensanden und Flugaschen eingehend zu untersuchen um die Reaktionsfähigkeit- und Geschwindigkeit und somit die Festigkeitsentwicklung zu steigern.
6. Die frühe Reaktion der Hauptklinkerphasen ist weitgehend untersucht und beschrieben, wobei entsprechende Studien meist hochverdünnte Modellsysteme betrachten. Jedoch gibt es kaum Hinweise inwiefern diese Erkenntnisse auf konzentrierte Systeme bei realistischen Wasser-Feststoff Verhältnissen übertragen werden können. Entsprechende Untersuchungen sind nötig um die Wechselwirkungen von Portlandzement und SCM in der Frühphase der Reaktion zu beschreiben.

Stand der Wissenschaft

7. In verdünnten Systemen führt steigender Ca-Gehalt zu einer niedrigeren Auflösungsrate von C_3S und C_2S.
8. Bestimmende Faktoren der Auflösung von C_3S sind sowohl die Untersättigung bezüglich C_3S als auch die Übersättigung in Bezug auf C-S-H.
9. Erhöhte Al-Konzentrationen führen zur Verzögerung der Hydratation von C_3S. Dies kann begründet sein durch die Einbindung von Al in C-S-H und eine dadurch bedingte deutlich langsamere Wachstumsrate von C-(A)-S-H. Ebenfalls scheint ein verzögernder Effekt von Al auf die Auflösung von C_3S möglich.

10. Die Oberfläche von Kalkstein bietet besonders gute Bedingungen für die Keimbildung von C-S-H, so dass im Vergleich zu anderen SCM in Anwesenheit von Kalkstein deutlich mehr C-S-H Keime gebildet werden.
11. Die Reaktivität von Hüttensand und Flugasche wird einerseits durch die Korngrösse, andererseits jedoch auch durch die intrinsische Reaktivität des amorphen Anteils selbst bestimmt.
12. In amorphen (Calcium)Aluminosilikaten führt ein steigender Gehalt an Netzwerkmodifizierern, wie z.B. CaO, zu einem stärker depolymerisierten Glasnetzwerk und damit zu steigender Reaktivität. Die Wirkung von amphoteren Oxiden (Al_2O_3, Fe_2O_3) die sowohl als Netzwerkmodifizierer als auch als Netzwerkbildner auftreten können ist nicht vollständig geklärt.
13. CO_2 haltige Monophasen besitzen im Vergleich zu Monosulfoaluminat eine höhere thermodynamische Stabilität, wodurch Ettringit stabilisiert wird. Durch das hohe spezifische Volumen von Ettringit wird ein Maximum an Raumausfüllung, dadurch eine geringere Porosität und in Folge ein Maximum an Festigkeit erreicht.
14. Kalkstein reagiert nur in geringem Ausmaß entsprechend dem zur Reaktion vorhandenen Al_2O_3, wobei sich zunächst Hemicarboaluminat, später Monocarboaluminat bildet. Dabei wird Al_2O_3 nicht nur durch den Portlandzement selbst, sondern auch durch die Auflösung von SCM, insbesondere von Flugasche, zur Verfügung gestellt.

Methodik

15. Der Einfluss von SCM auf die frühe Hydratation von Portlandzement in binären (d.h. Hüttensand oder Flugasche oder Quarz) und ternären (d.h. Flugasche und Kalkstein) Systemen wurde mittels isothermer Kalorimetrie und Porenlösungsanalysen untersucht. Über die chemische Zusammensetzung der Porenlösung ermittelte Sättigungsindices und Löslichkeitsprodukte wurden in Bezug zur Wärmeentwicklung gesetzt. Basierend auf den ermittelten Daten wurde evaluiert, inwiefern Mechanismen die die Hydratation von reinen Klinkerphasen in verdünnten Systemen bestimmen ebenfalls in Zementpasten unter realistischen Bedingungen maßgebend sind.
16. Der Einfluss der chemischen Zusammensetzung auf die Reaktivität von Gläsern bei hohem pH (>13) wurde mittels Ionenchromatographie in hoch verdünnten Systemen untersucht. Puzzolanitätstests wurden an vereinfachten Modellsystemen sowie an Portlandzement-Glass-Systemen durchgeführt. Das Reaktionsverhalten der Gläser wurde über isotherme Kalorimetrie und thermogravimetrische Experimente untersucht. Über Massenbilanzkalkulationen kann der Gehalt an gebundenem Wasser in Funktion der Menge an reagiertem Glas berechnet werden. Ein Abgleich mit gebundenem Wasser bestimmt über thermogravimetrische Untersuchungen erlaubt es, den Reaktionsgrad der Gläser abzuschätzen. Zusätzliche Experimente mittels selektiver Lösung wurden zu Vergleichszwecken durchgeführt.
17. Die Reaktionskinetik von quaternären Pasten die sowohl Kalksteinmehl als auch Hüttensand und Flugasche enthalten wurden bis zum Alter von 28 Tagen mittels isothermer Kalorimetrie und Experimenten zum chemischen Schwinden untersucht. Ergänzend wurden Festigkeitsprüfungen an Mörtelprismen durchgeführt.
18. Quaternäre Pasten wurden ebenfalls hinsichtlich der gebildeten Hydratphasen bis zu einem Alter von 182 Tagen untersucht. Hierzu wurden basierend auf thermodynamischen Modellierungen volumetrische Berechnungen zum gesamten Phasenvolumen als Funktion des Kalkstein- und des Flugaschen- bzw. Hüttensandgehalts durchgeführt. Ergänzt durch thermogravimetrische Ermittlung des Gehalts an gebundenem Wasser

und Portlandit, sowie mittels qualitativen röntgendiffraktometrischen Untersuchungen wurden die Ergebnisse der thermodynamischen Berechnungen mit der Festigkeitsentwicklung von Mörtelprismen abgeglichen.

19. Porenlösungen von quaternären Systemen wurden bis zu einem Alter von 728 Tagen mittels Ionenchromatographie und pH-Bestimmung analysiert. Über die ermittelten Konzentrationen wurden Sättigungsindices für relevante Phasen ermittelt. Im Hinblick auf den Einfluss des Hüttensandes wurden Porenlösungen für ausgewählte Systeme bei verschiedenen Hüttensandgehalten (20 und 30 M.%) bei 91 Tagen, sowie für die gesamten Matrix bis zu 91 Tagen, auf verschiedene Schwefelspecies untersucht.

Im Wesentlichen erzielte Ergebnisse

20. Untersuchungen zur frühen Reaktionskinetik von binären Systemen zeigten einen stärkeren Wärmefluss in Anwesenheit von SCM, bedingt durch erhöhte für die Keimbildung zur Verfügung stehende Oberfläche sowie eine geringere (Über)Sättigung bezüglich C-S-H. Erhöhte Ca-Konzentrationen führten nicht zu langsamerer Auflösung von C_3S, wie dies für reine Phasen bei hoher Verdünnung beobachtet wurde. Im Gegensatz zu Untersuchungen in Reinstsystemen führten höhere Ca-Konzentrationen nicht zu geringeren Reaktionsraten von C_3S. Die schnellste Reaktion wurde bei Anwesenheit von Kalkstein, d.h. den höchsten Ca-Konzentrationen, beobachtet. Die grundsätzliche Reaktionscharakteristik zeigt einen inversen Bezug zur Untersättigung bezüglich C_3S, wobei höhere Untersättigung zu schnellerer Reaktion führt. Wie ebenfalls in Reinstsystemen bei hoher Verdünnung beobachtet, führt die Anwesenheit von Aluminium zur Verzögerung der Reaktion. Höhere SO_4^{2-}-Konzentrationen wurden in Anwesenheit von Flugasche beobachtet was die Ettringitausfällung verhinderte und zu höheren Al-Konzentrationen führt. Dieser Mechanismus führt zu höheren Al-Konzentrationen in Gegenwart von Quarz, Hüttensand und Kalkstein im Gegensatz zu Anwesenheit von Flugasche.
21. Die frühe Hydratation von quaternären Systemen wird in Anwesenheit von Kalkstein deutlich beschleunigt, während Flugasche zu einer Verzögerung führt. Im Gegensatz zu einem Referenzsystem mit inertem Quarz konnte mittels isothermer Kalorimetrie und chemischem Schwinden eine Reaktionsbeschleunigung in Anwesenheit von Hüttensand nachgewiesen werden. Weitere Zugaben an Flugasche, Kalkstein oder Mischungen von beiden führten zu einer weiteren Beschleunigung, wobei die Unterschiede zwischen diesen Materialien zu gering sind um eine klare Unterscheidung zu ermöglichen.
22. Bei allen zur Glasauflösung- bzw. Reaktivität durchgeführten Experimenten zeigten sich identische Trends, d.h. steigende Reaktivität und Auflösungsgeschwindigkeit mit steigendem Anteil an Netzwerkmodifizierern innerhalb der Glasstruktur. Die Ergebnisse weisen darauf hin, dass Al_2O_3 in sämtlichen betrachteten Glaszusammensetzungen vorwiegend als Netzwerkmodifizierer vorliegt. Die thermogravimetrische Bestimmung von gebundenem Wasser bei den Modellsystemen und den glashaltigen Zementen kann über Massenbilanzberechnungen als Funktion des Anteils an reagiertem Glas zur Abschätzung des Glasreaktionsgrades verwendet werden.
23. Zu frühen Zeiten von bis zu 7 Tagen hat der Anteil an Hüttensand, Flugasche oder Kalkstein keinen wesentlichen Einfluss auf die Festigkeitsentwicklung. Zu späteren Zeiten wurde über thermodynamische Berechnungen ein Reaktionsgrad des enthaltenen $CaCO_3$ (Calcit) von 2 bis 5 M.% ermittelt. Dies führt zur Bildung von Hemicarboaluminat und Monocarboaluminat wodurch Ettringit indirekt stabilisiert wird. In Folge ergibt sich ein höheres absolutes Volumen der gebildeten Hydratphasen und damit

höhere Festigkeiten wie Festigkeitsuntersuchungen an Mörtelprismen zeigen. Dabei hängt der Reaktionsgrad des $CaCO_3$ vom verfügbaren Al_2O_3 ab, welches neben dem Portlandzement selbst auch durch die Reaktion von Hüttensand, im Besonderen aber durch die Auflösung der Flugasche zur Verfügung steht.

24. Allgemein hat die Anwesenheit von Hüttensand und Flugasche in Gegenwart von Kalkstein wenig Einfluss auf die gebildeten Hydratphasen. Die sukzessive Substitution von Hüttensand durch Flugasche führt zu einer geringen Abnahme von Portlandit und C-S-H und begünstigt die Bildung von mehr Monocarboaluminat und Hemicarboaluminat. Portlandit reagiert puzzolanisch mit der Flugasche wobei sich C-S-H bildet. Dennoch führt die geringe Reaktivität der Flugasche zu geringerem Gehalt an C-S-H was wiederrum sinkendes gesamtes Hydratphasenvolumen und damit niedrigere Festigkeitswerte generiert. Allerdings ist der Einfluss gering und alle untersuchten Systeme erreichen die Festigkeitsklasse 42.5 N entsprechend EN 196-1.
25. Analog zur Hydratphasenbildung zeigten Untersuchungen der Porenlösungschemie von quaternären Systemen durchweg ähnliche Ergebnisse. Entsprechend dem Gehalt an Flugasche sind die stärksten Variationen in den Al-Konzentrationen zu verzeichnen, welche mit steigendem Gehalt an Flugasche und mit fortschreitender Hydratation ansteigen. Weiterhin ist zu späteren Zeiten Portlandit bei hohen Gehalten an Flugasche zusehends untersättigt, während die Untersättigung bezüglich Strätlingit abnimmt, was auf die Auflösung von Portlandit hinweist.
26. Der absolute Gehalt an SO_3 in der Porenlösung wird dominiert von Sulfat (SO_4^{2-}), während die Konzentrationen von Sulfit (SO_3^{2-}) und Thiosulfat ($S_2O_3^{2-}$) sehr niedrig waren. Nach 2 Tagen lagen ca. 90 % des gesamten Schwefels in Form von SO_4^{2-} vor. Nach 91 Tagen waren dies ca. 36 % während ca. 28 % als $S_2O_3^{2-}$ vorlagen. Bei höheren Gehalten an Hüttensand sind dabei nach 7 Tagen höhere Konzentrationen an SO_3^{2-} und $S_2O_3^{2-}$ feststellbar.

Abstract

Problem definition and research objectives

1. The production of Portland cement clinker causes approx. 5 % to 8 % of the annual man-made CO_2 emissions. This is due to the usage of mainly fossil fuel (approx. 40 % of the total CO_2) and because of the decarbonation of limestone as a main component of the raw meal (approx. 60 % of the total CO_2).
2. Various strategies are applied in order to reduce the green-house gas-emissions, such as optimizing the process of clinker production, the use of alternative fuel and the partial substitution of the clinker in blended cement by so-called SCM (supplementary cementitious materials). Hereby blast-furnace slag, fly ash and limestone are the most used materials.
3. Quaternary systems containing three SCM simultaneously besides Portland cement contribute to the reduction of CO_2 emissions due to the decrease of the clinker content. In addition, such systems allow to use blast-furnace slag and fly ash in the most economic way and provide the possibility to account for shortages of SCM on the market.
4. Blast-furnace slag and fly ash show similarities in their principal chemical compositions such that similar hydrates are formed during their reaction in presence of Portland cement. Compared to ternary systems based on blast-furnace slag or fly ash besides limestone, quaternary systems that contain both, blast-furnace slag and fly ash, simultaneously besides limestone, are expected to perform similar in terms of phase assemblage and strength development.
5. The use of SCM as cement replacing materials is limited due to their generally slower reaction compared to neat cement which also leads to lower strength development, especially in the early stage of the hydration up to 28 d. To account for this it is necessary to study the reactivity of SCM such as blast-furnace slag and fly ash in detail in order to develop strategies to enhance the reactivity and thereby the strength development of SCM-containing systems.
6. The early hydration of clinker phases is studied in detail, mainly in diluted systems. It is unclear if processes that were found to control the reaction of such model systems are also prevailing in concentrated cement pastes under realistic water-to-solid ratios. Deeper insight to this aspect is needed to better understand interactions of neat Portland cement and SCM in the first hours of hydration.

State-of-the-art

7. Increasing Ca-concentrations lead to decreasing dissolution rates of C_3S and C_2S in diluted systems.
8. The hydration kinetics of C_3S is controlled by the interplay of undersaturation with respect to C_3S and oversaturation with respect to C-S-H.
9. Increasing Al-concentrations lead to a retardation of the hydration of C_3S. It is unclear if the uptake of aluminum in C-S-H to form C-(A)-S-H which has a significantly lower growth rate than pure C-S-H or a retarding effect of Al on the dissolution of C_3S causes this phenomenon.

10. The surface of limestone provides excellent conditions for the nucleation and growth of C-S-H such that significantly more C-S-H nuclei are formed in presence of limestone compared to other SCM.
11. The reactivity of blast-furnace slag and fly ash depends on the particle size as well as on the intrinsic reactivity of especially the amorphous phases.
12. An increase in network modifying oxides (e.g. CaO) in the chemical composition of amorphous (calcium)aluminosilicates leads to an increasingly depolymerized network which in turn causes increasing reactivity. The role of amphoteric oxides (Al_2O_3, Fe_2O_3) that can be present as network modifying oxides as well as network forming oxides is not completely solved.
13. CO_2-containing AFm-phases are thermodynamically more stable than monosulfoaluminate. This indirectly stabilizes the voluminous ettringite which causes a higher total volume of hydrates and lower porosity whereby higher compressive strength is reached.
14. Only a few percent of limestone in blended cement reacts chemically dependent on the Al_2O_3 available for reaction. Al_2O_3 that is provided by the reaction of Portland cement but also by the dissolution of SCM, especially by fly ash, reacts to form hemicarboaluminate which is transformed to monocarboaluminate as the hydration proceeds.

Methodology

15. The influence of SCM on the early hydration of Portland cement in binary (including blast-furnace slag or fly ash or limestone or quartz) and ternary (including fly ash and limestone) systems was investigated applying isothermal calorimetry and analysis of the pore solution chemistry. Calculated saturation indices and solubility products of relevant phases were correlated with heat development. Based on the gained data it was reviewed if mechanisms that control the hydration of pure phases in diluted systems are also prevailing in cement pastes under realistic conditions.
16. The influence of the chemical composition of synthetic glasses on their dissolution at high pH was investigated in highly diluted systems using ion chromatography. Pozzolanity tests were conducted on pastes using simplified model systems and glass-blended Portland cements. The process of the glass dissolution was investigated by isothermal calorimetry and by thermogravimetry. Correlation of experimentally determined total bound water with bound water determined by mass balance calculations as a function of amount of glass reacted allowed to estimate the degree of glass reaction in the pastes. Furtheron selective dissolution experiments were carried out to crosscheck the results of the bound water/mass balance approach.
17. The reaction kinetics of quaternary pastes containing blast-furnace slag and fly ash simultaneously in the presence of limestone were investigated up to 28 d using isothermal calorimetry and chemical shrinkage measurements. In addition strength tests on mortar bars were carried out.
18. Pastes of quaternary blends were also investigated in terms of hydrate assemblage at ages of up to 182 d. Thermodynamic calculations regarding total volume of hydrates as a function of limestone and fly ash/blast-furnace slag content were conducted. The calculations were supported by thermogravimetric determination of bound water and portlandite content as well as qualitative X-ray diffraction. The results were correlated with strength tests on mortar bars.

19. The pore solutions of hydrated quaternary blends were extracted and investigated by means of ion chromatography at ages of up to 728 d. Based on the ion concentrations in the solutions saturation indices were calculated for relevant phases. In order to gain better insight to the blast-furnace slag reaction sulphate speciation was carried out at two blast furnace slag levels (20 and 30 wt.%) for selected samples up to 91 d of hydration and at 91 d for the whole matrix under investigation.

Main results

20. Investigations on the early hydration kinetics of binary systems showed a higher heat flow in presence of SCM compared to neat Portland cement. This is caused by the higher surface area that is available for the nucleation of hydrates and by the lower (over)saturation with respect to C-S-H. An increase in the Ca-concentration in the pore solution did not cause lower dissolution rates of C_3S as was reported for pure phases in diluted systems. The highest dissolution was observed in the presence of limestone, i.e. at the highest Ca-concentration. The general trend of the reaction rate is inversely related to the degree of undersaturation with respect to C_3S. The more undersaturated the faster the observed reaction. The presence of increasing Al-concentrations caused a retardation of the reaction which is in line with investigations on pure phases in diluted systems. Higher sulphate concentrations could be detected for the fly ash containing blend which possibly hindered ettringite precipitation and results in higher Al-concentrations. Correspondingly the low sulphate concentrations lead to lower Al-concentrations in the presence of quartz, blast-furnace slag and limestone compared to fly ash.
21. The early hydration kinetics of quaternary systems is significantly accelerated in the presence of limestone while fly ash leads to retardation. Compared to reference systems containing inert quartz, investigations by means of isothermal calorimetry and chemical shrinkage revealed an acceleration caused by blast-furnace slag. Additions of fly ash, limestone or mixtures thereof introduced another acceleration but differences are too small to be significant and clear distinguishing between the various SCM is not possible.
22. Investigations on the reactivity of synthetic glasses showed that increasing amounts of network modifying oxides caused an increase in reactivity and dissolution rates. The results reveal that Al_2O_3 acts mainly as network modifying oxide in all investigated glasses. Experimentally determined bound water (thermogravimetric experiments) in model systems and blended cements can be compared with bound water determined by mass balance calculations carried out as a function of the amount of glass reacted. This enables to estimate the degree of glass reaction.
23. The actual content of blast-furnace slag, fly ash or limestone does not exert significant influence on the development of compressive strength up to 7 d. At later ages thermodynamic calculations predict a degree of $CaCO_3$ reaction of 2 to 5 wt.%. This leads to the formation of hemicarbonate and monocarbonate whereby ettringite is indirectly stabilized. As a result the total amount of solids is increased and compressive strength shows a slight maximum. Hereby the degree of $CaCO_3$ reaction depends on the Al_2O_3 available for reaction which is not only provided by the dissolution of Portland cement but especially by the dissolution of the fly ash.
24. In general the presence of blast-furnace slag and fly ash in the presence of limestone exerts little influence on the hydrate assemblage. The substitution of some of the blast-furnace slag by fly ash leads to a slight decrease of portlandite and C-S-H and

gives rise to the formation of more monocarbonate and hemicarbonate. Portlandite is consumed in a pozzolanic reaction with the fly ash whereby C-S-H is formed. However, the low reactivity of the fly ash causes a decrease in the amount of C-S-H formed. Thereby a lower total volume of hydrates is generated which is in line with slightly lower compressive strength in case of increasing fly ash content. The overall influence is small and all systems investigated reach strength class 42.5 N according to EN 196-1.

25. Corresponding to the investigations of the hydrate assemblage the pore solution chemistry of quaternary systems showed only small variations. Depending on the fly ash content the highest variations are observed for aluminium, i.e. increasing fly ash content leads to higher Al-concentrations. Another effect of increasing fly ash contents is an increasing undersaturation with respect to portlandite and a decreasing undersaturation with respect to strätlingite indicating the dissolution of portlandite.
26. The total concentration of sulfur in the pore solution is controlled by sulphate (SO_4^{2-}) while the concentrations of sulphite (SO_3^{2-}) and thiosulphate ($S_2O_3^{2-}$) were very low. Up to 2 d of hydration about 90 % of the total sulphur is present as SO_4^{2-}. After 91 d this value is reduced to about 36 % while about 28 % are present as $S_2O_3^{2-}$. In general higher blast-furnace slag content leads to higher concentrations of sulphite and thiosulphate after 7 d.

Contents

Chapter 1

Introduction

1.1 Neat and blended Portland cement: A brief historical review[1]

Three fundamental human needs can be defined that were always present throughout the history of mankind from the stone age to the 21st century: Food, clothing and dwelling. In terms of the latter, which establishes the need for building materials, a remarkable development can be observed during the last 150 years. The development of modern society, the imposing results of modern architectural design and the high level of mobility that is closely linked to a highly developed infrastructure, all these aspects as we know them today would not be present without the invention of Portland cement (PC). It seems to be impossible to date the natal hour of Portland cement with any certainty. It is commonly believed in France that the work of Louis-Joseph Vicat [Vicat, 1818, Vicat, 1828] made way for the commissioning of the first French Portland cement plant that was built in 1840 in Boulogne-sur-Mer [Aïtcin, 2008]. However, the invention of Portland cement is most often mentioned at the same time with a patent of Joseph Aspdin first lodged in 1824: *"An Improvement in the Modes of Producing an Artificial Stone"* [Haegermann, 1970]. Indeed it is more likely that Aspdin's son, William Aspdin, produced a first Portland cement-prototype around 1850 when he fired a mixture of limestone (LS) and clay at a sufficient high temperature to produce the main clinker phase, tricalcium silicate (C_3S) [Blezard, 1998]. Whatever the case, the invention of Portland cement half-way through the nineteenth century opened up entirely new opportunities for civil engineering. Today, the success of this material is reflected in an estimated amount of 4.18 Gt of cement that was produced world-wide in 2014 [van Oss, 2015]. The importance of cement is also reflected in the amount of concrete produced as most Portland cement is used in making concrete. With an estimated annual consumption of 3.8 billion m^3 concrete is the most solid material used today.

Thirty-eight years after Aspdin's patent another invention is worth emphasizing. It was the German Emil Langen who discovered the latent hydraulic properties of blast-furnace slag (BFS) (a by-product of pig-iron production) that was quenched fast enough to almost completely avoid crystallization [Grün, 1928, Kollo, 1987]. The material was

[1] While a whole range of materials is used to produce multi-component cements only the three mineral additions (blast-furnace slag, Si-rich fly ash and limestone) that are investigated in the course of the present thesis are considered in the historical review.

available in vast amounts as it was mostly collected on slag heaps. Blast-furnace slag is used in ground and granulated form - hence often called ground granulated blast-furnace slag (GGBFS) - for cement production. In 1882 Godhard Prüssing blended Portland cement clinker with 30 wt.% of blast-furnace slag. This decision was in violation of the purity requirement that was launched in 1885 by the *"Verein Deutscher Cement-Fabrikanten"* and caused longstanding scientific and economic conflicts. Blast-furnace slag used as a component within the production of cement clinker was first used in 1882 by Theodor Narjes and August Bender. Clinker that was produced according to this procedure was interground with 30 wt.% blast-furnace slag. This cement was designated *"Eisenportlandzement"* (Iron-Portland cement) in 1901. Cements with higher shares of blast-furnace slag were know as *"Hochofenzement"* (blast-furnace cement) from 1907 on [VDZ, 2002]. Blast-furnace slag was always present as a topic in cement research ever since, which is also documented in early publications by Passow [Passow, 1908] and Fleißner [Fleißner, 1912]. The use of blast-furnace cements or blast-furnace slag as addition to concrete is well known, especially in countries with a pig-iron industry. As the demand for high and equal quality pig-iron increased differences in the quality of blast-furnace slag were reduced and the application of the latter within the production of construction materials expanded which is reflected in the number of corresponding cements that are included in the current European standard EN 197-1 (see Figure 1.1).

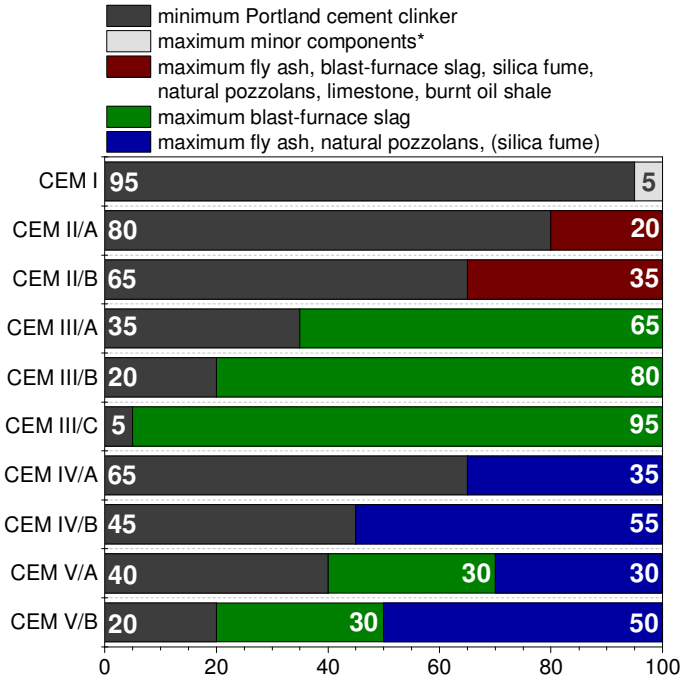

Figure 1.1: Cements standardized in EN 197-1. Further sub-groups are not displayed in the graphical depiction. Data refers to wt.%. *The amount of minor components (e.g. calcite, quartz, etc.) ranges from 0 to 5 wt.% for all cements as displayed for CEM I. Reproduced from [Deschner, 2014].

Besides blast-furnace slag, fly ash (FA) is another industrial by-product with an important role in cement production. This synthetic pozzolan is collected in the dedusting system of power plants that burn hard coal or lignite coal. According to [Joshi and Lohita, 1997] fly ash was first recognized as pozzolanic addition to concrete in 1914. However, it did not play an important role before the middle of the 19th century. The interest in the

material for the next decades was limited but still present. It was H.E. Davis who conducted comprehensive studies on the use of fly ash in concrete in 1937 [Davis et al., 1937]. From the 1960s on the number of publications concerning fly ash in cement or concrete increased but most of these studies until the 1980s (e.g. [Snyder et al., 1964, Berry and Malhotra, 1982, Swamy, 1986]) focused on Si-rich fly ash, simply because it was the most widespread available ash. Today, different types of fly ash are used for the production of Portland cement blends at shares of up to 55 wt.% as described in EN 197-1 (Figure 1.1).

Limestone plays an outstanding role in terms of cement production. It is one of the main components that constitute the raw mixture that is transformed to Portland cement clinker in the rotary kiln. Besides this application it is also used in pure form (i.e. pure limestone with a high share of calcite ($CaCO_3$)) to produce Portland cement-based blends. While blast-furnace slag and fly ash originate from other branches of industry, cement plants are almost exclusively located next to limestone quarries. Availability is therefore not an issue. The history of the use of limestone in blended Portland cement since the 1960s is documented by alterations in cement standards as presented in Table 1.1.

Besides blast-furnace slag, fly ash and limestone several other mineral additions are used in cement production. The current European standard EN 197-1 defines 27 different cements. While there is a falling demand in terms of neat Portland cement (CEM I) blended cements are becoming more and more important today (cf. Figure 1.3).

Table 1.1: Historical development of the limestone content in Portland cement blends in various standards.

year	alterations
1965	Cement with 20 wt.% limestone in Germany for special applications
1979	French cement standards allows limestone additions
1983	Canadian standard A5 allows up to 5 wt.% limestone in portland cement
1990	15±5 wt.% limestone blended cements routinely used in Germany
1992	UK specs allows up to 20 wt.% in limestone cement
2000	EN 197-1 allows 5 wt.% minor additional constituents (typ. limestone) in all 27 common cements (as was commonly practiced in various European cement standards prior to that)
2000	EN 197-1 creates CEM II/A-L (6 to 20 wt.%) and CEM II/B-L (21 to 35 wt.%)
2004	ASTM C 150 allows 5 wt.% in types I-V
2006	Canadian standard A3001 allows 5 wt.% in other types than general use hydraulic cement (GU)
2007	American Association of State Highway and Transportation Officials (AASHTO) M85 allows 5 wt.% in types I-V
2008	Canadian standard A3001 includes Portland limestone cement (PLC) containing 5 to 15 wt.% limestone

1.2 Context

The process of manufacturing cement is high up on the list of main sources of CO_2 emissions originating from industrial activities. Not regarding CO_2 generated due to the consumption of energy consumed by the cement plant (electric current etc.) these emissions are primarily generated by two sources:

- The combustion of huge amounts of fossil fuels which accounts for about 40 % of the CO_2 emissions, the so-called fuel-CO_2.
- The decomposition of $CaCO_3$ to CaO and CO_2 as limestone is one of the main components of the raw meal that is transformed to Portland cement clinker in the rotary kiln. CO_2 generated by this process accounts for about 60 % of the CO_2 emissions, the so-called process-CO_2.

Compared to other industries this output appears to be moderate. For example, the production of 1 t of steel causes approx. 2.0 t of CO_2 [Pardo et al., 2012] while the production of 1 t of Portland cement produces only 0.7 t to 1.0 t of CO_2 [Damtoft et al., 2008, Worrell et al., 2001]. However, due to the vast annual amounts of cement produced worldwide the green-house gas emissions produced by the cement industry are a serious issue. Figure 1.2 displays the expected annual demand of cement worldwide up to 2050. This graphical depiction clearly demonstrates the need for strategies that can be applied in order to reduce the green-house gas emissions in terms of cement production. According to [Marchal et al., 2012] the estimated man-made CO_2 emissions in 2050 reach 56 000 Gt. Without mitigation strategies the production of cement would be responsible for 4.1 % while the application of mitigation techniques enables to decrease the contribution to 2.8 %.

Strategies that aim at reducing the CO_2 emissions caused by cement production are already available or are under development. Different main groups can be defined in this regard:

- Applying the carbon dioxide capture and storage approach that seems to be particularly appropriate in cement industry due to the fact that there are large point sources of CO_2 with a high concentration in the flue gas composition [Barker et al., 2009].
- Switching from wet or semi-wet processes to a dry process of clinker production. Thereby the total energy of clinker production can be significantly lowered as the raw meal does not need to be dried.
- Process optimization by installing preheater and precalciner systems. This enables to reach a degree of decarbonation of the raw meal of up to 80 % by using hot air coming from the kiln whereby the raw meal reaches up to 800 °C when entering the rotary kiln. Due to the better energetic recovery of the heat generated the amount of fuel needed can be decreased.
- Alteration of the raw meal by using non-carbonatic Ca-sources. To this purpose slags or sewage sludge can be used.
- Utilizing alternative materials. This includes the use of fuels with different carbon content and heating value, e.g. used tires and waste oil.

- Reusing potential industrial by-products like blast-furnace slag and fly ash to reduce the clinker content in blended cements is considered as the most promising and practical way to reduce accumulation of industrial by-products and especially to reduce the CO_2 emissions generated by the cement industry.

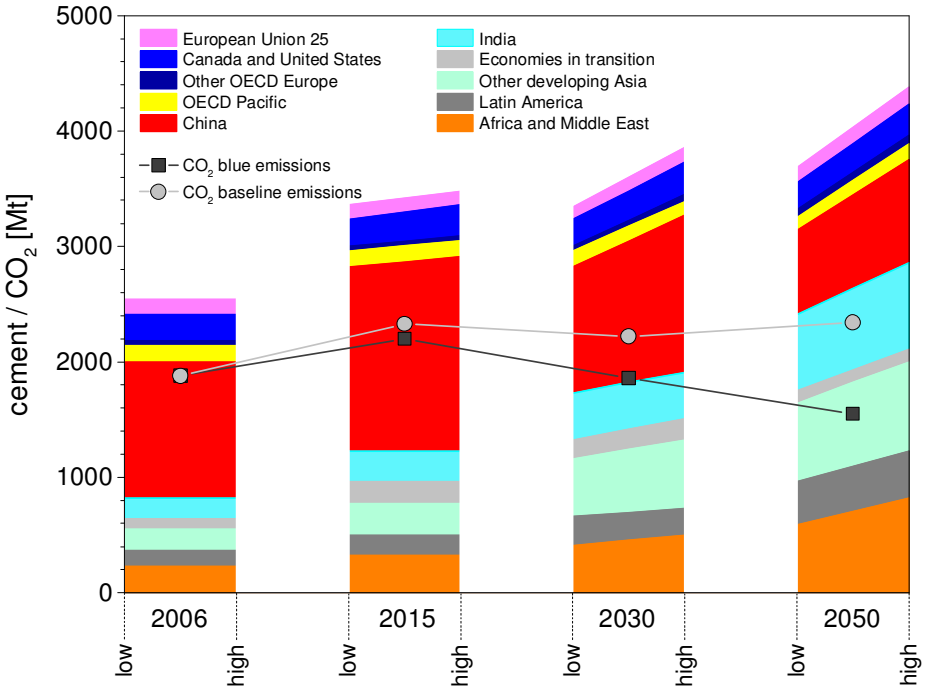

Figure 1.2: Expected global cement production till 2050. Both, a high demand scenario and a low demand scenario are depicted. The two continuous lines represent estimations of the global CO_2 emissions by cement plants. Blue emission is defined as future emissions by considering application of mitigation technologies and policies, baseline emissions is defined as future emissions without applying any mitigation actions. Data taken from [Schneider et al., 2011, Benhelal et al., 2013].

Reducing the clinker content by blending Portland cement with mineral additions or supplementary cementitious materials (SCM) is not a new approach. As already displayed in Figure 1.1 most of the cements available today are blended systems including SCM. The availability of materials and the properties of the resulting cement or concrete have been the driving force to promote this approach. The global debate on climate change adds a new motive for research and development in this field. As can be drawn from Figure 1.3, the demand for unblended Portland cement (CEM I) in Europe was reduced by about 20 % between 2000 and 2010 while the demand for blended cements, especially the sub-types of CEM II, increased in the same period. A detailed view on the European demand for CEM II sub-types shows that the most important cement is Portland limestone cement with limestone content of up to 35 wt.%. The second most important cement is Portland composite cement that is allowed to include up to 35 wt.% of SCM as displayed in Figure 1.1 followed by Portland slag cement and Portland fly ash cement. This clearly shows that there is a vast demand for SCM that will further increase due to the expected increase of cement consumption in the decades to come.

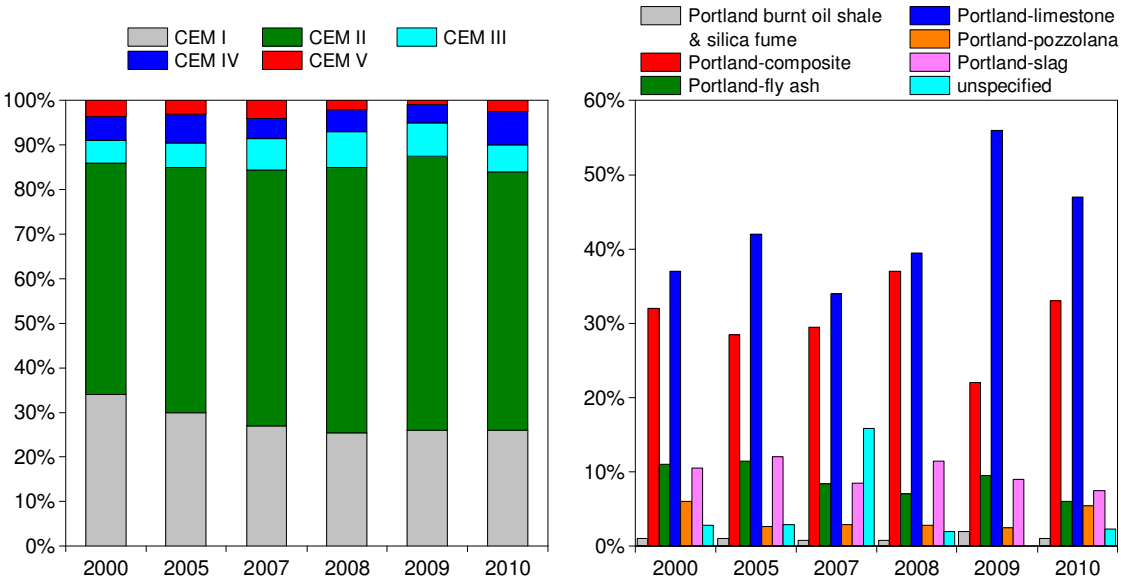

Figure 1.3: (left) Domestic deliveries by cement type and (right) domestic deliveries of CEM II sub-type within Europe between 2000 and 2010. Reproduced from [Cembureau, 2012].

The use of SCM in blended cements is limited due to several reasons. Not discussing details on the underlying processes, the allowed maximum amount of limestone that can be used in Portland limestone cement is determined by reasons of performance and durability. In terms of blast-furnace slag and especially fly ash, the general lower reactivity of these SCM causes the limited allowed amounts as early strength is one of the quality characteristics that is used to classify cements.[2] Another important factor is the availability of SCM which is especially noteworthy in case of blast-furnace slag of excellent quality. With regard to the above discussed environmental considerations efforts are being made to expand the European standard EN 197-1. New cement compositions that are investigated by CEN/TC 51 WG 6 Ad-Hoc-Group "CEM X"[3] [CEN/TC 51, 2012, Espion et al., 2013, VDZ, 2012] are displayed in a ternary (cement)-(limestone)-(blast-furnace slag or fly ash or pozzolan)-diagram in Figure 1.4 along with the currently included cement compositions. These investigations consider only ternary systems including Portland cement and limestone and blast-furnace slag or fly ash or pozzolans. Quaternary systems including three SCM simultaneously along with Portland cement might be interesting future cement compositions. This is mainly due to similarities in the chemical composition of the SCM which might result in similar phase assemblage and properties in hydrated systems [Iñiguez Sánchez et al., 2011]. While comprehensive studies on binary and ternary cements are available [Espion et al., 2013, Vance et al., 2013, Menendez and Irassar, 2003, El Houda Khalifa et al., 2013, De Weerdt et al., 2011c, De Weerdt et al., 2011a, Bleszynski et al., 2002, Lothenbach et al., 2008a, Deschner et al., 2012] there is a lack of knowledge on the behavior of quaternary systems. Along with the reduction of green-house gas emissions the availability of SCM is another aspect that supports the interest in quaternary cements. The high demand on the most required SCM, blast-furnace

[2] In case of fly ash also the consumption of portlandite plays a role as fly ash reacts in a pozzolanic reaction with the portlandite formed during the hydration of Portland cement.

[3] CEM X corresponds to the working title for new cement compositions in the process of standardization. The new cement compositions will be included in EN 197-1 as CEM II/C and CEM VI.

slag and fly ash, can lead to bottlenecks in the supply. Once corresponding compositions are developed to market maturity, industrial by-products can be used "resource-saving" while shortages on the market can be compensated. These environmental and economical considerations provide the driving force for the challenging task of developing complex quaternary Portland-cement based systems.

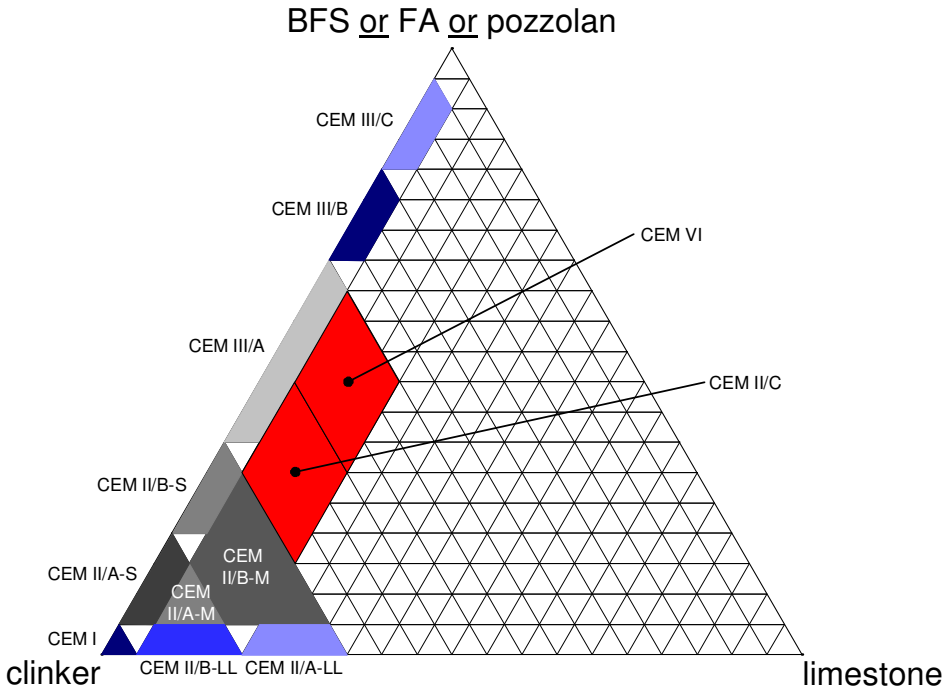

Figure 1.4: New cement compositions (red areas) as included in the European draft standard prEN 197-1:2014. Adapted from [VDZ, 2012].

1.3 Research objectives

As discussed above, the interest in quaternary cements along with the lack of information concerning such systems form the basis for corresponding studies. However, not only quaternary systems are investigated but also aspects concerning the effect of SCM on the hydration of blended cements or the reaction of SCM themselves. On this basis three general research objectives can be defined as follows:

- Detailed knowledge on the hydration mechanisms of pure clinker phases has been generated in recent years. While model systems are often used due to their lower complexity compared to "real" systems the described mechanisms are rarely investigated in Portland cement-based systems. Studies on binary SCM-blended systems investigate the early hydration in the first few hours in order to clarify if mechanisms that are prevailing for pure clinker phases are present and/or dominant in realistic systems as well (Chapter 4).

- Along with the amount of amorphous content, the intrinsic reactivity of SCM glasses is one of the key parameters that determine the SCM reaction in blended cements. Investigations on synthetic SCM glasses target at the determination of

the dependence of the intrinsic reactivity on the chemical composition of the glasses (Chapter 5).

- Investigation of quaternary Portland cement based compositions containing blast-furnace slag, Si-rich fly ash and limestone simultaneous. The main interest is to determine the kinetic behavior in presence of various SCM (Chapter 6) as well as the development and the composition of the hydrate assemblage and the corresponding effects on compressive strength depending on the actual composition (Chapter 7). In addition to investigations of the solid phases the composition of the pore solution corresponds to the solid phases present and is therefore of interest as well (Chapter 8).

1.4 Structure of the thesis

The investigation of quaternary Portland-cement based cements is a challenging task due to the complexity of these systems. Accordingly a multi-method approach was chosen. Different aspects like hydrate assemblage, hydration kinetics, pore solution chemistry and pozolanic reactivity of SCM were investigated. The following breakdown shortly describes the content of the different chapters:

Chapter 2 gives an overview on the use of SCM in blended Portland cements summarizing the state-of-the-art of aspects relevant to the investigations carried out in the context of the present thesis.
Chapter 3 provides detailed descriptions of the materials, the analytical techniques and strategies used in this work.
Chapter 4 deals with the effect of SCM on the very early hydration of up to 6 h in binary Portland cement blends. The investigations aim at clarifying correlations between the kinetic behavior and the pore solution chemistry taking into account theories based mainly on investigations in diluted systems.
Chapter 5 investigates the effect of glass composition on the reactivity of synthetic glasses based on compositions as they are prevailing in the glass phases of blast-furnace slag and fly ash.
Chapter 6 focuses on the kinetic behavior of quaternary Portland cement blends as well as on the development of compressive strength at ages of up to 28 d of hydration.
Chapter 7 presents results on investigations of the hydrate assemblage of ternary and quaternary Portland cement blends. The impact of the mix design on the hydrate assemblage and thereby on the total volume of hydrates and the resulting effect on compressive strength is discussed.
Chapter 8 investigates the pore solution of the systems studied in the two previous chapters at ages of up to 728 d. In addition saturation indices are calculated for relevant phases. In order to gain better insight to the blast-furnace slag reaction at early ages sulfate speciation was carried out for selected samples at ages of up to 91 d of hydration.
Chapter 9 provides general conclusions on the present thesis and gives an outlook along with suggestions for future work.

Chapter 2

The use of supplementary cementitious materials in Portland cement: A state-of-the-art review

This chapter contains a brief summary of research into neat SCM and Portland cement interground or blended with SCM relevant to the present thesis, namely blast-furnace slag, Si-rich fly ash and limestone (cf. Figure 2.1). The major aspects covered focus on the hydration of SCM-containing cements, the development and composition of the hydrate assemblage and the pore solution and on factors affecting the reactivity of the SCM themselves. With regard to the numerous studies available on relevant topics this overview does not claim to be thorough. It is referred to appropriate specialized literature whenever possible.

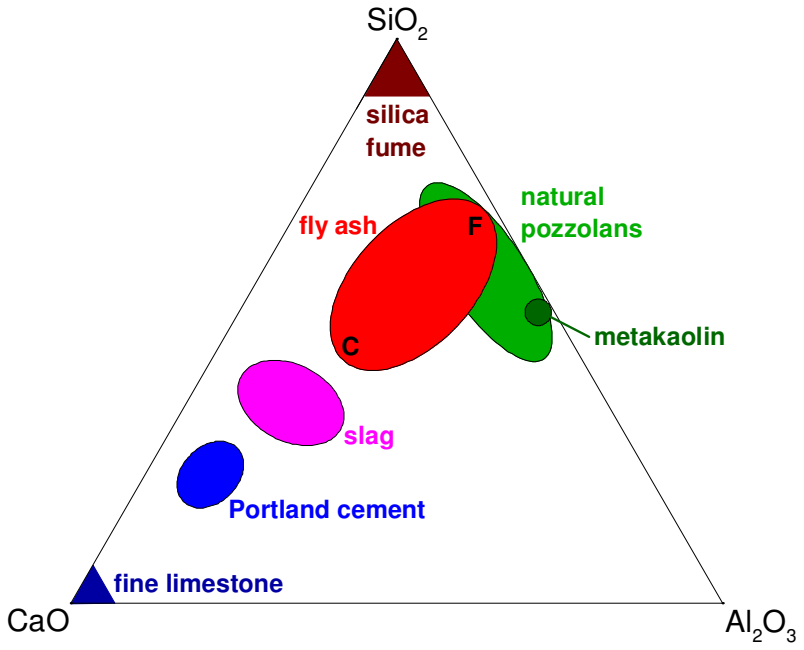

Figure 2.1: CaO-Al_2O_3-SiO_2 ternary diagram of cementitious materials. Reproduced from [Lothenbach et al., 2011].

2.1 Relevant types of SCM

2.1.1 Blast-furnace slag

Blast-furnace slag is a by-product of the production of pig-iron. It is defined as *"a non-metallic product consisting essentially of silicates and aluminosilicates of calcium and of other bases, that is developed in a molten condition simultaneously with iron in a blast-furnace"* [RILEM, 1988]. In the blast-furnace a mixture of iron oxide ore, coke and limestone (fluxing agent) are heated/molten at temperatures of about 1500 °C. Thereby the iron oxide is reduced into metallic iron due to the presence of coke while a slag is formed on top of the molten iron which consists of silicates and alumina originating from the iron ore and oxides from the limestone. When the blast furnace is tapped, the molten slag is cooled by use of high pressure water jets. The rapid quenching results in a wet and sandy granular material. Due to the high rate of cooling the formation of larger crystals is suppressed such that contents of amorphous/glassy phases (calcium aluminosilicates) of up to 100 wt.% are obtained. This granular material is further processed by drying and milling, hence its denotation "ground granulated blast-furnace slag". As can be seen from Table 2.1 the chemical composition shows significant variations, especially in the main constituents CaO, SiO_2, Al_2O_3 and MgO which are primarily caused by variations in the chemical composition of the iron ore used for the pig-iron production. Note that sulphur in the amorphous part of blast-furnace slag exists mainly in a sulphide state (S^{2-}) [Roy, 2009].

Table 2.1: Chemical composition of different blast-furnace slags presented in [wt.%].[a] n.a. = data not available.

	BFS_I	BFS_{II}	BFS_{III}	BFS_{IV}	BFS_V	BFS_{VI}	BFS_{VII}	BFS_{VIII}
L.O.I.[b]	0.80	0.40	n.a.	n.a.	0.03	n.a.	0.30	0.62
SiO_2	38.20	36.40	41.60	37.20	36.61	35.30	38.20	41.25
Al_2O_3	12.00	11.30	7.00	16.70	12.21	11.40	13.19	7.57
Fe_2O_3	1.60	1.40	1.30	1.40	0.85	1.70	0.86	0.38
CaO	35.80	33.40	39.10	35.00	41.59	33.90	39.72	36.43
MgO	7.70	13.20	7.20	6.40	7.18	13.80	8.55	9.67
SO_3[c]	1.40	0.36	1.30	1.00	0.63	n.a.	0.56	1.51
K_2O	1.20	1.00	0.60	0.50	0.28	0.90	0.41	0.62
Na_2O	0.41	0.52	0.50	0.50	0.18	n.a.	0.28	0.37
TiO_2	0.50	0.47	0.30	0.20	0.35	1.20	0.63	0.30
Mn_2O_3	1.50	1.40	1.10	1.00	0.14	1.00	0.69	0.71
P_2O_5	0.03	0.02	n.a.	n.a.	0.01	n.a.	n.a.	0.02
BaO	n.a.	n.a.	n.a.	n.a.	n.a.	n.a.	0.09	n.a.
Amorphous[d]	98.5	99.5	96.0	99.0	99.5	99.8	100.0	98.5

[a] Data taken from [Ben Haha et al., 2012] (BFS_I, BFS_{II}), [Ben Haha et al., 2011] (BFS_{III}, BFS_{IV}), [Kocaba, 2009] (BFS_V), [Escalante et al., 2001] (BFS_{VI}), [Bougara et al., 2010] (BFS_{VII}), [Schöler et al., 2015] (BFS_{VIII}),.

[b] Gain on ignition due to oxidation of S^{2-} during L.O.I. measurement.

[c] Present as S^{2-}.

[d] Amorphous content is typically determined by XRD-Rietveld methods using internal or external standard.

According to ASTM C989, blast-furnace slag is classified in three strength grades (80, 100 and 120) which are determined by respective mortar strength when the blast-furnace slag is mixed with an equal mass of Portland cement. These grades are classified according

to the slag activity index which is the average compressive strength of the slag-reference cement (SP), divided by the average compressive strength of the reference cement (P), multiplied by 100.

$$Slag\ activity\ index = \frac{SP}{P} \cdot 100[\%] \tag{2.1}$$

In accordance with EN 197-1 blast-furnace slag must contain at least two thirds by mass of amorphous phases while the overall composition must contain at least two thirds of CaO, MgO and SiO_2. The remaining third contains Al_2O_3 and minor compounds. The mass ratio (CaO+MgO)/(SiO_2) has to be greater than 1.0.

2.1.2 Fly ash

Fly ash is an industrial by-product that is generated by burning pulverized coal in coal combustion power plants. In the process of coal combustion, molten impurities in the coal (i.e. clay, feldspar, quartz and shale) rise and solidify into spherical particles containing amorphous/glassy phases due to the high rate of cooling. The composition of these particles that are collected in the power plants dedusting system is highly variable (cf. Table 2.2). The chemical composition of the fly ash depends mainly on the composition of the burned coal and the degree of coal pulverization while the morphology and the mineralogy of the fly ash are subject mainly to the mode of firing [Ravina, 1981].

Table 2.2: Chemical composition of different fly ashes presented in [wt.%].[a] n.a. = data not available.

	Si-rich FA				Ca-rich FA			
	$FA_{Si\text{-}I}$	$FA_{Si\text{-}II}$	$FA_{Si\text{-}III}$	$FA_{Si\text{-}IV}$	$FA_{Ca\text{-}I}$	$FA_{Ca\text{-}II}$	$FA_{Ca\text{-}III}$	$FA_{Ca\text{-}IV}$
L.O.I.	3.5	8.2	2.1	n.a.	n.a.	n.a.	n.a.	n.a.
SiO_2	50.9	49.1	56.8	67.0	20.7	42.3	33.6	31.5
Al_2O_3	24.7	19.2	26.0	24.8	5.5	19.8	18.2	17.8
Fe_2O_3	7.3	10.4	5.1	3.1	2.7	8.2	6.4	6.0
CaO	3.7	8.5	3.2	1.0	65.7	20.7	26.5	28.0
MgO	1.8	2.0	1.3	0.6	1.5	2.2	6.4	5.4
SO_3	0.4	0.3	0.1	0.1	2.6	1.4	2.2	4.4
K_2O	3.9	0.8	2.5	1.6	0.4	1.5	0.4	0.4
Na_2O	0.9	0.3	0.3	0.6	0.2	0.3	1.9	1.8
TiO_2	1.1	1.0	1.4	1.0	0.3	0.7	1.3	1.6
Mn_2O_3	0.1	0.1	0.0	0.0	0.0	0.0	0.0	0.1
P_2O_5	0.8	0.4	0.4	0.2	0.2	0.3	0.9	2.1
Amorphous[b]	83.3	60.6	68.8	79.1	89.7	85.9	75.1	90.7

[a] Data taken from [Deschner et al., 2012] ($FA_{Si\text{-}I}$), [Valentim et al., 2009] ($FA_{Si\text{-}II}$), [Schöler et al., 2015] ($FA_{Si\text{-}III}$), [Ward and French, 2006] ($FA_{Si\text{-}IV}$), [Durdziński et al., 2015] ($FA_{Ca\text{-}I}$, $FA_{Ca\text{-}II}$, $FA_{Ca\text{-}III}$), [Bumrongjaroen et al., 2007] ($FA_{Ca\text{-}IV}$).

[b] Amorphous content is typically determined by XRD-Rietveld methods using internal or external standard.

The contribution of fly ash on the hardening of pastes and the properties of those depends on the reactivity of the contained phases and on their amount contained in the fly ash. Based on the content of SiO_2, CaO, Al_2O_3 and/or Fe_2O_3 different systems are available in existing standards that classify fly ash in class F (Si-rich) and class C (Ca-rich) (ASTM C618) or type V (Si-rich) and type W (Ca-rich) (EN 197-1) for the use in

cement and concrete. The higher the amount of CaO, the higher the ability of the fly ash to participate in the hydration, assumed a sufficient high degree of reactivity is reached.

2.1.3 Limestone

Limestone is a sedimentary rock primarily of calcium carbonate ($CaCO_3$) that belongs to the group of carbonate rocks which are composed of more than 50 wt.% carbonate minerals, generally the minerals calcite (pure $CaCO_3$) or dolomite (calcium-magnesium carbonate, $CaMg(CO_3)_2$) or both. Besides calcite limestone contains dolomite, clay minerals, quartz and traces of manganese, lead, cobalt, magnesium, barium, strontium, zinc and rare earth elements in the ppm range. Limestone is not only one of the main compounds in the raw meal that is processed to Portland cement clinker, it is also used to be mixed with the clinker in blended cements [Hawkins et al., 2003]. As its composition may vary it has to fulfill several requirements in order to be suitable for cement production. According to EN 197-1 the $CaCO_3$ calculated from the CaO content must at least be 75 wt.% while the clay content[4] is not allowed to exceed 1.2 g/100 g. In addition the total content of organic carbon (TOC) classifies the limestone into type LL (TOC $\leq$ 0.2 wt.%) and type L (TOC $\leq$ 0.5 wt.%).[5]

2.2 Factors affecting the early hydration of SCM-blended cements

SCM affect the reaction of Portland cement in different ways by acting as inert addition and due to their chemical reaction, depending on the type of SCM and the stage of hydration. Initially where no or little reaction of the SCM occurs, these materials influence the hydration of the PC mainly by the so-called "filler effect" [Gutteridge and Dalziel, 1990a, Gutteridge and Dalziel, 1990b] which actually consists of two aspects:

(i) The presence of additional and different surface sites on the SCM can accelerate the hydration during the first hours as more surface for nucleation and growth of hydrates is present [Sharma and Pandey, 1999, Thomas et al., 2009, Kadri et al., 2009]. This effect has been observed to be most distinct for limestone but is also generally observed if PC is blended with quartz or blast-furnace slag. For fly ash both, retardation and acceleration have been reported.

(ii) The effective water-to-cement ratio (w/c) is increased in such blends as initially little SCM reacts. This additional water promotes the amount of Portland cement reacted after 1 d and longer as more water [Danielson, 1960, Yan et al., 2003, Justs et al., 2014] and more space [Baert et al., 2008, Bentz, 2006, Lam et al., 2000] for the growth of hydrates is available.

Recent investigations showed that the number of C-S-H nuclei on the limestone particles is significantly higher than on quartz and blast-furnace slag [Berodier and Scrivener, 2014]. While the underlying processes that cause this effect remain unclear, the effect itself explains the accelerating effect of limestone in blended cement [Poppe and De Schutter, 2005]. In the case of fly ash a different behavior can be observed. Blending Portland

[4] The test procedure for the content of clay using the methylene blue test is specified in EN 933-9.
[5] The determination of TOC is described in EN 13 639.

cement with fly ash can lead to retardation of the hydration, especially if a very fine fly ash is used at constant cement replacement level and constant w/s [Dittrich et al., 2014]. It has been argued that this effect is caused by interactions of alumina from the fly ash and calcium from the pore solution or by chemisorption of calcium ions on the surface of the fly ash [Fajun et al., 1985, Ogawa et al., 1980, Dittrich et al., 2014].

In contrast to the early promotion of PC reaction in the presence of SCM due to the presence of additional nucleation sites, the use of a higher water-to-cement ratio generally retards the early hydration of alite and PC in general [Yan et al., 2003, Justs et al., 2014, Gruyaert et al., 2010, Kirby and Biernacki, 2012]. A possible explanation could be the higher calcium concentrations due to lower pH values in a diluted system and the absence of additional nucleation sites.

Factors affecting the alite hydration

Investigations on laboratory synthesized C_3S and C_2S carried out at high water-to-binder ratios showed that higher CaO-concentrations in solution decrease the dissolution rates of C_3S and C_2S significantly [Nicoleau et al., 2013, Garrault and Nonat, 2001, Garrault-Gauffinet and Nonat, 1999], while any factor decreasing calcium concentration, e.g. the precipitation of portlandite, accelerates the reaction of alite and belite. Similarly, the acceleration of the alite hydration at a low water-to-solid ratio of 0.35 in the presence of alkali hydroxides [Mota et al., 2015, Kumar et al., 2012, Sant et al., 2012] has been related to a decrease of the calcium concentrations at higher pH values [Kumar et al., 2012]. Based on that line of thought, an increase of the calcium concentrations in the pore solution would retard the alite reaction. Thus, any increase of the water-to-cement ratio would be expected to retard the alite reaction as more water lowers the alkali hydroxide concentrations and the pH in the pore solution which results due to the common ion effect in higher calcium concentrations.

Alite dissolution is fast at higher undersaturation and slow at near equilibrium conditions [Nicoleau et al., 2013]. The effect of the degree of undersaturation on dissolution kinetics is strong if the solutions are moderately undersaturated, while at high degree of undersaturation the reactions are rather limited by the number of surface sites and changes in the degree of undersaturation have little effect as discussed in detail in [Nicoleau et al., 2013, Nicoleau et al., 2014, Juilland et al., 2010]. Also the suppressing effect of calcium in solution discussed above can be rationalized in terms of undersaturation as shown in Nicoleau et al. [Nicoleau et al., 2013], as the solutions containing water only are much more undersaturated with respect to alite (thus dissolving faster) than C_3S [Nicoleau et al., 2013] in saturated lime solution, which reacts very slow. Investigations by Bullard et al. [Bullard et al., 2012] indicate that both, the interplay of undersaturation with respect to C_3S and oversaturation with respect to C-S-H determines the overall hydration kinetics of alite. The presence of more C-S-H nuclei leads to faster C-S-H growth as visible by lower oversaturation with respect to C-S-H [Bullard et al., 2012]. The lower calcium and silicon concentrations resulting from the faster C-S-H formation result in higher undersaturation with respect to C_3S and thus to a faster alite dissolution. This interplay between precipitation and dissolution reactions is the reason why nucleation processes can play such an important role for the reaction kinetics.

Aluminium has been observed to retard the reaction of alite [Nicoleau et al., 2014, Begarin et al., 2011, Matschei and Costoya, 2012], which has been related to a hindered growth of C-S-H due to a poisoning by aluminium [Begarin et al., 2011, Minard, 2003, Garrault et al., 2011] and/or to hindered dissolution of alite due to binding of aluminium on the alite surface sites [Nicoleau et al., 2014]. The retardation of the alite reaction

in blended cements containing fly ash could thus be related to the presence of more aluminium in the pore solution.

While the accelerating effect of limestone has been studied in binary cement blends at a low water-to-solid ratio of 0.4 using calorimetric and microscopic techniques, knowledge on the influence of aluminium and calcium results mainly from investigations of dissolution of laboratory synthesized clinker phases in diluted suspensions. As information on the behavior of concentrated systems, i.e. pastes at realistic water-to-solid ratios, is limited it needs to be investigated if the hydration of such systems is subject to the mechanisms that are prevailing in diluted systems or if other factors have to be considered as well.

2.3 Reactivity of SCM

As already mentioned before, blast-furnace slag from pig-iron production or fly ash from coal combustion are the most commonly used SCM in blended cements. While latent hydraulic blast-furnace slag can replace up to 95 wt.% of cement clinker (CEM III/C) the use of fly ash is limited to 35 wt.% (CEM II/B) by current European standards [EN197-1, 2011]. In case of fly ash the restricted replacement levels in blended cements are due to the limited strength development at early ages ($\leq$ 28 d) compared to neat cement [Deschner et al., 2012, De Weerdt et al., 2011c]. This phenomenon is caused by the slower reaction of SCM compared to neat cement. Therefore, and due to economic and environmental considerations on the use and consumption of SCM better knowledge on SCM reactivity is one key aspect towards optimized multi-component cements. This is also supported by further positive effects like similar late strength compared to neat cement and i.e. the suppression of deleterious alkali-silica reaction (ASR) in Si-rich fly ash containing concrete [Shafaatian et al., 2013, Venkatanarayanan and Rangaraju, 2013],

Different aspects like the particle size distribution (PSD), the amount of reactive phases and their chemical composition influence the kinetics of the SCM reaction. A frequently used approach to increase the reactivity is to lower the particle size, which provides a higher specific surface available for reaction and leads to higher early compressive strength [Kumar et al., 2008, Payá et al., 2000, Day and Shi, 1994]. However, grinding is energy and cost-intense which has to be considered if environmentally friendly cements are developed. Furthermore it has to be taken into account that SCM like blast-furnace slag and fly ash contain not only amorphous phase but also inert or very low reactive crystalline phases, such as quartz, mullite, merwinite and melilite or other reactive phases like C_2F, C_4AF, $C_2\overline{S}$, C_2S and others. Although glass is the main reactive phase, its content cannot directly be linked to hydraulicity [Pal et al., 2003]. The glass contains generally mainly SiO_2, Al_2O_3 and CaO, while other oxides such as MgO, Na_2O, Fe_2O_3, K_2O and TiO_2 are present in lower concentrations. The chemical composition of these glasses can be highly variable, not only between different types of SCM but also between different batches from one plant as conditions during the production and variations in the oven within a batch (coal, iron ore) are unpreventable. Strongly different populations of chemical composition in the amorphous phase of fly ashes have been reported [Durdziński et al., 2015, Chancey et al., 2010]. The incorporation of minor amounts of network-modifying oxides such as K_2O, Na_2O and MgO leads to glasses with very different reactivities. An illustration of chemical compositions that are typical for glasses in blast-furnace slag,

Si-rich fly ash ($CaO_{reactive}$ <10 wt.%) and Ca-rich fly ash ($CaO_{reactive}$ >10 wt.%)[6] is presented in Figure 2.2.

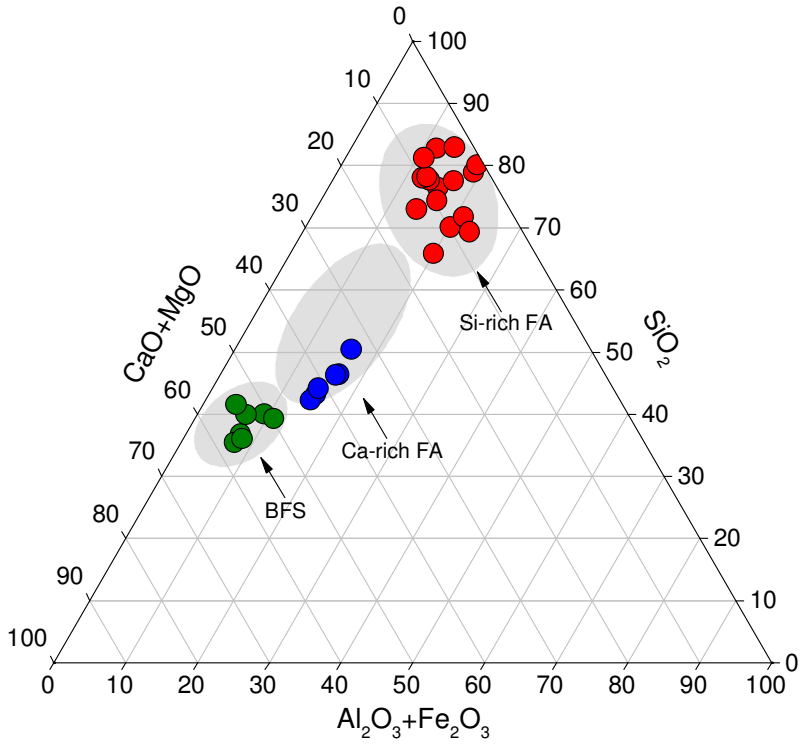

Figure 2.2: (CaO+MgO)-SiO_2-(Al_2O_3+Fe_2O_3) ternary system (in mol-%). Typical regions of glass compositions in Si-rich fly ashes [Valentim et al., 2009, Deschner et al., 2012, Schöler et al., 2015, Ward and French, 2006, Yan and Neretnieks, 1995, Bumrongjaroen et al., 2007], Ca-rich fly ashes [Tishmack et al., 1999] and blast-furnace slags [Ben Haha et al., 2011, Ben Haha et al., 2012, Kocaba, 2009, Escalante et al., 2001, Bougara et al., 2010, Schöler et al., 2015]. The compositions are either directly taken from the indicated literature or estimated from QXRD and XRF data.

Silica is generally the main constituent of the glasses present in blast-furnace slag and fly ash. In vitreous silica the minimum Si-O and O-O distances are consistent with the distances found in crystalline silicate minerals. While there is no long-range order present, the short-range order in vitreous silica is maintained due to the high degree of internal order of the silicon-oxygen tetrahedron [Shelby, 2005]. The inclusion of alkali metals and alkaline earth metals however decreases the degree of internal order. This process is directly linked to the degree of glass polymerization which can be described as ratio of network modifying oxides (NWM) to network forming oxides (NWF). The degree of polymerization significantly influences the reactivity of (calcium) aluminosilicate glasses [Chao et al., 2010]. Different approaches can be found to describe this relation. Typically hydraulic or basicity indices [Winnefeld et al., 2015, Ehrenberg et al., 2008] or, as common in glass science, the number of non-bridging oxygen atoms to oxygen atoms in tetragonal coordination (NBO/T) [Mysen et al., 1982, Mills et al., 2011] are used for this purpose. It is extremely difficult to gain data on the actual glass structure, especially on amphoteric oxides like Al_2O_3 and Fe_2O_3 which can act in both ways, as NWM or NWF, depending on

[6] Classification according to EN 197-1.

the overall glass composition. Consequently all these approaches can serve as estimates only. Detailed considerations on the informative value of different moduli describing the reactivity of blast-furnace slags with compressive strength and degree of reaction can be found in [Winnefeld et al., 2015].

Despite these difficulties it is generally agreed that a higher degree of depolymerization of the glass network leads to higher reactivity [Moesgaard et al., 2011, Duxson and Provis, 2008]. This is also reflected in the lower reactivity of Si-rich fly ash compared to Ca-rich fly ash and to blast-furnace slag as the content of NWM increases from the first to the latter. Investigations on the reactivity of industrially produced SCM in blended cements are very complex [Scrivener et al., 2015], due to the numerous variables. While identification and quantification of the crystalline phases and the amorphous content can be determined using quantitative X-ray diffraction techniques, investigations on the chemical composition of the amorphous phases are more difficult. An often used method is to subtract the crystalline phases and readily soluble compounds from the total chemical composition determined by X-ray fluorescence. However, the accuracy of this approach depends on the accuracy of the analytical data required and cannot account for different glass populations that might be present in the amorphous content of the SCM. In addition, the particle size distribution of fly ash and blast-furnace slag typically contains particles smaller than 1 µm. These "ultra fines" that can have different composition or amorphous content compared to larger particles, especially in the case of fly ash, exert significant influence on the reaction of the SCM themselves. Thus, the use of synthetic SCM glasses with well-defined compositions and particle size distributions is a possibility to pave the way towards better understanding of the chemical factors controlling SCM reactivity.

2.4 Hydration of composite cements containing SCM

The addition of low amounts of limestone (which mainly consists of $CaCO_3$) to Portland cement results in the formation of mono- and/or hemicarbonate instead of monosulfate after 1 d or longer [Lothenbach et al., 2008a, Zajac et al., 2014] when all calcium sulfates are depleted [Zajac et al., 2014]. Depending on the Al_2O_3/SO_3 ratio, just a small quantity of about 2 to 3 wt.% calcite takes actively part in a chemical reaction.

As far as hydrates present are concerned, the already mentioned formation of monocarbonate due to the addition of $CaCO_3$ prevents the destabilization of ettringite to monosulfate as monocarbonate ($C_4A\bar{C}H_{11}$) and ettringite ($C_6A\bar{S}_3H_{32}$) are more stable than monosulfate ($C_4A\bar{S}H_{12}$) and calcite ($C\bar{C}$) [Lothenbach et al., 2008a, Matschei et al., 2007b, Damidot and Glasser, 1992, Damidot et al., 1994]:

$$3C_4A\overline{S}H_{12} + 2C\overline{C} + 18H \rightarrow C_6A\overline{S}_3H_{32} + 2C_4A\overline{C}H_{11} \tag{2.2}$$

The stabilization of ettringite and monocarbonate in the presence of $CaCO_3$ increases the total volume of the solid phases [Lothenbach et al., 2008a, De Weerdt et al., 2011a], which has been shown to result in higher compressive strength in PC with low additions of limestone. The amounts of ettringite and monocarbonate formed in the hydrated system depends on the quantity of Al_2O_3 and SO_3 in the system as described in detail in [Matschei et al., 2007a]. However, not only the total amount of Al_2O_3 in the system,

but also the reaction degree of the aluminum containing phases (C_3A, C_4AF, SCM) is an important factor [De Weerdt et al., 2011a]. The amount and fineness of calcite plays a minor role [Zajac et al., 2014].

Similar effects have been observed for blends of PC with fly ash or blast-furnace slags [Carrasco et al., 2005, Menendez and Irassar, 2003, De Weerdt et al., 2011b, Moesgaard et al., 2011]. The presence of fly ash, which contains generally more Al_2O_3 than PC, leads to the formation of more AFt and AFm phases, such that the effect can be more pronounced. Investigations in PC-limestone and PC-fly ash-limestone cements have shown that this volume increase correlates strongly with the development of compressive strength and an increase in compressive strength has been observed up to 10 wt.% limestone [Carrasco et al., 2005, De Weerdt et al., 2011b, Moesgaard et al., 2011]. The contribution of Si-rich fly ash to the formation of AFt and AFm phases is limited due to its low reaction degree. It has been reported that after 1 year only 25 to 30 wt.% of the fly ash present in Portland cement blends has reacted [Ben Haha et al., 2010, De Weerdt et al., 2012, Deschner et al., 2013].

2.5 Summary and conclusions

The mechanisms controlling the hydration of the main clinker phases are well studied especially in pure systems, often at high dilutions. In contrast to that knowledge investigations on the early hydration of "real" concentrated systems are rare. Investigations in that regard are not only necessary to better understand the early reaction of Portland cements but also of blended systems containing SCM as these become more and more important in the curse of the reduction of CO_2 emissions. These blended systems are a promising method to contribute to lower the carbon footprint of cements. However, the used mineral additions like blast-furnace slag and especially fly ash show a slower reaction compared to Portland cement. This is mainly due to the reaction of the glass content of the used SCM that is the most important reactive part. It is well known from glass science that increasing amounts of network modifying oxides in the glass network leads to a more polymerized network and thereby to a higher reactivity. However, investigations of the reactivity of (calcium) aluminosilicate glasses are, if available, often carried out at low pH (<13) while the dissolution at high pH (>13) is of special interest for blended cements. Here especially the role of Al_2O_3 is of importance as this oxide can act in both ways, as network forming or as network modifying oxide. Knowledge derived from such investigations on synthetic glasses can contribute to better understand the reactivity of the amorphous content of blast-furnace slags and fly ashes such that corresponding SCM can be better applied in blended systems depending on the characteristics of the glass network present. All these before mentioned considerations are necessary to expand the number of available cement blends from ternary systems to quaternary systems that contain three SCM simultaneously besides Portland cement. Similar effects as in binary blends have been reported for ternary blends, e.g. the indirect stabilization of ettringite due to small amounts of limestone which leads to a higher total volume of hydrates and to a slight strength maximum at about 2 to 3 wt.% limestone. Quaternary systems might behave similar as SCM like blast-furnace slag and fly ash in principal lead to similar hydrate assemblages from a qualitative point of view as they show similarities in their chemical composition.

Chapter 3

Experimental

3.1 Materials

For investigations of multi-component cements two different batches of raw materials were used. The materials were chosen to show as little differences as possible in order to guarantee comparability of studies carried out with different batches. Table 3.1 allocates the different bathes to the corresponding studies and chapters within this thesis. In the following description of the raw materials the different batches are indicated by subscript numbers.

Table 3.1: Allocation of the different batches of raw materials to the corresponding investigations and chapters within the present thesis.

Investigations	Chapter	Batch
Early hydration studies	4	2
Synthetic glasses study	5	2
Kinetics of quaternary pastes	6	1
Hydrate assemblage of quaternary pastes	7	1
Pore solution chemistry of quaternary pastes	8	2

The cement used was a Portland cement CEM I 52.5 R designated as PC. Set regulators were bassanite and gypsum with shares of 3.2 wt.% and 1.2 wt.% (batch 1) or 1.0 wt.% and 3.1 wt.% (batch 2), respectively. Three SCM have been considered: blast-furnace slag, Si-rich fly ash (type V according to EN 197.1) and limestone with a calcite content of >99% (batch 1) or >95 wt.% (batch 2). The chemical and mineralogical compositions as well as the physical properties of the used materials are provided in Table 3.2 and Table 3.4 for batch 1 as well as in Table 3.3 and Table 3.5 for batch 2. The blast-furnace slag as well as the fly ash and the limestone were separately ground in a laboratory ball mill. The Portland cements and a quartz powder that serves as inert reference material were used as received. Figure 3.1 and Figure 3.2 show the PSD of the raw materials measured by laser diffraction with a Malvern Mastersizer using a 300 mm lens and isopropanol as dispersant. The overall PSD of the Portland cement, the blast-furnace slag and the fly ash do not differ significantly from each other while the limestone shows a distinct higher fraction of particles with a diameter larger than 10 µm. The grain size of the quartz was

chosen slightly shifted to larger particle sizes to avoid a pozzolanic reaction which might be possible at higher fineness.[7]

Table 3.2: Chemical composition[a] and physical properties of the used raw materials. n.d. = not detected.

	PC_1	BFS_1	FA_1	LS_1
SiO_2	19.86	41.25	56.77	2.35
Al_2O_3	4.64	7.57	26.03	0.78
TiO_2	0.26	0.30	1.37	0.04
MnO	0.10	0.71	0.03	0.01
Fe_2O_3	3.52	0.38	5.07	0.28
CaO	63.67	36.43	3.19	53.18
MgO	1.11	9.67	1.34	0.33
K_2O	0.63	0.62	2.53	0.18
Na_2O	0.14	0.37	0.31	n.d.
SO_3	2.89	1.51	0.06	n.d.
P_2O_5	0.14	0.02	0.40	0.02
L.O.I.[b]	2.13	0.62[h]	2.12	42.33
Total	99.09	98.83	99.22	99.50
CO_2[c]	0.70	0.00	0.16	42.20
C_{total}[d]	n.d.	n.d.	1.28	n.d.
$K_2O_{water\ soluble}$[e]	0.43	0.01	0.04	n.d.
$Na_2O_{water\ soluble}$[e]	0.06	0.01	0.03	n.d.
SA_{Blaine} [cm^2/g]	5180	4200	3360	4650
Density [g/cm^3][f]	3.13	2.91	2.22	2.72
d_{50} [µm][g]	10	14	10	16

[a] Determined by XRF analysis [wt.%].
[b] 950 °C (PC, BFS), 1050 °C (FA, LS).
[c] Calculated from TGA .
[d] C-content determined by combustion analysis. TOC = 1.22 [wt.%].
[e] Readily soluble alkalis calculated from the concentrations of alkalis measured in the solution after 5 min agitation at a w/s of 10.
[f] Determined with a Micromeritics AccuPycII 1340 helium pycnometer.
[g] The d_{50} is the size in microns that splits the distribution with half above and half below this diameter. Calculated from the PSD as presented in Figure 3.1.
[h] Gain on ignition due to oxidation of S^{2-}.

[7] Quartz: $d_{50} = 20\,\mu m$; Blaine $= 3520\,cm^2/g$; $\rho = 2.65\,g/cm^2$

Table 3.3: Chemical composition[a] and physical properties of the used raw materials.

	PC_2	BFS_2	FA_2	LS_2
SiO_2	19.61	39.26	56.68	2.28
Al_2O_3	4.90	8.40	23.33	0.98
TiO_2	0.26	0.29	1.12	0.05
MnO	0.20	0.59	0.03	0.02
Fe_2O_3	3.32	0.38	6.54	0.27
CaO	62.89	38.55	1.61	52.84
MgO	1.39	8.40	1.01	0.45
K_2O	0.58	0.58	2.01	0.22
Na_2O	0.15	0.41	0.45	0.00
SO_3	2.85	1.85	0.15	0.01
P_2O_5	0.18	0.02	0.22	0.03
L.O.I.[b]	1.69	0.34 [j]	2.25	42.41
Total	98.02	98.73	98.40	99.56
CO_2[c]	0.5	0.1	1.1	42.4
C_{total}[d]	n.d.	n.d.	1.41	n.d.
$K_2O_{water\ soluble}$[e]	0.42	0.03	0.03	$<$ 0.01
$Na_2O_{water\ soluble}$[e]	0.04	0.01	0.03	$<$ 0.01
$SO_{4\ water\ soluble}$[e]	1.20	0.22	0.63	$<$ 0.01
SA_{Blaine} [cm^2/g]	4870	3940	3080	n.d.
Density [g/cm^3][f]	3.13	2.90	2.33	2.77
d_{50} [µm][g]	9	14	12	17
d_{50} [µm][h]	10	14	13	18
SA [m^2/g][i]	3700	2700	3400	2600

[a] Determined by XRF analysis [wt.%].
[b] 950 °C (PC, BFS) 1050 °C (FA, LS).
[c] Calculated from TGA.
[d] C-content determined by combustion analysis. TOC = 1.27 [wt.%].
[e] Readily soluble alkalis calculated from the concentrations of alkalis measured in the solution after 5 min agitation at a w/s of 10.
[f] Determined with a Micromeritics AccuPycII 1340 helium pycnometer.
[g] The d_{50} is the size in microns that splits the distribution with half above and half below this diameter. Calculated from the PSD as presented in Figure 3.2.
[h] Calculated from the PSD measured with a 100 mm lens as used in the early hydration study discussed in Chapter 4 (cf. Appendix 3).
[i] Surface area (SA) calculated form PSD (measured with a 100 mm lens) and density.
[j] Gain of ignition due to oxidation of S^{2-}.

Table 3.4: Mineralogical composition of the used raw materials determined by XRD Rietveld [wt.%].[a]

	PC_1		BFS_1	FA_1	LS_1
C_3S	62.9	Mullite	-	19.2	-
$\alpha'C_2S$	5.5	Free lime	-	0.2	-
βC_2S	3.2	Maghemite	-	0.9	-
C_3A_{cubic}	1.4	Quartz	0.2	10.2	0.5
$C_3A_{othorh.}$	4.2	Calcite	0.4	0.4	99.1
C_4AF	12.4	Anhydrite	-	0.4	-
Calcite	1.5	Akermanite	0.2	-	-
Arcanite	0.7	Merwinite	0.4	-	-
Periclase	0.2	Gypsum	0.3	-	-
Portlandite[b]	1.7	Illite	-	-	0.4
Bassanite	3.2	Amorphous	98.5	68.8	-
Gypsum	1.2				
Syngenite[c]	1.4				
Quartz	0.2				
Total	100.0		100.0	100.0	100.0

[a] The uncertainties are in the range of 4.1 to 6.5% for C_3S, 2.8 to 5.5% for C_2S, 0.9 to 2.5% for C_3A, 1.3 to 2.4% for C_4AF, 1.0 to 1.6% for gypsum and 1.5 to 3.8% for calcite as investigated by round robin tests [Leon-Reina et al., 2009].
[b] Free lime in PC = 1.65, detected according to [Franke, 1941].
[c] Syngenite originates from slight prehydration of the cement due to the presence of calcium and alkali sulfates.

Table 3.5: Mineralogical composition of the used raw materials determined by XRD Rietveld [wt.%].[a]

	PC_2		BFS_2	FA_2	LS_2
C_3S	68.2	Calcite	1.7	0.9	95.6
$\alpha'C_2S$	3.0	Gypsum	0.8	-	-
βC_2S	4.1	Hematite	-	0.6	-
C_3A_{cubic}	2.0	Maghemite	-	0.8	-
$C_3A_{othorh.}$	3.1	Mayenite	0.2	-	-
C_4AF	11.4	Merwinite	0.7	-	-
Arcanite	0.8	Mullite	-	11.4	-
Bassanite	1.0	Others	2.3	-	3.5
Calcite	1.3	Quartz	0.2	14.3	0.9
Portlandite[b]	0.8	Amorphous	94.1	72.0	-
Gypsum	3.1				
Periclase	0.6				
Total	100.0		100.0	100.1	100.0

[a] The Uncertainties are in the range of 4.1-6.5% for C_3S, 2.8-5.5% for C_2S, 0.9-2.5% for C_3A, 1.3-2.4% for C_4AF, 1.0-1.6% for gypsum and 1.5-3.8% for calcite as investigated by round robin tests [Leon-Reina et al., 2009].
[b] Free lime in PC = 0.6, detected according to [Franke, 1941].

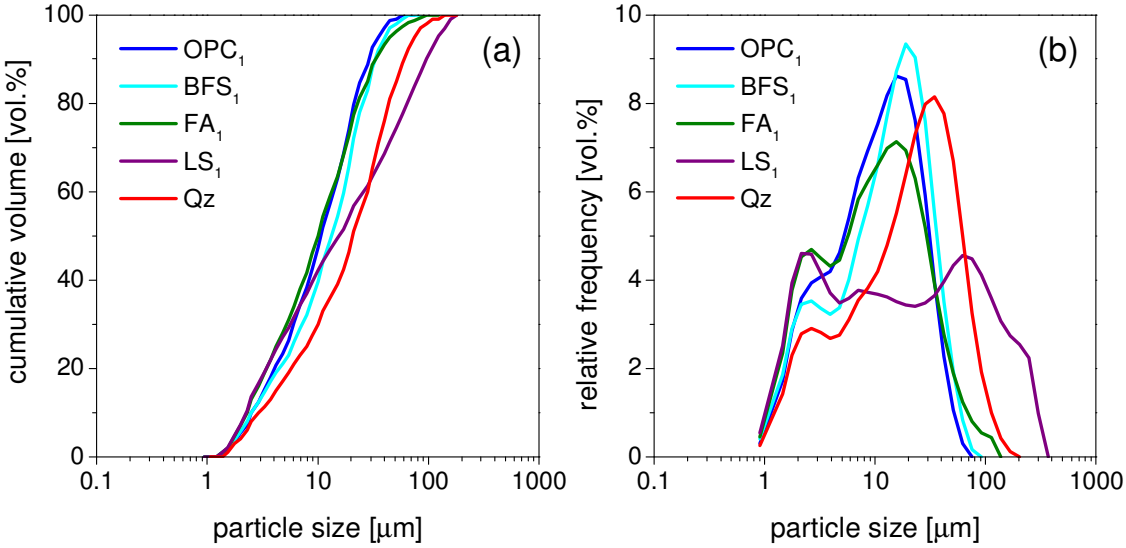

Figure 3.1: Particle size distribution for batches 1 depicted as (a) cumulative volume and (b) relative frequency determined by means of laser diffraction.

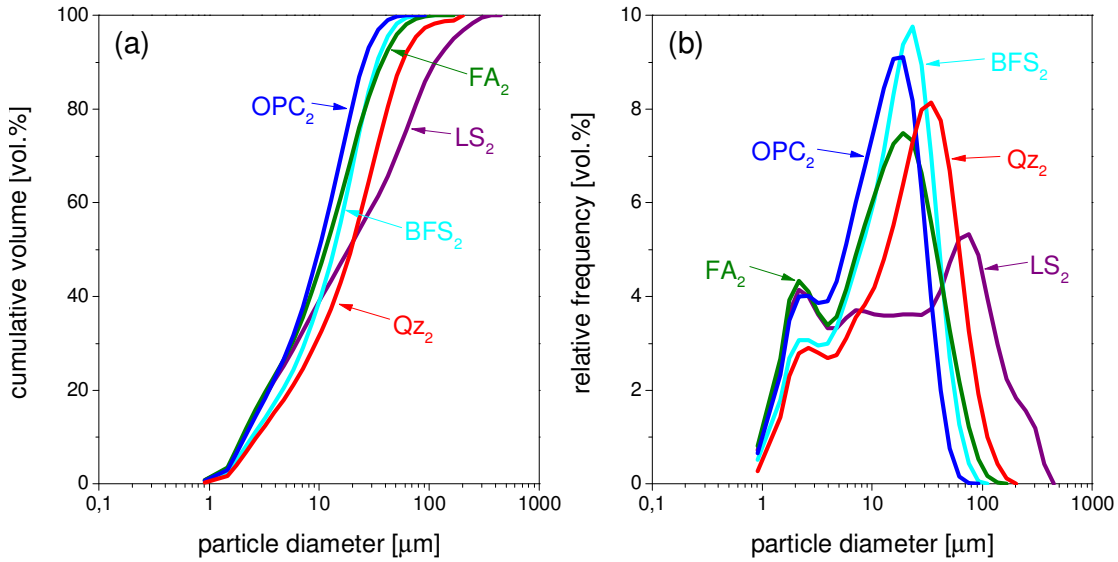

Figure 3.2: Particle size distribution for batches 2 depicted as (a) cumulative volume and (b) relative frequency determined by means of laser diffraction.

Blast-furnace slag and fly ash both consist of amorphous and crystalline compounds. The average amorphous content can be determined and quantified by QXRD. However, no information on the chemical composition of the amorphous content, which is needed as input parameter for accurate thermodynamic calculations, can be derived by QXRD. Thus, the average composition of the amorphous content of the blast-furnace slag and the fly ash was calculated by subtracting the readily soluble alkalis and the fraction of crystalline phases from the total XRF composition and normalizing the results to 100 wt.% (Table 3.6). Due to the low crystalline content of the blast-furnace slag, the composition of the amorphous content differs only slightly from the total composition. The amorphous content of the fly ash shows clear differences to the total composition, especially in the SiO_2 and Al_2O_3 content. This is mainly due to the presence of significant amounts of mullite and quartz.

Table 3.6: Average glass composition of blast-furnace slag and fly ash [wt.%]. Values are estimated by subtracting the water soluble alkalis and the fraction of crystalline phases from the total XRF composition.

	SiO_2	Al_2O_3	Fe_2O_3	CaO	MgO	K_2O	Na_2O	TiO_2	P_2O_5	Si/Al
BFS_1	42.7	7.9	0.4	37.5	10.0	0.6	0.4	0.3	0.0	5.4
BFS_2	41.7	9.0	0.3	38.5	9.1	0.6	0.4	0.3	0.0	4.6
FA_1	62.2	18.5	6.3	3.9	2.0	3.8	0.5	2.1	0.6	3.4
FA_2	62.6	22.5	7.6	1.6	0.0	2.9	0.6	1.7	0.3	2.8

3.2 Mix design

3.2.1 Early hydration study

The mix designs of the investigated systems are given in Table 3.7. The cement replacement level of the blended systems is always 50 wt.%. While the total SO_3 content of the neat cement is 2.8 wt.% the blended systems contain 1.4 wt.%. Additionally, the fly ash and blast-furnace slag containing systems were also adjusted to 2.8 wt.% total SO_3 using anhydrite. The sulfur incorporated in the amorphous phases of the fly ash and the blast-furnace slag were not taken into account; only SO_3 originating from PC and from the gypsum impurities in the blast-furnace slag (SO_3 = 0.37 wt.%) were considered.

Table 3.7: Mix design and surface area of the investigated blended systems. C -Portland cement, S - blast-furnace slag, FA - fly ash , L - limestone, Q - quartz.

Notation[a]	PC_2 [wt.%]	BFS_2 [wt.%]	FA_2 [wt.%]	LS_2 [wt.%]	Qz [wt.%]	Total [wt.%]	w/s	SA[b] [cm^2/g PC]
C[c]	100	-	-	-	-	100	0.75	3700
C-S	50	50	-	-	-	100	0.75	6400
C-S-$[d]	50	50	-	-	-	100	0.75	6400
C-FA	50	-	50	-	-	100	0.75	7100
C-FA-$[d]	50	-	50	-	-	100	0.75	7100
C-FA-L	50	-	30	20	-	100	0.75	6780
C-L	50	-	-	50	-	100	0.75	6300
C-Q	50	-	-	-	50	100	0.75	5700

[a] C - Portland cement, S - blast-furnace slag, FA - Si-rich fly ash, L - limestone, Q - quartz.
[b] Surface areas of dry mixtures calculated from surface areas of raw materials as given in Table 3.3.
[c] Neat PC is also investigated at water-to-solid ratios of 0.5, 1.0 and 1.5 by isothermal calorimetry.
[d] These systems were also investigated with an increased SO_3 content of 2.6 wt.%.

3.2.2 Synthetic glasses study

Investigations of synthetic glasses were carried out in diluted systems as well as pastes for model systems and glass-blended cement. The corresponding mix designs are presented in Table 3.8.

Table 3.8: Mix design of samples for dissolution experiments, model systems and blended cements.

	unit	glass dissolution	model system	blended cement
PC_2	[g]	-	-	50.0
synthetic glass	[g]	0.1	55.7	50.0
$Ca(OH)_2$	[g]	-	38.8	-
$CaCO_3$	[g]	-	5.5	-
$\sum$ solids	[wt.%]	100.0	100.0	100.0
0.3 M KOH solution	[g]	100.0	-	-
deionized H_2O	[g]	-	1.0	50.0
water/solid	[g/g]	1000.0	1.0	0.5

3.2.3 Kinetics and hydrate assemblage studies of quaternary pastes

Table 3.9 summarizes the compositions of the investigated quaternary cements.[8] The cement substitution level is always 50 wt.%, while the SO_3 level of all systems is ad-

[8] For the adjustment of the total SO_3 content SO_3 originating from the PC was taken into account while SO_3 originating from all other materials was neglected due to its low content. The limestone as contained in the PC was considered in the adjustment of the limestone as well. Consequently the actual compositions slightly differ from the ones as presented in Table 3.9. The simplified compositions were chosen to keep easy readability. All calculations are carried out using the defacto compositions as presented in Appendix 1.

justed with anhydrite to 3 wt.%. Two blast-furnace slag levels of 20 and 30 wt.% were investigated. At both of these levels fly ash is gradually replaced by limestone in steps of 5 wt.% up to a limestone content of 20 wt.%.

Table 3.9: Composition of the investigated composite cements. Data in [wt.%].

System	PC_1	BFS_1	FA_1	LS_1	Qz
0-0-0-50	50.0	-	-	-	50.0
20-0-0-30	50.0	-	-	-	30.0
30-0-0-20	50.0	-	-	-	20.0
20-30-0-0	50.0	20.0	30.0	-	-
20-25-5-0	50.0	20.0	25.0	5.0	-
20-20-5-0	50.0	20.0	25.0	5.0	-
20-15-15-0	50.0	20.0	15.0	15.0	-
20-10-20-0	50.0	20.0	10.0	20.0	-
30-20-0-0	50.0	30.0	20.0	-	-
30-15-5-0	50.0	30.0	15.0	5.0	-
30-10-10-0	50.0	30.0	10.0	10.0	-
30-5-15-0	50.0	30.0	5.0	15.0	-
30-0-20-0	50.0	30.0	-	20.0	-

3.2.4 Pore solution analysis of quaternary pastes

The mix design of the investigated systems is given in Table 3.10.[8] The cement replacement level of the blended systems is always 50 wt.% while the total SO_3 content was adjusted to 3.0 wt.% using anhydrite.

Table 3.10: Composition of the investigated composite cements. Data in [wt.%].

System	PC_2	BFS_2	FA_2	LS_2	Qz
20-0-0-30	50.0	-	-	-	30.0
20-30-0-0	50.0	20.0	30.0	-	-
20-25-5-0	50.0	20.0	25.0	5.0	-
20-15-15-0	50.0	20.0	15.0	15.0	-
20-10-20-0	50.0	20.0	10.0	20.0	-
30-15-5-0	50.0	30.0	15.0	5.0	-
30-5-15-0	50.0	30.0	5.0	15.0	-
30-0-20-0	50.0	30.0	-	20.0	-

3.3 Methods

3.3.1 Sample preparation

Dry mixtures were homogenized from the raw materials by mixing batches of 1700 g of the dry powder for 2 h in a Turbula blender (Willy A. Bachofen AG, Switzerland) using

2000 ml wide neck bottles equipped with two alumina ceramic mixing balls of 30 mm diameter.

3.3.1.1 Early hydration

Paste samples investigates in Chapter 6 and Chapter 7 were prepared from 200 g of dry material with water-to-solid ratio of 0.45 using a Twister Evolution vacuum mixer from Renfert. The pastes were mixed for 2 min at 300 rpm and filled in 60 ml PE vessels. The samples were capped, sealed with parafilm and stored at 20 °C in 60 ml for thermogravimetric analysis (TGA) and XRD studies[9].

Pastes as investigated in Chapter 8 were prepared from one batch of 1700 g dry mixture using a Type 1551 mixer from Toni Technik, Berlin. After addition of water according to a water-to-solid ratio of 0.5 mixing was done for 60 s at stage 1 followed by hand-mixing for 30 s and 90 s final mixing at stage 2. The paste amples for pore solution were cast in 500 ml polyethylene (PE) bottles, caped, sealed and stored at 90 % relative humidity at 20 °C. Except for the increased water-to-solid ratio of 0.75 this procedure also applies for the pore solution samples prepared for investigations of the early hydration as discussed in Chapter 4.

3.3.1.2 Glass dissolution samples

For dissolution experiments mixtures of 0.1 g glass powder and 100 g 0.3 M KOH-solution were prepared using a high liquid-to-solid ratio of 1000 in order to prevent the precipitation of hydration products as far as possible. The ratio of the surface area of the glass powder to the volume of KOH-solution (SA/V) ranges from 0.30 cm^2/cm^3 to 0.39 cm^2/cm^3 (Table 3.14). The samples were prepared in 100 ml PE-vessels that were sealed and stored at 20 °C on a shaking platform at a speed of 100 rpm until analysis. At corresponding sample ages (0.5 h, 1 h, 2 h, 4 h, 8 h, 16 h, 24 h, 48 h and 168 h) 15 ml of the solution was collected in a syringe and filtered through a 0.45 µm nylon filter in order to remove possibly remaining glass particles. Each sample was diluted by a factor of 1, 5, 10, 100 and 1000 using Milli-Q water[10] and subsequently analyzed by ion chromatography. In addition about 4 ml of undiluted solution was used for measurement of pH.

3.3.1.3 Pozzolanity tests in model systems and glass-blended Portland cements

The glass pozzolanity was investigated in simplified model systems and in PC-glass blends. The mix designs of the used model systems is presented in Table 3.8. Portlandite was used to serve as calcium reservoir for the formation of C-S-H. In order to allow the formation of monocarbonate in agreement with the conditions present in PC after 1 d of hydration, the samples were prepared with a small amount of calcite [Deschner et al., 2011]. Blended cements were prepared using a cement replacement of 50 wt.%. 1.3 g of dry mixture was mixed with 1.3 g of 0.3 M KOH solution (model systems) or 0.65 g of deionized water (blended cements) and mixed by hand for 2 min in a 60 ml PE vessel. The vessels were capped, sealed and stored at 20 °C and 90 % RH until investigation. The mix design and analytical data of the used PC are presented in Table 3.8, Table 3.3 and Table 3.5.

[9] In addition samples for XRD and TGA were prepared with a water-to-solid ratio of 0.5. these samples were used for long term investigations of up to 728 d of hydration. TGA and XRD data as presented in Appendix 6 and Appendix 7 result from these samples.

3.3.2 Isothermal calorimetry

Isothermal calorimetry experiments were carried out at 20 °C with an eight channel TAM Air Isothermal Calorimeter from TA Instruments, U.S.A. The samples were mixed ex-situ which is characterized by the loss of the initial peak but allows a better control of the quality of the mixing [Costoya Fernandez, 2008]. All investigated pastes were prepared according to the mix designs as presented in 3.2. Mixing of solid and liquid was done in glass ampoules of known weight and by use of an electric stirrer for 1 min at 550 rpm. The heat flow of two separate runs for each system was recorded for 24 h in the early hydration study and for 168 h in all other experiments. By integration of the recorded heat flow the total heat of hydration was calculated. Exclusion of the first 30 min (60 min in case of the model systems investigated in the synthetic glasses study) from this calculation allowed to start from a point when the calorimeter has reached equilibrium again after inserting the vials.

3.3.3 Chemical shrinkage

Chemical shrinkage experiments were carried out at 20 °C according to procedure A described in ASTM standard C-1680-07 [ASTM, 2007]. Data was collected up to 28 d of hydration.

3.3.4 Strength tests on mortar bars

Compressive strength of mortar prisms was determined according to EN 196-1.

3.3.5 Thermogravimetric analysis

For TGA, paste samples were gently crushed with a mortar and pestle in case of hardened samples. To stop the hydration the resulting material was immersed in isopropanol for 15 min and afterwards filtrated using a Büchner funnel and an aspirator pump followed by washing the filtrate with diethylether in order to remove all remaining isopropanol. Drying of the filter cake in a compartment dryer at 40 °C for 8 min assured the elimination of remaining diethylether. The analysis was carried out directly afterwards on approximately 50 mg of the resulting powder using a Mettler Toledo TGA/SDTA851e by monitoring the weight while heating up from 30 to 980 °C at a heating rate of 20 K/min under nitrogen atmosphere (flow rate 30 ml/min). The detected weight loss was corrected for weight loss of a blank pan measured prior to each series of experiments.

The corresponding changes in bound water and portlandite were calculated as percentage of the dry sample weight at 550 °C according to

$$BW = \frac{m_{total} - m_{dry\ solids}}{m_{dry\ solids}} \cdot 100[\%], \tag{3.1}$$

and

$$CH = \frac{m_{H_2O\ CH}}{m_{dry\ solids}} \cdot \frac{M(Ca(OH)_2)}{M(H_2O)} \cdot 100[\%] = \frac{m_{H_2O\ CH}}{m_{dry\ solids}} \cdot \frac{74}{18} \cdot 100[\%], \tag{3.2}$$

with m_{total} = total mass of "wet" paste, $m_{dry\ solids}$ = mass of dry paste corresponding to sample weight at 550 °C, $m_{H_2O\ CH}$ = weight loss due to dehydroxylation of portlandite obtained by the tangent method, $M_{(Ca(OH)_2)}$ = molar mass of portlandite and $M_{(H_2O)}$ = molar mass of H_2O. For further in-depth considerations on thermogravimetric analysis of cementitious systems it is referred to [Lothenbach et al., 2015].

3.3.6 X-ray Diffraction

For XRD experiments, slices of approx. 3 mm thickness where immersed in isopropanol for 20 min followed by drying at 40 °C for 15 min. As immersion in isopropanol is known to affect hydrate phases [Kocaba, 2009] this procedure was kept as short as possible. All samples were placed in a PANalytical X'Pert Pro MPD diffractometer in a Θ-2Θ configuration with an incident beam monochromator and CuKα_1 radiation. The samples were scanned for 120 min between 5° and 75° with an X'Celerator detector. For the evaluation of the gained data in terms of phase identification the X'Pert High Score Plus program version 3.0e from PANalytical was used. Details on the used instrument settings are given in Table 3.11.

Table 3.11: XRD instrument settings.

Diffractometer	PANalytical X'Pert Pro MPD
Goniometer	Θ-2Θ, Radius 240 mm
Source	CuKa$_1$
Generator	40 mA, 45 kV
Sample	
Surface diameter	27 mm
Preparation	backloading
Incident optics	
Monochromator	Johansson (Ge(111))
Divergence slit	0.5°
Anti scatter slit	1.0°
Beam mask	15 mm
Receiving optics	
Detector	X'Celerator
Soller slit	0.04rad

3.3.7 Pore solution chemistry

3.3.7.1 Pore solution extraction

Pore solutions from not yet hardened paste samples were extracted using pressure filtration. The pastes were filled in a steel cylinder that was equipped with a sieve and a 0.45 µm nylon filter at the bottom. After closing the device with a capped screw an

overpressure was generated by compressed air and the pore solution was extracted. For extraction of the pore solution of hardened pastes the steel die method [Barneyback and Diamond, 1981] was applied at pressures of up to 2500 N/mm^2. After extraction the solutions were immediately filtered through a 45 µm nylon filter and further processed for analysis by means of ion chromatography, ICP-OES, pH measurements and sulphur speciation techniques.

3.3.7.2 Ion chromatography and pH measurements

The K, Na, Ca, Al, Si, Cl and sulphur concentrations were measured using a Dionex DP ICS-3000 ion chromatograph. Each sample was diluted by a factor of 1, 5, 10, 100 and 1000 by Milli-Q water[10]. Standards with 0.1 and 50 mg/l were used for all ions of interest to define the lower (l.d.l) and upper (u.d.l.) detection limit. The relative uncertainty is ±10%. The pH was measured on the neat pore solution with a Knick pH meter (pH Meter 766) equipped with a Knick SE100 electrode. The pH electrode was calibrated against KOH solutions of known concentrations (0.05, 0.1, 0.2, 0.5 and 1.0 mol/l) and the free OH^- concentrations were calculated. From the measured elemental concentrations in the pore solution and the corresponding activities, the saturation indices (SI) of the solid phases can be calculated. The SI with respect to the solids are given by $\log(IAP/K_{S0})$, where K_{S0} is the theoretical solubility product of the respective solid, while IAP is the ion activity product calculated from the measured concentrations. A saturation index near 0 indicates that the phase is at or near equilibrium with the solution. A positive saturation index indicates oversaturation and that the phase is present or should precipitate while a negative saturation index indicates undersaturation and that the phase is not present or should dissolve. As the use of SI can be misleading when comparing phases which dissociate into a different number of ions, effective SI were calculated by dividing the SI by the number of ions participating in the reactions to form the solids, as described in [Lothenbach et al., 2008b].

3.3.7.3 Sulphur speciation

Sulfur contained in blast-furnace slag is mainly present in reduced form (S^{2-}). In order to gain better knowledge on the reaction of the blast-furnace slag at early ages concentrations of SO_4^{2-} (sulphate), SO_3^{2-} (sulphite), $S_2O_3^{2-}$ (thiosulphate) and HS^- (sulphide) in the pore solution were investigated for selected samples up to 28 d and for the whole matrix at 91 d. The concentrations of SO_4^{2-}, SO_3^{2-} and $S_2O_3^{2-}$ were analyzed by ion chromatography (Metrohm Compact IC 761) after stabilization with formaldehyde solution. HS^- was stabilized with zinc acetate and measured by colorimetry. The total sulfur concentration was determined by ICP-OES. The adapted protocol as presented in Figure 3.3 is based on a procedure as described in [Gruskovnjak et al., 2006, Lothenbach et al., 2012].

[10] Milli-Q water refers to ultrapure water typically 18.2 mS cm at 25 °C

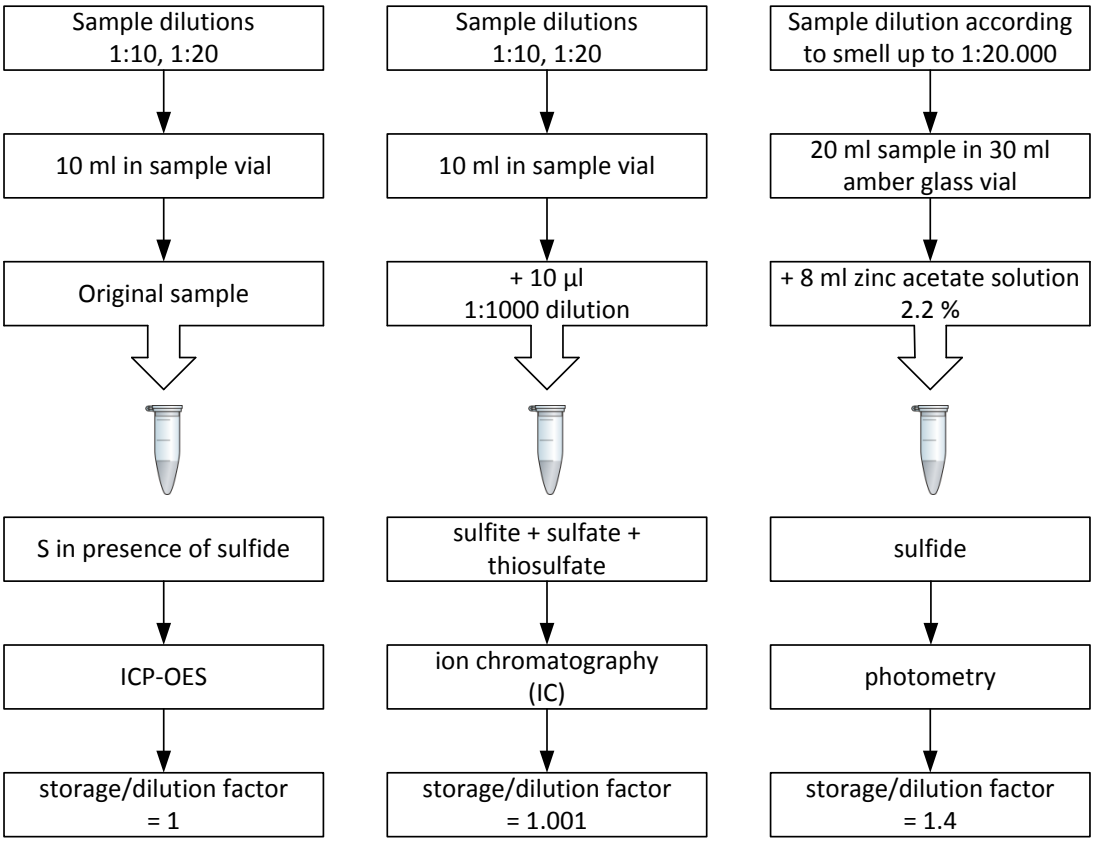

Figure 3.3: Sample preparation of cement pore solutions for sulfate speciation analysis.

3.3.7.4 Inductively coupled plasma atomic emission spectroscopy

The total concentrations of Al, Ca, K, Na, and Si as investigated in the early hydration study were determined using inductively coupled plasma optical emission spectroscopy (ICP-OES Varian Vista-Pro). Therefore 25 ml undiluted solution plus 5 ml HNO_3 were distributed to prevent any precipitation of solids.

3.3.8 Thermodynamic modeling

Thermodynamic modeling was carried out using the geochemical modeling program GEMS [Kulik et al., 2013] together with thermodynamic data from the PSI-GEMs database [Thoenen and Kulik, 2003, Hummel et al., 2002] supplemented by cement specific data [Lothenbach et al., 2008b, Matschei et al., 2007c]. The use of a solid solution model allows the description of varying C/S ratios in the C-S-H. The activities of the different species were calculated from the measured total concentrations at the respective temperatures using GEMs. The activity coefficients of aqueous species y_i were computed with the built-in expanded extended Debye-Hückel equation in Truesdell-Jones form with common parameter a_i of 3.67 for KOH solutions:

$$log\ y_i = \frac{-A_y z_i^2 \sqrt{I}}{1 + B_y a_i \sqrt{I}} + b_y I, \tag{3.3}$$

where z_i denotes the charge of species i, I the effective molal ionic strength, b_y is a semi-empirical parameter (~0.123 for KOH at 25 °C), and A_y and B_y are P, T-dependent coefficients. This activity correction is thought to be applicable up to approx. 1 M ionic strength [Helgeson et al., 1981]. Data on the density and the molar volume of phases considered in the thermodynamic calculations are given in Table 3.12.

3.3.8.1 Hydrate assemblage

Different long-term degrees of reaction were assumed to calculate the phase assemblage (Chapter 7). The used degrees of reaction are 100 wt.% for PC, 70 wt.% for the blast-furnace slag and 30 wt.% for the fly ash. The values for the SCM are based on investigations of blast-furnace slag and fly ash blended Portland cements after one year of hydration [Ben Haha et al., 2010, Deschner et al., 2013, Kocaba et al., 2012, Lothenbach et al., 2008b]. As the crystalline phases in both SCM are either considered to be non-reactive (e.g. quartz or mullite) or are only present in very low amounts, only the amorphous content was assumed to react. The XRD data indicate no significant reaction of the quartz and mullite present in fly ash up to 91 d of hydration. This in turn means that the before mentioned overall long term degrees of reaction have to be based on the amorphous part of the blast-furnace slag and the fly ash which leads to elevated values of 71.1 wt.% and 43.6 wt.%, respectively. For the calculation of C-S-H a solid solution of Ca-rich C-S-H ($C_{1.67}S_{1.0}H_{2.1}$) and Si-rich C-S-H ($C_{0.83}S_{1.0}H_{1.33}$) with varying C/S ratio has been implemented as described in detail in [Lothenbach et al., 2008b, Kulik, 2011]. The oxide composition as given in Table 3.6 was used as input for the equilibrium calculations which give the mass, the volume and the composition of the modeled systems as output.

Table 3.12: Density and molar volume of hydrates used in the thermodynamic calculations [Lothenbach et al., 2008b].

Mineral	Formula	Density [g/cm^3]	Molar volume [cm^3/mol]
Monosulfate	$Ca_4Al_2(SO)_4(OH)_{12}\cdot 6\,H_2O$	2.01	309
Hemicarbonate	$Ca_4Al_2(CO_3)_{0.5}(OH)_{13}\cdot 5.5\,H_2O$	1.98	285
Monocarbonate	$Ca_4Al_2(CO_3)(OH)_{12}\cdot 5\,H_2O$	2.17	262
Ettringite	$Ca_6Fe_2(SO_4)_3(OH)_{12}\cdot 26\,H_2O$	1.77	707
Portlandite	$Ca(OH)_2$	2.24	33
Si-rich C-S-H	$(CaO)_{0.83}(SiO_2)(H_2O)_{1.33}$	2.50	59
Ca-rich C-S-H	$(CaO)_{1.67}(SiO_2)(H_2O)_{2.1}$	2.67	78
Hydrotalcite	$Mg_4Al_2(OH)_{14}\cdot 3\,H_2O$	2.01	220
FH	$FeO(OH)$	2.61	34
Calcite	$CaCO_3$	2.71	37

3.3.8.2 Early hydration - thermodynamic framework

Based on the concentrations in the pore solutions saturation indices were calculated in order to display the degree of oversaturation/undersaturation of the pore solution with respect to C_3S, C-S-H and portlandite. In addition to the database expansion with respect to cement relevant phases data for C-S-H were used as described by [Kulik, 2011]. The saturation indices calculated relate to ettringite, portlandite, Ca-rich C-S-H and alite. Corresponding solubility products are given in Table 3.13. Note that a −0.5 log unit lower solubility product for C-S-H was used than suggested by [Kulik, 2011] to avoid apparent undersaturation as this C-S-H model tends to overestimate silicon concentrations as shown in [Lothenbach and Nonat, 2015]. In addition, saturation with respect to the "experimental" solubility product of alite ($C_3S_{exp.}$), i.e. of the protonated surface sites as suggested by Nicoleau et al. [Nicoleau et al., 2013] were calculated.

Table 3.13: Mineral phases and corresponding solubility products as used in the thermodynamic calculations.

Mineral	Reaction	log K_{S0}
ettringite	$Ca_6Al_2(SO_4)_3(OH)_{12}{\cdot}12\,H_2O \rightarrow$ $6\,Ca^{2+}+2\,Al(OH)_4^-+3\,SO_4^{2-}+4\,OH^-+26\,H_2O$	−44.9[a]
portlandite	$Ca(OH)_2 \rightarrow Ca^{2+}+2\,OH^-$	−5.2[b]
C-S-$H_{Ca\text{-}rich}$	$(CaO)_{1.5}(SiO_2)(H_2O)_{2.5}+H_2O \rightarrow 1.5\,Ca^{2+}+Si(OH)_4^0+3\,OH^-$	−17.2[c]
alite	$(CaO)_3SiO_2+5\,H_2O \rightarrow 3\,Ca_2^+ +Si(OH)_4^0+6\,OH^-$	−10.6[d]
$alite_{exp.}$	$(CaO)_3SiO_{2,\,surface}+5\,H_2O \rightarrow 3\,Ca_2^+ +Si(OH)_4^0+6\,OH^-$	−22.0[e]

[a] [Lothenbach et al., 2008b, Matschei et al., 2007c].
[b] [Hummel et al., 2002].
[c] [Kulik, 2011].
[d] Based on the Gibbs free energy of −2784.3 kJ/mol for C_3S given by Babushkin et al. [Babushkin, 1985].
[e] log K_{S0} according to [Nicoleau et al., 2013]. The $SiO(OH)_3^+$ and $CaSiO_2(OH)_2(aq)$ complexes present in the PSI thermodynamic data base [Hummel et al., 2002] were deactivated for these calculations to correspond to the Phreeqc thermodynamic data base [Parkhurst and Appelo, 2013] used by [Nicoleau et al., 2013].

To ease comparison with the data measured by [Nicoleau et al., 2013] in diluted systems also ion activity products for the dissolution of C_3S (Π_{C_3S}) were calculated: $\Pi_{C_3S} = \{Ca^{2+}\}^3\ \{Si(OH)_4^0\}\ \{OH^-\}^6/\{H_2O\}^5)$, where {} denotes activity of the respective species and the activity of water is near to 1. The activity of the different species $\{Ca^{2+}\}$, $\{Si(OH)_4^0\}$, $\{OH^-\}$ and $\{H_2O\}$ were calculated with GEMS from the measured concentrations as given in Appendix 2. As [Nicoleau et al., 2013] used the Phreeqc thermodynamic data base [Parkhurst and Appelo, 2013] the $SiO(OH)_3^+$ and $CaSiO_2(OH)_2(aq)$ complexes present in the PSI thermodynamic data base [Hummel et al., 2002] were deactivated for these calculations in order to enable comparability.

3.3.8.3 Estimation of glass reaction

The amount of bound water and of portlandite in the investigated model systems and the cement blends was calculated as a function of glass reacted. The input composition was corrected for the defacto content of $Ca(OH)_2$ and $CaCO_3$, both derived from TGA. The amount of predicted phases was normalized to dry sample weight (corresponding to TGA at 550 °C).

3.3.9 Preparation and characterization of synthetic glasses

All glasses as depicted in Figure 3.4 were synthesized from reagent-grade oxides (SiO_2, Al_2O_3, Fe_2O_3, TiO_2) and carbonates ($CaCO_3$, $MgCO_3$, K_2CO_3, Na_2CO_3). Appropriate amounts of precursors were weighed in to result in 110 g of decarbonated material. These mixtures were filled in 250 ml PE bottles along with 150 g of alumina mixing balls of 5 mm diameter and subsequently rotated on a low profile roller at 100 rpm overnight. Afterwards the mixtures were decarbonated in a platinum crucible at 900 °C for 1 h. Melting was carried out at 1500 °C. The furnace was first heated to the target temperature before the raw mixtures were inserted. After a dwell time of 2 h the molten glasses were quenched on air, coarsely crushed after cooling and stored in PE vessels in an evacuated desiccator until further processing. The degree of polymerization of the glass network of the synthetic glasses (expressed as NBO/T as given in Table 3.16) was calculated according to Eq. 3.4 adapted from Mills et al. [Mills et al., 2011]:

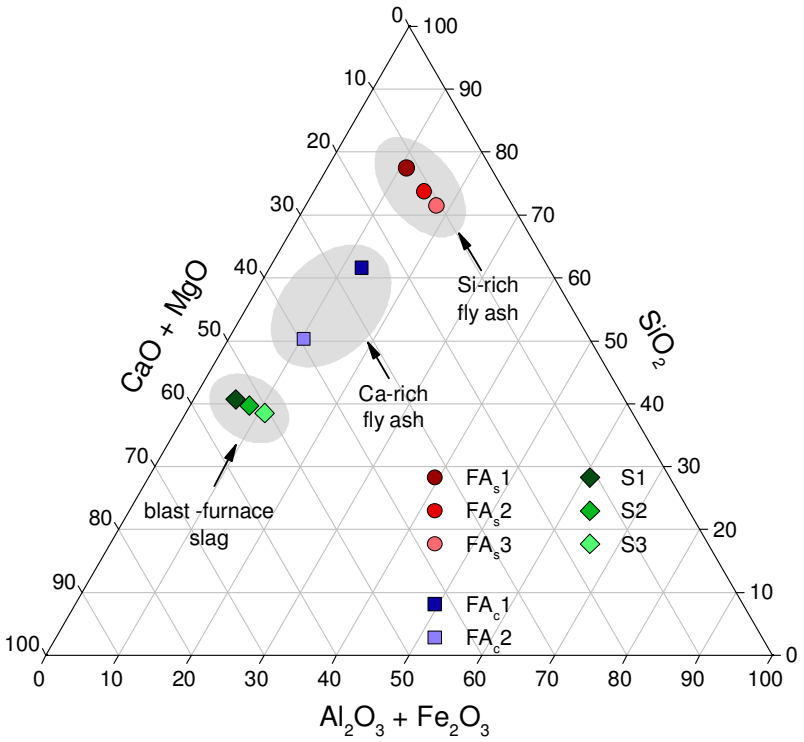

Figure 3.4: Glass compositions used in this study. Note that this depiction considers only the indicated components normalized to 100 mol-%. For the actual compositions of the synthesized glasses including minor compounds and alkalies see Table 3.16.

$$\frac{NBO}{T} = \frac{2(CaO + MgO + K_2O + Na_2O + 3fFe_2O_3 + 3fAl_2O_3 - (1-f)Fe_2O_3 - (1-f)Al_2O_3)}{SiO_2 + TiO_2 + 2(1-f)Fe_2O_3 + 2(1-f)Al_2O_3} \tag{3.4}$$

The variable f [11] describes the distribution of the amphoteric oxides Al_2O_3 and Fe_2O_3 between NWM and NWF. NBO/T values can be located in the range from 0 to 4 corresponding to a fully polymerized structure (NBO/T = 0) or a fully depolymerized structure (NBO/T = 4) consistent of isolated tetrahedra.

Fragments of each glass were embedded in low-viscosity bisphenol-A-epoxy-resin under vacuum and subsequently polished down to 0.1 µm using diamond pastes in order to check homogeneity of the glasses. Prior to the analysis the specimens were coated with a thin carbon layer in order to avoid charging effects. For SEM investigations a Philips ESEM FEG-XL30 microscope with an accelerating voltage of 15 kV and a spot size of 4 was used. For all glasses SEM images showed a uniform grey level throughout which reveals homogeneity.

In order to obtain a fine powder the glasses were ground dry in a planetary ball mill at 250 rpm. The grain size fraction between 30 µm and 63 µm was obtained by dry sieving. In order to remove remaining ultrafine particles smaller than 30 µm the sieved powders were ultrasonically washed in two cycles, first in ultrapure water and then in acetone. The solution was discarded and the remaining glass powder was dried at 110 °C for 10 min after each cycle. This procedure was applied twice. As inert reference material commercially available quartz powder (Millisil B12 from Sibelco) was sieved and washed as was done with the glasses. The particle size distributions were analyzed in Fraunhofer mode with a Malvern Mastersizer X using a 100 mm lens and isopropanol as dispersant. All glasses show similar values (Figure 3.5 and Table 3.14). The peak of the passing volume is located at about 75 µm. The PSD of the quartz is slightly shifted towards higher fineness.

In order to check if the glasses are amorphous, XRD analysis was carried out using a PANalytical X'PertPro MPD diffractometer in a Θ-2 Θ configuration with an incident beam monochromator and CuKα_1 radiation. The samples were scanned for 60 min between 5° and 70° with an X'Celerator detector. Data was evaluated with the X'Pert High Score Plus program version 3.0e from PANalytical. Figure 3.6a shows the gained X-ray patterns. The absence of reflections that would indicate long-range structural order indicates the amorphous character of the glasses. The amorphous humps of the Si-rich fly ash glasses and the slag glasses do not vary significantly amongst each other. The positions of the amorphous humps are shifted towards higher angles with increasing CaO content (Figure 3.6b) which is strongly linked to the ratio of network modifiers to network formers. This effect is dominated by the CaO content of the glasses [Diamond, 1983]. In addition the chemical compositions of the glasses were determined by X-ray fluorescence (XRF) in order to check if any variations are present compared to the target compositions as given in Table 3.16. Very good agreement was found between the

[11] A value of 0.92 was used for Al_2O_3 and Fe_2O_3 in the calculations as this was found to be the most reasonable approach. Thereby all relevant oxides are completely assigned to NWF by f = 0 or to NWM by f = 1. For detailed descriptions it is referred to 5.2.1. It should also be noted that different f values can be used for each amphoteric oxide. Due to the low amounts of Fe_2O_3 this does not significantly alter the results and was therefore not taken into account.

experimentally determined and the calculated compositions (Table 3.15).

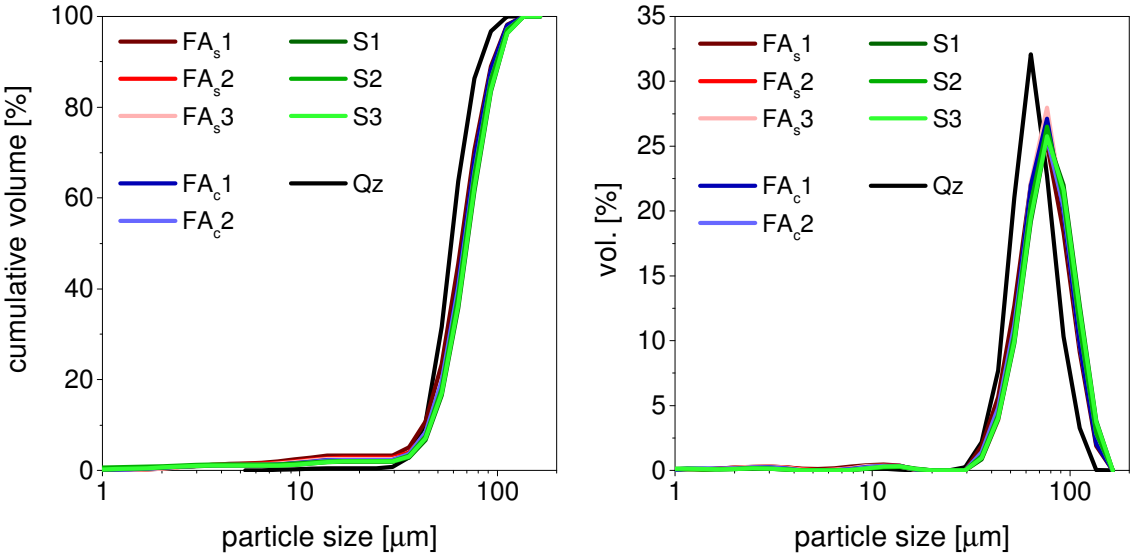

Figure 3.5: Particle size distribution determined by laser diffraction.

Table 3.14: Physical properties of the synthesized glasses.

	density[a] [g/cm^3]	d_{50}[b] [µm]	SA[c] [m^2/g]	SA/V [cm^2/cm^3]
FA$_s$1	2.45	71.7	0.039	0.39
FA$_s$2	2.48	75.1	0.036	0.36
FA$_s$3	2.46	74.3	0.036	0.36
FA$_c$1	2.63	75.2	0.034	0.34
FA$_c$2	2.78	76.6	0.032	0.32
S1	2.91	73.7	0.030	0.30
S2	2.89	77.1	0.029	0.29
S3	2.88	74.5	0.030	0.30
Qz	2.66	58.5	0.038	0.38

[a] Determined with a Micromeritics AccuPycII 1340 helium pycnometer.
[b] Calculated from laser diffraction analysis (Figure 3.5).
[c] Calculated from PSD and density.

The specific surface of the obtained glass powders was calculated from the particle size distribution and the density. The latter was determined with a Micromeritics AccuPycII 1340 Helium Pycnometer. The results are presented in Table 3.14.

Table 3.15: Actual oxide compositions of the synthesized glasses as measured by XRF analysis.[a] Data given in [wt.%].

	FA_s1		FA_s2		FA_s3		FA_c1	
	XRF	Δ^b	XRF	Δ^b	XRF	Δ^b	XRF	Δ^b
SiO_2	67.62	0.75	62.54	0.95	59.86	0.69	55.54	−0.24
Al_2O_3	16.41	−0.47	22.26	−0.64	25.53	−0.33	18.82	0.01
Fe_2O_3	0.71	−0.02	0.96	−0.03	1.14	−0.04	0.81	0.00
CaO	7.33	−0.12	6.93	−0.23	6.37	−0.10	16.11	0.10
MgO	1.55	0.16	1.46	0.12	1.36	0.13	3.40	0.44
K_2O	3.53	−0.01	3.21	0.05	3.14	−0.06	2.87	−0.07
Na_2O	1.74	0.02	1.62	0.01	1.61	−0.10	1.41	0.00
TiO_2	0.83	−0.03	0.84	−0.04	0.82	−0.02	0.81	−0.01
Total	99.72	0.27	99.82	0.19	99.83	0.17	99.77	0.22
	FA_c2		S1		S2		S3	
	XRF	Δ^b	XRF	Δ^b	XRF	Δ^b	XRF	Δ^b
SiO_2	46.54	0.46	39.85	0.44	38.11	0.46	36.25	0.45
Al_2O_3	16.31	−0.31	9.77	−0.37	13.38	−0.27	17.33	−0.27
Fe_2O_3	0.70	−0.01	0.42	−0.02	0.58	−0.02	0.74	−0.01
CaO	26.26	−0.41	37.80	−0.56	36.22	−0.60	34.43	−0.51
MgO	5.55	0.57	8.07	0.75	7.69	0.75	7.32	0.71
K_2O	2.34	0.02	2.00	0.02	1.96	−0.03	1.83	0.00
Na_2O	1.19	−0.01	1.03	−0.01	0.98	−0.01	0.94	−0.02
TiO_2	0.83	−0.03	0.82	−0.02	0.83	−0.03	0.82	−0.02
Total	99.72	0.28	99.76	0.26	99.75	0.26	99.66	0.33

[a] L.O.I. in total 0.12-0.24 wt.%, minor compounds (Cr_2O_3,MnO,P_2O_5,SO_3) in total 0.06-0.10 wt.%. Both parameters are neglected in the calculations, hence the total values slightly deceed 100 wt.%.

[a] Δ is calculated as difference of calculated composition (Table 3.16) and XRF data.

Table 3.16: Targeted compositions and oxide ratios of the synthesized glasses as well as calculated NBO/T.

glass type	Si-rich fly ash			Ca-rich fly ash		blast-furnace slag		
	FA_s1	FA_s2	FA_s3	FA_c1	FA_c2	S1	S2	S3
Oxide composition [wt.%]								
SiO_2	68.37	63.49	60.55	55.30	47.00	40.29	38.57	36.70
Al_2O_3	15.94	21.62	25.20	18.83	16.00	9.40	13.11	17.06
Fe_2O_3	0.69	0.93	1.10	0.81	0.69	0.40	0.56	0.73
CaO	7.21	6.70	6.27	16.21	25.85	37.24	35.62	33.92
MgO	1.71	1.58	1.49	3.84	6.12	8.82	8.44	8.03
K_2O	3.52	3.26	3.08	2.80	2.36	2.02	1.93	1.83
Na_2O	1.76	1.63	1.51	1.41	1.18	1.02	0.97	0.92
TiO_2	0.80	0.80	0.80	0.80	0.80	0.80	0.80	0.80
total	100.00	100.00	100.00	100.00	100.00	100.00	100.00	100.00
Oxide composition [mol-%]								
SiO_2	73.64	70.25	68.21	59.12	48.58	39.54	38.56	37.45
Al_2O_3	10.11	14.09	16.73	11.86	9.74	5.43	7.72	10.26
Fe_2O_3	0.28	0.39	0.47	0.33	0.27	0.15	0.21	0.28
CaO	8.32	7.94	7.57	18.56	28.62	39.15	38.16	37.08
MgO	2.74	2.61	2.50	6.12	9.44	12.91	12.57	12.21
K_2O	2.42	2.30	2.21	1.91	1.55	1.26	1.23	1.19
Na_2O	1.84	1.75	1.65	1.46	1.18	0.97	0.94	0.91
TiO_2	0.65	0.67	0.68	0.64	0.62	0.59	0.60	0.61
total	100.00	100.00	100.00	100.00	100.00	100.00	100.00	100.00
Oxide ratios [g/g]								
MgO/CaO	0.24	0.24	0.24	0.24	0.24	0.24	0.24	0.24
Al_2O_3/SiO_2	0.23	0.34	0.42	0.34	0.34	0.46	0.34	0.34
CaO/Al_2O_3	0.45	0.31	0.25	3.96	2.72	1.99	0.86	1.62
CaO/SiO_2	0.11	0.11	0.10	0.92	0.92	0.92	0.29	0.55
Na_2O/SiO_2	0.03	0.03	0.02	0.03	0.03	0.03	0.03	0.03
K_2O/SiO_2	0.05	0.05	0.05	0.05	0.05	0.05	0.05	0.05
Fe_2O_3/Al_2O_3	0.04	0.04	0.04	0.04	0.04	0.04	0.04	0.04
Oxide ratios [mol/mol]								
MgO/CaO	0.33	0.33	0.33	0.33	0.33	0.33	0.33	0.33
Al_2O_3/SiO_2	0.14	0.20	0.25	0.20	0.20	0.14	0.20	0.27
CaO/Al_2O_3	0.82	0.56	0.45	1.57	2.94	7.21	4.94	3.62
CaO/SiO_2	0.11	0.11	0.11	0.31	0.59	0.99	0.99	0.99
Na_2O/SiO_2	0.02	0.02	0.02	0.02	0.02	0.02	0.02	0.02
K_2O/SiO_2	0.03	0.03	0.03	0.03	0.03	0.03	0.03	0.03
Fe_2O_3/Al_2O_3	0.03	0.03	0.03	0.03	0.03	0.03	0.03	0.03
Degree of polymerization								
NBO/T	1.14	1.46	1.67	1.97	2.66	3.37	3.67	4.00

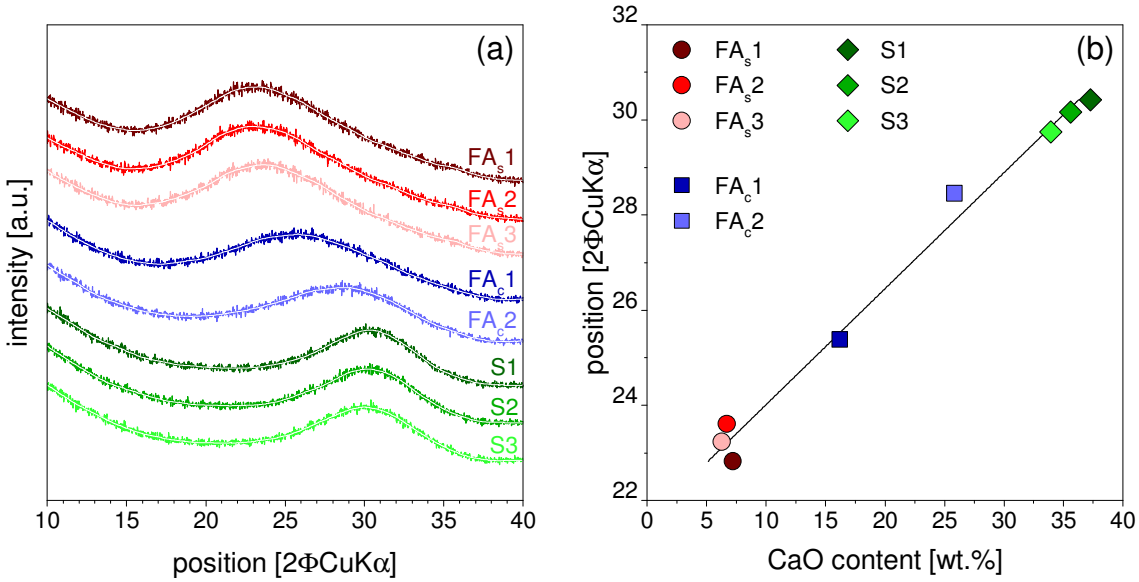

Figure 3.6: (a) X-ray powder diffraction patterns of the synthetic glasses showing a distinctive shift of the diffuse scattering maximum towards higher angles with increasing CaO content and (b) correlation of the maximum of the amorphous hump with the CaO-content in the synthetic glasses.

3.3.10 Degree of glass reaction

3.3.10.1 Diluted systems

The measured concentration of aluminium in the KOH-solution was used to follow the glass dissolution as congruent dissolution can be assumed for (calcium) aluminosilicate glasses [Snellings, 2013]. From the Al concentrations the amount of Al_2O_3 dissolved was calculated. Due to the assumption of a congruent dissolution the calculated amount of Al_2O_3 dissolved corresponds to the total amount of glass dissolved.

3.3.10.2 Pastes of model systems and blended cements

Correlation of the bound water content as obtained from TGA with the modeled total bound water content allows to directly estimate the amount of glass reacted at a given sample age. The pozzolanic reaction could also be traced by the portlandite development/consumption as has been shown in several studies [Deschner et al., 2012, De Weerdt et al., 2011a]. However, using portlandite for the determination of glass reacted depends on the composition of C-S-H. As the composition of C-S-H in presence of portlandite can vary over time and depending on the water to solid ratio [Rossen, 2014] as well as on the aluminum available for reaction ($C/S_{PC} < C/S_{PC/FA}$), the use of portlandite only can introduce a considerable error in the calculated degree of reaction. Consequently, total bound water normalized to dry sample weight at 550 °C was chosen as a sum parameter as it is expected to give the most accurate results possible.

In addition to the mass balance/TGA approach selective dissolution experiments were carried out after 91 d of hydration for both, pastes of the model systems and the blended cements. Therefore the EDTA/NaOH procedure as described by [Ben Haha et al., 2010] was used. In the cited study parts of the investigated SCM were found to dissolve in the dissolution test. To account for this the unhydrated raw materials were tested under

the same conditions as the hydrated pastes. Table 3.17 presents the residues of the raw materials. While almost all PC was dissolved the glasses were only slightly affected by the treatment with residues of $\geq$ 97.8 wt.% . Hereby a loss of 1 wt.% due to sample preparation and filtration is expected. The residues of the raw materials were used to correct the results of the hydrated pastes.

Table 3.17: Assessment of the EDTA/NaOH selective dissolution technique using raw unhydrated materials: Residues R_U as a % of the initial mass.

	PC	FA_s1	FA_s2	FA_s3	FA_c1	FA_c2	S1	S2	S3
R_U	0.5	99.6	99.6	97.8	99.7	99.1	98.2	99.1	98.8

[a] The amount of bound water is very low and might also originate from a water-film on the glass surface besides precipitated hydrates.

As suggested by [Lumley et al., 1996] and adapted by [Lothenbach et al., 2012] the amount of glass reacted in the selective dissolution tests was corrected for hydrotalcite as hydrotalcite is not dissolved by the EDTA/NaOH approach:

$$x_{ht} = 100 \cdot \frac{R_u - R_{HP}}{R_u \cdot (1 - h \cdot M)} \tag{3.5}$$

Where R_U and R_{HP} are the residues of the unhydrated and the hydrated systems, both corrected for bound water (sample weight at 550 °C during TGA). h = 2.35 (= mass of dried hydrotalcite in g) formed from 1 g of MgO in the glass and M = MgO content of the glass.

Chapter 4

Early hydration of SCM-blended cements: A pore solution and isothermal calorimetry study[12]

While the accelerating effect of limestone has been studied in binary cement blends at a water-to-solid ratio of 0.4 using calorimetric and microscopic techniques, knowledge on the influence of aluminium and calcium results mainly from investigations of dissolution of laboratory synthesized clinker phases in diluted suspensions. The complexity of the systems increases dramatically from pure phases and lab clinkers towards industrial available "real" materials and blends thereof at realistic water-to-binder ratios where the combination of both, dissolution and precipitation reaction determines the observed hydration kinetics. For an advanced understanding of the controlling factors within the first hours of hydration in SCM-blended cements it is necessary to detect if the mechanisms that are prevailing for pure clinker phases in diluted systems are present in realistic systems as well and to which extend these control the reaction of such complex systems.

In this chapter the hydration kinetics and the development of ion concentrations in the pore solution of binary cement pastes containing different supplementary cementitious materials (blast-furnace slag, Si-rich fly ash, limestone, quartz) at a cement replacement of 50 wt.% and a water-to-solid-ratio of 0.75 are discussed during the first 6 h of hydration. The pore solution chemistry was investigated using inductively coupled plasma optical emission spectroscopy. For investigations of the kinetic behavior of the investigated systems isothermal calorimetry experiments were applied.

4.1 Experimental

The present study was carried out with materials from batch 2 as described in 3.1. Detailed information on the pore solution extraction and analysis as well as on the isothermal calorimetry experiments and thermodynamic calculations are given in 3.3.

[12] An extended version of this chapter has been submitted as a manuscript to Cement and Concrete Research as: Early hydration of SCM-blended cements: A pore solution and isothermal calorimetry study, A. Schöler, B. Lothenbach, F. Winnefeld, M. Ben Haha, M. Zajac, H.-M. Ludwig

4.2 Results and discussion

4.2.1 Effect of SCM on specific heat flow

The influence of the water-to-cement ratio on the specific heat flow of Portland cement within the first 24 h of hydration is presented in Figure 4.1. While no significant change is observed until the minimum is reached for all systems at about 2 h a less strong increase of the heat flow rate during the acceleration period is visible with increasing water-to-cement ratio. The slope of the curves is clearly lower at higher water-to-cement ratios during the acceleration period and the onset is slightly shifted to later ages. In addition the second heat flow maximum is successively lower with increasing water-to-cement ratio. This behavior reveals a strong influence of the water content on the alite reaction as the heat released during the period of the highest heat flow can be attributed mainly to the alite reaction while the second aluminate reaction is visible as shoulder or peak after the main reaction [Jansen et al., 2011, Hesse et al., 2011]. After 1 d and longer, however, a higher heat flow is observed at higher water-to-cement ratios as more water is available. This leads to higher total released heat at later ages as has been shown e.g. by [Yan et al., 2003, Justs et al., 2014, Danielson, 1960].

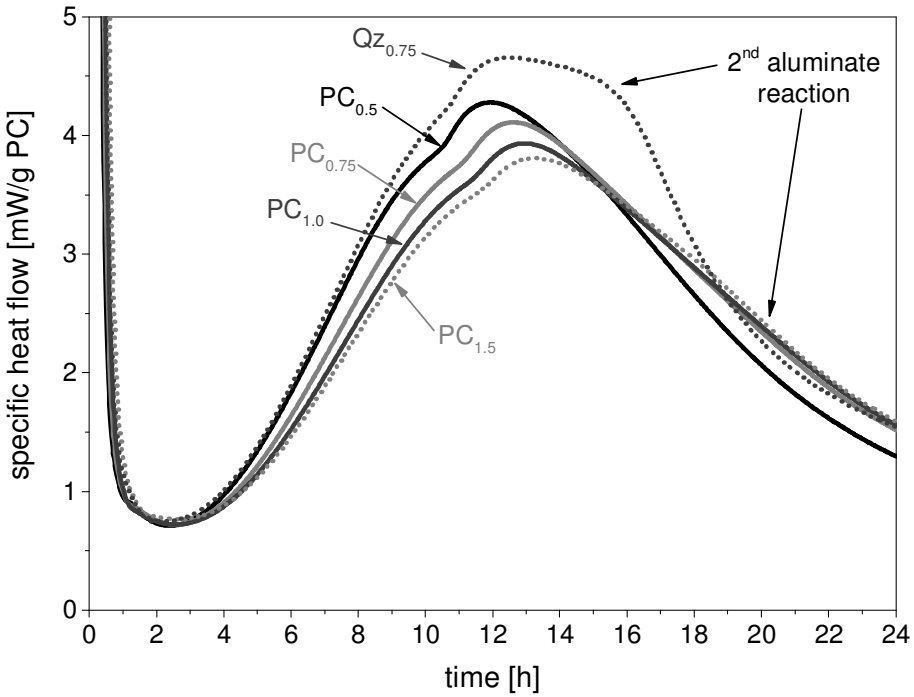

Figure 4.1: Specific heat flow within the first 24 h of hydration for neat PC at various water-to-cement ratios. The water-to-solid ratio of the Qz blend (50 wt.%) corresponds to an effective water-to-cement ratio of 1.5. Note that the subscript numbers represent the water-to-solid ratio. All curves are normalized to the mass of PC in the system.

While the water-to-cement ratios of the neat Portland cement systems are identical with the water to-solid ratios, the water-to-solid ratio of the quartz blend (0.75) reflects an effective water-to cement ratio of 1.5 as 50 wt.% of the cement is replaced by quartz. Despite this, the Portland cement in the quartz blend reacts considerably faster than $PC_{0.75}$ and $PC_{1.5}$ and its reaction is comparable to $PC_{0.5}$ during the acceleration period.

As the reaction of quartz is negligible, the acceleration of the alite reaction seems to be related to the presence of additional surfaces for the nucleation of C-S-H which increases from 3700 cm^3/g PC for neat Portland cement to 5700 cm^3/g PC for the quartz blend. This effect, which is also reflected in the higher heat maximum at about 2 h as well as in the more pronounced aluminate reaction between 12 h and 16 h, prevails.

Also blast-furnace slag and fly ash, which both react significantly slower than Portland cement, can be considered to be almost inert during the early hydration. Although they have a comparable surface area to quartz, each solid exerts a different influence in the early hydration as can be seen from the specific heat flow curves as depicted in Figure 4.2a. The fly ash blend and the neat cement proceed similar except for the somewhat slower reaction of the neat cement during the initial period up to 1.5 h at the same effective water-to-cement ratio which is caused by the absence of additional nucleation sites. This means that the fly ash has little influence on the overall behavior of the system during the early hydration compared to neat cement. However, at constant water-to-binder ratio (curve C and C-FA in Figure 4.2b) a slightly slower reaction of the fly ash blend can be observed. Thus, the apparent retarding effect of the fly ash (prolonged induction period) is partially related to the presence of higher effective water-to-cement ratio in the fly ash blend compared to neat Portland cement. The retarding effect observed is often more distinct (see e.g. [Deschner et al., 2012, Dittrich et al., 2014]) than reported here as additional aspects like the chemical composition of the pore solution or surface characteristics can also have an important influence on the kinetics of reaction. However, Figure 4.2a shows that the effect of additional nucleation sites seems to be much more pronounced for quartz and blast-furnace slag than for fly ash although they have a comparable surface area, indicating that not only the specific surface area plays an important role.

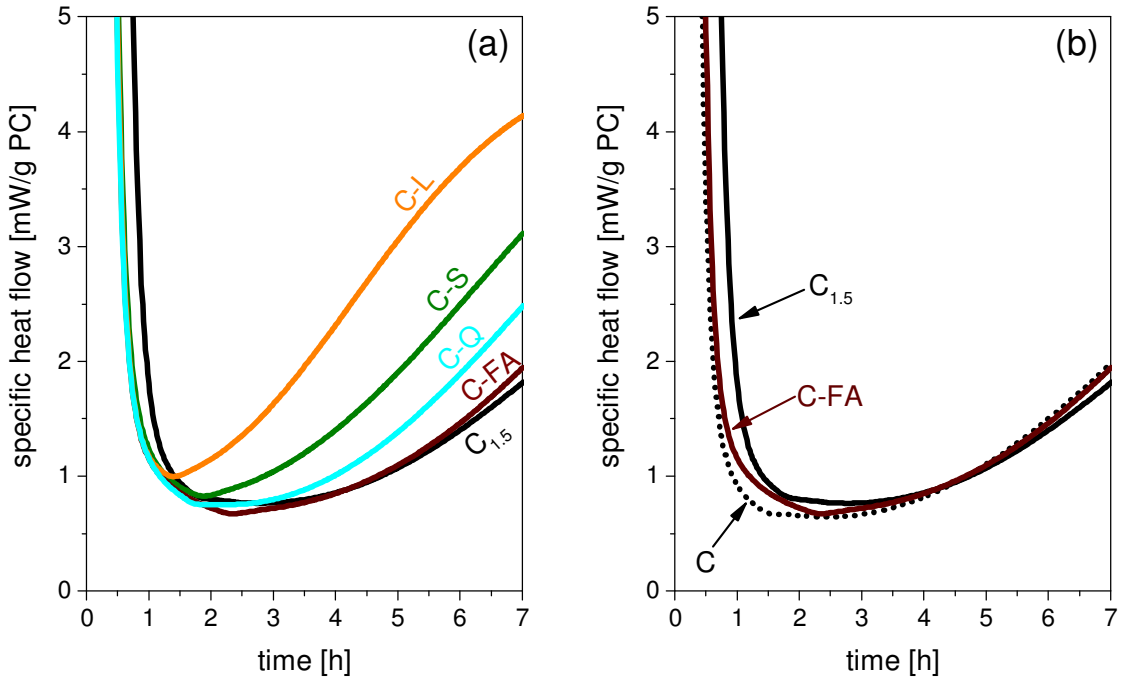

Figure 4.2: (a) Specific heat flow in the first 7 h of hydration depicted for the whole matrix under investigation. (b) Comparison of specific heat flow of the fly ash blend and neat cement at different water-to-solid ratios. All systems at a water-to-solid ratio of 0.75 except otherwise stated in subscript numbers. Note that all curves are normalized to the mass of PC in the system.

The fastest reaction is observed in the presence of limestone. The surface of limestone provides excellent conditions for the formation of C-S-H nuclei [Berodier and Scrivener, 2014] such that the overall hydration reaction can be considerably accelerated. Similary the system containing limestone together with fly ash shows significant faster reaction compared to the fly ash blend although it is reacting slower than the limestone blend due to the lower amount of limestone incorporated. The blast-furnace slag and fly ash blend were also studied with increased total SO_3 content (total of 2.5 wt.%), which did not significantly affect the specific heat flow related to the main peak. These results are summarized in Appendix 3.

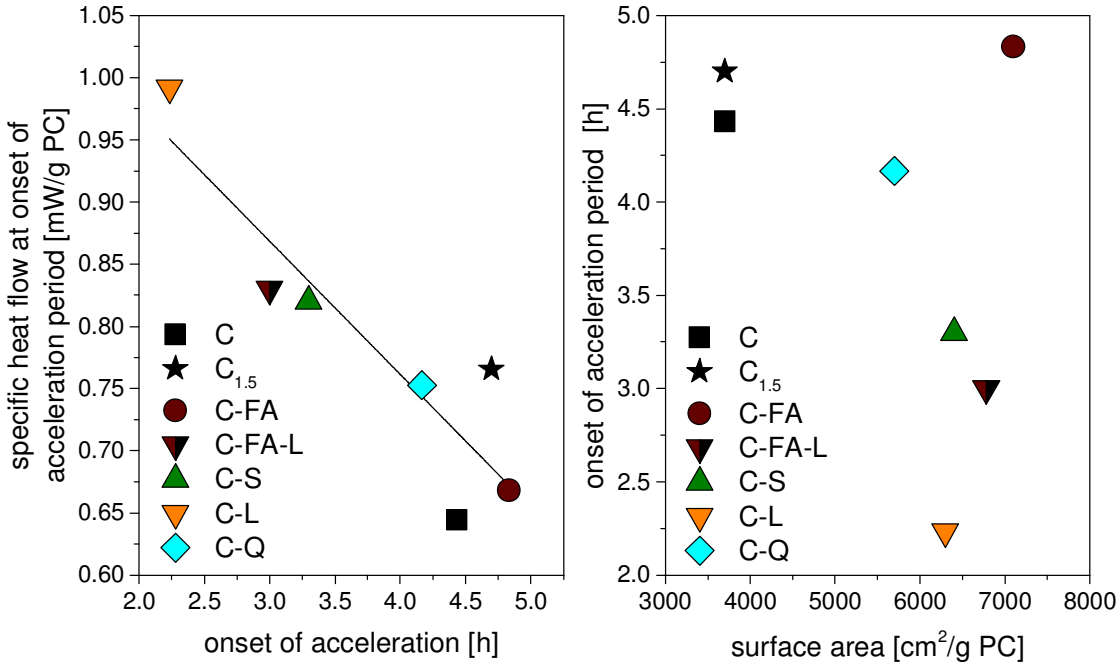

Figure 4.3: (a) Specific heat flow at the onset of the acceleration period plotted in function of the temporal appearance of the onset and (b) temporal appearance of the onset in function of the specific surface. Note that only blended systems are considered in the linear fit of inset (a). Heat flow and specific surface are normalized to the amount of PC in the system. The water-to-solid ratio is 0.75 except otherwise stated in subscript numbers.

In Figure 4.3a, the specific heat flow at the onset of the acceleration period is depicted as a function of the temporal appearance of the onset. The time of the onset and the corresponding heat flow are strongly correlated. If the neat cement is used as reference the fly ash slightly retards the onset while an increasing acceleration is observed from quartz to blast-furnace slag to limestone. Figure 4.3b shows the temporal appearance of the onset of the acceleration period as a function of the specific surface area per g PC. As already discussed before, the higher effective water-to-cement ratio in the quartz blend which would lead to a retardation in case of neat cement (cf. slightly later onset of $C_{1.5}$ compared to C) can be compensated by the additional surface which leads to a slightly earlier onset. A different behavior can be observed for the fly ash where the highest specific surface is present but even a slight retardation compared to the neat cements is present. The retarding effect has also been reported by [Dittrich et al., 2014] where a very fine fly ash ($d_{50} = 2.1\,\mu m$) significantly retarded a fly ash blended Portland cement compared to neat cement at equal water-to-solid ration of 0.5. Differences in the surfaces of the blended systems are relatively small. With the exception of the fly ash this is true for the effect of surface differences on reaction kinetics as well. This has also been shown

by [Berodier and Scrivener, 2014] for SCM of similar PSD compared to Portland cement. However, the influence of the surface on the kinetics increases with increasing fineness of the SCM [Gutteridge and Dalziel, 1990a, Dittrich et al., 2014, Rossen et al., 2015].

4.2.2 Effect of SCM on the pore solution

Figure 4.4 shows that the presence of SCM affects the composition of the pore solution, in particular the pH values. Silicon and sulfate concentrations are decreased in the blends compared to the neat cement while calcium concentrations are higher. Aluminum concentrations are lower in most blended systems compared to PC with the exception of the fly ash blend, where aluminum is increased.

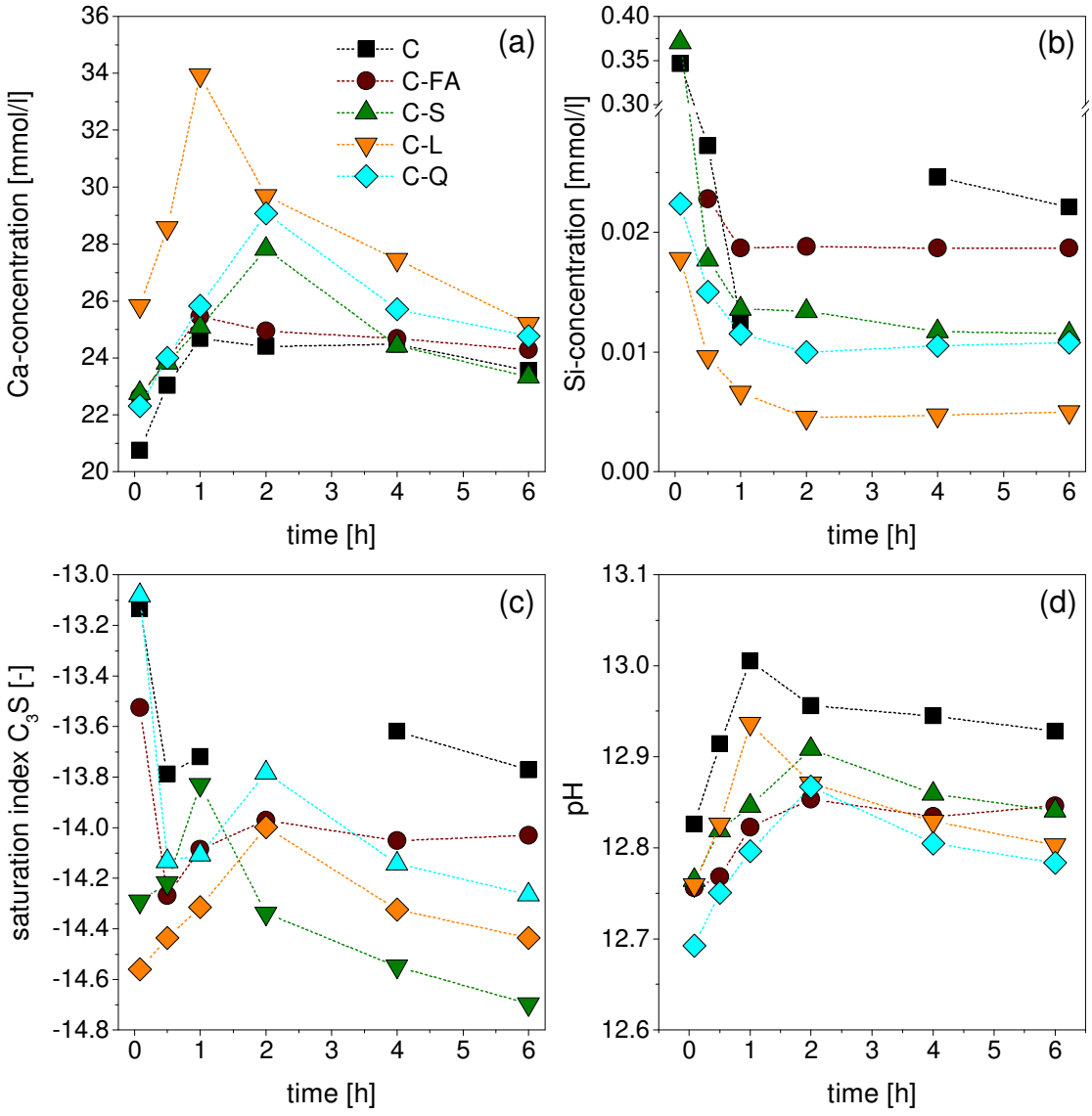

Figure 4.4: Concentrations of (a) calcium and (b) silicon in the pore solutions, (c) calculated saturation index of C_3S and (d) pH values. Note the different scales of the ordinates.

As discussed in the introduction, several studies have shown a decreasing dissolution rate of C_3S and C_2S in the presence of higher Ca-concentrations in diluted systems where

precipitation is limited or prevented [Nicoleau et al., 2013, Garrault-Gauffinet and Nonat, 1999, Garrault and Nonat, 2001] and as the silicon concentrations are very low. Thus if the calcium concentration would be the controlling factor at realistic water-to-binder ratios, a decreasing Ca-concentration from the limestone containing system over blast-furnace slag and quartz to the fly ash blend and neat cement would be expected based on the kinetic behavior shown in Figure 4.2. However, the measured Ca-concentrations as presented in Figure 4.4a show a partially opposite behavior. The calcium concentration in the pore solution of the slow reacting neat cement along with the fly ash and of the faster reacting blast-furnace slag blend are located close to each other and are relatively low. The quartz blend, which reacts slower than the blast-furnace slag blend has higher Ca-concentrations, and the limestone blend as the fastest reacting system shows the highest calcium concentrations throughout. These findings indicate that relating kinetics to calcium concentrations only is too simplistic for concentrated suspensions where both, dissolution and precipitation occur. As discussed in the introduction, the controlling factor for alite dissolution is rather the degree of undersaturation with respect to C_3S (referring to the experimental solubility products derived by [Nicoleau et al., 2013]) and the degree of oversaturation with respect to C-S-H. The saturation indices with respect to C_3S are presented in Figure 4.5. In all cases the solutions are initially oversaturated and at later ages near saturation with respect to C-S-H and near saturation with respect to portlandite (for data see Appendix 2). Although the differences are small, the saturation indices with respect to calcium rich C-S-H are higher for the plain Portland cement than for the blended cements and lowest for the limestone blend.

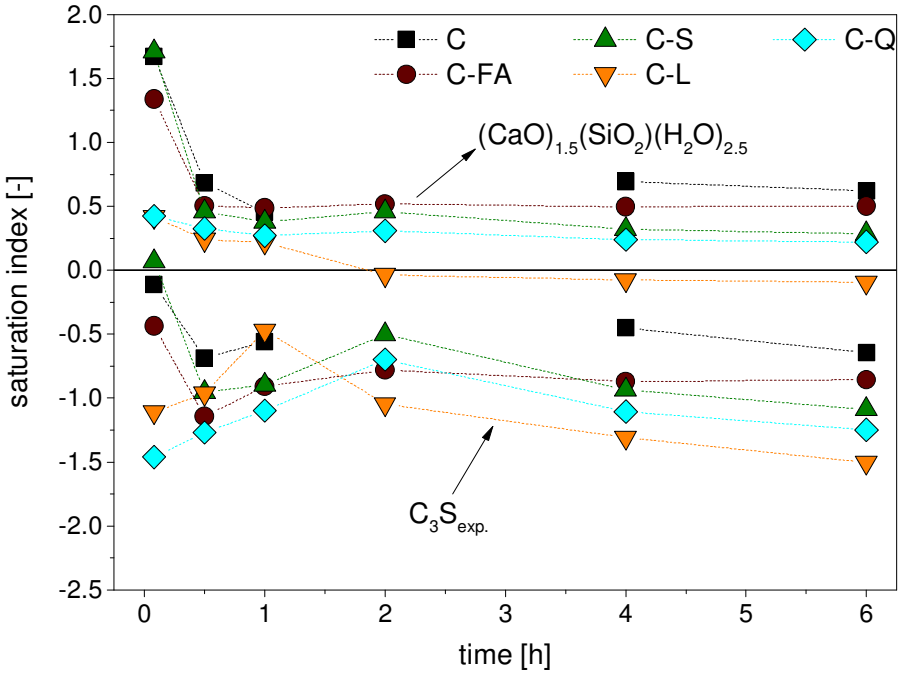

Figure 4.5: Saturation indices for C-S-H and for C_3S with respect to the "experimental" solubility product of alite.

The lower degree of oversaturation observed for the limestone containing sample is probably related to the presence of more C-S-H nuclei formed on the surface of limestone. Berodier and Scrivener [Berodier and Scrivener, 2014] have shown that the number of

C-S-H nuclei on the surface of limestone after 90 min is significantly higher compared to cement and quartz. Additional C-S-H nuclei lead to faster C-S-H precipitation and to lower oversaturation. Thus the observed sequence in oversaturation with respect to C-S-H can be inversely related to the expected number of C-S-H nuclei; i.e. limestone > other blends > neat cement. This is also reflected in the faster reaction observed at approx. 90 min (Figure 4.4a).

All solutions are undersaturated with respect to C_3S. A strong undersaturation is calculated if for C_3S the solubility product of log $K_{S0,\ C_3S} = -10.6$ is used based on the Gibbs free energy of −2784.3 kJ/mol of solid C_3S given by Babushkin et al. [Babushkin, 1985] (data given in Figure 4.4). [Nicoleau et al., 2013] argued that the dissolution reaction is controlled by hydroxylated surface species and defined a much lower "experimental" solubility product, $K_{S0,\ C_3S_{exp.}} = -22.0$. Figure 4.6 shows that initially the two depicted systems (neat cement and limestone-blended cement) are close to the "experimental" solubility product and approach the C-S-H solubility product as the reaction proceeds. The solutions are only moderately undersaturated with respect to the "experimental" solubility product. Figure 4.5 shows that the solutions are most undersaturated with respect to $C_3S_{exp.}$ for limestone-blended Portland cement and the least for the plain Portland cement, while the differences between C-S, C-Qz and C-FA are relatively small. The faster C-S-H precipitation due to more C-S-H nuclei on limestone leads to a higher undersaturation with respect to C_3S and thus to its faster dissolution.

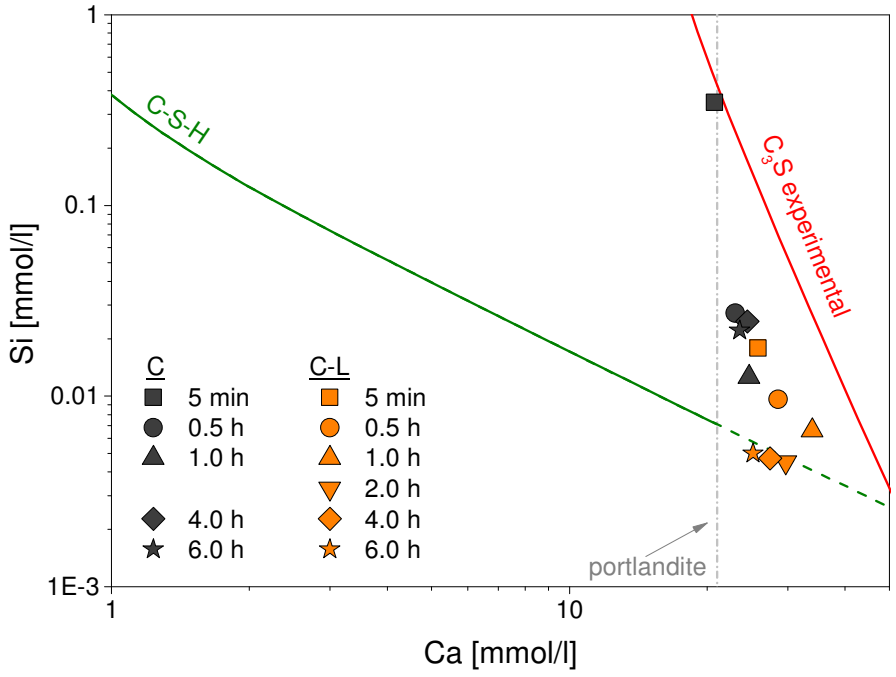

Figure 4.6: Ca and Si Concentrations measured in the pore solutions for neat and limestone blended cement. The solid lines represent the solubility of C-S-H, C_3S and portlandite.

Thus the general trends of dissolution (and precipitation reactions) are consistent with the observed degree of undersaturation at least along the lines of plain Portland cement, quartz and limestone blend which is also present when estimating the dissolution rates for these systems using the data from [Nicoleau et al., 2013] (Figure 4.7 and Table 4.1). However, the relatively slow reaction of C-FA and the faster reaction of the C-S cannot be explained by the degree of undersaturation only.

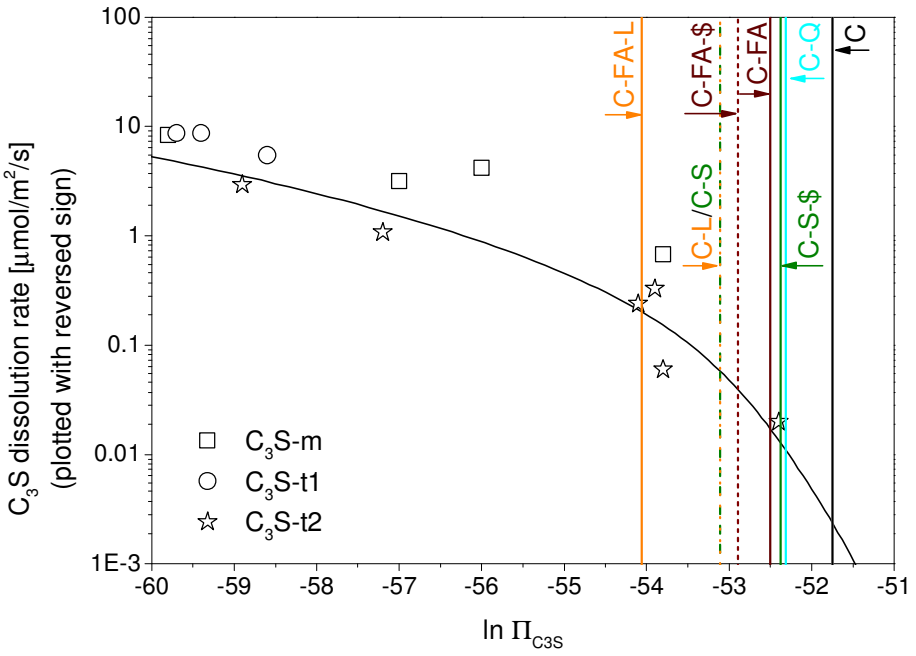

Figure 4.7: Dissolution rate of C_3S (plotted with a reversed sign) compared to ln Π measured in this study after 2 h of hydration (4 h of hydration in the case of neat cement (C)). Data points for the C_3S polymorphs are taken from [Nicoleau et al., 2013].

Table 4.1: Estimated C_3S dissolution rates calculated from ln $\Pi_{C_3S,\,exp.}$ at 2 h of hydration.

System	C_3S dissolution rate [mol/m^2/s]
C[a]	−0.002
C-FA	−0.017
C-FA-$	−0.040
C-FA-L	−0.202
C-S	−0.058
C-S-$	−0.013
C-L	−0.058
C-Q	−0.011

[a] Data for C correspond to 4 h of hydration.

Another factor known to suppress the alite reaction is the amount of aluminium and sulfate in the solution. In fact the highest aluminium concentration (Figure 4.4a) is present for the cement with fly ash while it decreases over neat cement, quartz and blast-furnace slag to limestone; the same order as observed for the heat discussed above. The aluminium concentrations during the first hours support the observation that aluminium hinders alite hydration [Begarin et al., 2009]. Plotting the heat flow as a function of the Al-concentration after 2 h hours of hydration (Figure 4.8a) clearly reveals a decrease in the recorded heat flow with an increase in aluminium. This indicates that the retarding effect of aluminium on the dissolution of alite as observed for pure alite [Nicoleau et al., 2014,Begarin et al., 2011] is one of the main factors affecting the alite reaction in Portland cement and blended cements.

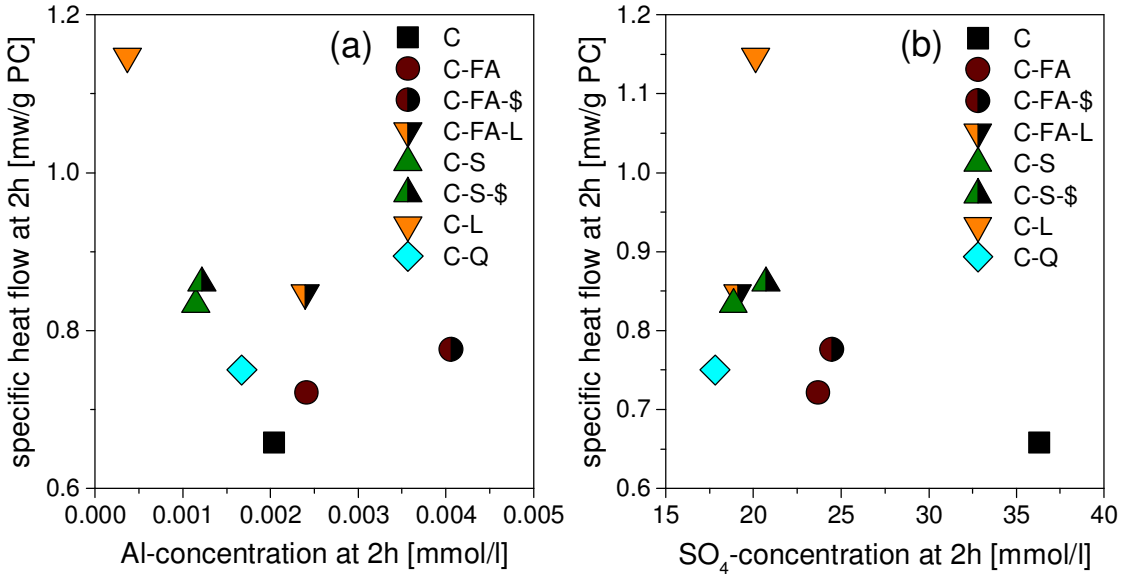

Figure 4.8: Specific heat flow at 2 h of hydration in function of the (a) Al-concentrations and (b) SO_4-concentrations at 2 h of hydration. Heat flow values are normalized to the amount of PC in the system.

The reason for these different aluminium concentrations observed is difficult to reveal. During the early hydration, part of the aluminium reacts and the aluminium released is precipitating as ettringite. The PC and the blend with fly ash both show the highest oversaturation with respect to ettringite (see data in the Appendix 2) indicating that the precipitation of ettringite is more slowly in these two systems than in the other blends with quartz, limestone or blast-furnace slag, hence the high aluminium observed. The kinetic hindrance of the ettringite precipitation is probably related to the higher sulphate concentration in these systems as Damidot [Damidot, 2007] has shown that higher sulphate (and aluminium) concentrations can lead to higher oversaturation with respect to ettringite. While in the case of neat Portland cement the low calcium concentrations (due to higher pH) are responsible for the relatively high sulphate concentrations, the readily soluble sulfate from the fly ash (Table 3.3) causes the high sulfate concentrations in the fly ash blend. Note that the presence of additional solid calcium sulfate (sample C-FA-$ and C-S-$) did not significantly affect the aluminum and sulfate concentrations, as the solutions are saturated with respect to $CaSO_4$ anyway.

A comparison of the specific heat flow after 2 h of hydration with the "experimental" solubility product of alite calculated at 2 h of hydration is presented in Figure 4.9. Similar to Figure 4.6, along the line of neat Portland cement, quartz and limestone these data correlate well with the heat development.

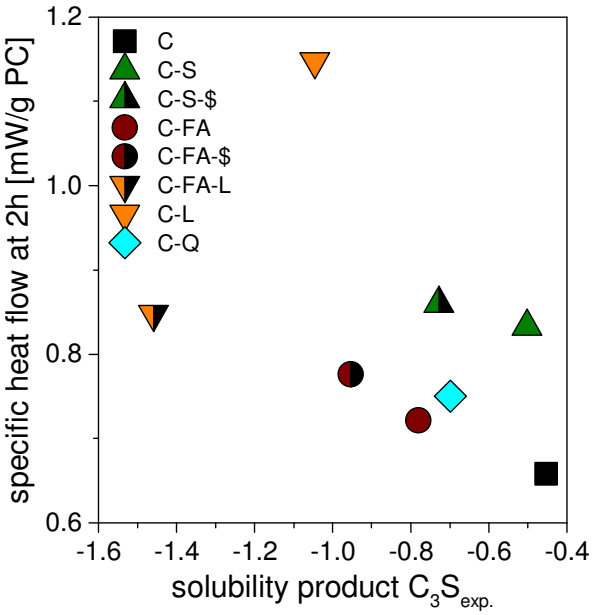

Figure 4.9: "Experimental" solubility product of alite calculated at 2 h of hydration ($C_3S_{exp.}$) plotted in function of the specific heat flow after 2 h of hydration. Note that $C_3S_{exp.}$ was calculated for 4 h of hydration in case of C.

In contrast to the Al-concentrations that have been shown to clearly affect the hydration of blended Portland cements, and indirectly also the sulfate concentrations, no such systematic effect can be observed for calcium as can be seen from Figure 4.10.

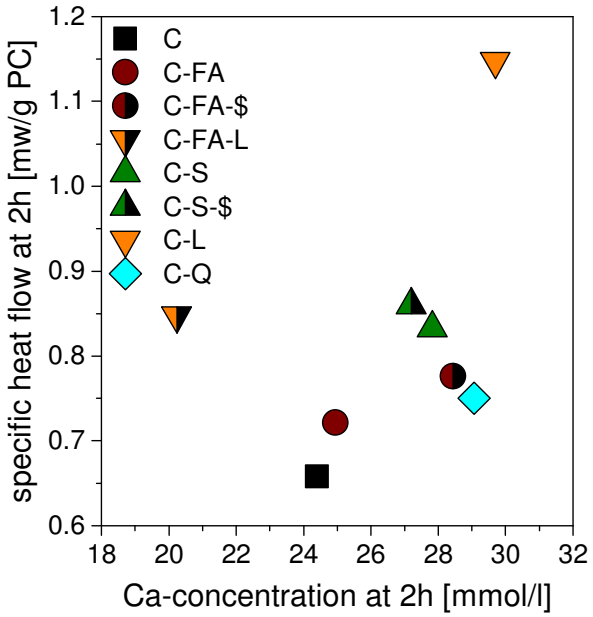

Figure 4.10: Specific heat flow at 2 h of hydration as a function of Ca-concentration. Note that the heat flow is normalized to the amount of PC in the system.

4.3 Conclusions

The results presented in this study compare the early hydration of Portland cement blends with different types of SCM. The experimental results lead to the following conclusions:

(i) The presence of additional surface sites for nucleation in blended cements leads to a faster heat development and to a lower degree of (over)saturation with respect to C-S-H. The observed decrease of saturation of the solutions is most distinct for the limestone blended cement, as on limestone C-S-H nucleation occurs more easily, and less for the quartz, blast-furnace slag and fly ash blended cements, while the highest oversaturation with respect to C-S-H is present for the neat cement, where the least surface is available for nucleation.

(ii) Higher calcium concentrations does not lead to a systematic decrease of the reaction rate of C_3S and C_2S with increasing Ca-concentration. In contrast the fastest reacting blend with limestone shows the highest calcium concentrations.

(iii) The general trend of the reaction rate is inversely related to the degree of undersaturation with respect to C_3S (which depends on pH, calcium and silicon concentrations). The more undersaturated the faster the observed reaction. The limestone containing blend which is more strongly undersaturated reacts faster than the other blends which are less undersaturated. The least undersaturation is observed for the plain cement, which also shows the slowest reaction. The difference between the different blends however, could not be explained by undersaturation only.

(iv) A higher Al concentration in the pore solution retards the hydration as visible by the very fast reaction of the limestone blended sample with the lowest aluminium concentration compared to the fly ash sample with the highest aluminium concentrations. Consequently, the presence of aluminium retards the hydration in the blended systems in agreement with the observed effect of aluminium on alite dissolution in diluted systems.

(v) The lower aluminium concentration in most blends (quartz, blast-furnace slag and limestone) seems to be related to the lower sulfate concentrations which enable a faster ettringite precipitation.

The investigations of the changes in the pore solution during the early hydration have shown that the same factors as in diluted systems dominate the kinetics. Higher degree of undersaturation with respect to C_3S and lower aluminium concentration accelerate the reaction, while higher aluminium concentrations have an opposite effect. Similarly additional C-S-H nuclei (due to more surface or the presence of limestone) lead to faster C-S-H precipitation and thus also to faster hydration. The exact interplay between these factors in real systems depends on many factors. The aluminium concentrations are strongly affected by the kinetics of ettringite precipitation, which can be hindered at high sulfate concentrations. The numerous factors controlling the hydration make investigations in cement pastes challenging and further research is needed both on pure phases and in cements to better understand the factors controlling the early hydration of Portland cement in the presence of SCM.

Chapter 5

The effect of glass composition on the reactivity of synthetic glasses[13]

Compared to Portland cement the reaction of blast-furnace slag and especially fly ash is slower. This is caused by the low reactivity of the glass phase of these SCM. The main factor that controls the intrinsic reactivity of the glass phase is the glass composition which determines the characteristics and properties of the glass network. For a better application of SCM in blended cements the dependance of the reactivity of glasses on their chemical composition needs to be understood in detail. Thus the reaction of synthetic glasses that correspond to the glass composition as present in Si-rich and Ca-rich fly ashes and blast-furnace slags was studied. Different approaches were chosen to characterize the glass reactivity, all at high pH (>13) to mimic conditions that are prevailing in cement pore solutions. The dissolution of the glasses was investigated in 0.3 M KOH-solution at far-from-equilibrium conditions. Isothermal calorimetry and TGA experiments were conducted on model systems containing portlandite and calcite and on glass-blended Portland cement. Bound water content derived from TGA was used together with thermodynamic modeling in order to calculate the degree of glass reaction in both systems. Additionally EDTA/NaOH selective dissolution experiments were conducted.

5.1 Glass synthesis, glass powder preparation and characterization

Detailed descriptions on the synthesis of the glasses as well as on the characterization and on the preparation of the actual glass powders that were investigated in this chapter are given in 3.3.9. The mix designs as well as all used methods and strategies are described in 3.2 and 3.3.

Three groups of glasses were investigated, FA_s, FA_c and S corresponding to glass compositions as present in Si-rich and Ca-rich fly ashes and blast-furnace slags. In groups FA_s and S Al_2O_3/Si_2O_3 was varied while in group FA_c and in selected samples from groups FA_s and S this ratio was fixed. All other ratios possible were kept constant.

[13] An extended version of this chapter has been submitted as a manuscript to Journal of the American Ceramic Society, as: The effect of glass composition on the reactivity of synthetic glasses, A. Schöler, F. Winnefeld, M. Ben Haha, B. Lothenbach

With this approach the influence of decreasing SiO_2 content at the expense of an increase of CaO as well as the role of Al_2O_3 could be investigated.

5.2 Results and discussion

5.2.1 Glass dissolution at far-from-equilibrium conditions

The measured concentrations of aluminium in the KOH-solutions during the first hours can be used to follow the glass dissolution as congruent dissolution can be assumed for (calcium)aluminosilicate glasses [Snellings, 2013]. The data presented in Table 5.1 show the determined Al concentrations in the KOH solutions. All values increase with increasing sample age. Thereby the highest values can be found for the Ca-rich slag glasses while the lowest ones are present for the Si-rich fly ash glasses.

Table 5.1: Al concentrations obtained in the dissolution tests and calculated percentage of glass reacted.

age	FA_s1	FA_s2	FA_s3	FA_c1	FA_c2	S1	S2	S3
				Al concentration [mmol/l][a]				
0.5 h	<0.004	<0.004	<0.004	<0.004	<0.004	<0.004	0.004	***0.004***
1 h	<0.004	<0.004	<0.004	<0.004	<0.004	<0.004	***0.007***	***0.008***
2 h	<0.004	<0.004	<0.004	<0.004	***0.004***	<0.004	***0.010***	***0.011***
4 h	<0.004	<0.004	<0.004	<0.004	***0.006***	***0.008***	***0.017***	***0.019***
8 h	<0.004	***0.018***	***0.004***	***0.006***	***0.010***	***0.014***	***0.032***	***0.036***
16 h	<0.004	***0.023***	***0.005***	***0.009***	***0.021***	***0.021***	***0.054***	***0.060***
1 d	***0.005***	***0.026***	***0.009***	***0.011***	***0.019***	***0.037***	***0.079***	***0.088***
2 d	***0.011***	***0.035***	***0.019***	***0.029***	***0.051***	0.047	0.108	0.121
7 d	0.023	0.074	0.046	0.066	0.097	0.066	0.149	0.166
				glass reacted [wt.%][b]				
0.5 h	0.0	0.0	0.0	0.0	0.0	0.0	1.5	1.3
1 h	0.0	0.0	0.0	0.0	0.0	0.0	3.1	2.6
2 h	0.0	0.0	0.0	0.0	1.5	0.0	4.1	3.5
4 h	0.0	0.0	0.0	0.0	1.9	4.9	7.3	6.2
8 h	0.0	4.4	0.8	1.6	3.4	8.4	13.6	11.4
16 h	0.0	5.7	1.0	2.5	7.2	12.8	22.8	19.2
1 d	1.6	6.4	1.9	3.3	6.3	22.2	33.4	28.0
2 d	3.7	8.7	4.0	8.2	17.5	28.2	45.7	38.3
7 d	7.7	18.4	9.8	18.9	33.1	39.9	62.9	52.8

[a] Determined by ion chromatography. The relative error is ~10%. Values in italics correspond to the initial linear dissolution as presented in Table 5.2 and Figure 5.1.

[b] Calculated from the obtained Al concentrations in the dissolution tests assuming congruent dissolution. Values are corrected for hydrotalcite formation (see Appendix 4).

The samples were prepared with a water-to-solid ratio of 1000 to prevent the precipitation of solids. Saturation indices calculated from the measured concentrations in solution showed that the solutions were always clearly undersaturated with respect to Ca-rich C-S-H, Si-rich C-S-H, strätlingite and AH_3, with exception of the blast furnace slag glasses

after $\geq$ 1 d, where the solutions start to be saturated with respect to C-S-H. Besides C-S-H, hydrotalcite might form due to the presence of MgO in the glasses. Mg could not be determined by IC due to its very low concentrations below the detection limit of <0.004 mmol/l. Thus the solid samples were analyzed for the presence of hydrates after 7 d in the dissolution tests. While XRD data do not give clear evidence regarding the presence of crystalline phases, TGA (c.f. Appendix 4) confirmed the formation of C-S-H and hydrotalcite for blast-furnace slag glasses and FA_c2. For comparison TGA data from pure phases as described in [Lothenbach et al., 2015] were used.

The Al-concentrations were used to calculate the amount of Al_2O_3 dissolved from the glass which corresponds to total amount of reacted glass. The formation of Al-containing hydrates (hydrotalcite) was taken into account, as else the reaction of the glasses is underestimated. For the calculations a composition of OH^--hydrotalcite ($Mg_4Al_2(OH)_{14}{\cdot}3\,H_2O$) was used. The values of calculated glass reacted as presented in Table 5.1 are corrected according to this procedure. Based on these data the highest glass reaction was observed for Ca-rich slag glass (S2 and S3) while the lowest reaction was observed for the Si-rich glasses (FA_s). The Al-rich samples S3 and FA_s3 showed higher degree of reaction than the samples S1 and FA_s1, which contained approx. 40 wt.% less aluminium. The Si-concentrations (Appendix 2) show a significantly larger scatter throughout the whole dataset.

Based on a strategy suggested by [Snellings, 2013] initial dissolution rates (r_+) were calculated from the Al concentrations taking into account the initial stage only, where relatively little of the glasses has dissolved, i.e. prior to a rate drop (cf. Figure 5.1) and with respect to the initial surface areas:

$$r_{+,\mathrm{Al}} = \frac{d(Al)}{\Delta t} \cdot \frac{\nu_{Al}}{m \cdot S \cdot V_{Solution}} \tag{5.1}$$

The slope of the straight line that corresponds to the initial stage of dissolution (c.f. Figure 5.1) is given by d(Al), Δt [s] is the duration of the initial linear stage, the cation fraction of the tracer element in the glass sample is given by ν_{Al} [mol], m [g] is the mass of the glass sample, S [m^2/g] represents the initial specific surface area of the glass sample as calculated from PDS and density and $V_{Solution}$ [l] corresponds to the solution volume. Linear behavior was found up to 48 h for FA_s1-FA_c2 and up to 24 h for S1-S3. The calculated initial dissolution rates expressed are in the range of $10^{-8.0}$ mol/m^2/s to $10^{-9.4}$ mol/m^2/s (see Table 5.2). The obtained dissolution rates are slightly lower than the dissolution rates determined by Snellings ($10^{-7.0}$ mol/m^2/s to $10^{-8.5}$ mol/m^2/s) [Snellings, 2013] which might be caused by different surface areas as Snellings used BET values and a broader PSD ranging from 30 µm to 300 µm.

Table 5.2: Initial dissolution rates as calculated from the Al concentrations expressed as log r_+. Data given in [mol/m^2/s].

	FA_s1	FA_s2	FA_s3	FA_c1	FA_c2	S1	S2	S3
log r_+	−9.40	−9.20	−9.11	−9.13	−9.00	−8.72	−8.29	−8.12

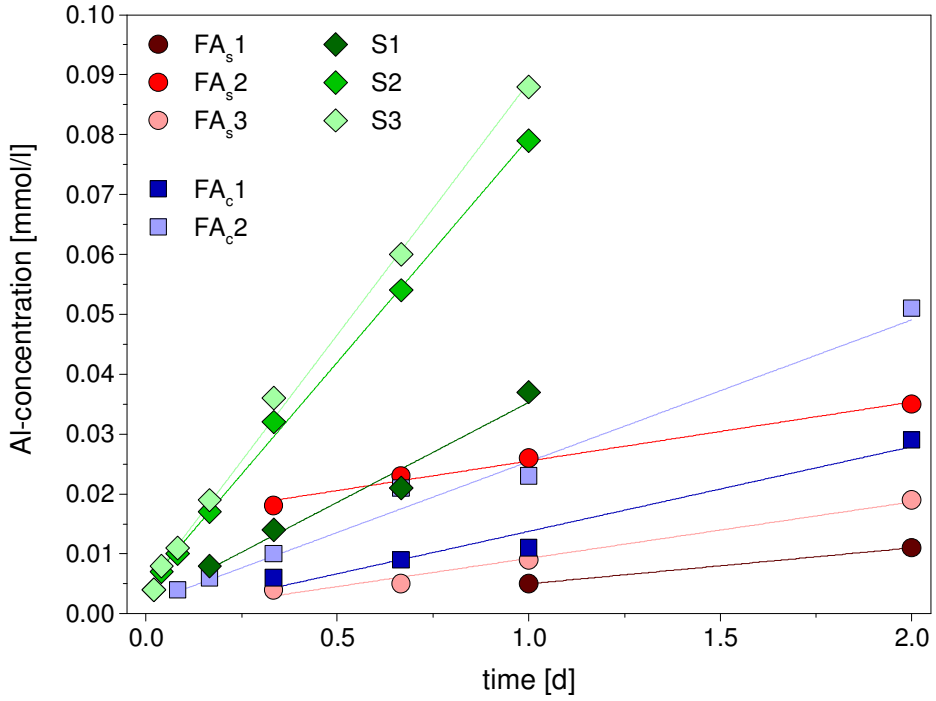

Figure 5.1: Al concentrations of the dissolution tests as determined by ion chromatography depicted for the initial linear increase. The relative error is ~10%. Initial dissolution rates are calculated from the linear increase in solution concentrations over time which is indicated by the straight solid lines.

Figure 5.2 shows log r_+ plotted in function of CaO/SiO_2. It is clearly visible that increasing Al_2O_3 contents lead to faster dissolution in the groups FA_s and S. Hence the effect of Al_2O_3 also has to be taken into account. Based on this observation the ratio of non-bridging oxygen atoms to oxygen atoms in tetragonal coordination (NBO/T) was calculated (cf. 3.3.9). Thereby alkalies and alkaline earths act as network modifying oxides (NWM) such that an increase of such oxides leads to a more depolymerized network and thereby to higher reactivity. Intermediate oxides like Al_2O_3 might also act as NWM as is indicated by the results presented in Figure 5.2. A value of NBO/T = 0 refers to a fully interconnected network and NBO/T = 4 represents a fully depolymerized network. Assigning 0.92 % of Al_2O_3 to NWM enables to calculate NBO/T values in a range of 0 and 4.

The groups with varying Al_2O_3-SiO_2-ratio (FA_s1 to FA_s3 and S1 to S3) show an increasing reaction with increasing Al_2O_3 content, i.e. FA_s3 and S3, indicating that aluminum is not acting as network former but rather as network modifier. This justifies the chosen approach in the NBO/T calculations, i.e. assigning 92% of Al_2O_3 (and Fe_2O_3) to NWM using an f value of 0.92.

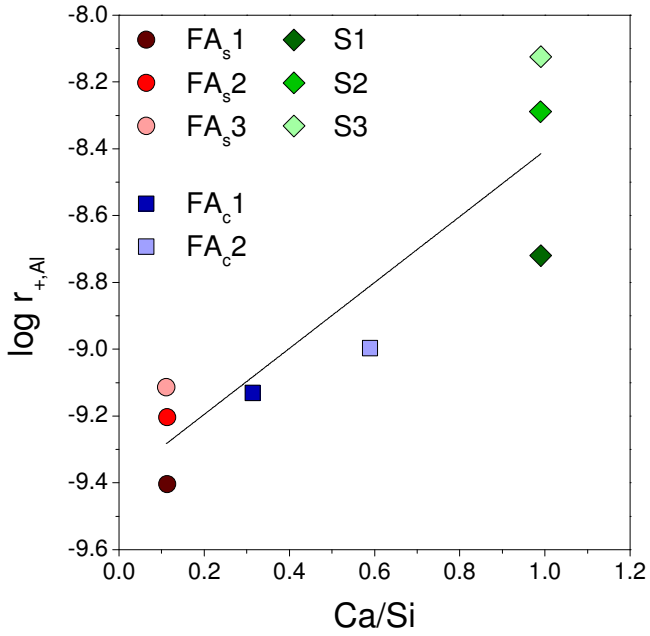

Figure 5.2: Log $r_{+,Al}$ plotted in function of CaO-SiO_2-ratio of the synthetic glasses.

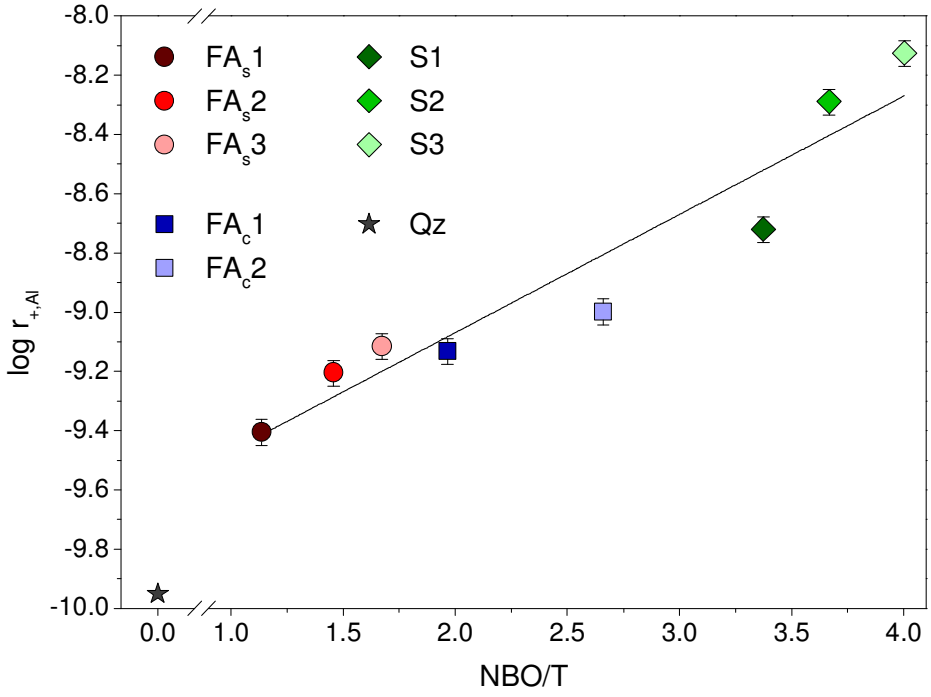

Figure 5.3: Logarithm of the initial dissolution rate plotted against NBO/T. Data for quartz at pH = 12.2 is taken from [Brantley, 2008].

5.2.2 Glass reaction in model systems

5.2.2.1 Calorimetry

The reaction of the different glasses was determined in model systems containing glass, portlandite and calcite in 0.3M KOH solution as described in detail in 3.2.2. The recorded specific heat flow curves gained by isothermal calorimetry from the model systems are presented in Figure 5.4. As the model systems contain only $Ca(OH)_2$ and $CaCO_3$ besides glass, the heat generated is related to the reaction of the glass as confirmed by the very low heat generated by the quartz reference sample. All Si-rich fly ash glasses and FA_c1 generated a similar and relatively low heat flow between 0.75 µW/g and 1.25 µW/g. The constant heat flow indicates a uniform progress of reaction during the 7 d studied. The samples containing more SiO_2 (within the groups FA_s and S) generated less heat than the samples containing more CaO or more Al_2O_3. This is caused by different intrinsic reactivity of the glasses whereby different enthalpies of formation for different phases or amounts of phases formed could also affect the heat. It should be mentioned that specific heat flow does not directly correspond to the degree of reaction; however, the overall development tentatively indicates a higher reactivity for glasses with lower SiO_2 content. FA_c2 also shows a uniform heat development but somewhat higher heat flow than the other fly ash glass samples. In contrast to the fly ash glasses the blast-furnace slag glasses show clearly higher heat flow, a significant maximum during the first days indicating an induction and acceleration period. Again the samples containing more SiO_2 generated less heat than the samples containing more CaO or more Al_2O_3.

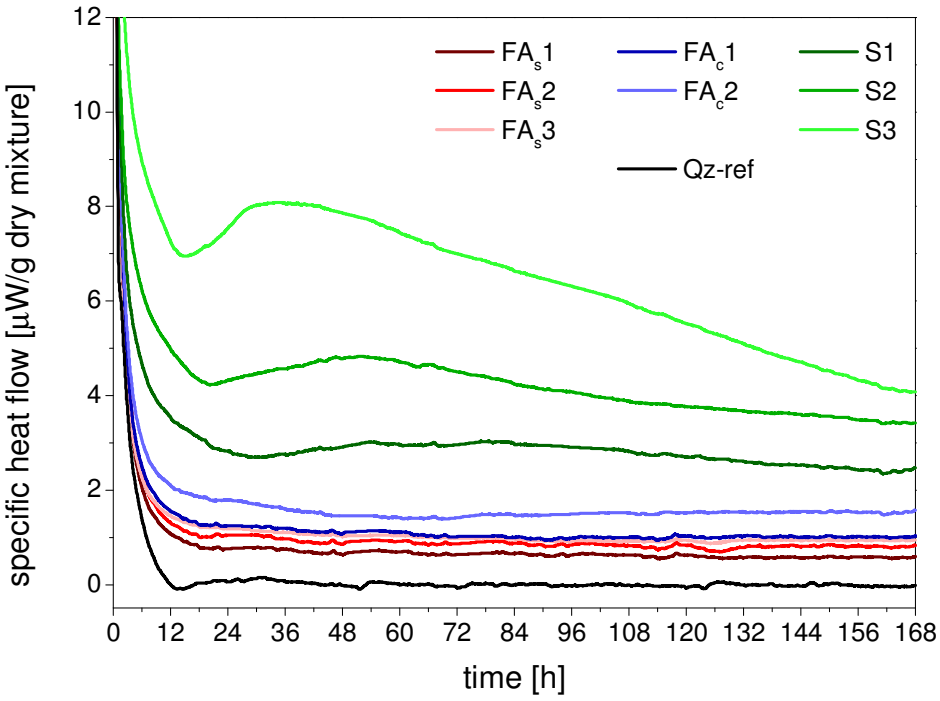

Figure 5.4: Specific heat flow of pozzolanity test samples as recorded at 20 °C.

The calculated released heat of hydration up to 7 d is presented in Figure 5.5. The Si-rich fly ash glasses and FA_c1 are all located close to each other and do not reach values exceeding 7 J/g after 7 d. For all other glasses an increasingly steeper progression and thereby higher released heat after 7 d is present at higher CaO and lower SiO_2 content in the glasses. This is in agreement with the observations from the dissolution tests.

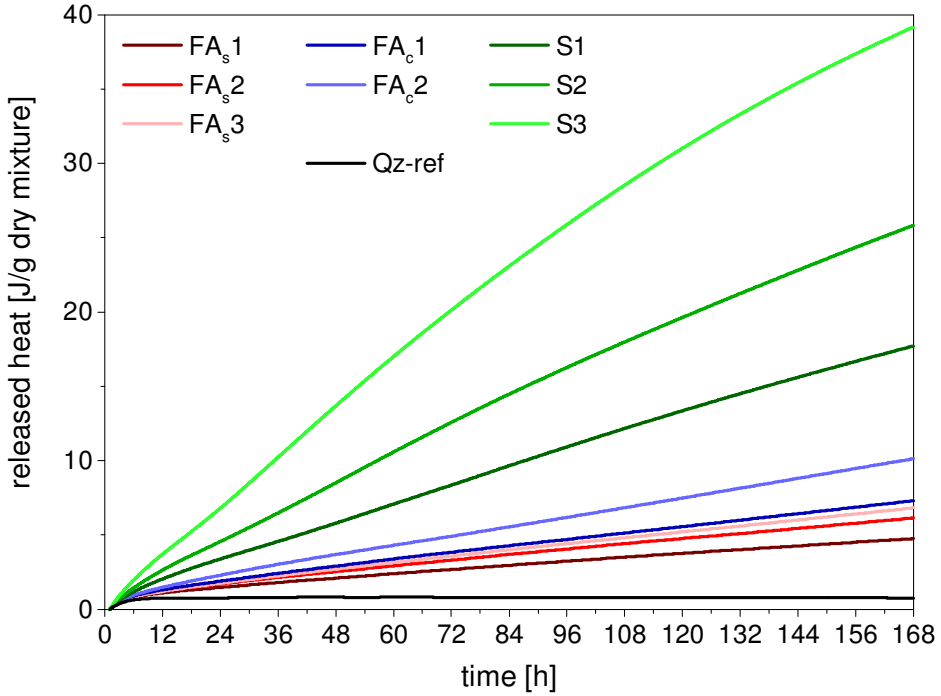

Figure 5.5: Released heat of pozzolanity test samples as recorded at 20 °C.

5.2.2.2 Bound water content and calculation of the degree of SCM reaction

Bound water in the model systems originates from the presence of C-S-H, AFm phases, hydrotalcite and portlandite as can be seen from the TGA curves of selected samples (Figure 5.6). The total bound water content as obtained from TGA is presented in Figure 5.7a. The increase of bound water and the decrease of portlandite reveal a higher amount of glass reacted at later ages as a function of glass composition, i.e. an increase from Si-rich fly ash glasses to blast-furnace slag glasses (see also Figure 5.6) and also a higher reaction of the Al_2O_3-rich S3 and FA_s3 compared to S1 and FA_s1 which contain approx. 40 wt.% less Al_2O_3. The mean initial total bound water content of the dry mixtures which originates from the added portlandite is 9.0 g/100 g dry solids. Taking into account the relative uncertainty of ±10% due to sample preparation and measurement, additional bound water due to the formation of hydrate phases is clearly visible after 7 d (S2, S3), 14 d (S1), 28 d (FA_c2) and 91 d (FA_s1-FA_c1). This progression is as well present in the calculated amount of glass reacted (Figure 5.7b). These results correlate with the successive decrease of the degree of polymerization in the glass network from Si-rich glasses towards Ca-rich glasses. Similar trends can be observed for total released heat after 7 d of hydration and for the amount of glass reacted in the dissolution tests. Note that in the dissolution tests (cf. 5.2.1) where a high liquid to solid ratio was present and the samples were permanently shaken the degree of reaction is notably higher. The results of selective dissolution experiments (Appendix 4) show a large scatter such that the suitability of the EDTA/NaOH approach for the glasses needs to be investigated in

more detail.

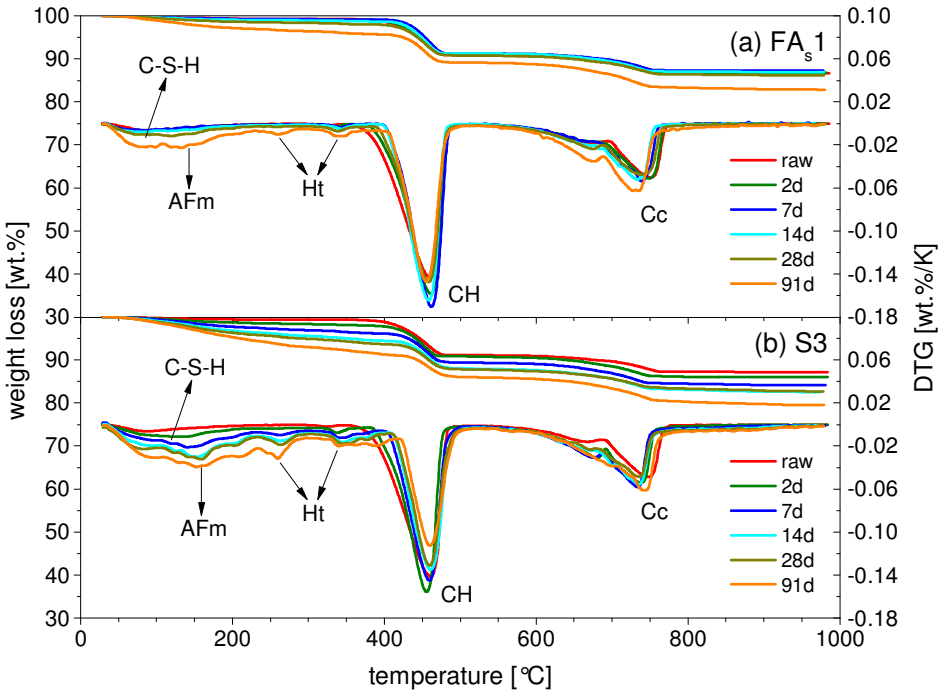

Figure 5.6: (a) Weight loss and (b) differential thermogravimetry (DTG) curves for selected pozzolanity test samples. AFm - monocarbonate and/or hemicarbonate, Cc - calcite, CH - portlandite, C-S-H - calcium silicate hydrate, E - ettringite, Ht - hydrotalcite.

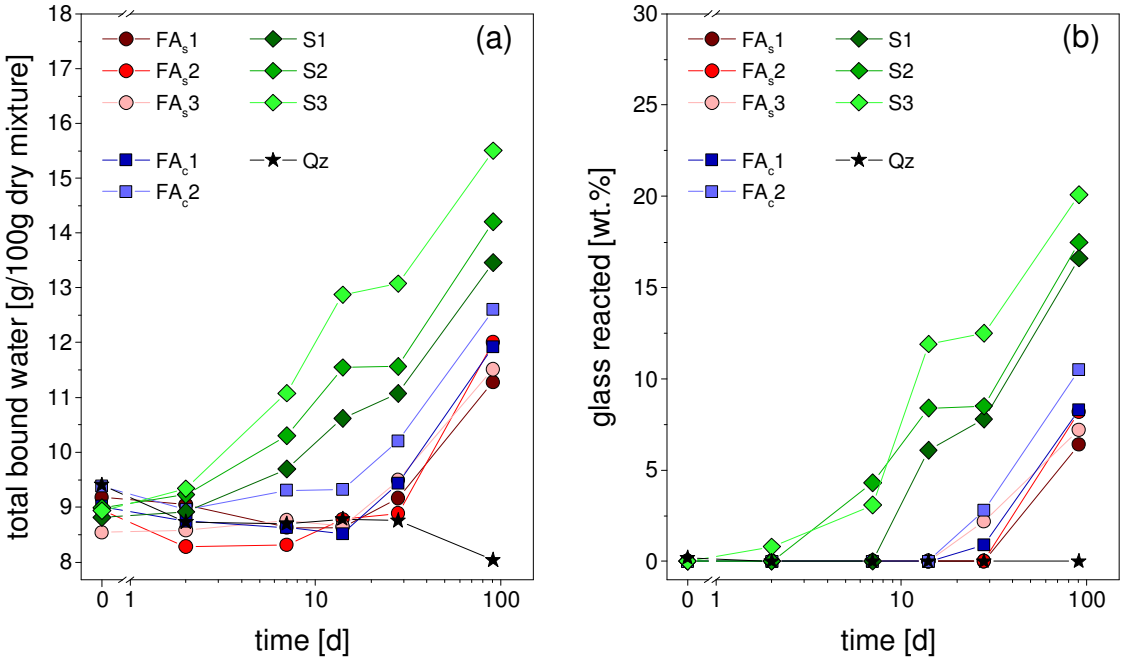

Figure 5.7: (a) Total bound water content as calculated from TGA and (b) calculated percentage of reacted glass as a function of time.

5.2.3 Glass reaction in blended cements

Blends of Portland cement and glass were investigated by isothermal calorimetry, mass balance/TGA and by EDTA/NaOH selective dissolution. Recorded specific heat flow and calculated released heat (Appendix 4) revealed no significant influence of the glass composition on the early hydration within the first 7 d as all curves including the quartz containing reference were superimposed not showing any significant variations. This indicates that the heat is dominated by the reaction of Portland cement and shows a low degree of glass reaction during the first 7 d. The glass reaction was also studied by TGA. The bound water content is similar for all systems up to 7 d (Figure 5.8a). Later a higher increase is visible for the blast-furnace slag glasses while the Si-rich fly ash glasses and FA_c1 are comparable to the quartz reference. As the reaction of the glasses is relatively slow, their contribution to heat or bound water is not well visible during the first 7 d of hydration. Only at later ages where little Portland cement reaction occurs the reaction of the glass is clearly visible. This is supported by the different bound water values depending on the type of glass as they are present from 14 d on. The development of portlandite content in the blended cements is presented in Figure 5.8b. The actual portlandite content was calculated using the tangential method in the region of the portlandite peak in the DTG curve (typically in the region of 370 °C to 500 °C). It is difficult to differentiate between the various glasses as all values are located in narrow borders. Only after 91 d lower portlandite content is present for all glass containing samples compared to the quartz reference indicating a reaction of the glasses.

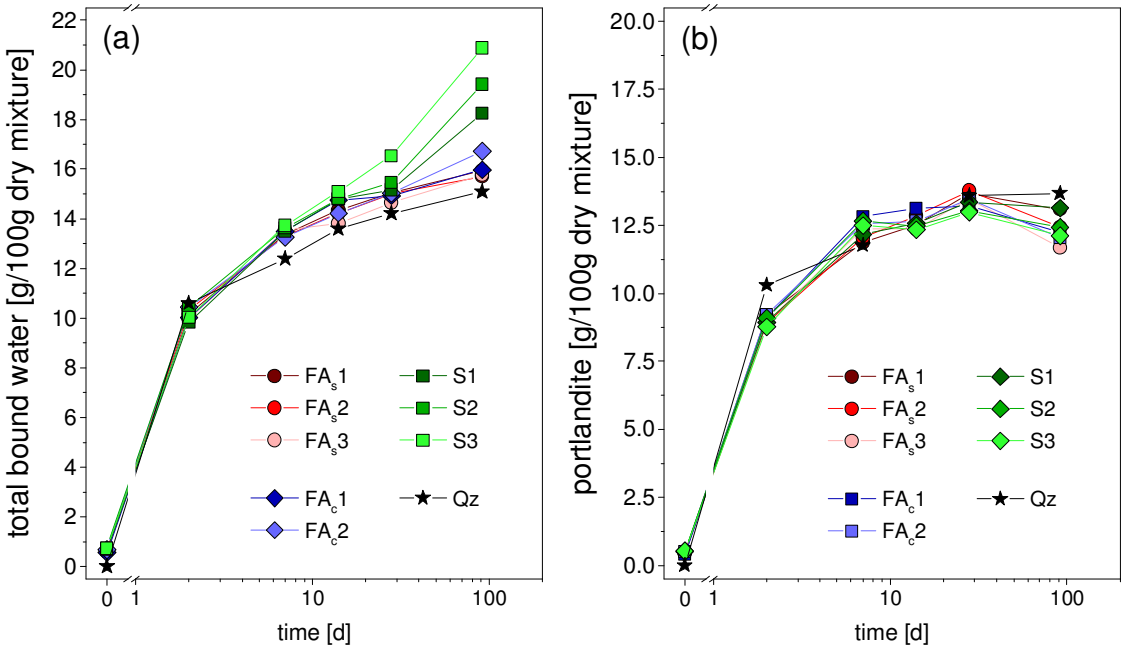

Figure 5.8: Blended cements: (a) Bound water excluding water contributed by the dehydroxylation of portlandite. Values are corrected for water present in the unhydrated dry mixtures. (b) Development of portlandite. The relative error due to sample preparation and measurement is between ± 5% and 10%.

Table 5.3: Amount of glass reacted for blended cements after 91 d of hydration determined by the bound water/mass balance approach.

	FA_s1	FA_s2	FA_s3	FA_c1	FA_c2	S1	S2	S3
glass reacted [wt.%]	0.6	0.2	0.5	0.8	2.5	8.0	10.4	13.5

In order to determine the amount of glass reacted, the difference in the bound water content of the various systems with respect to the quartz reference after 91 d of hydration was calculated from TGA data and used to estimate the amount of glass reacted as was done for the model systems. In contrast to the model systems portlandite is not just present as a reactant but is also formed during the hydration of Portland cement. Therefore bound water excluding water contributed by the dehydroxylation of portlandite was used to determine the amount of glass reacted. The results in Table 5.3 show the same trends that can be observed by all experiments as described before, i.e. increasing amount of glass reacted from Si rich glasses towards increasingly Ca-rich and Al-rich glasses.

A comparison of the amount of glass reacted in the blended cements determined by the bound water/mass balance approach and by the EDTA/NaOH selective dissolution technique for samples hydrated for 91 d is presented in Figure 5.9a. The results of both methods show the same behavior of the glasses, i.e. higher reactivity with increasing amount of network modifiers. The bound water/mass balance approach does not reveal any significant difference among the Si-rich glasses (group FA_s shows almost no reaction) while glasses containing more modifiers show clearly higher reaction. In contrast to this observation the selective dissolution experiments show successively increasing reaction for all glasses with increasing amount of network modifying oxides in the glass composition. Thereby the determined amount of glass reacted is higher compared to the bound water/mass balance approach throughout. While in general the same trends are observed as determined in the dissolution tests and in the model systems the reason for the mentioned differences is not clear. As discussed by [Ben Haha et al., 2010] the detailed evaluation of suitable solvents is a rather time-consuming procedure. Further experiments in this regard might reveal the suitability of the EDTA/NaOH solvent for the used glasses in more detail.

5.3 Glass reaction

5.3.1 Glass reaction in dissolution, model systems and blended cements

In Figure 5.9b the calculated amount of glass reacted in the blended cements is plotted in function of calculated amount of glass reacted in the pozzolanity tests both determined by bound water/mass balance at 91 d of hydration. The results show similar characteristics as the dissolution experiments, i.e. a low degree of reaction was obtained for the Si-rich fly ash glasses while the slag glasses showed a significant reaction. The offset of about 6 wt.% between the blended cements and the model systems might be caused by a higher water-to-solid ratio for the latter.

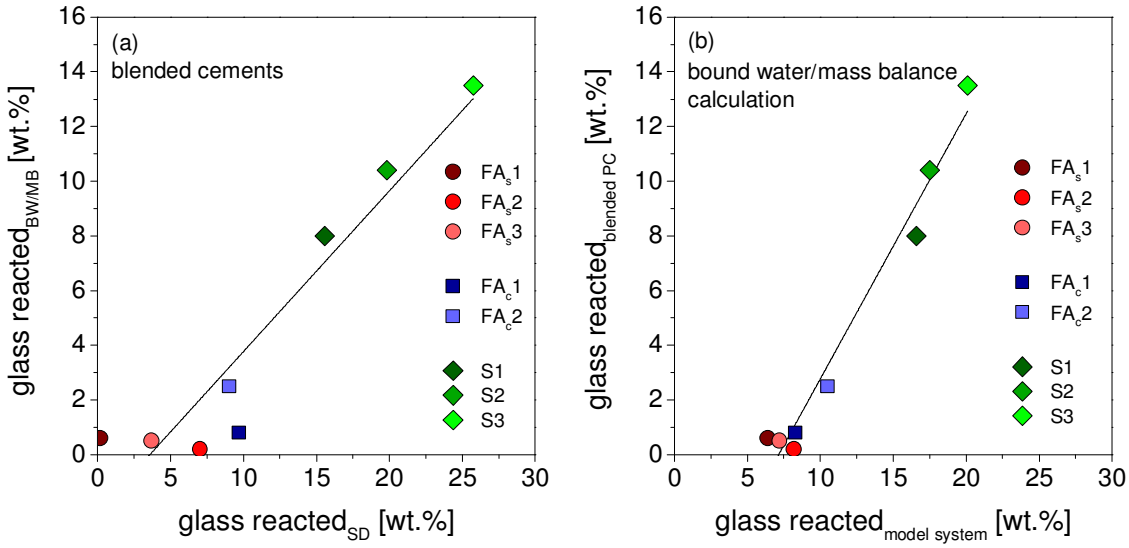

Figure 5.9: Calculated amount of glass reacted in the (a) blended cements depicted as bound water/mass balance approach vs. EDTA/NaOH selective dissolution and (b) for blended cements vs. model systems determined by bound water/mass balance. All values for samples hydrated for 91 d. BW/MB = bound water/mass balance, SD = selective dissolution.

5.3.2 Effect of glass composition

A comparison of the degree of glass reacted calculated for all applied methods plotted in function of NBO/T is provided in Figure 5.10. These general trends also give support to the calculation strategy for NBO/T, i.e. assigning 92% of Al_2O_3 to NWM. Only the results for the model systems obtained in the selective dissolution experiments show a different behavior (c.f. Appendix 4).

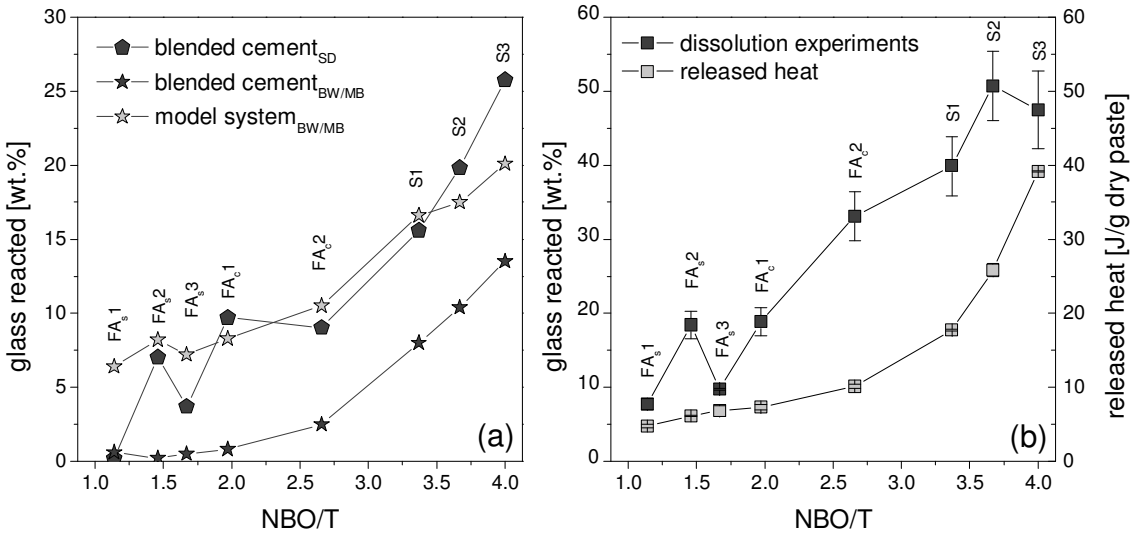

Figure 5.10: (a) Estimated amount of glass reacted as a function of NBO/T depicted for selective dissolution experiments and bound water/mass balance calculations for model systems and blended cements after 91 d of hydration. (b) Amount of glass reacted calculated for dissolution experiments in diluted systems and released heat for model systems, both at 7 d of reaction/hydration. SD = selective dissolution (EDTA/NaOH), BW/MB = bound water/mass balance approach.

5.4 Conclusions

The present work shows that the chemical composition and thereby the degree of polymerization of the glass network is a primary factor affecting the reactivity of glasses in high alkaline environments.

i Dissolution experiments in diluted suspensions and investigations on model systems containing portlandite and calcite showed the same trend. Dissolution or reactivity increases with decreasing polymerization of the glass network, i.e. Si-rich fly ash glasses show the lowest reactivity and blast-furnace slag glasses show the highest reactivity while Ca-rich fly ash glasses are located in between. The data indicate that not only higher quantities of CaO but also of Al_2O_3 increased the reaction of the glasses.

ii Model systems based on $Ca(OH)_2$ and $CaCO_3$ can be used to study the glass reaction under less complex conditions as they are prevailing in Portland cement-based composite cements. The reactivity determined from total bound water content and thermodynamic calculations follows the same characteristics as the dissolution tests, although values are lower throughout caused by the different concentration gradients in the solution. The same trends of glass reaction as in simplified model systems are also observed in blended cements, although the progress of glass reaction is slower in the blended cements than in the model systems.

iii Applying the presented pozzolanity test in model systems, the degree of glass reaction in blended cements can be calculated using the amount of additional bound water with respect to an inert quartz reference. Results of both, model systems and blended cements, show a clear linear relation.

iv Selective dissolution experiments can be used to determine the degree of glass reaction in blended cement. However, a large scatter was present in the results obtained in the model systems.

Chapter 6

Hydration kinetics of quaternary pastes[14]

In contrast to well investigated ternary cements there is a lack of information on the behavior of quaternary blended Portland cement systems containing simultaneously clinker, blast-furnace slag, Si-rich fly ash and limestone. The phase composition of these systems is similar to Portland cement based composites including Si-rich fly ash or blast-furnace slag [Iñiguez Sánchez et al., 2011, Schöler et al., 2015]. Yet, the nature of such systems is very complex and consequently it is extremely difficult to gain adequate information on the occurring hydration mechanisms and to link them to the resulting properties of the binder. The before mentioned mineral additions show little reaction in the first hours of hydration. Despite this early inactivity these SCM exert influence on the hydration of Portland cements from the very beginning. The dilution of Portland cement with inert material leads to a higher effective water-to-cement ratio and provides additional specific surface for nucleation and growth of hydrate phases. These mechanisms that promote the reaction of OPC are known as "filler effect" as discussed in detail in Chapter 2. Later on a chemical reaction occurs depending on the type of SCM present. Both effects contribute to the hydration in blended systems. In order to understand interactions of different SCM in multi-component cements knowledge on the kinetic behavior of such systems is needed.

In this chapter investigations of hydration kinetics of quaternary cement pastes with a water-to solid ratio of 0.5 containing limestone, blast-furnace slag and siliceous fly ash at 50 wt.% cement replacement are presented over a hydration time of up to 28 d. Varying limestone and fly ash additions were studied at two constant blast-furnace slag levels of 20 wt.% and 30 wt.%. The investigations were carried out by applying isothermal conduction calorimetry and chemical shrinkage experiments at 20 °C. In addition compressive strength was measured on mortar samples in order to correlate the kinetic behavior and thereby the influence of SCM with strength development.

6.1 Experimental

For detailed information on the chemical and mineralogical compositions as well as physical properties of the raw materials from batch 1 and the mix design of the matrix under

[14] An extended version of this chapter will be submitted as a manuscript to Materials and Structures as: Hydration kinetics of quaternary Portland cement blends containing blast-furnace slag, Si-rich fly ash and limestone, A. Schöler, B. Lothenbach, F. Winnefeld

investigation it is referred to 3.1 and 3.3. This also applies for in-depth considerations on the used analytical techniques.

6.2 Results and discussion

6.2.1 Effect of blast-furnace slag and quartz on heat development

The development of the specific heat flow for neat PC as well as for quartz-blended PC and a mixture of blast-furnace slag and quartz is shown in Figure 6.1. For a comparison of different filler materials similar PSD is required (Figure 3.1) as higher fineness can exert significant influence on the heat flow characteristics [Dittrich et al., 2014]. As described earlier one of the main characteristics of the filler effect is a higher effective water-to-cement ratio. In neat PC pastes higher water-to-cement ratios lead to slower development of the specific heat flow within the acceleration period [Danielson, 1960]. A slight decrease of the maximum heat flow at the end of the acceleration period can be observed with increasing water-to-cement ratio [Gruyaert et al., 2010, Kirby and Biernacki, 2012] (cf. Chapter 4). In contrast to this consideration, the investigated systems that were blended with SCM, which react little in the first 24 h of hydration, do not show significant difference in the acceleration period compared to neat PC. Except for slight differences in the duration and the minimum heat flow during the dormant period, the blended systems and the neat PC show an almost similar progression of the first increasing branch that is associated with the silicate reaction. Accordingly the additional specific surface that is provided for nucleation and growth of hydrates can compensate for the higher effective water-to-cement ratio. For the neat PC a shoulder is visible at 12 h. This is due to the second C_3A reaction that starts when all calcium sulfates are consumed. The weakly defined character of this shoulder corresponds to the low C_3A content of the PC. For the blended systems it has to be taken into account that they are all adjusted to a total SO_3-level of 3 wt.%. At a cement replacement of 50 wt.% this increases the SO_3 content to 6 wt.% with respect to the OPC. This higher sulfate content in the cement shifts the second C_3A reaction to later times in the blends where it is visible as small shoulder at 16 h. As the sulphate depletion peak becomes less distinct with increasing SO_3/Al_2O_3 ratio [Quennoz et al., 2011] it is not very pronounced in the blended systems.

The cumulative heat for the before discussed systems is given in Figure 6.2. The blends start to release more heat compared to the neat PC at 16 h as the higher effective water-to-cement ratio promotes the clinker reaction. At 36 h the heat release of the quartz blend becomes less steep and proceeds parallel to the neat PC from 48 h on. This indicates that the quartz exclusively acts as filler and does not react itself. In addition to the filler effect a contribution of the blast-furnace slag can be obtained from 36 h on for the blast-furnace slag/quartz blend when the system starts to release more heat than the quartz blend. The blast-furnace slag reaction is also indicated by the steeper increase of the blast-furnace slag/quartz blend compared to the quartz blend from 48 h on.

6.2.2 Effect of fly ash and limestone on heat development

Figure 6.3 presents the development of specific heat flow of samples with a blast-furnace slag share of 30 wt.% as well as for samples incorporating only quartz or quartz and blast-furnace slag as cement substituting material. Only one of the two measurements

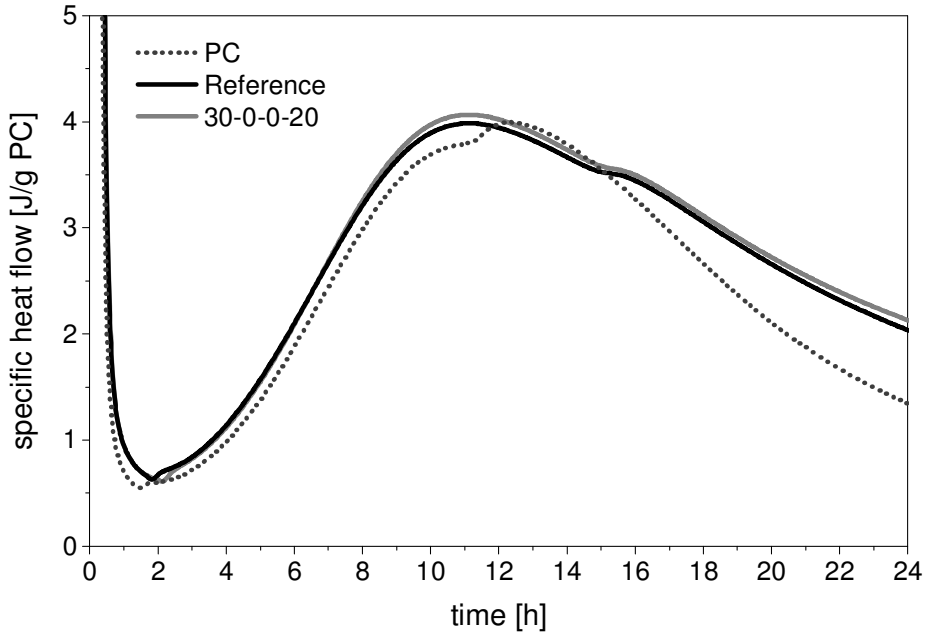

Figure 6.1: Influence of PC replacement by quartz or quartz and blast-furnace slag on the specific heat flow. All data is normalized to the mass of PC in the systems. Sample code: BFS-FA-LS-Qz.

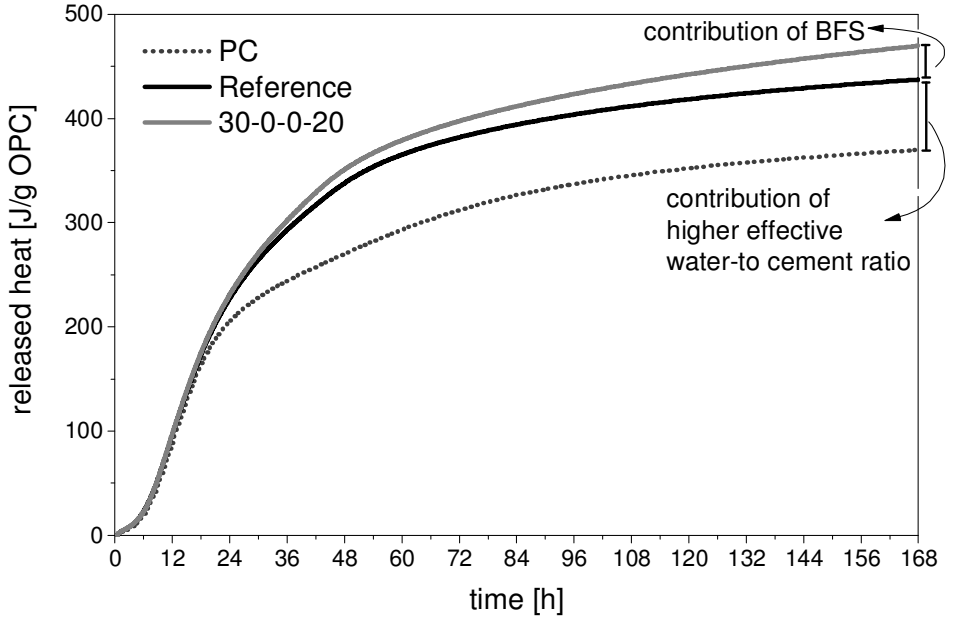

Figure 6.2: Influence of PC replacement by quartz or quartz and blast-furnace slag on released heat. All data is normalized to the mass of PC in the systems. Sample code: BFS-FA-LS-Qz.

that were carried out for each system is depicted as the curves are superimposed by each other, representing a negligible standard deviation.

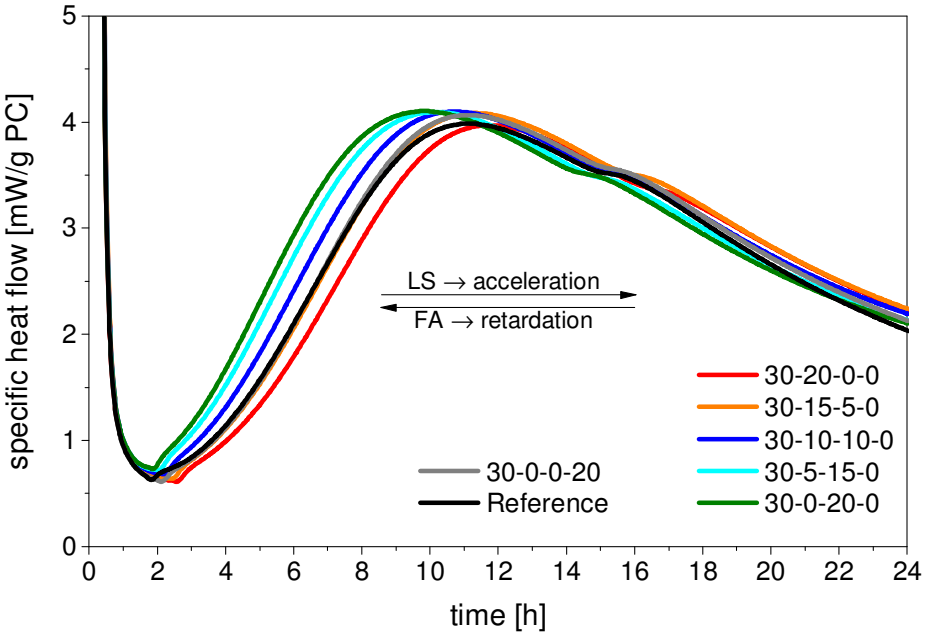

Figure 6.3: Specific heat flow of systems containing 30 wt.% blast-furnace slag. All data is normalized to the mass of PC in the systems. Sample code: BFS-FA-LS-Qz.

All systems show a similar progression within the induction period. In the subsequent acceleration period that is associated with a fast portlandite (CH) and C-S-H formation [Hesse et al., 2011] all systems show a steep increase. This increase becomes steeper with increasing limestone content in the first hours untill all curves progress parallel from about 6 h on. A clear acceleration of the reaction with increasing limestone content can be observed. At a low amount of 5 wt.% additional limestone the progression is equal to the quartz containing systems while higher additions lead to an acceleration. The maximum heat flow of the main reaction shows similar characteristics like the minimum. The soonest appearance is detectable for maximum limestone content at 10 h. Stepwise lower contents cause an increasing delay with the latest appearance at limestone absence at 12 h.

The deceleration period of the second reaction again proceeds parallel for all systems untill a small shoulder, representing the aluminate reaction, is reached between 14 h and 17 h with the same delay as observed before at the heat flow maximum caused by decreasing limestone content. The further progression of the descending branch is again parallel.

The overall observed accelerating effect of limestone or $CaCO_3$ on PC or C_3S has been reported by numerous researchers [Bonavetti et al., 2003, Péra et al., 1999, Vance et al., 2013]. Chapter 4 shows that this effect is related to an increased C-S-H nucleation on limestone which results in a higher degree of undersaturation with respect to C_3S and thus to a faster alite reaction. Calcite itself only reacts after the depletion of all sulfates which depends on the Al_2O_3/SO_3 ratio and happens at about 1 d as has been shown by [Lothenbach et al., 2008a]. The sulfate depletion in all investigated systems in this study appears after the second maximum within the silicate reaction. Consequently the

increasing acceleration with increasing limestone content has to be related to the effect of nucleation on the limestone surface. Analysis of the pore solution indicate an increase of calcium and a decrease of silicon and the pH in presence of more calcite. These changes are mirrored in a lower degree of oversaturation with respect to C-S-H due to better nucleation. This also leads to a faster alite reaction [Zajac et al., 2014].

i) Limestone particles offer additional nucleation sites for heterogeneous nucleation of hydrate phases after the first day of hydration.

ii) In a chemical reaction proceeding at ages later than 24 h limestone serves as a reactant for alumina that is mainly provided by C_3A dissolution to form hemi- and monocarboaluminate. A resulting beneficial effect is the indirect stabilization of ettringite [Bonavetti et al., 2001]. As this reaction is limited by the availability of alumina [Zajac et al., 2014], excess limestone will not further react and serve only as inert filler. However, the very fast reaction of C_3A is delayed and controlled by the sulfate set regulators and a limited amount of alumina is present in the pore solution [Lothenbach et al., 2008a] at early ages.

In contrast to the accelerating effect of limestone a slight delay of about 30 min was detected at a maximum fly ash content of 20 wt.%. Most possibly the negatively charged fly ash surface at high pH leads to chemisorption of Ca^{2+} ions on the surface of the fly ash [Fajun et al., 1985, Ogawa et al., 1980, Dittrich et al., 2014].

Figure 6.4 depicts the cumulative heat of hydration. Up to 30 h the heat release is equal for all systems. Between 30 h and 48 h some very slight differences are noticeable that result from the shifted main reactions (Figure 6.3). Thereafter all curves representing the systems in absence of quartz are superimposed by each other. The enlarged excerpt of Figure 6.4 reveals that the blast-furnace slag increases the released heat by 30 J/g compared to the sample only containing quartz. Fly ash, limestone or mixtures thereof lead to another contribution of up to 15 J/g. However, the differences are very small. Due to these very slight variations it is not possible to identify a specific trend concerning the actual composition of the systems.

As the observed differences of systems with different blast-furnace slag content are very small and do not alter the results of the calorimetric experiments qualitatively, only systems incorporating 30 wt.% blast-furnace slag are discussed in the foregoing. Additionally, Figure 6.5 gives information on the effect of changes in the blast-furnace slag content. At higher blast-furnace slag content the onset of the acceleration period appears slightly earlier independent from the fly ash/limestone content (Figure 6.5a). This contribution can also be seen in terms of the released heat at seven days of hydration (Figure 6.5b).

6.2.3 Long term effects

To investigate the progression of hydration for longer hydration times of up to 28 d chemical shrinkage was measured (Figure 6.6). Similar to released heat (Figure 6.4) the quartz reference shows higher shrinkage than the neat PC due to the filler effect. All other systems behave in the same way up to 36 h and show superposition. Between 1.5 d and 7 d the superposition more or less persists except for the system containing only quartz as cement substitution, which shows lower shrinkage. This indicates a significant reaction of blast-furnace slag, fly ash, limestone or mixtures thereof in addition to the

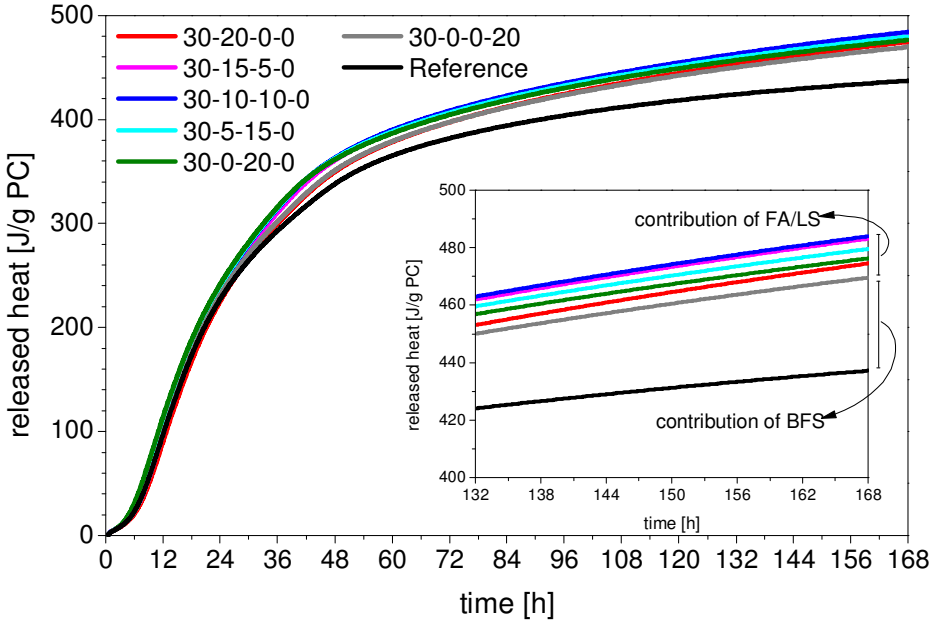

Figure 6.4: Released heat of systems containing 30 wt.% blast-furnace slag. All data is normalized to the mass of PC in the systems. Sample code: BFS-FA-LS-Qz.

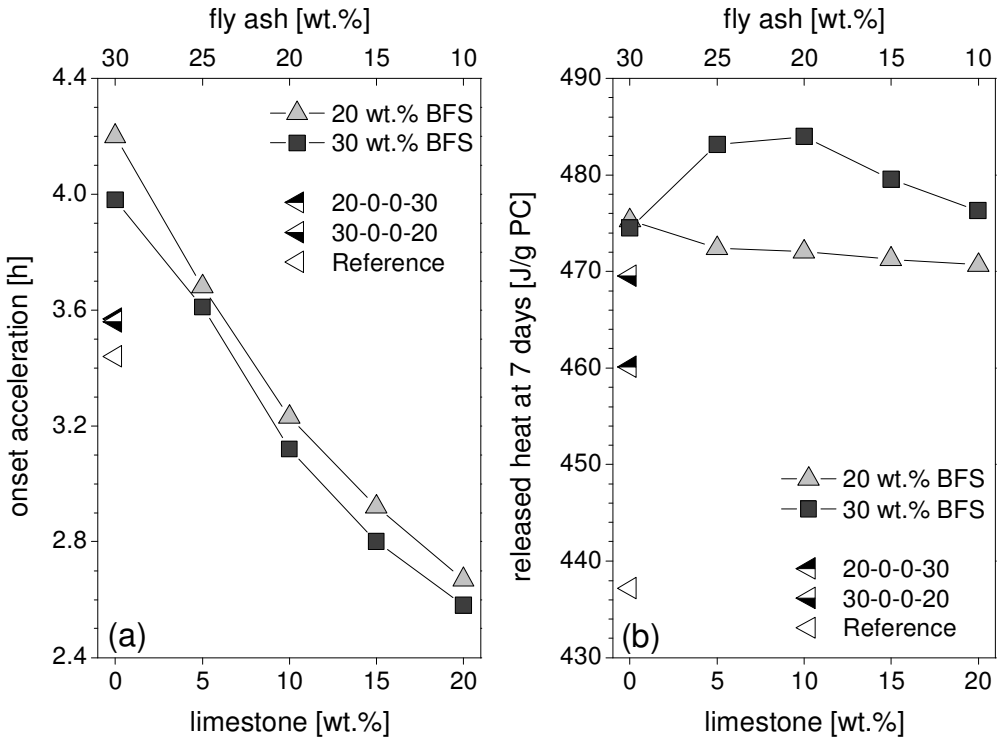

Figure 6.5: Onset of the acceleration period (a) and total released heat after seven days of hydration (b) depicted as a function of additional limestone/fly ash content for both blast-furnace slag levels. Released heat is normalized to the mass of PC in the systems. Note that the fly ash values correspond to samples including 20 wt.% blast-furnace slag. For samples containing 30 wt.% blast-furnace slag the fly ash content is 10 wt.% lower as indicated on the abscissa. Sample code: BFS-FA-LS-Qz.

filler effect that is generated by the presence of inert quartz. The shrinkage behavior in the first seven days of hydration is in good correlation with released heat calculated from the calorimetric experiments (Figure 6.4). At later ages from 7 d on the sample containing only quartz shows only a slight increase in shrinkage and comes close to stagnation from 16 d on. The cement reacts faster than the investigated SCM and the higher effective water-to-binder ratio and the increased nucleation space even accelerate this reaction. All other systems are still located close to each other with a parallel progression in shrinkage. Despite the small standard deviation it is not possible to see clear trends or differences. At the end of the chemical shrinkage experiment at 28 d the main statement is the same than with the results of released heat at seven days (Figure 6.4). Blast-furnace slag is clearly beneficial while a slight further contribution by fly ash, limestone or mixtures thereof is detectable with differences that are too small to allow distinction between the different SCM.

A correlation between chemical shrinkage and released heat up to 7 d is depicted in Figure 6.7. The contributing effect of higher blast-furnace slag contents is barely visible. Only the quartz-containing systems are located at lower values compared to all other systems while quartz in combination with blast-furnace slag increases both, released heat and shrinkage. Fly ash and/or limestone in the presence of blast-furnace slag leads to values located close to each other. A clear distinction is not possible.

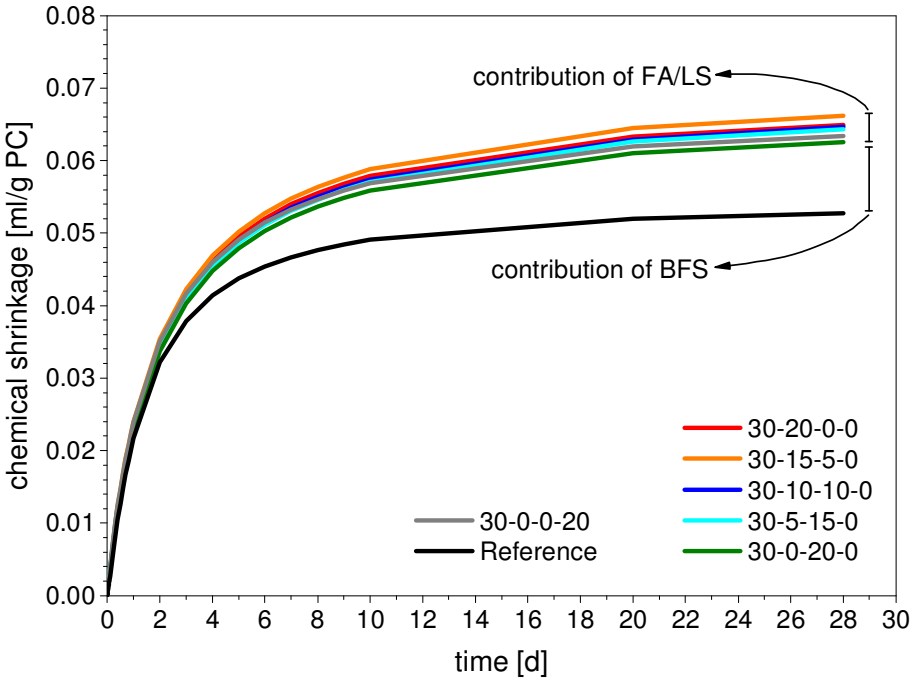

Figure 6.6: Chemical shrinkage of systems incorporating 30 wt.% blast-furnace slag. Note that all data is normalized to the mass of PC in the systems. Sample code: BFS-FA-LS-Qz.

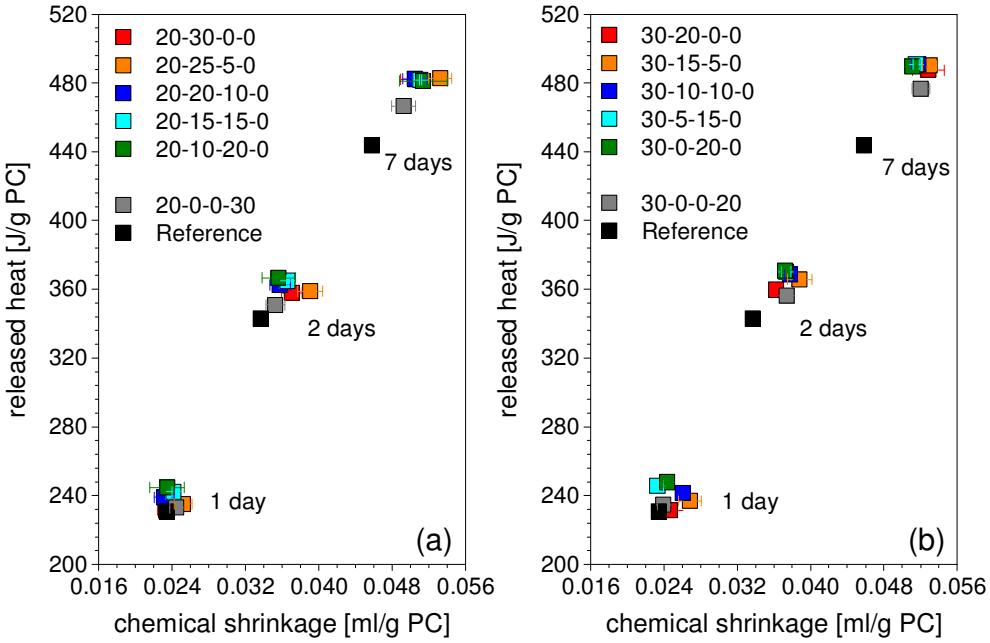

Figure 6.7: Correlation of chemical shrinkage with released heat at 1, 2 and 7 d of hydration for the complete matrix under investigation. Note that all data is normalized to the mass of PC in the systems. Sample code: BFS-FA-LS-Qz.

6.3 Compressive strength

The results of the compressive strength testing for both blast-furnace slag levels at 2 d, 7 d and 28 d are depicted in Figure 6.8. At 2 d all systems reach values between 16 MPa and 17 MPa independent from the blast-furnace slag level or the fly ash/limestone content. As the hydration proceeds, compressive strength is increased by approximately 11 MPa at seven days where all systems are located between 27 MPa and 28 MPa. At 28 d of hydration the strength increases from absence of limestone to limestone addition (or fly ash substitution) of 5 wt.%. Further addition of LS or substitution of fly ash, respectively, leads to a decrease in strength. A similar optimum of 5 wt.% limestone in PC or fly ash blended PC has been reported by [De Weerdt et al., 2011c, Tsivilis et al., 2002]. While the progression is the same for both blast-furnace slag levels from a qualitative point of view the blast-furnace slag content itself leads to quantitative differences. At the higher level of 30 wt.% slightly higher compressive strength is reached by about 2 MPa for all systems after 28 d of hydration. This can be related to a faster reaction of the blast-furnace slag compared to the fly ash. This beneficial effect can be seen with the quartz containing systems as well. Generally speaking, all systems, except the quartz references, fulfil the requirements of strength class 42.5 N according to EN 197-1. The hindrance in reaching the next higher class (42.5 R) is based on the 2 d values. While 42.5 R requires minimum 28 d strength of 40 MPa, the minimum 2 d strength is 18 MPa. Accordingly the main challenge in improving multi component cements with respect to existing standards is to increase early age strength.

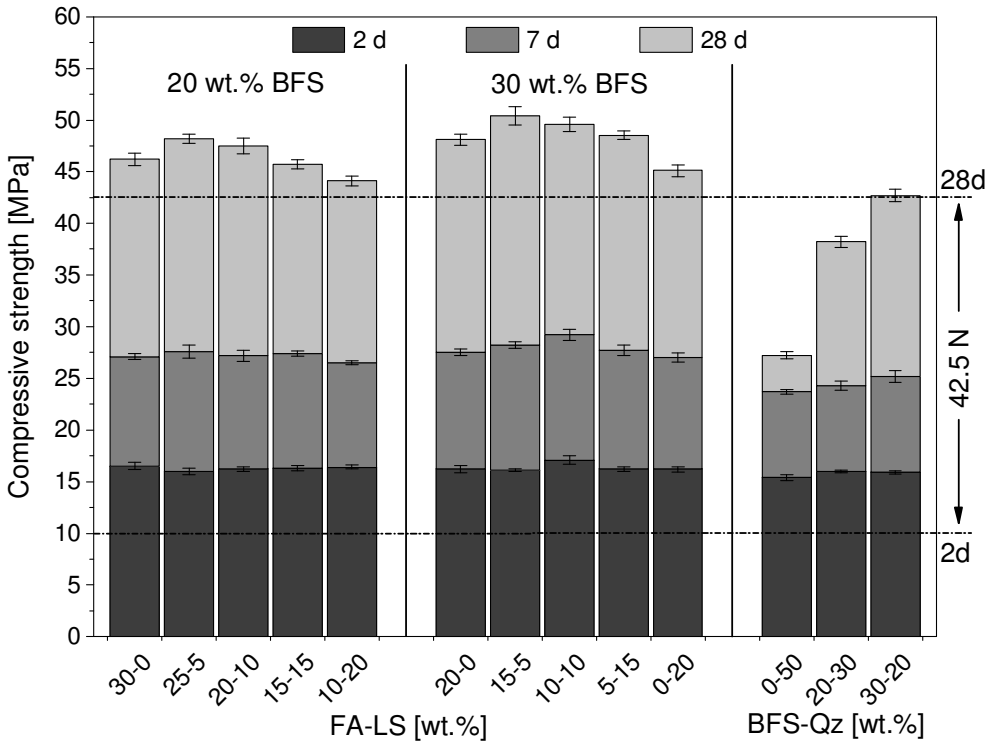

Figure 6.8: Compressive strength at 2, 7 and 28 d of hydration for systems containing 20 wt.% and 30 wt.% blast-furnace slag.

Figure 6.9a and Figure 6.9b correlate the calculated released heat with compressive strength. At 2 d the differences in released heat do not exert influence on the strength development. After 7 d days the quartz containing samples show lower released heat at lower strength. All other systems are close together by means of released heat while minor additions of limestone slightly improve compressive strength.

The correlation of chemical shrinkage with strength development (Figure 6.9c and Figure 6.9d) shows that the detected shrinkage at 2 d is not influenced by the composition of the systems. At 2 d the quartz containing samples show lower values for both, shrinkage and strength while blast-furnace slag addition improves both values slightly. All other systems are located close together, partially superimposed. After 28 d the sample containing only quartz besides PC is still located at the bulk of the seven day values but the blast-furnace slag addition does now clearly contribute to strength

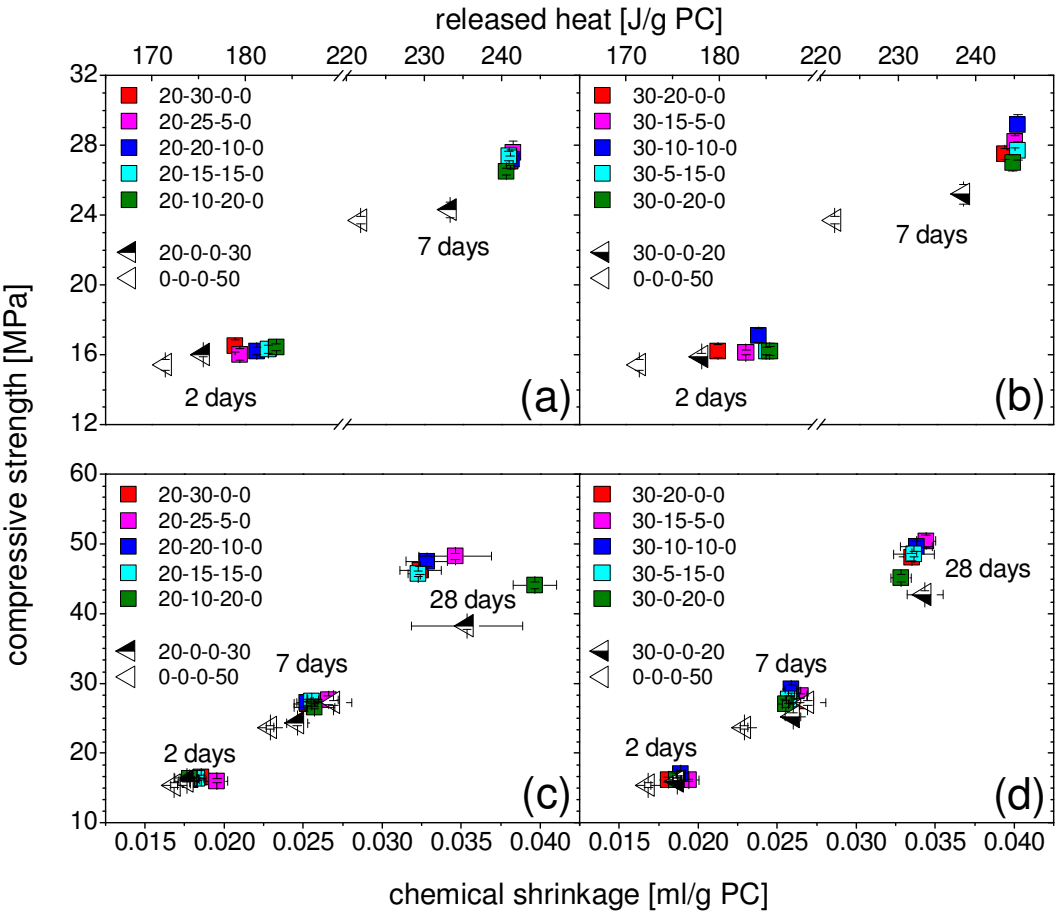

Figure 6.9: Correlation of released heat (a), (b) and chemical shrinkage (c), (d) with compressive strength for systems containing 20 and 30 wt.% blast-furnace slag. Note that all values are normalized to the mass of PC in the systems. Sample code: BFS-FA-LS-Qz.

6.4 Conclusions

This study investigates the hydration kinetics of quaternary cements containing PC, blast-furnace slag, fly ash and limestone simultaneously at high cement substitution of 50 wt.% and a water-to-binder ratio of 0.45. The analysis of the acquired results summarizes as follows:

(i) Compared to a system incorporating only Portland cement and quartz in equal shares, additions of blast-furnace slag lead to acceleration of the hydration in the first 24 h as observed by both, released heat and chemical shrinkage.

(ii) In addition to the contribution of blast-furnace slag complete substitution of quartz by limestone cause further acceleration. On the contrary the complete quartz substitution by fly ash leads to retardation. The acceleration is due to the limestone as its surface provides excellent conditions for the C-S-H nucleation such that the number of C-S-H nuclei is significantly higher as on other SCM. This leads to undersaturation with respect to C_3S and to oversaturation with respect to C-S-H. The

more this effect is pronounced the faster the alite dissolution. Mixtures of limestone all show a faster reaction compared to only fly ash while this effect depends on the actual content of both materials. However, the differences in the systems are too small to be significant which does not allow for clear distinction between the contributions of the different SCM.

(iii) In terms of strength development maximum strength is reached at 5 wt.% additional limestone. Yet, it is only present at 28 d. This maximum is visible at both blast-furnace slag levels while the higher one leads to a slight strength increase. All systems fulfil the requirements of strength class 42.5 N according to EN 196-1.

(iv) By applying isothermal conduction calorimetry to cement pastes it is possible to get insight to the early hydration reaction. Furthermore the gained data provide possibilities to predict the development of compressive strength within certain limits. Chemical shrinkage experiments are useful to cross-check the calorimetric experiments and to obtain data at later ages.

Concluding it can be stated that it is possible to make use of blast-furnace slag, fly ash and limestone simultaneously to produce quaternary binders without a decline in mechanical properties. However, quaternary systems are not well investigated at present and it is indispensable to gain deeper knowledge on the actual hydration reactions and the influence of the chemical and mineralogical composition of the raw materials. With a better knowledge thereof mechanical properties of multicomponent cements can be further improved.

Chapter 7

Hydrate assemblage of quaternary pastes[15]

New cement compositions that are already included in the prenorm prEN 197-1:2014 (CEM II/C , CEM VI) are ternary systems containing clinker, limestone and either blast-furnace slag, fly ash or pozzolans. In contrast, quaternary systems including three SCM simultaneously are not considered. However, such systems have similar composition in terms of phase composition [Iñiguez Sánchez et al., 2011] and might therefore be promising compositions. The investigations presented in this chapter aim to contribute to this purpose by investigating quaternary Portland cement systems containing blast-furnace slag, type V fly ash and limestone and the relationship between the types and contents of SCM and the hydrate assemblage. Data were collected at up to 182 d of hydration by applying thermogravimetric analysis and X-ray diffraction techniques. In addition thermodynamic modeling was used to calculate the total volume of hydrates. The results were correlated with strength tests in order to show the relation of the phase assemblage and the volume of hydrates on mechanical properties.

7.1 Experimental

These investigations were carried out with the same materials that were used for investigations of the kinetic behavior as discussed in the previous chapter. Chemical and mineralogical compositions as well as physical properties of the used raw materials from batch 1 are given in 3.1. The mix design as presented in Table 3.9 was not altered. The quartz containing reference samples were not considered in this study

For investigations of cement pastes, paste samples were prepared with a water-to-binder ratio of 0.45. Investigations were carried out using thermogravimetric and X-ray diffraction techniques. The investigations were supplemented by thermodynamic calculations. For detailed information on the analytical strategies and techniques used it is referred to 3.3.

[15] An extended version of this chapter has been published as: A. Schöler, B. Lothenbach, F. Winnefeld, M. Zajac, Hydration of quaternary Portland cement blends containing blast-furnace slag, siliceous fly ash and limestone powder, Cement & Concrete Composites 55 (2015) 374-382.

7.2 Results and discussion

7.2.1 Characterization of the hydrate assemblage

7.2.1.1 Thermodynamic modeling

Thermodynamic modeling was applied to investigate the influence of limestone on the hydrate assemblage (Figure 7.1). To illustrate the effect of limestone a CO_2-free PC containing 30 wt.% fly ash and 20 wt.% blast-furnace slag was chosen as starting composition. In the absence of $CaCO_3$, C-S-H and monosulfate are calculated to be the main hydrates in a ternary system with 20 wt.% blast-furnace slag.

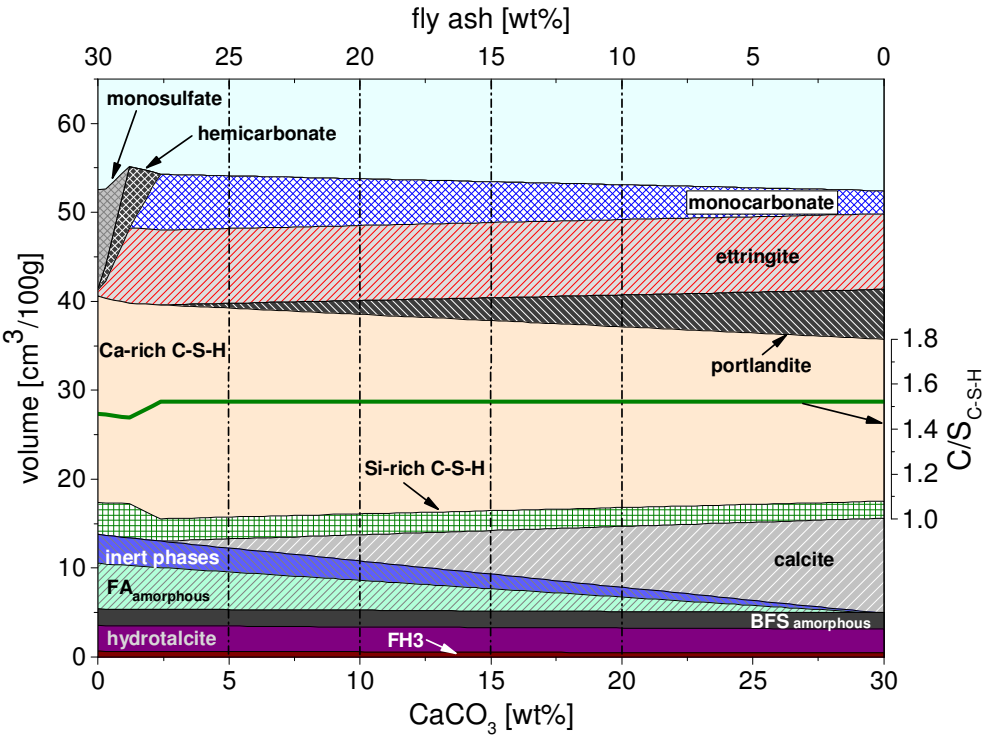

Figure 7.1: Hydrates as predicted by thermodynamic modeling as a function of $CaCO_3$/fly ash content at 20 wt.% blast-furnace slag. The dash-dot lines represent the compositions of the systems under investigation. Volume expressed as $cm^3/100g$ unhydrated binder.

The partial replacement of fly ash by $CaCO_3$ is calculated to lead to the consumption of portlandite as the SiO_2 present in the fly ash will react with $Ca(OH)_2$ according to Eq.(7.1):

$$yCa(OH)_2 + SiO_2 + xH_2O \rightarrow yCaO \cdot SiO_2 \cdot (y+x)H_2O \tag{7.1}$$

The complete replacement of fly ash by $CaCO_3$ leads to the presence of more portlandite as no pozzolanic reaction occurs.

A replacement of fly ash by $CaCO_3$ leads to the formation of hemicarbonate, monocarbonate and more ettringite instead of monosulfate according to Eq.(7.2) and Eq.(7.3) (additional information on the stoichiometry of AFm and AFt phases is presented in Table 7.1).

$$3C_4A\overline{S}H_{12} + CH + C\overline{C} + 19H \rightarrow C_6A\overline{S}_3H_{32} + 2C_4A\overline{C}_{0.5}H_{12} \quad (7.2)$$
$$(3 \cdot 309cm^3 + 33cm^3 + 37cm^3 \rightarrow 707cm^3 + 2 \cdot 285cm^3;\ \Delta V = 28vol.\%)$$

$$3C_4A\overline{S}H_{12} + 2C\overline{C} + 18H \rightarrow C_6A\overline{S}_3H_{32} + 2C_4A\overline{C}H_{11} \quad (7.3)$$
$$(3 \cdot 309cm^3 + 2 \cdot 37cm^3 \rightarrow 707cm^3 + 2 \cdot 262cm^3;\ \Delta V = 23vol.\%)$$

Table 7.1: Compositions of AFm and AFt phases as used in the thermodynamic calculations..

Mineral	Reaction
Ettringite	$Ca_6Al_2(SO_4)_3(OH)_{12}{\cdot}26H_2O \rightarrow 6Ca^{2+}{+}2Al(OH)_4^-{+}3SO_4^{2-}{+}4OH^-{+}26H_2O$
Monosulfate	$Ca_6Al_2(SO_4)(OH)_{12}{\cdot}6H_2O \rightarrow 4Ca^{2+}{+}2Al(OH)_4^-{+}SO_4^{2-}{+}4OH^-{+}6H_2O$
Hemicarbonate	$Ca_4Al_2(CO_3)_{0.5}(OH)_{13}{\cdot}5.5H_2O \rightarrow 4Ca^{2+}{+}2Al(OH)_4^-{+}0.5CO_3^{2-}{+}5OH^-{+}5.5H_2O$
Monocarbonate	$Ca_4Al_2(CO_3)(OH)_{12}{\cdot}5H_2O \rightarrow 4Ca^{2+}{+}2Al(OH)_4^-{+}CO_3^{2-}{+}4OH^-{+}5H_2O$

Numbers in parentheses show the molar volume of solids and the volume gain due to the reaction with respect to the reactants. Data on the density and the molar volume of phases considered in the thermodynamic calculations are given in Table 3.12. In the presence of more $CaCO_3$, monocarbonate is stable according to Eq.(7.3). From the diffractograms given in Figure 7.4 it can be seen that both, hemicarbonate and monocarbonate are present at 182 d days of hydration. In experimental studies, initially the formation of hemicarbonate is observed as the formation of monocarbonate is kinetically slow [Zajac et al., 2014]. In the long term a transformation of hemicarbonate to monocarbonate is observed. These effects result in a maximum volume of stable hydrates at about 3 wt.% $CaCO_3$ content, similar to the effects observed for ternary PC-blast-furnace slag-fly ash and PC-fly ash-limestone systems [Menendez and Irassar, 2003, De Weerdt et al., 2011a]. Investigations of PC-limestone and PC-fly ash-limestone cements have shown that this volume maximum correlates with a maximum of compressive strength [Carrasco et al., 2005, De Weerdt et al., 2011b, Moesgaard et al., 2011, Damidot et al., 2011]. This positive effect is enhanced by increasing Al_2O_3 content as more ettringite can be stabilized by $CaCO_3$. Thus, the partial substitution of PC by blast-furnace slag and fly ash should increase the positive effect of the presence of $CaCO_3$. However, the contribution of blast-furnace slag and fly ash to the amount of Al_2O_3 that is available to form monocarbonate and to stabilize ettringite is limited as both materials exhibit slower reaction rates than PC. Furthermore, the used blast-furnace slag has a low Al_2O_3 content. After one year, the reaction of approximately 25 to 30 wt.% of fly ash and 70 wt.% of blast-furnace slag has been reported [Ben Haha et al., 2010, De Weerdt et al., 2012, Deschner et al.,

2013, Kocaba et al., 2012, Lothenbach et al., 2012]. Considering the only partial reaction of fly ash and blast-furnace slag, blast-furnace slag contributes approx. 6 wt.% and fly ash approx. 8 wt.% of reactive Al_2O_3. Thus, their presence increases the amount of available Al_2O_3 in the long term.

Thermodynamic modeling was also used to study the influence of different fractions of fly ash and blast-furnace slag on the hydrate assemblage. In a ternary system containing 50 wt.% of blast-furnace slag and 5 wt.% of $CaCO_3$ as shown on the left hand side of Figure 7.2, the main hydrates are calcium silicate hydrate (C-S-H), ettringite, monocarbonate, hydrotalcite and portlandite. Successive replacement of blast-furnace slag by fly ash exerts different effects:

i) The total volume of hydrated binder and the amount of C-S-H is slightly reduced due to the lower degree of reaction of the fly ash compared to the blast-furnace slag.

ii) Decrease of the volume of portlandite caused by the pozzolanic reaction with the SiO_2 from the fly ash.

iii) The higher Al_2O_3 and the lower MgO content of the fly ash lead to an increase in monocarbonate and a decrease in hydrotalcite.

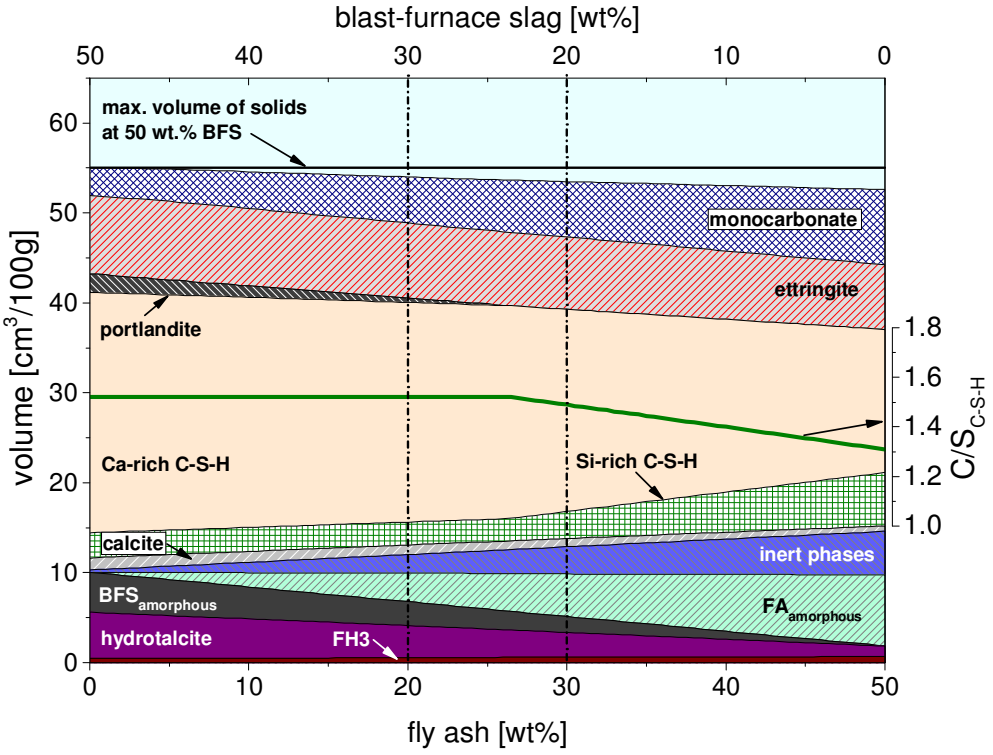

Figure 7.2: Changes in the total volume of hydrates as an effect of different additions of blast-furnace slag and fly ash in a quaternary OPC containing 5 wt.% $CaCO_3$. The dash-dot lines represent the two blast-furnace slag levels that were investigated. Volume expressed as $cm^3/100g$ unhydrated binder.

If a complete reaction of the binder would have been assumed a slightly higher total volume of hydrates would be obtained for the fly ash rich blends, mainly due to the formation of additional C-S-H. Furthermore the complete depletion of portlandite and the formation of strätlingite at high fly ash contents would be calculated as has been shown elsewhere [Lothenbach et al., 2011].

Thermodynamic modeling predicts no or very little portlandite, as a homogeneous system with C-S-H of C/S ~1.5 is predicted. In real systems generally the presence of significant quantities of portlandite is still observed while C-S-H with a more variable C/S from 1.2 to 1.6 is present [De Weerdt et al., 2011a, Deschner et al., 2012]. Due to inhomogeneities and a disconnected pore network portlandite can persist in some parts of the microstructure while in other areas a low C/S is present. SEM/EDX investigations in blended Portland cements showed a very inhomogeneous microstructure [De Weerdt et al., 2011a, Kocaba, 2009]; in some areas portlandite persisted while in others the C/S of the C-S-H equaled to 1.2. Such inhomogeneous distribution of the C/S cannot be captured by thermodynamic modeling.

In this study quaternary blends with two different blast-furnace slag levels were investigated as indicated in Figure 7.2. The calculated total volume of solids as shown in Figure 7.1 decreases only very slightly by 1 vol.% from 20 wt.% to 30 wt.% blast-furnace slag content. The corresponding changes in bound water, C-S-H and portlandite are calculated using GEMs as given in Table 7.2.

Table 7.2: Amount of bound water, C-S-H and portlandite at 20 and 30 wt.% blast-furnace slag and 30 and 20 wt.% fly ash, respectively. Calculated by thermodynamic modeling; referred to weight of dry hydrates. Data in [wt.%].

BFS content	30	20
Bound water	26.2	25.0
C-S-H	66.7	62.1
CH	1.0	0.0

7.2.1.2 Hydrates present

Results of TGA and XRD investigations at 182 d of hydration for selected samples containing 20 wt.% blast-furnace slag at different fly ash and limestone quantities are depicted in Figure 7.3 and Figure 7.4. In absence of limestone, the main phases detected by XRD and TGA are calcium silicate hydrate (C-S-H), ettringite, AFm phases (mainly hemicarbonate and a mixed AFm containing sulfate, carbonate and hydroxide [Pöllmann, 2006]) and portlandite. The presence of limestone leads to the formation of hemicarbonate and monocarbonate instead of the monosulfate phases [Lothenbach et al., 2008a]. Furthermore slightly more ettringite is detected as can be seen from the TGA data. XRD data recorded at different sample ages (cf. Appendix 7) show that during the first weeks only hemicarbonate is observed, while hemi- and monocarbonate are both present at later ages. However, from a thermodynamic point of view only monocarbonate is stable. This initial kinetic hindrance of the monocarbonate formation has previously been reported, e.g. by [Lothenbach et al., 2008a, Zajac et al., 2014]. The formation of mono-

carbonate and hemicarbonate prevents the monosulfate formation, indirectly stabilizes ettringite (Figure 7.1) and is the cause for the increased ettringite content as can be seen from Figure 7.3. The slight increase of portlandite in the presence of 5 wt.% and 15 wt.% limestone is due to the simultaneous reduction of the fly ash content whereby less portlandite is consumed to form C-S-H (see Figure 7.5).

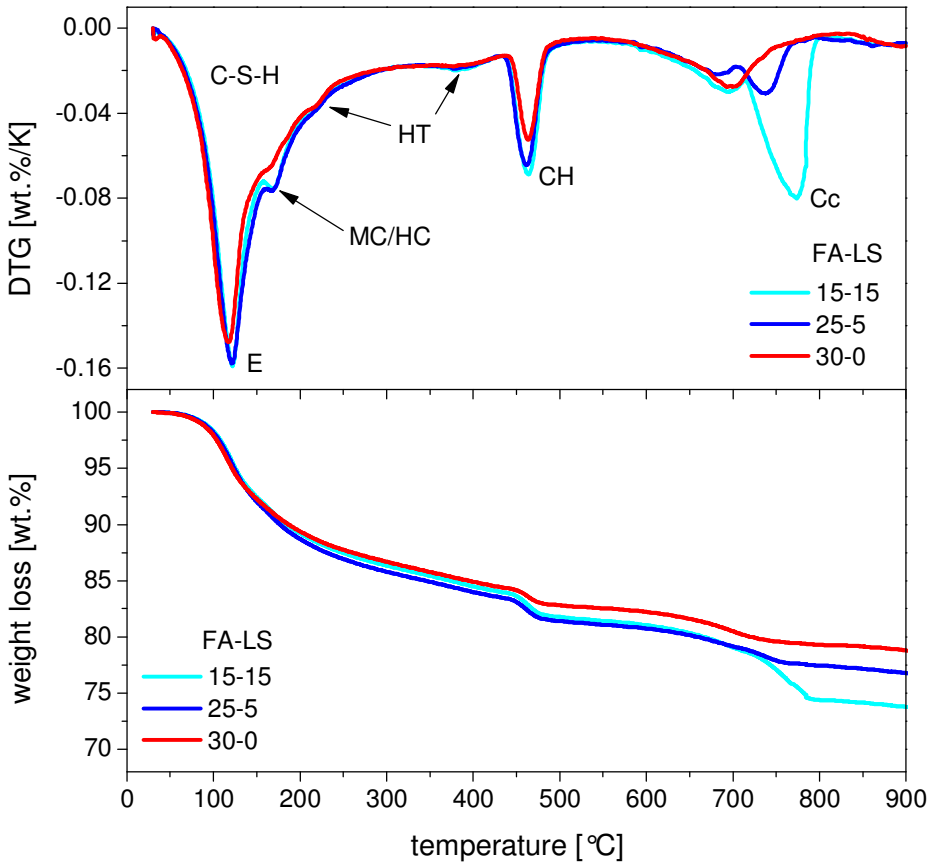

Figure 7.3: TGA curves for samples containing 20 wt.% blast-furnace slag at 182 d of hydration. Cc - calcite, CH - portlandite, C-S-H - calcium silicate hydrate, E - ettringite, HC - hemicarbonate, HT - hydrotalcite, MC - monocrbonate. Sample code: FA-LS.

XRD experiments on systems containing 30 wt.% blast-furnace slag do not show differences to the data presented in Figure 7.4. As shown in Table 7.3 the bound water content increases up to 91 d in all systems. After 91 d and 182 d the total bound water content is comparable to calculated values (as given in Table 7.2). The samples with higher blast-furnace slag content have slightly more bound water in agreement with the modeling. This observation underpins the faster reaction of the blast-furnace slag. The portlandite content does not vary significantly between the two blast-furnace slag levels and does not indicate a strong influence of the fly ash used on the extent of the pozzolanic reaction.

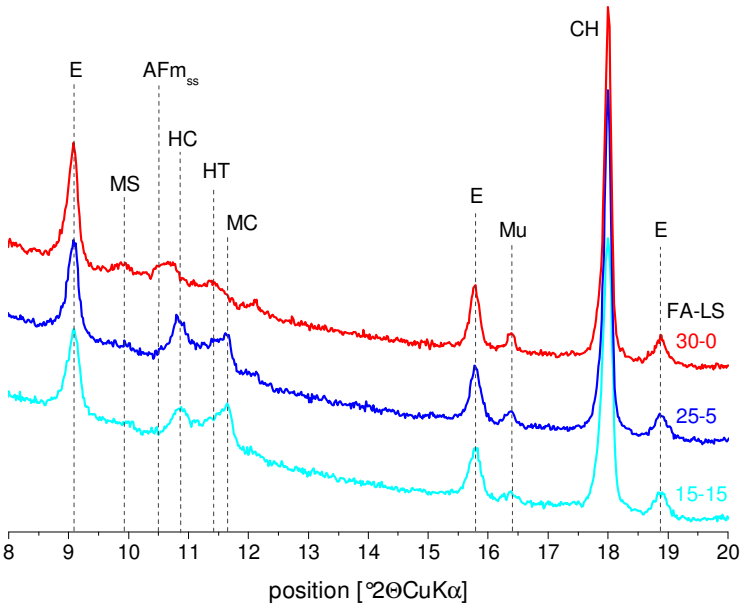

Figure 7.4: X-ray diffractograms of samples containing 20 wt.% blast-furnace slag and 30 wt.% fly ash or mixtures of fly ash and limestone at 182 d of hydration. AFm$_{ss}$ - solid solution of menicarbonate and OH^- substituted monosulfate, CH - portlandite, E - ettringite, HC - hemicarbonate, HT - hydrotalcite, MC - monocarbonate, MS - monosulphate, Mu - mullite.

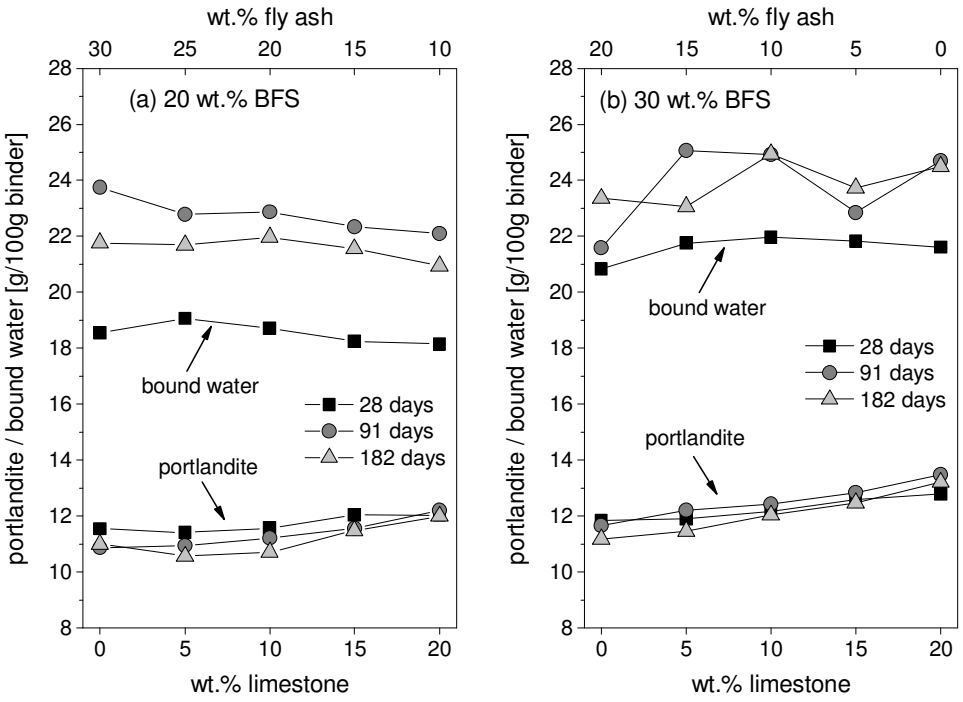

Figure 7.5: Content of bound water (excluding portlandite) and portlandite obtained from TGA for both blast-furnace slag levels of (a) 20 wt.% and (b) 30 wt.% at 28, 91 and 182 d of hydration. The relative error due to preparation and measurement is between ± 5% and 10%.

The portlandite content is slightly lower in the samples containing more fly ash which is in agreement with the calculated trends in Figure 7.1 and Figure 7.2. The absolute portlandite quantities determined by TGA decrease slowly with time but are considerably higher than the modeled ones even after 182 d. This could be related to a lower degree of fly ash reaction than assumed or also due to an inhomogeneous system with lower C/S ratio of C-S-H, as has been observed by [De Weerdt et al., 2011a, De Weerdt et al., 2011b].

Table 7.3: Bound water (excluding portlandite) and portlandite as calculated from TGA for ages from 1 d to 182 d of hydration. Data is given in [wt.%].

BFS-FA-LS	Time [d]	BW	CH	BFS-FA-LS	Time [d]	BW	CH
20-10-20	1	10.4	9.3	30-0-20	1	10.4	9.4
	2	14.9	11.6		2	15.0	11.7
	7	18.0	11.6		7	18.1	12.6
	28	18.1	12.0		28	21.6	12.8
	91	22.1	12.2		91	24.7	13.5
	182	20.9	12.0		182	24.5	13.2
20-15-15	1	10.8	9.1	30-5-15	1	10.5	9.1
	2	14.4	10.7		2	14.7	11.1
	7	17.3	11.0		7	18.5	12.6
	28	18.2	12.0		28	21.8	12.6
	91	22.2	11.6		91	22.8	12.8
	182	21.6	11.5		182	23.7	12.5
20-20-10	1	10.6	8.7	30-10-10	1	10.7	9.2
	2	14.5	11.1		2	14.5	11.3
	7	18.0	11.6		7	18.4	12.1
	28	18.7	11.6		28	22.0	12.2
	91	22.9	11.2		91	25.0	12.4
	182	22.0	11.7		182	25.0	12.0
20-25-5	1	10.5	8.9	30-15-5	1	10.5	9.3
	2	14.3	10.9		2	14.7	11.0
	7	18.2	11.5		7	19.3	12.3
	28	19.0	11.4		28	21.8	11.9
	91	22.8	11.0		91	25.1	12.2
	182	21.7	10.6		182	23.1	11.5
20-30-0	1	10.2	8.6	30-20-0	1	10.5	8.6
	2	14.8	10.8		2	14.6	10.9
	7	18.0	11.4		7	18.1	11.6
	28	18.6	11.5		28	20.8	11.8
	91	23.7	11.9		91	21.6	11.7
	182	21.8	11.0		182	23.4	11.2

7.2.2 Effect of total volume of hydrates on compressive strength

The development of compressive strength up to 28 d as shown in Figure 7.6 shows maximum values at 5 wt.% limestone content after 28 d for both blast-furnace slag levels. $CaCO_3$ is able to take part actively in the hydration reaction up to 2 to 3 wt.% as shown in the thermodynamic calculations presented in Figure 7.1. This chemical reaction of limestone has also been reported by [Lothenbach et al., 2008a, Bonavetti et al., 2001]. At higher shares the remaining calcite will only act passively as filler. The filler effect itself is characterized by supplying higher specific surface available for nucleation and a higher effective water-to-cement ratio [Bonavetti et al., 2001, Gutteridge and Dalziel, 1990a, Gutteridge and Dalziel, 1990b]. The amount of calcite that is able to react depends on the available Al_2O_3 and thereby on the present SCM and their composition.

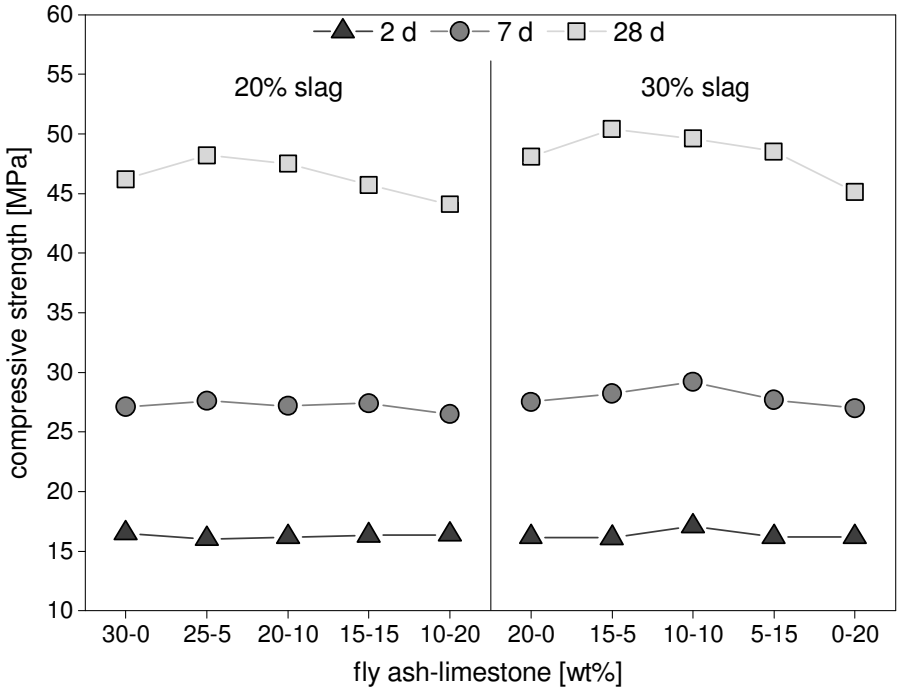

Figure 7.6: Compressive strength at 2 d, 7 d and 28 d of hydration for systems containing 20 wt.% and 30 wt.% blast-furnace slag.

The calculated effect of the blast-furnace slag and fly ash contents as a function of $CaCO_3$ on the total volume of solids is depicted in Figure 7.7. All systems blended with blast-furnace slag and/or fly ash show a slightly lower volume of solids compared to PC. Cement substitution by blast-furnace slag leads to slightly higher calculated volume of solids than substitution by fly ash due to the limited reactivity of the latter. When both materials are incorporated the volume of solids increases with increasing blast-furnace slag content. Blast-furnace slag can form significantly more C-S-H than fly ash due to its faster reaction. The Al_2O_3 available for reaction from the fly ash leads to more monocarbonate but this cannot compensate for the lower C-S-H content. The steeper decrease of the blast-furnace slag system that is visible from about 2 wt.% $CaCO_3$ originates from a decrease in blastfurnace slag content and thereby a decrease in hydrotalcite as well. The formation of hydrotalcite requires both Al_2O_3 and MgO. The first is provided by the fly ash and the latter by blast-furnace slag. Al_2O_3 is known to be preferably bound in

hydrotalcite [Ben Haha et al., 2011, Ben Haha et al., 2012]. As this phase remains constant in the fly ash containing systems a less steep decrease is visible that mainly results from a decrease in C-S-H with decreasing blast-furnace slag content. A slightly higher calculated total volume of solids with higher blast furnace slag content goes along very well with the slightly higher compressive strength observed for corresponding systems Figure 7.7.

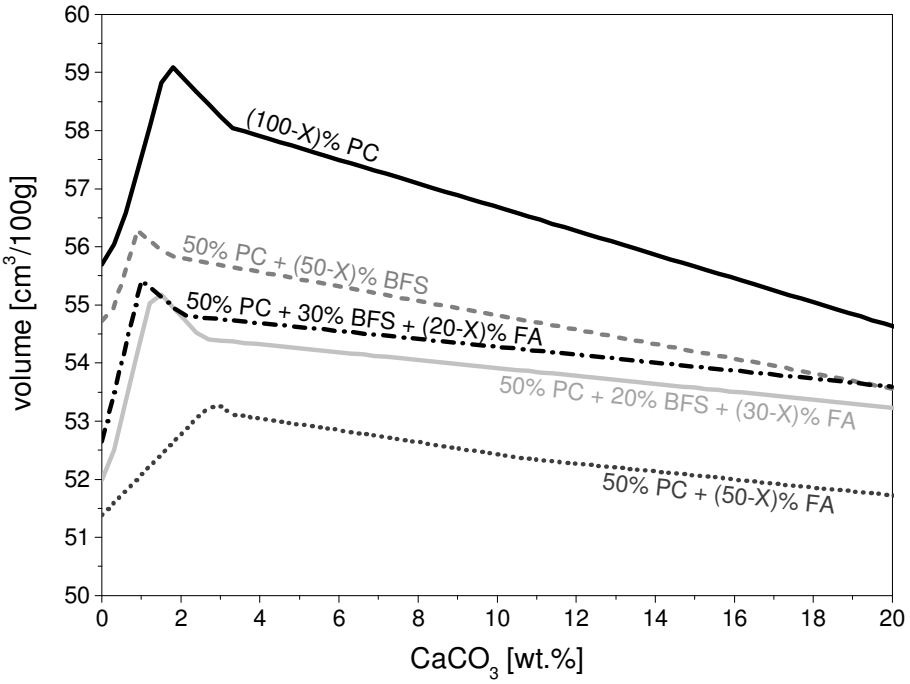

Figure 7.7: The effect of limestone in cement blends containing blast-furnace slag and/or fly ash calculated by thermodynamic modeling. Assumed degrees of reaction are 100% for OPC, 70% for blast-furnace slag and 30% for fly ash. Volume expressed as $cm^3/100g$ unhydrated binder. The X represents the weight fraction of added $CaCO_3$.

7.3 Conclusions

The present study shows the effect of the binder composition in quaternary PC systems with 50 wt.% cement substitution by blast-furnace slag, siliceous fly ash and limestone.

(i) The relative fraction of blast-furnace slag, siliceous fly ash or limestone in PC-blends with 50 wt.% substitution exerts no significant influence on strength development at early ages up to 7 d. At later ages, a $CaCO_3$ content of 2 to 5 wt.% leads to the stabilization of monocarbonate and ettringite, a maximum volume of hydrates (Figure 7.1 and Figure 7.7) and thus to a higher compressive strength as shown in Figure 7.6.

(ii) The ideal amount of additional limestone depends on the composition and amounts of incorporated fly ash and/or blast-furnace slag as well as the total SO_3. Further on the amount of $CaCO_3$ that is already incorporated in PC has to be taken into account.

(iii) The types of hydrates present in ternary or quaternary blends with 50 wt.% of PC are similar to PC. However, there are some differences in the volume of hydrates and less portlandite is present in blended PC while more C-S-H and AFm phases can be observed.

(iv) The presence of both, fly ash and blast-furnace slag, has little effect on the hydrate assemblage. The replacement of some blast-furnace slag by fly ash leads to a slight decrease in the amount of portlandite and C-S-H and to the formation of more AFm phases (monocarbonate and hemicarbonate). Portlandite is consumed in the pozzolanic reaction with the fly ash to form C-S-H. However, the limited assumed degree of reaction as well as the low amorphous content of the fly ash itself leads to lower calculated C-S-H. The low reactivity also causes the slightly reduced total volume of solids and compressive strength at high fly ash content. Yet, these effects are small and consequently amounts of up to 30 wt.% fly ash can be used in quaternary blends without significant loss of compressive strength.

Chapter 8

Pore solution chemistry

In this chapter the pore solution chemistry of cement pastes containing different supplementary cementitious materials (blast-furnace slag, Si-rich fly ash, limestone, quartz) at a cement replacement of 50 wt.% is discussed up to 728 d of hydration. In addition sulfate speciation was carried out for selected samples up to 91 d and at 91 d for the whole matrix under investigation. The pore solution analysis was carried out using ion chromatography and inductively coupled plasma optical emission spectroscopy.

8.1 Experimental

The investigated pore solutions were extracted from cement pastes prepared with materials from batch 2 as described in 3.1. This section also provides detailed descriptions on the matrix under investigation, the strategies used for sample preparation, pore solution extraction and pore solution analysis.

8.2 Results and discussion

As the pore solution chemistry of all investigated systems does not show significant differences between all investigated systems only two systems representing the compositions leading to the most favorable results in terms of total volume of hydrates and compressive strength (cf. 6.3, 7.2.1 and 7.2.2) are discussed in detail in terms of ion concentrations and saturation indices. Summarizing figures including values for the whole matrix under investigation are presented in order to elucidate the similar characteristics among the investigated systems. For a complete data-set it is referred to Appendix 2.

8.2.1 Ion concentrations

Ion concentrations of all investigated species are presented for the whole matrix under investigation at all ages in Figure 8.1. The symbols in the graphical depiction represent the mean values of all eight investigated systems while the error bars correspond to the lowest and highest values detected for a given ion at a given age such that variations are visible. Most variations are too small to be significant especially if the relative uncertainty of ± 10% is taken into account. Only the Al-concentrations show noteworthy differences

that are mainly caused by the different fly ash contents of the systems such that a higher fly ash content leads to higher Al-concentrations towards later ages.

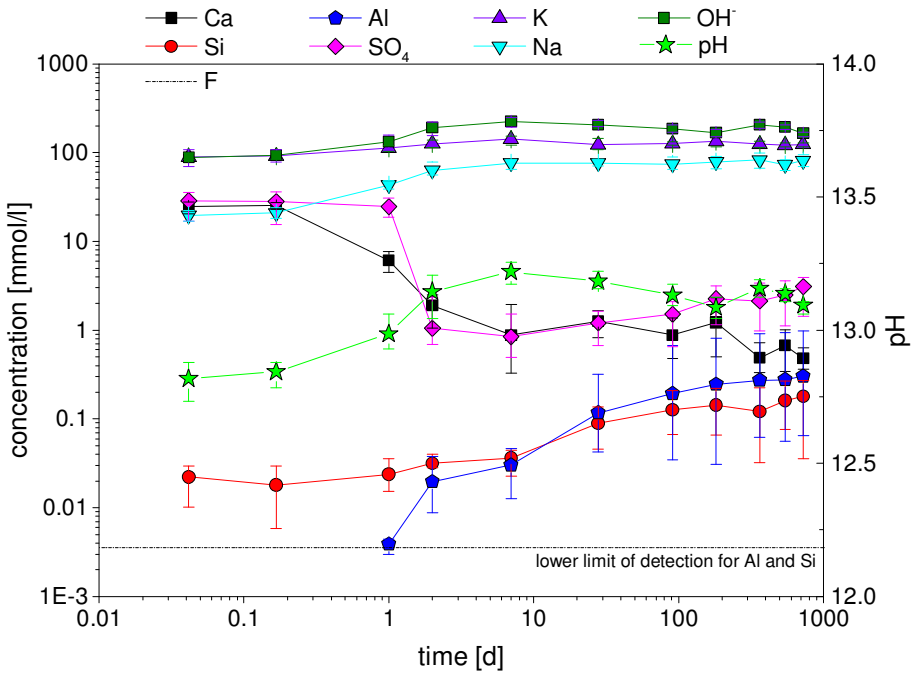

Figure 8.1: Ion concentrations for all investigated ions depicted for the whole matrix under investigation at all ages. The symbols represent the mean values while the error bars correspond to the highest and lowest values that were detected for a corresponding ion at a given age such that variations in concentrations are visible. Note the different scales of the ordinates for concentrations (logarithmic) and pH (linear).

Figure 8.2 and Figure 8.3 show a comparison of the pore solution composition for the two selected systems containing 5 wt.% limestone at 20 wt.% and 30 wt.% blast-furnace slag, respectively. The development of alkalies proceeds identical for both systems which is also the case for OH^-. After the depletion of the calcium sulphates the pH rises to 13.1±0.1 from an initial value of 12.8±0.1 at 1 h. The high pH of values >13 is preserved up to 728 d. In contrast to studies of [Deschner et al., 2012] who investigated Portland fly ash cements no tendentious decrease of alkalies and OH^- can be observed towards later ages. Alkalies can be bound in C-S-H and a tendency of decreasing C/S ratio of the C-S-H which can be observed toward later ages for blended cements [Deschner et al., 2012] can bind more alkalies compared to a lower C/S ratio [Hong and Glasser, 1999]. The changes in C-S-H towards lower C/S ratio at later ages are also reflected in the increasing Si-concentrations along with the decreasing Ca-concentrations and in the calculated phase assemblages as discussed in Chapter 7.

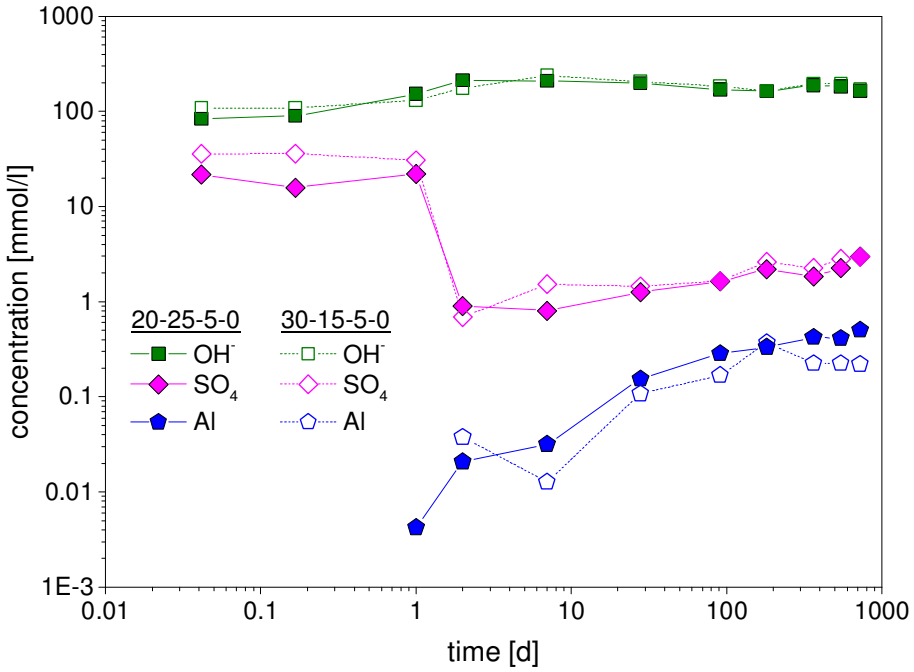

Figure 8.2: Development of the SO_4, Al and OH^- concentrations in the pore solutions of the systems 20-25-5-0 and 30-15-5-0. The relative error of measurement is ~10%. Notation: BFS-FA-LS-Qz.

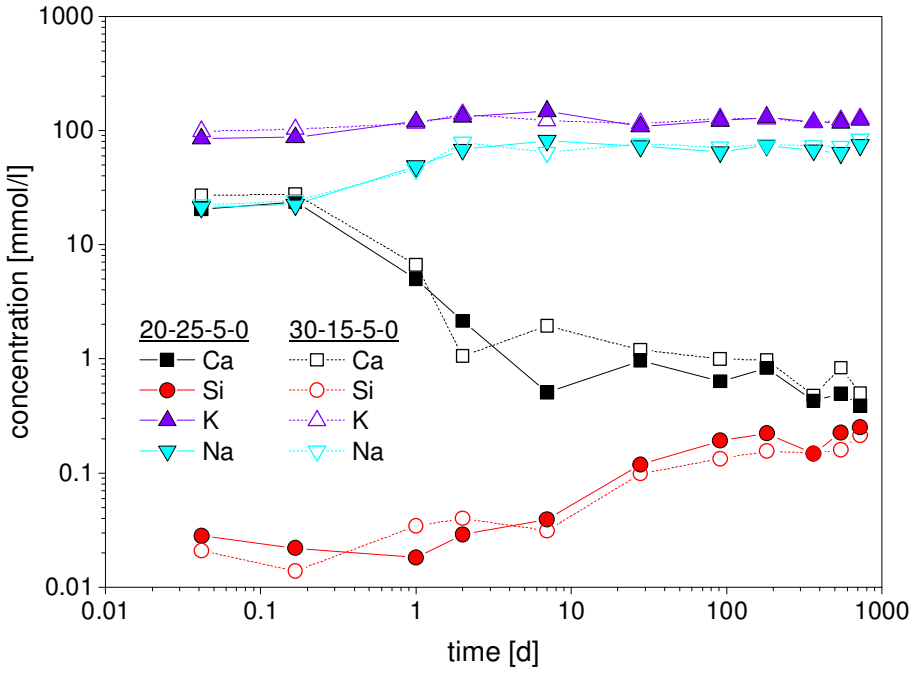

Figure 8.3: Development of the Ca, Si, K and Na concentrations in the pore solutions of the systems 20-25-5-0 and 30-15-5-0. The relative error of measurement is ~10%. Notation: BFS-FA-LS-Qz.

As already stated before, the main variations are present in terms of aluminium. The extend of these variations depends on the fly ash content and on the sample age as fly ash is the main contributor in terms of additional aluminium (not originating from the clinker itself) but will contribute significantly only after some days as the fly ash reacts comparatively slow. Aluminium was not detectable before 1 d of hydration and shows similar values for both systems with a tendency towards higher values for higher fly ash content. The increasing values along with the increasing Si-concentrations correspond to the dissolution of the fly ash glass and correspond to findings of other studies [Luke and Lachowski, 2008, Deschner et al., 2012].

8.2.2 Effective saturation indices

Using the measured ion concentrations as input along with the corresponding activities, saturation indices (SI) of solids of interest were calculated. While a positive SI implies oversaturation, a negative SI implies undersaturation. As the use of SI can be misleading when comparing phases which dissociate into a different number of ions, effective SI were calculated by dividing the SI by the number of ions participating in the reactions to form the solids, as described by [Lothenbach et al., 2008b]. Calculations were carried out for Ca-rich C-S-H, Si-rich C-S-H, portlandite, strätlingite, ettringite, gypsum, monosulfate and monocarbonate. The results for the whole matrix under investigation at all ages is summarized in Figure 8.5.

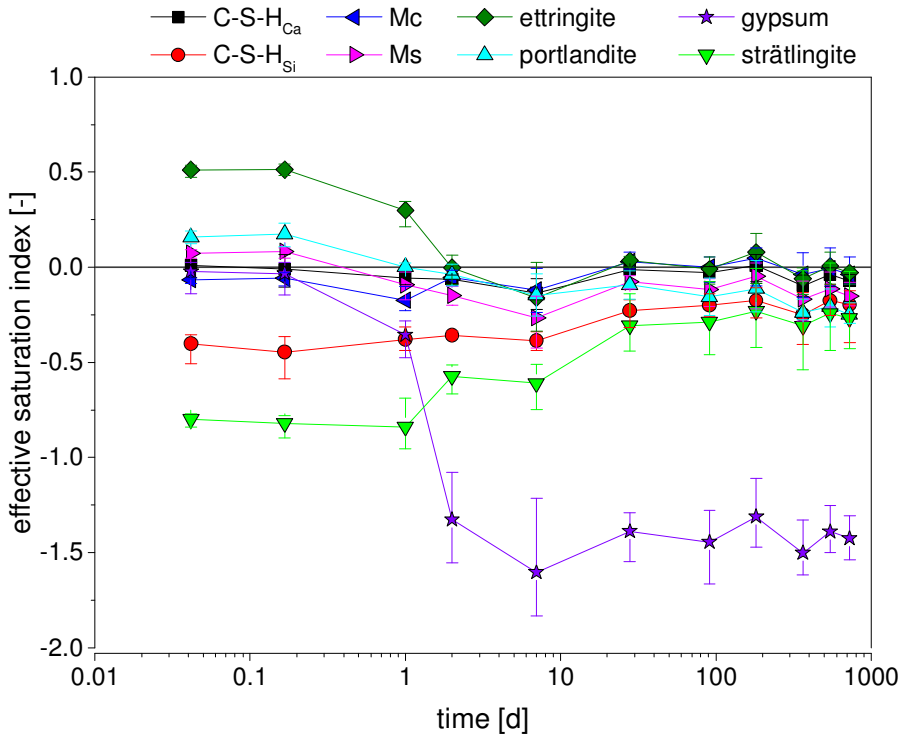

Figure 8.4: Effective saturation indices for all phases of interest for the whole matrix under investigation at all ages. The symbols represent the mean values while the error bars correspond to the highest and lowest values that were calculated for a corresponding phase at a given age such that variations are visible.

The calculated indices do not show significant changes among the investigated systems. Ca-rich C-S-H is close to saturation throughout while Si-rich C-S-H is undersaturated throughout and only shows a trend towards saturation at later ages. Portlandite is slightly oversaturated in the early stage and slightly undersaturated after 1 d in the samples containing fly ash, indicating the dissolution of portlandite in these systems. Strätlingite is clearly undersaturated and slowly approaches saturation towards later ages which corresponds to the tendency of portlandite to be undersaturated at late ages, especially for fly ash containing systems. Ettringite is oversaturated in the early stage and close to saturation after 2 d. The depletion of calcium sulfate is reflected in its clear undersaturation after 1 d. Monosulfate and monocarbonate are both close to saturation throughout. The absence of significant difference within the calculated effective saturation indices reflects the results of ion-concentrations where no significant differences could be observed as well.

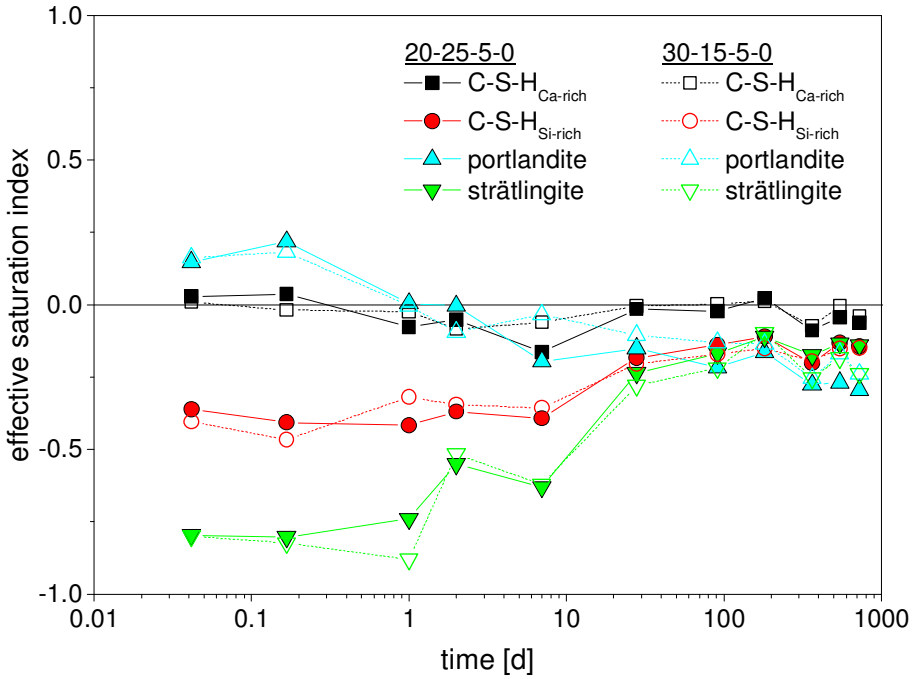

Figure 8.5: Effective saturation indices of Ca-rich and Si-rich C-S-H, portlandite and strätlingite calculated by the elemental concentrations in the pore solutions for the systems 20-25-5-0 and 30-15-5-0. Notation: BFS-FA-LS-Qz.

Figure 8.5 presents a comparison of the two selected systems already discussed in detail in terms of ion concentrations in the previous subsection. Ca-rich C-S-H is dominating throughout, i.e. it is always close to saturation. Si-rich C-S-H is clearly undersaturated throughout. However, due to the increasing Si-concentration and the decreasing Ca-concentration the Si-rich C-S-H becomes less undersaturated towards later ages after 7 d. Similar to the ion-concentrations this behavior corresponds to the dissolution of the fly ash glass which alters the pore solution composition such that the precipitated phases, here C-S-H, are affected as well. The saturation with respect to portlandite starts to decrease after 4 h of hydration and becomes undersaturated after 1 d due to the consumption of portlandite by the pozzolanic reaction. Strätlingite is clearly undersaturated at early ages and becomes less undersaturated as the hydration proceeds towards later

ages. This corresponds to the portlandite consumption along with the additional Al and Si supplied by the reaction of especially the fly ash.

8.2.3 Interplay of hydrates present and pore solution composition

Figure 8.6 presents diffractogram of the discussed two systems at after 7 d and 728 d of hydration. The variations among the different systems are small and the hydrate assemblage is not altered from a qualitative point of view. The small variations over time that were observed in the composition of the pore solution correspond well to the investigations on the solids as discussed in detail in Chapter 7.

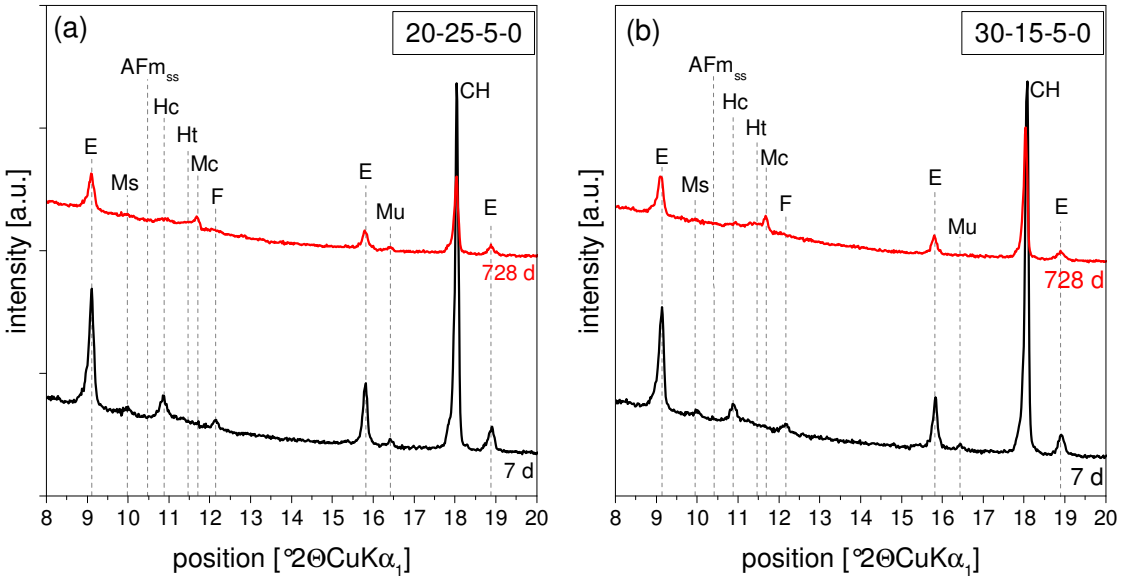

Figure 8.6: X-ray diffractograms of systems containing 5 wt.% limestone at (a) 20 wt.% and (b) 30 wt.% blast-furnace slag depicted at 7 d and 728 d of hydration. AFm_{ss} - solid solution of hemicarbonate and OH^- substituted monosulfate, CH - portlandite, E - ettringite, F - brownmillerite, Hc - hemicarbonate, Ht - hydrotalcite, Mc - monocarbonate, Ms - monosulfate, Mu - mullite. Note that the lower intensities at 728 d for hydrates (especially ettringite) are caused by tube degradation over time.

8.2.4 Sulphur speciation

Figure 8.7 provides a comparison of the investigated sulfur species at 20 wt.% and 30 wt.% blast-furnace slag for systems not containing fly ash up to 91 d of hydration. The development of sulphide is directly linked to the dissolution of the blast-furnace slag at early ages while it becomes less important towards later ages [Lothenbach et al., 2012]. However, sulphide (HS^-) originating from the dissolution of the blast-furnace slag was below the detection limit of 0.019 mmol/l. Sulphite (SO_3^{2-}) and especially thiosulphate ($S_2O_3^{2-}$) which are both intermediates during the oxidation of HS^- to SO_4^{2-} could be detected. In the presence of 30 wt.% blast furnace slag clearly higher values of SO_3^{2-} and $S_2O_3^{2-}$ could be detected than for samples containing 20 wt.% blast-furnace slag. While this shows a dissolution of the blast-furnace slag the effect is clearly less pronounced compared to slag cements [Gruskovnjak et al., 2006, Lothenbach et al., 2012] due to the lower blast-furnace slag content. The concentrations of sulphate (SO_4^{2-}) are superimposed

for both blast-furnace slag levels up to 1 d. After 1 d a drop in the concentration occurs and after 7 d the values are slightly increasing again with higher blast-furnace slag content leading to higher concentrations. S_{total} is controlled by sulphate at early age and by sulphate and thiosulphate after 91 d. Further details are given in Appendix 2.

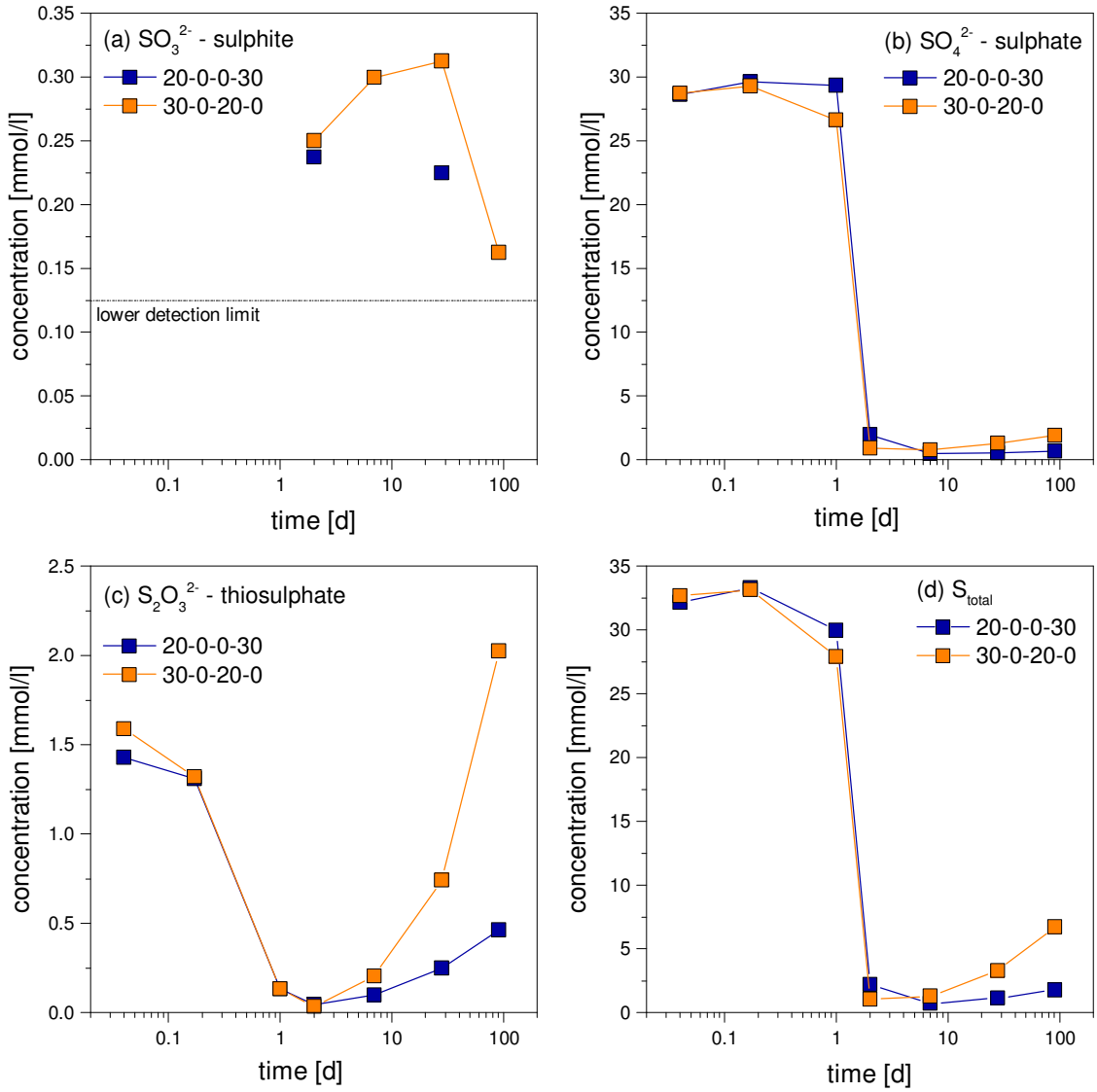

Figure 8.7: Sulphur speciation in the pore solution of selected samples at ages of up to 91 d as detected by ICP-OES. Missing data-points for SO_3^{2-} as well the S^{2-}-concentrations for all investigated samples were found to be below the lower detection limit. Corresponding lower detection limits are 12.5×10^{-2} mmol/l (SO_3^{2-}) and 1.9×10^{-2} mmol/l (S^{2-}). Note the different scaling of the ordinates. Notation: BFS-FA-LS-Qz.

Results of the sulphur speciation for the whole matrix under investigation after 91 d of hydration are presented in Figure 8.8. All values are higher compared to the quartz-containing reference at 20 wt.% blast furnace slag while a higher blast-furnace slag level leads to higher values throughout.

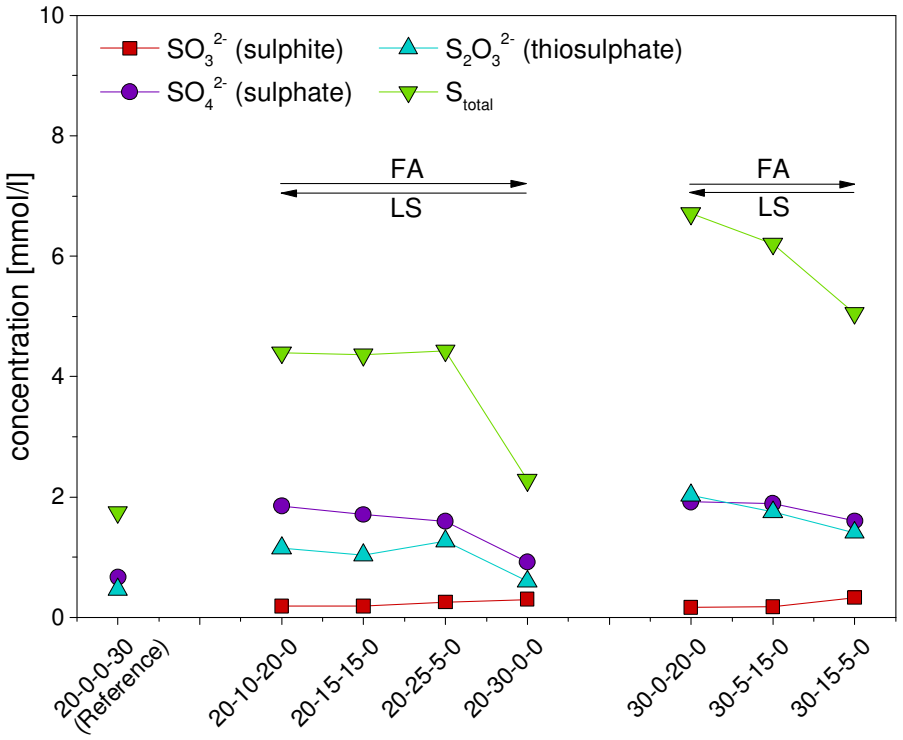

Figure 8.8: Sulphur speciation in the pore solution for the whole matrix under investigation of samples at 91 d as detected by ICP-OES. Missing data-points for SO_3^{2-} were found to be below the lower detection limit of 0.125 mmol/l. Notation: BFS-FA-LS-Qz.

8.3 Conclusions

This study investigates the pore solution of quaternary cements containing PC, blast-furnace slag, fly ash and limestone simultaneously at high cement substitution of 50 wt.% at a water-to-binder ratio of 0.5. The analysis of the acquired results summarizes as follows:

- Investigations of the pore solution do not show significant differences among the different systems. This corresponds to the presence of the same hydrates in all systens (cf. Chapter 7) despite the variations in the mix design. Only Al- and Si- concentrations vary over time, mainly as a funtion of the fly ash reaction. As a consequence the calculated effective saturation indices do not show significant differences as well.
- The pH is not significantly affected due to the different mix designs and remains at values slightly higher than 13 up to 728 d.

- The total SO_3 content of the pore solution is controlled by sulphate SO_4^{2-}. All other species are either present below the lower limit of detection or show similar values for both blast-furnace slag levels. After 7 d slightly higher concentrations are present for higher blast-furnace slag content.

Chapter 9

Concluding remarks

9.1 General summary and conclusions

In the present thesis several aspects related to the use of SCM in multi-component systems were investigated using a multi-method approach. Three mineral additions, blast-furnace slag, fly ash and limestone were used. The main aspects considered are, i) the effect of SCM on the early hydration in binary and ternary Portland cement blends, ii) the effect of chemical composition of synthetic glasses[16] on their reactivity and iii) kinetic behavior and composition of the hydrate assemblage of quaternary Portland cement blends including all of the three before mentioned SCM simultaneously. The general conclusions on these aspects in the order of appearance in the thesis are listed below:

9.1.1 The effect of SCM on the early hydration of SCM-blended cements

The investigation of the early hydration of binary cements containing either blast-furnace slag, Si-rich fly ash or limestone are discussed in detail in Chapter 4. Based on theories obtained mainly from experiments conducted on pure phases in diluted systems, the aim was to investigate if these theories are valid in "real" systems at realistic conditions (e.g. water-to-cement ratio of 0.5) as well. The findings in this regard can be summarized as follows:

The presence of additional surface sites for nucleation in blended cements that are provided by the SCM leads to a faster heat development and to a lower degree of (over)saturation with respect to C-S-H. This observed decrease of saturation of the solutions is most distinct for the limestone blended cement, as on limestone C-S-H nucleation occurs more easily, and less for the quartz, blast-furnace slag and fly ash blended cements, while the highest oversaturation with respect to C-S-H is present for the neat cement, where the least surface is available for nucleation. These findings, especially with regard to the role of limestone, are supported by the contributions of [Berodier and Scrivener, 2014] and [Oey et al., 2013] which showed that limestone provides excellent conditions for the nucleation of C-S-H.

[Nicoleau et al., 2013] showed that increasing Ca-concentration of the pore solution decreases the dissolution rate of C_3S and C_2S in diluted systems. Higher calcium concentrations in the pore solution do not lead to a systematic decrease of the reaction rate

[16] The glasses were designed to correspond to the chemical compositions present in the glass phase of blast-furnace slag, Ca-rich and Si-rich fly ashes.

of C_3S and C_2S in realistic systems. In contrast the fastest reacting blend with limestone shows the highest calcium concentrations in solution.

The general trend of the reaction rate is related to the degree of undersaturation with respect to C_3S (which depends on pH, calcium and silicon concentrations). The more undersaturated the faster the observed reaction. Indirectly the overall reaction of C_3S is controlled by the interplay of undersaturation with respect to C_3S and oversaturation with respect to C-S-H as discussed in detail in [Bullard et al., 2012]. The limestone containing sample, where a higher number of C-S-H nuclei leads to a lower oversaturation with respect to C-S-H compared to quartz, blast-furnace slag, fly ash and neat cement (in this order), is most strongly undersaturated with respect to C_3S and shows thus the fastest reaction. The least undersaturation is observed for the plain cement, which also shows the slowest reaction. The differences in reaction between the different blends however, can not be explained by undersaturation only.

An increase of the Al-concentrations in the pore solutions was found to notably retard the hydration as visible by the very fast reaction of the limestone blended sample with the lowest aluminium concentration compared to the fly ash sample with the highest aluminium concentrations. Consequently, the presence of aluminium retards the hydration in the blended systems in agreement with the observed effect of aluminium on alite dissolution in diluted systems [Nicoleau et al., 2014].

Higher sulphate concentrations could be detected for the fly ash containing blend which possibly hindered ettringite precipitation and resulted in higher Al-concentrations. Similarly the low sulphate concentrations could be the reason for the lower Al-concentrations in the presence of quartz, blast-furnace slag and limestone compared to fly ash.

Overall it can be stated that the investigations of the changes in the pore solution during the early hydration have shown that the same factors as in diluted systems dominate the kinetics. A higher degree of undersaturation with respect to C_3S along with lower aluminium concentration accelerates the reaction. An increase in the aluminium concentration leads to the opposite effect. Due to the presence of more or better surface available for C-S-H nucleation faster C-S-H precipitation is caused which in turn leads to faster hydration. In real systems many factors affect the exact interplay between the mentioned aspects. The aluminium concentrations are strongly affected by the kinetics of ettringite precipitation, which can be hindered at high sulfate concentrations. The numerous factors that are involved in the early hydration make investigations in cement pastes challenging. In order to better understand the factors controlling the early hydration of Portland cement in the presence of SCM further research is needed both on pure phases and in cements.

9.1.2 The dependance of glass reactivity on the glass composition

Most SCM contain significant amounts of amorphous phases that can basically be described as (calcium) aluminosilicate glasses. The glass content is the most reactive part of corresponding SCM (especially blast-furnace slag and fly ash[17]). The reactivity of these SCM depends on the particle size distribution, the glass content and the intrinsic reactivity of the contained glass itself. The glass reactivity is directly linked to the degree of glass polymerization which can be described as ratio of network modifying oxides (NWM) to network forming oxides (NWF). The degree of polymerization significantly

[17] Note that other reactive phases such as free lime or anhydrite might be present in fly ash in relatively small amounts compared to the amorphous content.

influences the reactivity of (calcium) aluminosilicate glasses [Chao et al., 2010]. Different approaches are known to describe this relation. Hydraulic or basicity indices [Winnefeld et al., 2015, Ehrenberg et al., 2008] or, as common in glass science, the number of non-bridging oxygen atoms to oxygen atoms in tetragonal coordination (NBO/T) [Mysen et al., 1982, Mills et al., 2011] are used for this purpose. It is extremely difficult to gain information on the actual glass structure, especially on amphoteric oxides like Al_2O_3 and Fe_2O_3 which can act in both ways, as NWM or NWF. In addition most of the studies available on glass reactivity consider conditions that are not relevant for cements (pH <13).

The study presented in Chapter 5 investigates the reactivity of synthetic glasses with similar chemical compositions as the composition of the glass phases in blast-furnace slag, Ca-rich fly ash and Si-rich fly ash at high pH (>13) similar to cement pore solutions with the aim to gain better knowledge on the influence of the glass composition on the glass reactivity. Such a better understanding will help to select optimum SCM for blended cements depending on the types and amounts of SCM used or to develop efficient methods for glass activation. The main findings of the study are summarized in the following:

Dissolution experiments at far-from-equilibrium conditions as well as investigations on model systems showed the same trends. The initial dissolution rate and the glass reactivity both increased with decreasing polymerization of the glass network (e.g. increase in network modifying oxides such as CaO and alkali oxides). Thereby Si-rich fly ash glasses showed the lowest reactivity, blast-furnace slag glasses showed the highest reactivity and Ca-rich fly ash glasses are located in between. The results indicate that not only higher quantities of CaO but also of Al_2O_3 lead to an increase of reactivity. A customized approach of the calculation of NBO/T (ratio of non-bridging oxygen atoms to oxygen atoms in tetragonal coordination) that defines the amphoteric Al_2O_3 (and also Fe_2O_3) mainly as network modifying oxide (approx. 90%) appears most realistic.

Model systems based on $Ca(OH)_2$ and $CaCO_3$ enabled to study the glass reaction in less complex conditions than prevailing in blended Portland cement systems. The same trends of glass reaction were observed in simplified model systems as in glass-blended cements, although the progress of glass reaction was slower in the blended cements than in the model systems.

The bound water content of model systems and glass-blended Portland cements can be calculated from TGA data. The correlation of experimentally determined bound water with bound water obtained from mass balance calculations as a function of the amount of glass reacted allows to estimate the degree of glass reaction. Results gained by this approach follow the same characteristics compared to the dissolution tests, although values are lower throughout caused by the presence of less water. Applying this approach the degree of glass reaction in blended cements can be calculated using the amount of additional bound water with respect to an inert quartz reference. Results of both approaches, pozzolanity tests and blended cements, show a clear linear relation. For both the glass-blended cements and the model systems the Si-rich fly ash glasses showed the lowest degree of reaction after 91 d of hydration.

9.1.3 Hydration of quaternary multi-component cements

Due to environmental considerations such as the reduction of the carbon footprint of cements but also due to economical reasons such as availability of SCM on the market most cements are blended with SCM nowadays. The presence of SCM causes differences

in the behavior of these blended systems compared to neat Portland cement. These phenomena are caused by the so-called "filler effect" that is discussed in detail in Chapter 2. While binary and ternary systems are well investigated there is a lack of information on the behavior of quaternary cements containing simultaneously clinker, blast-furnace slag, Si-rich fly ash and limestone. The phase composition of these systems is similar to Portland cement based composites including Si-rich fly ash or blast-furnace slag [Iñiguez Sánchez et al., 2011, Schöler et al., 2015]. The nature of such systems is very complex and consequently it is difficult to gain adequate information on the occurring hydration mechanisms and to link them to the resulting properties of the binder. The aim of investigations of quaternary systems is to contribute to this purpose by investigating Portland cement-based multi-component systems with fixed blast-furnace slag levels of 20 and 30 wt.% and varying shares of Si-rich fly ash and limestone of 30 and 20 wt.%, respectively. Corresponding studies were carried out regarding three aspects that are described in the following sections.

9.1.3.1 Kinetic aspects

The experiments presented in Chapter 6 investigate the hydration kinetics of quaternary cements containing Portland cement, blast-furnace slag, Si-rich fly ash and limestone simultaneously at high cement substitution of 50 wt.% and a water-to-binder ratio of 0.45. The main findings of these investigations summarizes as follows:

Compared to a system incorporating only Portland cement and quartz in equal shares, additions of blast-furnace slag lead to acceleration of the hydration in the first 24 h as observed by both released heat of hydration and chemical shrinkage. In addition to the contribution of blast-furnace slag a complete substitution of quartz by limestone causes further acceleration. On the contrary the complete quartz substitution by fly ash leads to retardation. The acceleration is due to the limestone as its surface provides excellent conditions for the C-S-H nucleation such that the number of C-S-H nuclei is significantly higher than on other SCM [Berodier and Scrivener, 2014]. This leads to a higher undersaturation with respect to C_3S and to a lower oversaturation with respect to C-S-H. The more this effect is pronounced the faster the alite dissolution. Mixtures containing limestone show a faster reaction compared to mixtures containing only fly ash. Thereby the characteristic of the acceleration of the reaction (with respect to inert quartz) depends on the actual limestone content. However, the differences in the systems are too small to be significant which does not allow for clear distinction between the contributions of the different SCM.

9.1.3.2 Hydrate assemblage

The study of the hydrate assemblage in quaternary pastes at a water-to-solid ratio of 0.45 and the effects on mechanical properties are discussed in detail in Chapter 7.

The influence of the relative fraction of blast-furnace slag, Si-rich fly ash and limestone in Portland cement blends at a cement replacement of 50 wt.% exerts no significant influence on strength development at early ages up to 7 d. After 28 d of hydration a strength maximum is reached in presence of 5 wt.% additional limestone. This maximum is visible at both blast-furnace slag levels of 20 and 30 wt.% while higher blast-furnace slag content leads to a slight strength increase. The presence of small amounts of $CaCO_3$ (2 to 5 wt.%) leads to the stabilization of monocarbonate and ettringite. Under these conditions also a maximum of hydrates is predicted by thermodynamic calculations such that the

strength maximum is related to the volume of hydrates and the degree of space filling. The ideal amount of additional limestone ($CaCO_3$-source) depends on the composition and amounts of incorporated fly ash and/or blast-furnace slag as well as on the total SO_3 content.

The types of hydrates present in ternary and quaternary systems at 50 wt.% cement replacement are similar to neat Portland cement. Differences in the total volume of hydrates are caused by a lower portlandite content in blended systems while more C-S-H and AFm phases are formed compared to neat Portland cement.

The hydrate assemblage is not significantly affected by the presence of both fly ash and blast-furnace slag. The successive replacement of blast-furnace slag by fly ash leads to a slight decrease in the amount of portlandite and C-S-H and to a more pronounced formation of hemicarbonate and monocarbonate. Portlandite is consumed in the pozzolanic reaction with the fly ash and C-S-H is formed. In the thermodynamic calculations it was accounted for the generally slower reaction of Si-rich fly ash compared to blast-furnace slag by assuming a lower degree of reaction such that lower amounts of C-S-H were calculated.

The low reactivity is also responsible for the slightly reduced total volume of solids and compressive strength at high fly ash content. Still these effects are small and consequently amounts of up to 30 wt.% fly ash can be used in quaternary blends in the presence of blast-furnace slag and limestone without significant loss of compressive strength. All investigated systems fulfill the requirements of strength class 42.5 N according to EN 196-1. Disregarding durability aspects these systems could therefore be potential candidates for standardization.

9.1.3.3 Long term development of the pore solution composition

Besides the kinetics and the hydrate assemblage of quaternary blends also the pore solution was investigated as it is the "missing link" between the dissolution of the binder and the formation of hydrates. The corresponding investigations as presented in Chapter 8 lead to the following conclusions[18]:

No significant differences are detectable in the pore solutions among the different systems. This is in line with the presence of the same hydrates in all systems despite the variations in the mix design. Clear differences are only observed for Al- and Si- concentrations, especially at later ages which is mainly caused by the amount of the fly ash contained and its dissolution. In consequence the calculated effective saturation indices of relevant phases do not show significant differences as well.

The pH is not significantly affected due to the different mix designs and remains at values slightly higher than 13 up to 728 d. This might be of special interest for future use of quaternary systems in the field with regard to steel passivation/corrosion in reinforced concrete.

Investigations by means of sulphur speciation up to 91 d of hydration revealed that the total sulphur content of the pore solution is dominated by sulphate (SO_4^{2-}) while concentrations of sulphite (SO_3^{2-}) and thiosulphate ($S_2O_3^{2-}$) were very low. After 7 d of hydration higher concentrations of sulphite and thiosulphate could be observed at higher content of blast-furnace slag.

[18] Note that the pore solution experiments were carried out with slightly different batches of raw materials compared to the investigations of kinetics and hydrate assemblage (c.f. Chapter 3). Also a slightly higher water-to-solid ratio of 0.5 was used to enable pore solution extraction at ages of up to 728 d.

9.2 Outlook and suggestions for future work

The work presented in this thesis covers aspects of the fundamental effects of SCM on the hydration of blended Portland cements, the reactivity of SCM as well as investigations on cement compositions that might be possible candidates for future standardization. New insights in the complex systems are provided which can help to develop more advanced eco-friendly Portland cement-based binders. In addition the extension from ternary to quaternary systems provides possibilities to use relevant SCM in a more economical way and to compensate shortages on the market. However, despite the contribution provided by this thesis quaternary systems need to be studied in more detail and it is indispensable to gain deeper knowledge on the actual hydration reactions and the influence of the chemical and mineralogical composition of the raw materials. In addition to deeper insights to the nature of pastes the application of new cement compositions, i.e. their use for the production of concrete has to be considered. To this purpose comprehensive studies on the mechanical characteristics and on durability of concretes need to be conducted. Based on these considerations a number of aspects can be listed that might serve as subjects for further research:

- Investigations on the first few hours of hydration in Portland cement blends can be further deepened by applying highly sensitive methods like ICP-MS that allow to detect very low concentrations of ions in pore solutions. In this regard special designed experimental set-ups as for instance used by [Nicoleau et al., 2013] seem to be promising approaches. It should be noted that investigations of the early stage of hydration in the first hours became more enlightening in recent years due to decreasing detection limits in terms of instrumental analysis. Further improvement of analytical methods will contribute in this regard.

- While the influence of network modyfying oxides versus network forming oxides was found to be a key parameter that determines the reactivity of synthetic glasses the role of amphoteric oxides such as Al_2O_3 (and Fe_2O_3) is not fully understood. For information on the actual coordination of such oxides solid state NMR might give better insight. Also the use of fourier transform infrared spectroscopy (FTIR) might reveal useful information.

- The pozzolanity test that was used for model systems and glass-blended cements was found to be a fast and comparatively easy method to evaluate and compare the reactivity of synthetic glasses. However, especially the composition of C-S-H that is used in thermodynamic calculations determines the accuracy of the results. This has also to be taken into account as highly variable C/S are observed in presence of SCM, especially in the case of fly ash. Any new insight to the composition of C-S-H in multi-component systems as well as any improvement in terms of C-S-H models will help to increase the accuracy of the pozzolanity test as presented in this thesis. This also applies for the alteration of the C-S-H composition due to the incorporation of e.g. aluminium.

- The quaternary cement pastes that were investigated are promising compositions. However, it should be considered that these systems were only investigated in terms of kinetics, hydrate assemblage, pore solution chemistry and compressive strength whereby raw materials with fixed particle size distribution were used. While this approach was chosen to understand the principal behavior of multi-component pastes optimization in terms of PSD with regard to particle packing has to be investigated once these systems are used as binders in mortar and concrete.

- With respect to a standardization that is essential in order to use new compositions in the construction sector comprehensive performance and durability studies need to be conducted in order to fulfill existing regulations and to ensure a long service life. The performance of the new cement compositions in mortar and concrete needs to be investigated more in detail concerning aspects such as creep performance, shrinkage behavior and E-modulus determinations as function of the actual binder composition, i.e. content of blast-furnace slag, fly ash and limestone. While phase assemblage calculations predict maximum volume filling in presence of a few wt.% limestone and thus minimum porosity such durability aspects need to be studied in detail. Based on studies including the before mentioned aspects the new binder compositions can be classified according to applicable exposure classes such that further progress towards standardization of promising formulations can be achieved.

References

[Aïtcin, 2008] Aïtcin, P.-C. (2008). *Binders for Durable and Sustainable Concrete*. Taylor & Francis.

[ASTM, 2007] ASTM (2007). C-1608-0 Standard Test Method for Chemical Shrinkage of Hydraulic Cement Paste.

[Babushkin, 1985] Babushkin (1985). *Thermodynamics of Silicates*. Springer Verlag Berlin Heidelberg.

[Baert et al., 2008] Baert, G., Hoste, S., De Schutter, G., and De Belie, N. (2008). Reactivity of fly ash in cement paste studied by means of thermogravimetriy and isothermal calorimetry. *Journal of Thermal Analysis and Calorimetry*, 94:485 – 492.

[Barker et al., 2009] Barker, D., Turner, S., Napier-Moore, P., Clark, M., and Davison, J. (2009). CO_2 capture in the cement industry. *Energy Procedia*, 1:87–94.

[Barneyback and Diamond, 1981] Barneyback, R. and Diamond, S. (1981). Expression and analysis of pore fluids from hardened cement pastes and mortars. *Cement and Concrete Research*, 11:279 – 285.

[Begarin et al., 2009] Begarin, F., Garrault, S., Nonat, A., and Nicoleau, L. (2009). Hydration of alite containing aluminium. In *29th Cement and Concrete Science Congress, Leeds, United Kingdom*, pages 9–12.

[Begarin et al., 2011] Begarin, F., Garrault, S., Nonat, A., and Nicoleau, L. (2011). Hydration of alite containing aluminium. *Advances in Applied Ceramics*, 110:127–130.

[Ben Haha et al., 2010] Ben Haha, M., De Weerdt, K., and Lothenbach, B. (2010). Quantification of the degree of reaction of fly ash. *Cement and Concrete Research*, 40:1620 – 1629.

[Ben Haha et al., 2011] Ben Haha, M., Lothenbach, B., Le Saout, G., and Winnefeld, F. (2011). Influence of slag chemistry on the hydration of alkali-activated blast-furnace slag - Part I: Effect of MgO. *Cement and Concrete Research*, 41:995 – 963.

[Ben Haha et al., 2012] Ben Haha, M., Lothenbach, B., Le Saout, G., and Winnefeld, F. (2012). Influence of slag chemistry on the hydration of alkali-activated blast-furnace slag - Part II: Effect of Al_2O_3. *Cement and Concrete Research*, 42:74 – 83.

[Benhelal et al., 2013] Benhelal, E., Zahedi, G., Shamsaei, E., and Bahadori, A. (2013). Global strategies and potentials to curb CO_2 emissions in cement industry. *Journal of Cleaner Production*, 51:142–161.

[Bentz, 2006] Bentz, D. P. (2006). Influence of water-to-cement ratio on hydration kinetics: Simple models based on spatial considerations. *Cement and Concrete Research*, 36:238–244.

[Berodier and Scrivener, 2014] Berodier, E. and Scrivener, K. (2014). Understanding the Filler Effect on the Nucleation and Growth of C-S-H. *Journal of the American Ceramic Society*, 97:3764–3773.

[Berry and Malhotra, 1982] Berry, E. and Malhotra, V. (1982). Fly ash for use in concrete - a critical review. *ACI Journal*, 2:59–73.

[Bleszynski et al., 2002] Bleszynski, R., Hooton, R., Thomas, M., and Rogers, C. (2002). Durability of ternary blend concrete with silica fume and blast-furnace slag: Laboratory and outdoor exposure site studies. *ACI Materials Journal*, 99:499–508.

[Blezard, 1998] Blezard, R. (1998). *Lea's Chemistry of Cement and Concrete*, chapter The history of calcareous cements, pages 1–23. Butterworth Heinemann.

[Bonavetti et al., 2003] Bonavetti, V., Donza, H., Menendez, G., Cabrera, O., and Irassar, E. (2003). Limestone filler cement in low w/c concrete: a rational use of energy. *Cement and Concrete Research*, 33:865 – 874.

[Bonavetti et al., 2001] Bonavetti, V., Rahhal, V., and Irassar, E. (2001). Studies on the

carboaluminate formation in limestone filler-blended cements. *Cement and Concrete Research*, 31:853 – 859.

[Bougara et al., 2010] Bougara, A., Lynsdale, C., and Milestone, N. (2010). Reactivity and performance of blastfurnace slags of differing origin. *Cement & Concrete Composites*, 32:319–324.

[Brantley, 2008] Brantley, S. (2008). *Kinetics of Water-Rock Interaction*. Springer.

[Bullard et al., 2012] Bullard, J., Scherer, G., and Thomas, J. (2012). Time dependent driving forces and the kinetics of tricalcium silicate hydration. *Cement and Concrete Research*, 72:26–34.

[Bumrongjaroen et al., 2007] Bumrongjaroen, W., Muller, I., and Pegg, I. (2007). Characterization of glassy phase in fly ash from iowa state university. Technical Report VSL-07R520X-1, Turner Fairbank Research Center, Federal Highway Administration.

[Carrasco et al., 2005] Carrasco, M., Menendez, G., Bonavetti, V., and Irassar, E. (2005). Strength optimization of tailor-made cement with limestone filler and blast furnace slag. *Cement and Concrete Research*, 32:1324 – 1331.

[Cembureau, 2012] Cembureau (2012). Cements for a low-carbon Europe: A review of the diverse solutions applied by the European cement industry through clinker substitution to reducing the carbon footprint of cement and concrete in Europe. Technical report, Cembureau - The European Cement Association.

[CEN/TC 51, 2012] CEN/TC 51 (2012). Cement and building limes, N 1146 - Presentation of WG 6, Definition and terminology of cement, Progress Report, Athens. Technical report, Comission for European Normalization.

[Chancey et al., 2010] Chancey, R., Stutzman, P., Juenger, M., and Fowler, D. (2010). Comprehensive phase characterization of crystalline and amorphous phases of a Class F fly ash. *Cement and Concrete Research*, 40:146–156.

[Chao et al., 2010] Chao, L., Henghu, S., and Li, L. (2010). A review: The comparison between alkali-activated slag (Si+Ca) and metakaolin (Si+Al) cements. *Cement and Concrete Research*, 40:1341–1349.

[Costoya Fernandez, 2008] Costoya Fernandez, M. (2008). *Effect of Particle Size on the Hydration Kinetics and Microstructural Development of Tricalcium Silicate*. PhD thesis, École Polytechnique Fédérale de Lausanne.

[Damidot, 2007] Damidot, D. (2007). Calculation of critical supersaturated domains with respect to ettringite in the CaO-Al_2O_3-$CaSO_4$-H_2O system at 20 °C. *Proceedings of the 12th international Congress on the Chemistry of Concrete, Montreal*.

[Damidot and Glasser, 1992] Damidot, D. and Glasser, F. (1992). Thermodynamic investigation of the CaO-Al_2O_3-$CaSO_4$-H_2O system at 50 °C and 85 °C. *Cement and Concrete Research*, 22:1179 – 1191.

[Damidot et al., 2011] Damidot, D., Lothenbach, B., Herfort, D., and Glasser, F. (2011). Thermodynamics and cement science. *Cement and Concrete Research*, 41:679 – 695.

[Damidot et al., 1994] Damidot, D., Stronach, S., Kindness, A., Atkins, M., and Glasser, F. (1994). Thermodynamic investigation of the CaO-Al_2O_3-$CaCO_3$-H_2O closed system at 25 °C and the influence of Na_2O. *Cement and Concrete Research*, 24:563 – 572.

[Damtoft et al., 2008] Damtoft, J., Lukasik, J., Herfort, D., Sorrentino, D., and Gartner, E. (2008). Sustainable development and climate change initiatives. *Cement and Concrete Research*, 38:115–127.

[Danielson, 1960] Danielson, U. (1960). Heat of hydration of cement as affected by water-cement ratio. In *Chemistry of Cement: Proceedings of the Fourth International Symposium, Washington*, volume 1, pages 519–526.

[Davis et al., 1937] Davis, R., Carlson, R., Kelly, J., and Davis, H. (1937). Properties of cements and concretes containing fly ash. *Journal of the American Concrete Institute*, 33:55–611.

[Day and Shi, 1994] Day, R. and Shi, C. (1994). Influence of the fineness of pozzolan on the strength of lime natural-pozzolan cement pastes. *Cement and Concrete Research*, 24:1485–1491.

[De Weerdt et al., 2011a] De Weerdt, K., Ben Haha, M., Le Saout, G., Kjellsen, K., Justnes, H., and Lothenbach, B. (2011a). Hydration mechanisms of ternary portland cements containing limestone powder and fly ash. *Cement and Concrete Research*, 41:279 – 291.

[De Weerdt et al., 2012] De Weerdt, K., Ben Haha, M., Le Saout, G., Kjellsen, K., Justnes, H., and Lothenbach, B. (2012). The effect of temperature on the hydration of composite cements containing limestone powder and fly ash. *Materials and Structures*, 45:1101–1114.

[De Weerdt et al., 2011b] De Weerdt, K., Justnes, H., Lothenbach, B., and Ben Haha, M. (2011b). The effect of limestone powder additions on strength and microstructure of fly ash blended cements. *Proceedings of the 13th international Congress on the Chemistry of Concrete, Madrid*.

[De Weerdt et al., 2011c] De Weerdt, K., Kjellsen, K., Sellevold, E., and Justnes, H. (2011c). Synergy between fly ash and limestone powder in ternary cements. *Cement & Concrete Composites*, 33:30 – 38.

[Deschner, 2014] Deschner, F. (2014). *Reaction of siliceous fly ash in blended Portland cement pastes and its effect on the chemistry of hydrate phases and pore solution*. PhD thesis, Friedrich-Alexander-Universität Erlangen-Nürnberg.

[Deschner et al., 2011] Deschner, F., Lothenbach, B., Winnefeld, F., Schwesig, P., Seufert, S., Dittrich, S., and Neubauer, J. (2011). Investigation of a model system to characterize the pozzolanic reactivity of two low Ca fly ashes and a quartz powder. In *Tagung Bauchemie : GDCh-Fachtagung, Hamburg*, pages 127–132.

[Deschner et al., 2013] Deschner, F., Münch, B., Winnefeld, F., and Lothenbach, B. (2013). Quantification of fly ash in hydrated, blended Portland cement pastes by backscattered electron imaging. *Journal of Microscopy*, 251:188–204.

[Deschner et al., 2012] Deschner, F., Winnefeld, F., Lothenbach, B., Seufert, S., Schwesig, P., Dittrich, S., Goetz-Neunhoeffer, F., and Neubauer, J. (2012). Hydration of Portland cement with high replacement by siliceous fly ash. *Cement and Concrete Research*, 42:1389 – 1400.

[Diamond, 1983] Diamond, S. (1983). On the glass present in low-calcium and in high-calcium flyashes. *Cement and Concrete Research*, 13:459–464.

[Dittrich et al., 2014] Dittrich, S., Neubauer, J., and Goetz-Neunhoeffer, F. (2014). The influence of fly ash on the hydration of OPC within the first 44 h - Aquantitative in situ XRD and heat flow calorimetry study. *Cement and Concrete Research*, 56:129–138.

[Durdziński et al., 2015] Durdziński, P., Dunant, C. F., Ben Haha, M., and Scrivener, K. (2015). A new quantification method based on SEM-EDS to assess fly ash composition and study the reaction of its individual components in hydrating cement paste. *Cement and Concrete Research*, 73:111–122.

[Duxson and Provis, 2008] Duxson, P. and Provis, J. L. (2008). Designing precursors for geopolymer cements. *Journal of the American Ceramic Society*, 91:3864–3869.

[Ehrenberg et al., 2008] Ehrenberg, A., Israel, D., Kühn, A., Ludwig, H.-M., Tigges, V., and Wassing, W. (2008). Granulated blast-furnace slag: reaction potential and production of optimized cements, part 2. *Cement International*, 6:82–92.

[El Houda Khalifa et al., 2013] El Houda Khalifa, N., Bouasker, M. Mounanga, P., and Benkahla, N. (2013). Physico-chemical study of cementitious materials based on binary and ternary binders. *Chemistry and Materials Research*, 4:19–24.

[EN197-1, 2011] EN197-1 (2011). Cement - Part 1: Composition, specifications and conformity criteria for common cements, European Comitee for Standardization, Brussels.

[Escalante et al., 2001] Escalante, J., Gómez, L., Johal, K., Mendoza, G., Mancha, H., and J., M. (2001). Reactivity of blast-furnace slag in Portland cement blends hydrated under different conditions. *Cement and Concrete Research*, 31:1403 – 1409.

[Espion et al., 2013] Espion, B., Lebon, B., Pierre, C., Germain, O., and Hellebois, A.

(2013). Characterisation of new ternary cements with reduced clinker content. *Proceedings of the First International Conference on Concrete Sustainability*, pages 145–152.

[Fajun et al., 1985] Fajun, W., Grutzeck, M. W., and Roy, D. M. (1985). The retarding effects of fly ash upon the hydration of cement pastes: The first 24 hours. *Cement and Concrete Research*, 15:174 – 184.

[Fleißner, 1912] Fleißner (1912). *Eisenhochofenschlacken, ihre Eigenschaften und ihre Verwendung*. Wilhelm Knapp Verlag, Halle.

[Franke, 1941] Franke, B. (1941). Bestimmung von Calciumoxyd und Calciumhydroxyd neben wasserfreiem und wasserhaltigem Calciumsilikat. *Zeitschrift für anorganische und allgemeine Chemie*, 247:180–184.

[Garrault and Nonat, 2001] Garrault, S. and Nonat, A. (2001). Hydrated layer formation on tricalcium and dicalcium silicate surfaces: Experimental study and numerical simulations. *Langmuir*, 17:8131–8138.

[Garrault et al., 2011] Garrault, S., Nonat, A., Sallier, Y., and Nicoleau, L. (2011). On the origin of the dormant period of cement hydratation. In *Proceedings of the 13th international Congress on the Chemistry of Concrete, Madrid*.

[Garrault-Gauffinet and Nonat, 1999] Garrault-Gauffinet, S. and Nonat, A. (1999). Experimental investigation of calcium silicate hydrate (C-S-H) nucleation. *Journal of Crystal Growth*, 200:565–574.

[Grün, 1928] Grün, R. (1928). *Der Hochofenzement und Seine Verwendung*. Verlag Zement und Beton, Berlin.

[Gruskovnjak et al., 2006] Gruskovnjak, A., Lothenbach, B., Holzer, L., Figi, R., and Winnefeld, F. (2006). Hydration of alkali-activated slag: comparison with ordinary portland cement. *Advances in Cement Research*, 18:119–128.

[Gruyaert et al., 2010] Gruyaert, E., Robeyst, N., and De Belie, N. (2010). Study of the hydration of Portland cement blended with blast-furnace slag by calorimetry and thermogravimetry. *Journal of Thermal Analysis and Calorimetry*, 102:941 – 951.

[Gutteridge and Dalziel, 1990a] Gutteridge, W. and Dalziel, J. (1990a). Filler cement: The effect of the secondary component on the hydration of Portland cement: Part 1: Fine non-hydraulic filler. *Cement and Concrete Research*, 20:778 – 782.

[Gutteridge and Dalziel, 1990b] Gutteridge, W. and Dalziel, J. (1990b). Filler cement: The effect of the secondary component on the hydration of Portland cement: Part 2: Fine hydraulic binders. *Cement and Concrete Research*, 20:853 – 861.

[Haegermann, 1970] Haegermann, G. (1970). Dokumente zur Entstehungsgeschichte des Portland-Cements. *Zement-Kalk-Gips*, 23:1–11.

[Hawkins et al., 2003] Hawkins, P., Tennis, P., and Detwiler, R. (2003). The Use of Limestone in Portland Cement: A State-of-the-Art Review. Technical report, Portland Cement Association.

[Helgeson et al., 1981] Helgeson, H., Kirkham, D., and Flowers, G. (1981). Theoretical prediction of the thermodynamic behaviour of aqueous electrolytes at high pressures and temperatures: IV. Calculation of activity coefficients, osmotic coefficients, and apparent molal and standard and relative partial molal porperties to 600 °C and 5 Kb. *American Journal of Science*, 281:1249 – 1516.

[Hesse et al., 2011] Hesse, C., Goetz-Neunhoeffer, F., and Neubauer, J. (2011). A new approach in quantitative in-situ XRD of cement pastes: Correlation of heat flow curves with early hydration reactions. *Cement and Concrete Research*, 41:123 – 128.

[Hong and Glasser, 1999] Hong, S.-Y. and Glasser, F. (1999). Alkali binding in cement pastes Part I. The C-S-H phase. *Cement and Concrete Research*, 29:1893–1903.

[Hummel et al., 2002] Hummel, W., Berner, U., Curti, E., Pearson, F., and Thoenen, T. (2002). Nagra/PSI chemical thermodynamic data base 01/01, Nagra Technical Report NTB 02-16. Technical report, Nagra, Nationale Genossenschaft für die Lagerung radioaktiver Abfälle, Wettingen, Switzerland.

[Iñiguez Sánchez et al., 2011] Iñiguez Sánchez, C., Gómez Zamorano, L., and Lothenbach,

B. (2011). Microstructure and mechanical properties of composite cements with ultra fine silica waste additions. In *Proceedings of the 13th international Congress on the Chemistry of Concrete, Madrid*.

[Jansen et al., 2011] Jansen, D., Goetz-Neunhoeffer, F., Stabler, C., and Neubauer, J. (2011). A remastered external standard method applied to the quantification of early OPC hydration. *Cement and Concrete Research*, 41:602–608.

[Joshi and Lohita, 1997] Joshi, R. and Lohita, R. (1997). *Fly ash in concrete*. Gordon and Breach Science Publishers, Amsterdam, The Netherlands.

[Juenger et al., 2011] Juenger, M., Winnefeld, F., Provis, J., and Ideker, J. (2011). Advances in alternative cementitious binders. *Cement and Concrete Research*, 41:1232–1243.

[Juilland et al., 2010] Juilland, P., Gallucci, E., Flatt, R., and Scrivener, K. (2010). Dissolution theory applied to the induction period in alite hydration. *Cement and Concrete Research*, 40:831–844.

[Justs et al., 2014] Justs, J., Wyrzykowski, M., Winnefeld, F., Bajare, D., and Lura, P. (2014). Influence of superabsorbent polymers on hydration of cement pastes with low water-to-binder ratio. *Journal of Thermal Analysis and Calorimetry*, 115:425–432.

[Kadri et al., 2009] Kadri, E. H., Aggoun, S., De Schutter, G., and Ezziane, K. (2009). Combined effect of chemical nature and fineness of mineral powders on Portland cement hydration. *Materials and Structures*, 43:665–673.

[Kirby and Biernacki, 2012] Kirby, D. M. and Biernacki, J. J. (2012). The effect of water-to-cement ratio on the hydration kinetics of tricalcium silicate cements: Testing the two-step hydration hypothesis. *Cement and Concrete Research*, 42:1147 – 1156.

[Kocaba, 2009] Kocaba, V. (2009). *Development and Evaluation of Methods to Follow Microstructural Development of Cementitious Systems Including Slags*. PhD thesis, École Polytechnique Fédérale de Lausanne.

[Kocaba et al., 2012] Kocaba, V., Gallucci, E., and Scrivener, K. (2012). Methods for determination of degree of reaction of slag in blended cement pastes. *Cement and Concrete Research*, 42:511–525.

[Kollo, 1987] Kollo, H. (1987). 125 Jahre Hüttensand - ein äußerst schätzbares Material. *Beton-Informationen*, 27:70.

[Kulik, 2011] Kulik, D. (2011). Improving the structural consistency of C-S-H solid solution thermodynamic models. *Cement and Concrete Research*, 41(5):477 – 495.

[Kulik et al., 2013] Kulik, D., Wagner, T., Dmytrieva, S., Kosakowski, G., Hingerl, F., Chudnenko, K., and Berner, U. (2013). GEM-Selektor geochemical modeling package: revised algorithm and GEMS3K numerical kernel for coupled simulation codes. *Computational Geosciences*, 17:1 – 24.

[Kumar et al., 2012] Kumar, A., Sant, G., Patapy, C., Gianocca, C., and Scrivener, K. (2012). The influence of sodium and potassium hydroxide on alite hydration: Experiments and simulations. *Cement and Concrete Research*, 42:1513–1523.

[Kumar et al., 2008] Kumar, S., Kumar, R., Bandopadhyay, A., Alex, T., Kumar, B., Das, S., and Mehrotra, S. (2008). Mechanical activation of granulated blast furnace slag and its effect on the properties and structure of portland slag cement. *Cement & Concrete Composites*, 30:679–685.

[Lam et al., 2000] Lam, L., Wong, Y., and Poon, C. (2000). Degree of hydration and gel/space ratio of high-volume fly ash/cement systems. *Cement and Concrete Research*, 30:747–756.

[Leon-Reina et al., 2009] Leon-Reina, L., De la Torre, A. G., Porras-Vazquez, J. M., Cruz, M., Ordonez, L. M., Alcobe, X., Gispert-Guirado, F., Larranaga-Varga, A., Paul, M., Fuellmann, T., Schmidt, R., and Aranda, M. (2009). Round robin on Rietveld quantitative phase analysis of Portland cements. *Journal of Applied Crystallography*, 42:906–916.

[Lothenbach et al., 2015] Lothenbach, B., Durdziński, P., and De Weerdt, K. (2015). *A Practical Guide to Microstructural Analysis of Cementitious Materials*, chapter Thermogravimetric analysis. CRC Press, Boca Raton, Florida.

[Lothenbach et al., 2012] Lothenbach, B., Le Saout, G., Ben Haha, M., Figi, R., and Wieland, E. (2012). Hydration of a low-alkali CEM III/B-SiO_2 cement (LAC). *Cement and Concrete Research*, 42:410 – 423.

[Lothenbach et al., 2008a] Lothenbach, B., Le Saout, G., Gallucci, E., and Scrivener, K. (2008a). Influence of limestone on the hydration of Portland cements. *Cement and Concrete Research*, 38:848 – 860.

[Lothenbach et al., 2008b] Lothenbach, B., Matschei, T., Möschner, G., and Glasser, F. (2008b). Thermodynamic modelling of the effect of temperature on the hydration and porosity of Portland cement. *Cement and Concrete Research*, 38:1–18.

[Lothenbach and Nonat, 2015] Lothenbach, B. and Nonat, A. (2015). Calcium silicate hydrates: Solid and liquid phase composition. *Cement and Concrete Research*, 78:57–70.

[Lothenbach et al., 2011] Lothenbach, B., Scrivener, K., and Hooton, R. (2011). Supplementary cementitious materials. *Cement and Concrete Research*, 41:1244 – 1256.

[Luke and Lachowski, 2008] Luke, K. and Lachowski, E. (2008). Internal composition of 20-year-old fly ash and slag-blended ordinary Portland cement pastes. *Journal of the American Ceramic Society*, 91:4084–4092.

[Lumley et al., 1996] Lumley, J., Gollop, R., Moir, G., and Taylor, H. (1996). Degrees of reaction of the slag in some blends with portland cements. *Cement and Concrete Research*, 26(1):139–151.

[Marchal et al., 2012] Marchal, V., Dellink, R., van Vuuren, D., Clapp, C., Château, J., Lanzi, E., Magné, B., and van Vliet, J. (2012). *OECD Environmental Outlook to 2050*, chapter 3. Climate Change, pages 71–152. OECD Publishing.

[Matschei and Costoya, 2012] Matschei, T. and Costoya, M. (2012). A contribution to an improved understanding of the hydration kinetics of OPC. *18. IBAUSIL, Weimar*, Paper No. V1-21.

[Matschei et al., 2007a] Matschei, T., Lothenbach, B., and Glasser, F. (2007a). The role of calcium carbonate in cement hydration. *Cement and Concrete Research*, 37:551 – 558.

[Matschei et al., 2007b] Matschei, T., Lothenbach, B., and Glasser, F. (2007b). The AFm phase in Portland cement. *Cement and Concrete Research*, 37:118 – 130.

[Matschei et al., 2007c] Matschei, T., Lothenbach, B., and Glasser, F. (2007c). Thermodynamic properties of Portland cement hydrates in the system CaO-Al_2O_3-SiO_3-$CaSO_3$-$CaCO_3$-H_2O. *Cement and Concrete Research*, 37:1379 – 1410.

[Mehrotra et al., 1982] Mehrotra, V., Sai, A., and Kapur, P. (1982). Plaster of paris activated supersulfated slag cement. *Cement and Concrete Research*, 12:463–473.

[Menendez and Irassar, 2003] Menendez, G.and Bonavetti, V. and Irassar, E. (2003). Strength development of ternary blended cement with limestone filler and blast-furnace slag. *Cement & Concrete Composites*, 25:61 – 67.

[Mills et al., 2011] Mills, K., Yuan, L., and Jones, R. (2011). Estimating the physical properties of slags. *The Journal of The Southern African Institute of Mining and Metallurg*, 111:649–658.

[Minard, 2003] Minard, H. (2003). *Etude intégrée des processus d'hydratation, de coagulation, de rigidification et de prise pour un système C_3S - C_3A - sulfates - alcalins*. PhD thesis, Université de Bourgogne.

[Moesgaard et al., 2011] Moesgaard, M., Herfort, D., Steenberg, M., Frank Kirkegaard, L., and Yue, Y. (2011). Physical performances of blended cements containing calcium aluminosilicate glass powder and limestone. *Cement and Concrete Research*, 41:359 – 364.

[Mota et al., 2015] Mota, B., Matschei, T., and Scrivener, K. (2015). The influence of sodium salts and gypsum on alite hydration. *Cement and Concrete Research*, 75:53–65.

[Mysen et al., 1982] Mysen, B., Virgo, D., and Seifert, F. (1982). The structure of silicate melts: Implications for chemical and physical properties of natural magma. *Reviews of Geophysics*, 20:353–383.

[Nicoleau et al., 2013] Nicoleau, L., Nonat, A., and Perrey, D. (2013). The di- and tricalcium silicate dissolutions. *Cement and Concrete Research*, 47:14–30.

[Nicoleau et al., 2014] Nicoleau, L., Schreiner, E., and Nonat, A. (2014). Ion-specific effects influencing the dissolution of tricalcium silicate. *Cement and Concrete Research*, 59:118–138.

[Odler, 2000] Odler, I. (2000). *Special Inorganic Cements*. Taylor & Francis, London.

[Oey et al., 2013] Oey, T., Kumar, A., Bullard, J., Neithalath, N., and Sant, G. (2013). The Filler Effect: The Influence of Filler Content and Surface Area on Cementitious Reaction Rates. *J. Am. Ceram. Soc.*, 96(6):1978–1990.

[Ogawa et al., 1980] Ogawa, K., Uchikawa, H., Takemoto, K., and Yasui, I. (1980). The mechanism of the hydration in the system C_3S-pozzolana. *Cement and Concrete Research*, 10:683 – 696.

[Pal et al., 2003] Pal, S., Mukherjee, A., and Pathak, S. (2003). Investigation of hydraulic activity of ground granulated blast furnace slag in concrete. *Cement and Concrete Research*, 33:1481–1486.

[Pardo et al., 2012] Pardo, N., Moya, J., and Vatopoulos, K. (2012). Prospective scenarios on energy efficiency and CO_2 emissions in the EU iron & steel industry. Technical report, European Commission - Joint Research Centre - Institute for Energy and Transport, Petten, The Netherlands.

[Parkhurst and Appelo, 2013] Parkhurst, D. and Appelo, C. (2013). *Description of Input and Examples for PHREEQC Version 3 - A Computer Program for Speciation, Batch-Reaction, One-Dimensional Transport, and Inverse Geochemical Calculations*. U.S. Geological Survey Techniques and Methods, book 6, chap. A43.

[Passow, 1908] Passow, H. (1908). *Die Hochofenschlacke in der Zementindustrie*. A. Sturbers Verlag, Würzburg.

[Payá et al., 2000] Payá, J., Monzó, J., Borrachero, M., Peris-Mora, E., and Amahjour, F. (2000). Mechanical treatment of fly ashes: Part IV. Strength development of ground fly ash-cement mortars cured at different temperatures. *Cement and Concrete Research*, 30:543–551.

[Péra et al., 1999] Péra, J., Husson, S., and Guilhot, B. (1999). Influence of finely ground limestone on cement hydration. *Cement & Concrete Composites*, 21:99 – 105.

[Pöllmann, 2006] Pöllmann, H. (2006). Syntheses, properties and solid solution of ternary lamellar calcium aluminate hydroxi salts (AFm-phases) containing SO_4^{2-}, CO_3^{2-} and OH^-. *Neues Jahrbuch für Mineralogie - Abhandlungen: Journal of Mineralogy and Geochemistry*, 182:173 – 181.

[Poppe and De Schutter, 2005] Poppe, A.-M. and De Schutter, G. (2005). Cement hydration in the presence of high filler contents. *Cement and Concrete Research*, 35:2290–2299.

[Quennoz et al., 2011] Quennoz, A., Gallucci, E., and Scrivener, K. (2011). Calcium silicate - calcium aluminate interactions and their influence on cement early hadration. *Proceedings of the 13th international Congress on the Chemistry of Concrete, Madrid*.

[Ravina, 1981] Ravina, D. (1981). Production and collection of fly ash for use in concrete. In Diamond, S., editor, *Proceedings of the sympossium of fly ash incorporation in hydrated cement systems, Boston*, pages 2–11.

[RILEM, 1988] RILEM (1988). TC 73-SBC - Final report: Siliceous by-products for use in concrete. Technical report, RILEM Publications SARL.

[Rossen, 2014] Rossen, J. (2014). *Composition and morphology of C-A-S-H in pastes of alite and cement blended with supplementary cementitious materials*. PhD thesis, École Polytechnique Fédérale de Lausanne.

[Rossen et al., 2015] Rossen, J., Lothenbach, B., and Scrivener, K. (2015). Composition of C-S-H in pastes with increasing levels of silica fume addition. *Cement and Concrete Research*, 75:14–22.

[Roy, 2009] Roy, A. (2009). Sulfur speciation in granulated blast furnace slag: An X-ray absorption spectroscopic investigation. *Cement and Concrete Research*, 39:659–663.

[Sant et al., 2012] Sant, G., Kumar, A., Patapy, C., Le Saout, G., and Scrivener, K. (2012). The influence of sodium and potassium hydroxide on volume changes in cementitious materials. *Cement and Concrete Research*, 42:1447–1455.

[Schneider et al., 2011] Schneider, M., Romer, M., Tschudin, M., and Bolio, H. (2011). Sustainable cement production-present and fu-

ture. *Cement and Concrete Research*, 41:642 – 650.

[Schöler et al., 2015] Schöler, A., Lothenbach, B., Winnefeld, F., and Zajac, M. (2015). Hydration of quaternary Portland cement blends containing blast-furnace slag, siliceous fly ash and limestone powder. *Cement & Concrete Composites*, 55:374–382.

[Scrivener et al., 2015] Scrivener, K., Lothenbach, B., De Belie, N., Gruyaert, E., Skibsted, J., Snellings, R., and Vollpracht, A. (2015). TC 238-SCM: hydration and microstructure of concrete with SCMs. *Materials and Structures*, 48:835–862.

[Shafaatian et al., 2013] Shafaatian, S., Akhavan, A., Maraghechi, H., and Rajabipour, F. (2013). How does fly ash mitigate alkali-silica reaction (ASR) in accelerated mortar bar test (ASTM C1567)? *Cement & Concrete Composites*, 37:143–153.

[Sharma and Pandey, 1999] Sharma, R. and Pandey, S. (1999). Influence of mineral additives on the hydration characteristics of ordinary Portland cement. *Cement and Concrete Research*, 29:1525–1529.

[Shelby, 2005] Shelby, J. (2005). *Introduction to Glass Science and Technology*. The Royal Society of Chemistry, Cambridge.

[Snellings, 2013] Snellings, R. (2013). Solution-controlled dissolution of supplementary cementitious material glasses at pH 13: The effect of solution composition on glass dissolution rates. *Journal of the American Ceramic Society*, 96:2467–2475.

[Snyder et al., 1964] Snyder, M., Roese, A., Hunter, R., and Gluck, P. (1964). Properties and uses of fly ash. *Battelle Technical Review, The Battelle Memorial Institute, Columbus, Ohio*, Fevruary:14–18.

[Swamy, 1986] Swamy, R., editor (1986). *Cement replacement materials*. Surrey University Press, Guildford.

[Thoenen and Kulik, 2003] Thoenen, T. and Kulik, D. (2003). Nagra/PSI chemical thermodynamic database 01/01 for GEMS-selektor (V.2-PSI) geochemical modeling code, http://gems.web.psi.ch/doc/pdf/TM-44-03-04-web.pdf PSI, Villingien.

[Thomas et al., 2009] Thomas, J., Jennings, H. M., and Chen, J. (2009). Influence of nucleation seeding on the hydration mechanisms of tricalcium silicate and cement. *The Journal of Physical Chemistry C*, 113:4327–4334.

[Tishmack et al., 1999] Tishmack, J., Olek, J., and Diamond, S. (1999). Characterization of High-Calcium Fly Ashes and Their Potential Influence on Ettringite Formation in Cementitious Systems. *Cement, Concrete, and Aggregates*, 21:82–92.

[Tsivilis et al., 2002] Tsivilis, S., Chaniotakis, E., Kakali, G., and Batis, G. (2002). An analysis of the properties of Portland limestone cements and concrete. *Cement & Concrete Composites*, 24:371 – 378.

[Valentim et al., 2009] Valentim, B., Guedes, A., Flores, D., Ward, C., and Hower, J. (2009). Variations in fly ash composition with sampling location: Case study from a portuguese power plant. *Coal Combustion and Gasification Products*, 1:14–24.

[van Oss, 2015] van Oss, H.-G. (January 2015). *Mineral Commodity Summaries*. U.S. Geological Survey, Reston, Virginia.

[Vance et al., 2013] Vance, K., Aguayo, M., Oey, T., Sant, G., and Neithalath, N. (2013). Hydration and strength development in ternary Portland cement blends containing limestone and fly ash or metakaolin. *Cement & Concrete Composites*, 39:93 – 103.

[VDZ, 2002] VDZ (2002). *Zement Taschenbuch*. Verein Deutscher Zementwerke e.V., Düsseldorf.

[VDZ, 2012] VDZ (2012). Güteüberwachung und Qualitätssicherung von Zement. VDZ-Tätigkeitsbericht 2009-2012. Technical report, Verein Deutscher Zementwerke e.V., Düsseldorf.

[Venkatanarayanan and Rangaraju, 2013] Venkatanarayanan, H.K. and, H. and Rangaraju, P. R. (2013). Decoupling the effects of chemical composition and fineness of fly ash in mitigating alkali-silica reaction. *Cement & Concrete Composites*, 43:54–68.

[Vicat, 1818] Vicat, L.-J. (1818). *Recherches expérimentales sur les chaux de construction, les bétons et les mortiers ordinaires*. Firmin Didot Publication, Paris.

[Vicat, 1828] Vicat, L.-J. (1828). *Résumé des connaissances positives actuelles, sur les qualités, le choix et la convenance réciproque des matériaux propres à la fabrication des Mortiers et Ciments Calcaires*. Firmin Didot Publication, Paris.

[Ward and French, 2006] Ward, C. and French, D. (2006). Determination of glass content and estimation of glass composition in fly ash using quantitative X-ray diffractometry. *Fuel*, 85:2268 – 2277.

[Winnefeld et al., 2015] Winnefeld, F., Ben Haha, M., Le Saout, G., Costoya, M., Ko, S.-C., and Lothenbach, B. (2015). Influence of slag composition on the hydration of alkali-activated slags. *Journal of Sustainable Cement-Based Materials*, 4:85–100.

[Worrell et al., 2001] Worrell, E., Price, L., Martin, N., Hendriks, C., and Meida, L. (2001). Carbon dioxide emissions from the global cement industry. *Annual Review of Environment and Resources*, 26:303–329.

[Yan and Neretnieks, 1995] Yan, J. and Neretnieks, I. (1995). Is the glass phase dissolution rate always a limiting factor in the leaching processes of combustion residues? *The Science of the Total Environment*, 172:95–118.

[Yan et al., 2003] Yan, P., Zheng, F., and Xu, Z. (2003). Hydration of shrinkage-compensating binders with different compositions and water-binder ratios. *Journal of Thermal Analysis and Calorimetry*, 74:201–209.

[Zajac et al., 2014] Zajac, M., Rossberg, A., Le Saout, G., and Lothenbach, B. (2014). Influence of limestone and anhydrite on the hydration of Portland cements. *Cement & Concrete Composites*, 46:99 – 108.

List of Figures

List of Tables

Glossary

Cement Notation

A	Al_2O_3
$\overline{C}$	CO_2
C	CaO
F	Fe_2O_3
K	K_2O
M	MgO
N	Na_2O
$\overline{S}$	SO_3
S	SiO_2

Abbreviations

AASHTO	American Association of State Highway and Transportation Officials
AFm	Al_2O_3-Fe_2O_3 (mono)
AFt	Al_2O_3-Fe_2O_3 (tri)
ASR	alkali-silica reaction
ASTM	American Society for Testing and Materials
BFS	blast-furnace slag
BW	bound water
C-(A)-S-H	calcium-alumino-silicate-hydrate
C/S	calcium-to-silicon ratio
CCS	carbon dioxide capture and storage
CEN	Comission for European Normalization
CH	portlandite or calcium hydroxide
CSA	Canadian Standards Association
C-S-H	calcium-silicate-hydrate
EN	European standard
FA	fly ash
FH	goethite or FeO(OH)
GEMS	Gibbs energy minimization software
GGBFS	ground granulated blast-furnace slag
GU	general use hydraulic cement
HC	hemicarbonate

HT	hydrotalcite
IAP	ion activity product
IC	ion chromatography
ICP-OES	inductively coupled plasma optical emission spectrometry
KOH	potassium hydroxide
LS	limestone
MC	monocarbonate
NBO/T	ratio of non-bridging oxygen atoms to oxygen atoms in tetragonal coordination
NWF	network forming oxide
NWM	network modifying oxide
OECD	Organisation for Economic Co-operation and Development
PC	Portland cement
PLC	Portland limestone cement
PSD	particle size distribution
PSI	Paul Scherrer Intitut
QXRD	quantitative X-ray diffraction
Qz	quartz
RH	relative humidity
rpm	rotations per minute
SA	surface area
SCM	supplementary cementitious material(s)
SEM/EDX	scanning electron microscopy - energy-dispersive X-ray spectroscopy
SEM-IA	scanning electron microscopy - image analysis
SI	saturation index
TC	Technical committee
TGA	thermogravimetric analysis
TOC	total content of organic carbon
WG	working group
XRD	X-ray diffraction
XRF	X-ray fluorescence

Appendices

Contents

Appendix 1 - Matrix under investigation: Actual compositions

Table A1-1 - Actual compositions of all systems as investigated. Data in [wt.%].

System	PC	BFS	FA	LS	Qz	AH
Kinetics and hydrate assemblage studies (Chapter 6 and Chapter 7)[a]						
20-10-20-0	51.1	19.0	9.5	18.2	-	2.3
20-15-15-0	51.1	19.0	14.2	13.4	-	2.3
20-20-10-0	51.1	19.0	19.0	8.7	-	2.3
20-25-5-0	51.1	19.0	23.7	4.0	-	2.3
20-30-0-0	50.7	18.8	28.2	-	-	2.3
30-0-20-0	51.1	28.4	-	18.2	-	2.3
30-5-15-0	51.1	28.4	4.7	13.4	-	2.3
30-10-10-0	51.1	28.4	9.5	8.7	-	2.3
30-15-5-0	51.1	28.4	14.2	4.0	-	2.3
30-20-0-0	50.7	28.2	18.8	-	-	2.3
20-0-0-30	50.7	18.8	-	-	28.2	2.3
30-0-0-20	50.7	28.2	-	-	18.8	2.3
0-0-0-50	50.7	-	-	-	47.0	2.3
Pore solution and sulfate speciation studies (Chapter 8)[b]						
20-10-20-0	50.6	18.8	9.4	18.1	-	3.1
20-15-15-0	50.6	18.8	14.1	13.4	-	3.1
20-25-5-0	50.6	18.8	23.5	4.0	-	3.1
20-30-0-0	50.3	18.6	28.0	-	-	3.1
30-0-20-0	50.6	28.2	-	18.1	-	3.1
30-5-15-0	50.6	28.2	4.7	13.4	-	3.1
30-15-5-0	50.6	28.2	14.1	4.0	-	3.1
20-0-0-30	50.3	18.6	-	-	28.0	3.1
30-0-0-20	50.3	28.0	-	-	18.6	3.1
0-0-0-50	50.3	-	-	-	46.6	3.1
Early hydration study (Chapter 4)[c]						
C	100.0	-	-	-	-	-
C-S	51.9	48.1	-	-	-	-
C-S-$	50.7	47.0	-	-	-	2.3
C-FA	51.9	-	48.1	-	-	-
C-FA-$	50.7	-	47.0	-	-	2.3
C-FA-L	51.9	-	28.9	19.2	-	-
C-L	51.9	-	-	48.1	-	-
C-Q	51.9	-	-	-	48.1	-

[a] Water-to-binder ratio = 0.45.
[b] Water-to-binder ratio = 0.50.
[c] Water-to-binder ratio = 0.75.

Appendix 2 - Pore solution chemistry - comprehensive tables

Table A2-1 - Detection limits for ion concentrations analyzed by ion chromatography (Chapter 5 and Chapter 8). Data given in [mmol/l].[a]

	Al	Ca	Cl	K	Na	Si	SO_4
l.d.l.	0.004	0.003	0.003	0.003	0.004	0.004	0.001
u.d.l.	1.9	1.2	1.4	1.3	2.2	1.8	0.5

[a] Values for lower detection limit (l.d.l.) correspond to 0.1 [mg/l], values for upper detection limit correspond to 50 [mg/l].

Table A2-2 - Early hydration study (Chapter 4): Measured ion concentrations in the pore solutions along with calculated OH^- concentrations and pH values. All valuzes exept pH in Ion concentrations as measured by ion chromatography, calculated OH^- concentrations and measured pH for glass dissolution experiments. Data except pH given in [mmol/l].

age [h]	Al	Ca	SO_4	K	Na	Si	OH^-	pH
				C				
0.083	0.006	20.8	41.0	87.1	17.9	0.350	89.2	12.83
0.5	0.002	23.0	37.8	89.0	19.4	0.027	109.7	12.91
1	0.002	24.7	35.1	96.4	22.2	0.013	135.6	13.01
2	0.002	24.4	36.3	94.4	16.5	n.d.[a]	120.9	12.96
4	0.002	24.5	31.4	81.1	17.5	0.025	117.3	12.95
6	0.001	23.6	33.0	82.1	18.0	0.022	112.8	12.93
				C-FA				
0.083	0.006	22.6	29.9	54.4	14.4	0.170	74.9	12.76
0.5	0.003	24.0	27.7	47.8	15.3	0.023	76.8	12.77
1	0.002	25.5	26.0	49.4	15.1	0.019	87.3	12.82
2	0.002	25.0	23.7	49.9	15.5	0.019	93.5	12.85
4	0.002	24.7	23.8	47.6	15.6	0.019	89.4	12.83
6	0.002	24.3	24.4	50.6	16.3	0.019	92.0	12.85
				C-FA-$				
0.083	0.005	21.4	27.6	45.5	13.9	0.029	65.4	12.70
0.5	0.004	24.5	25.7	46.4	13.8	0.017	79.7	12.78
1	0.004	26.7	25.3	46.7	14.3	0.012	87.5	12.82
2	0.004	28.4	24.5	46.6	14.5	0.009	94.3	12.86
4	0.004	28.4	24.1	47.6	14.8	0.008	97.3	12.87
6	0.003	26.2	23.6	45.4	14.8	0.009	89.8	12.84

Continued on next page

Table A2-2 – continued from previous page

age [h]	Al	Ca	SO_4	K	Na	Si	OH^-	pH
				C-FA-L				
0.083	0.005	21.6	25.7	44.1	10.7	0.080	63.3	12.70
0.5	0.004	24.6	23.7	42.3	11.3	0.078	74.3	12.77
1	0.003	19.8	19.6	38.4	9.6	0.023	65.6	12.72
2	0.002	20.2	19.1	37.9	8.6	0.020	66.0	12.72
4	0.003	24.5	18.8	42.8	10.9	0.018	87.1	12.84
6	0.002	23.4	19.3	43.2	11.7	0.020	84.8	12.83
				C-S				
0.083	0.002	22.8	23.1	46.0	9.9	0.370	75.6	12.76
0.5	0.002	23.8	21.4	46.9	10.5	0.018	86.0	12.82
1	0.001	25.1	21.2	47.8	10.9	0.014	91.6	12.85
2	0.001	27.8	18.9	48.5	11.2	0.013	106.0	12.91
4	0.001	24.4	20.6	49.1	11.8	0.012	94.5	12.86
6	0.001	23.3	21.3	49.2	12.2	0.012	90.4	12.84
				C-S-$				
0.083	0.002	23.9	22.9	39.6	9.0	0.014	69.8	12.73
0.5	0.001	24.6	21.4	42.5	9.4	0.019	80.0	12.79
1	0.002	26.1	20.8	43.1	9.5	0.017	86.6	12.82
2	0.001	27.2	20.7	44.0	9.7	0.016	91.2	12.84
4	0.001	26.0	22.4	45.0	10.2	0.015	85.5	12.82
6	0.001	25.1	22.8	45.7	11.1	0.015	84.4	12.81
				C-L				
0.083	0.001	25.8	23.2	41.2	8.1	0.018	74.7	12.76
0.5	0.001	28.6	22.0	42.3	8.5	0.010	87.4	12.83
1	0.001	33.9	20.2	46.9	9.7	0.007	113.6	12.94
2	0.001	29.7	20.1	43.0	9.2	0.005	97.1	12.87
4	0.001	27.5	21.6	42.8	9.8	0.005	88.1	12.83
6	0.001	25.2	22.1	43.1	11.0	0.005	82.8	12.80
				C-Q				
0.083	0.003	22.3	22.7	39.1	7.8	0.022	63.7	12.69
0.5	0.002	24.0	20.9	38.9	8.0	0.015	72.9	12.75
1	0.002	25.8	20.1	39.5	8.4	0.012	81.2	12.8
2	0.002	29.1	17.8	39.4	8.7	0.010	95.9	12.87
4	0.002	25.7	19.9	39.9	8.9	0.011	82.9	12.8
6	0.001	24.8	21.1	40.7	9.5	0.011	79.0	12.78

[a] n.d. = not detected.

Table A2-3 - Early hydration study (Chapter 4): Calculated saturation indices for all systems under investigations. Mc - monocarboaluminate, Ms - monosulfoaluminate, Cc - calcite, E - ettringite, CH - portlandite, Gp - gypsum.

age [h]	Mc	Ms	E	CH	Gp	C-S-H	$C_3S_{exp.}$	$\Pi_{C_3S,\ exp.}$
				C				
0.083	−0.25	1.41	8.47	0.00	0.06	1.67	−0.11	−50.96
0.5	−0.76	0.90	7.95	0.22	0.05	0.68	−0.69	−52.28
1	−0.35	1.28	8.27	0.42	0.02	0.45	−0.56	−51.99
2	−0.48	1.17	8.22	0.33	0.05	n.c.[a]	n.c.[a]	n.c.[a]
4	−0.60	1.03	8.02	0.33	0.02	0.69	−0.45	−51.74
6	−1.00	0.63	7.62	0.28	0.03	0.62	−0.64	−52.19
				C-FA				
0.083	−0.28	1.38	8.44	−0.04	0.06	1.34	−0.44	−51.71
0.5	−0.77	0.89	7.96	0.02	0.06	0.50	−1.14	−53.34
1	−0.55	1.10	8.14	0.16	0.04	0.49	−0.91	−52.80
2	−0.44	1.16	8.11	0.21	0.00	0.52	−0.78	−52.50
4	−0.56	1.05	8.02	0.17	0.01	0.50	−0.87	−52.71
6	−0.76	0.84	7.79	0.18	0.00	0.50	−0.86	−52.68
				C-FA-$				
0.083	−0.56	1.08	8.11	−0.15	0.04	0.51	−1.47	−54.08
0.5	−0.19	1.45	8.49	0.07	0.04	0.41	−1.14	−53.32
1	0.02	1.67	8.74	0.18	0.06	0.30	−1.03	−53.07
2	0.19	1.85	8.92	0.27	0.06	0.21	−0.95	−52.90
4	0.10	1.75	8.79	0.30	0.05	0.19	−0.92	−52.83
6	−0.40	1.23	8.24	0.20	0.03	0.19	−1.11	−53.25
				C-FA-L				
0.083	−0.64	0.99	8.00	−0.14	0.03	0.96	−0.99	−52.99
0.5	−0.34	1.29	8.30	0.05	0.03	1.05	−0.52	−51.89
1	−0.86	0.67	7.46	−0.11	−0.08	0.44	−1.45	−54.04
2	−1.06	0.47	7.26	−0.09	−0.08	0.38	−1.46	−54.06
4	−0.36	1.18	8.00	0.21	−0.06	0.50	−0.79	−52.51
6	−0.94	0.59	7.41	0.16	−0.07	0.52	−0.86	−52.68
				C-S				
0.083	−0.93	0.66	7.59	0.01	−0.01	1.71	0.07	−50.55
0.5	−0.92	0.65	7.55	0.15	−0.03	0.46	−0.95	−52.90
1	−1.18	0.40	7.30	0.22	−0.03	0.38	−0.90	−52.77
2	−0.73	0.82	7.67	0.38	−0.05	0.46	−0.50	−51.86
4	−1.35	0.20	7.06	0.23	−0.05	0.32	−0.94	−52.86
6	−1.49	0.07	6.93	0.17	−0.05	0.28	−1.09	−53.21

Continued on next page

Table A2-3 – continued from previous page

age [h]	Mc	Ms	E	CH	Gp	C-S-H	$C_3S_{exp.}$	$\Pi_{C_3S,\ exp.}$
				C-S-$				
0.083	−0.99	0.63	7.64	−0.02	0.03	0.28	−1.41	−53.96
0.5	−1.09	0.50	7.45	0.11	−0.01	0.48	−0.99	−52.98
1	−0.84	0.76	7.70	0.20	−0.01	0.47	−0.83	−52.60
2	−0.91	0.69	7.65	0.25	0.00	0.46	−0.73	−52.38
4	−1.16	0.46	7.44	0.17	0.02	0.41	−0.93	−52.85
6	−1.31	0.30	7.27	0.15	0.01	0.39	−1.01	−53.02
				C-L				
0.083	−1.36	0.28	7.33	0.07	0.05	0.42	−1.11	−53.26
0.5	−1.88	−0.23	6.80	0.23	0.04	0.24	−0.97	−52.93
1	−1.09	0.54	7.54	0.51	0.03	0.22	−0.47	−51.79
2	−1.66	−0.04	6.93	0.34	0.01	−0.04	−1.05	−53.11
4	−0.82	0.80	7.79	0.22	0.02	−0.08	−1.31	−53.72
6	−1.09	0.52	7.49	0.14	0.01	−0.10	−1.50	−54.17
				C-Q				
0.083	−1.06	0.56	7.53	−0.12	0.01	0.42	−1.46	−54.07
0.5	−1.07	0.53	7.47	0.03	−0.01	0.33	−1.27	−53.63
1	−0.81	0.78	7.72	0.15	−0.01	0.27	−1.10	−53.23
2	−0.40	1.17	8.06	0.34	−0.03	0.31	−0.70	−52.31
4	−0.89	0.69	7.61	0.16	−0.02	0.24	−1.11	−53.25
6	−1.16	0.44	7.39	0.10	0.00	0.22	−1.25	−53.58

[a] n.c. = not calculated as no Si was detected in the pore solution.

Table A2-4 - Synthetic glasses (Chapter 5): Ion concentrations as measured by ion chromatography, calculated OH^- concentrations and measured pH for glass dissolution experiments. Data except pH given in [mmol/l]. n.d. = not detected (either below lower limit of detection or not present).

age [h]	Al	Ca	Cl	K	Na	OH^-	Si	SO_4	pH
				FA_s1					
0.5	n.d.	n.d.	n.d.	290.3	1.6	303.3	n.d.	n.d.	13.34
1	n.d.	n.d.	n.d.	293.7	1.6	303.4	n.d.	0.01	13.34
2	n.d.	n.d.	n.d.	295.4	1.6	303.4	n.d.	n.d.	13.34
4	n.d.	n.d.	0.01	293.8	1.7	325.6	n.d.	n.d.	13.35
8	n.d.	n.d.	0.01	289.6	2.4	313.4	n.d.	n.d.	13.34
16	n.d.	n.d.	n.d.	296.7	1.6	281.2	0.019	n.d.	13.30
24	0.005	n.d.	0.03	308.8	1.6	279.9	n.d.	n.d.	13.29
48	0.011	n.d.	0.03	308.3	1.7	302.0	0.681	n.d.	13.32
168	0.023	n.d.	0.03	311.3	1.6	249.7	0.085	n.d.	13.24
				FA_s2					
0.5	n.d.	n.d.	n.d.	266.6	1.8	251.6	0.007	n.d.	13.27
1	n.d.	n.d.	n.d.	266.4	1.8	233.1	0.011	n.d.	13.24
2	n.d.	n.d.	n.d.	335.9	1.8	243.3	0.007	n.d.	13.25
4	n.d.	n.d.	n.d.	272.5	1.8	242.3	0.004	n.d.	13.25
8	0.018	n.d.	n.d.	280.5	2.3	242.5	0.473	n.d.	13.25
16	0.023	n.d.	n.d.	284.5	2.2	270.5	0.509	n.d.	13.29
24	0.026	n.d.	n.d.	282.2	2.2	270.5	0.488	n.d.	13.29
48	0.035	n.d.	n.d.	284.4	2.2	260.4	0.452	n.d.	13.27
168	0.074	n.d.	n.d.	279.6	2.2	251.9	0.325	n.d.	13.27
				FA_s3					
0.5	n.d.	n.d.	n.d.	291.2	1.6	303.3	n.d.	n.d.	13.34
1	n.d.	n.d.	n.d.	297.6	1.6	303.4	n.d.	0.01	13.34
2	n.d.	n.d.	n.d.	299.3	1.6	303.5	n.d.	0.01	13.34
4	n.d.	n.d.	0.01	292.2	1.6	313.4	n.d.	n.d.	13.34
8	0.004	n.d.	0.01	290.8	1.7	313.4	n.d.	n.d.	13.34
16	0.005	n.d.	n.d.	301.3	1.6	292.2	n.d.	n.d.	13.32
24	0.009	n.d.	0.03	303.9	1.6	290.6	n.d.	n.d.	13.30
48	0.019	n.d.	0.05	307.7	1.7	313.6	0.256	n.d.	13.34
168	0.046	n.d.	0.03	314.2	1.7	290.8	0.137	n.d.	13.30
				FA_c1					
0.5	n.d.	n.d.	0.02	289.3	1.7	279.6	n.d.	n.d.	13.29
1	n.d.	n.d.	0.03	292.3	1.6	301.7	0.012	n.d.	13.32
2	n.d.	n.d.	n.d.	311.4	1.9	260.8	0.024	n.d.	13.27
4	n.d.	n.d.	n.d.	310.5	1.9	303.6	0.018	n.d.	13.34
8	0.006	n.d.	n.d.	312.7	1.9	292.3	0.020	n.d.	13.32
16	0.009	n.d.	n.d.	306.1	1.9	270.9	0.060	n.d.	13.29
24	0.011	n.d.	n.d.	315.6	1.9	251.2	0.043	n.d.	13.25
48	0.029	n.d.	n.d.	296.4	1.9	303.4	0.061	n.d.	13.34
168	0.066	n.d.	n.d.	297.2	1.9	281.2	0.269	n.d.	13.30

Continued on next page

Table A2-4 – continued from previous page

age [h]	Al	Ca	Cl	K	Na	OH^-	Si	SO_4	pH
				FA_c2					
0.5	n.d.	n.d.	0.03	293.0	1.6	290.5	n.d.	n.d.	13.30
1	n.d.	n.d.	0.03	298.3	1.6	313.5	0.028	n.d.	13.34
2	0.004	n.d.	n.d.	296.2	2.3	281.2	0.034	n.d.	13.30
4	0.006	n.d.	n.d.	307.0	2.0	303.6	0.033	n.d.	13.34
8	0.010	n.d.	n.d.	309.4	1.9	303.6	0.046	n.d.	13.34
16	0.021	n.d.	n.d.	301.5	1.9	251.0	0.105	n.d.	13.25
24	0.019	n.d.	n.d.	307.1	1.9	270.9	0.109	n.d.	13.29
48	0.051	n.d.	n.d.	305.2	1.9	292.2	0.199	n.d.	13.32
168	0.097	n.d.	n.d.	303.3	1.9	281.3	0.439	n.d.	13.30
				S1					
0.5	n.d.	n.d.	n.d.	288.5	1.6	303.3	n.d.	n.d.	13.34
1	n.d.	n.d.	n.d.	296.5	1.6	303.4	0.005	n.d.	13.34
2	n.d.	n.d.	n.d.	299.5	1.6	303.5	0.006	n.d.	13.34
4	0.008	n.d.	0.02	294.4	1.7	313.4	n.d.	n.d.	13.34
8	0.014	n.d.	0.01	317.7	1.6	313.7	n.d.	n.d.	13.34
16	0.021	n.d.	n.d.	297.1	1.6	303.4	0.104	n.d.	13.34
24	0.037	n.d.	0.03	306.1	1.7	301.9	0.210	n.d.	13.32
48	0.047	0.1	0.03	311.1	1.7	313.7	0.514	n.d.	13.34
168	0.066	0.1	0.02	309.1	1.7	302.0	0.463	n.d.	13.32
				S2					
0.5	0.004	n.d.	n.d.	271.0	1.8	233.2	0.011	n.d.	13.24
1	0.007	n.d.	n.d.	281.9	1.8	242.5	0.015	n.d.	13.25
2	0.010	n.d.	n.d.	270.8	1.8	242.3	0.017	n.d.	13.25
4	0.017	n.d.	n.d.	274.7	1.8	233.3	0.020	n.d.	13.24
8	0.032	n.d.	n.d.	282.0	2.0	251.9	0.408	n.d.	13.27
16	0.054	n.d.	n.d.	265.2	2.0	270.2	0.465	n.d.	13.29
24	0.079	n.d.	n.d.	277.0	2.0	260.3	0.487	n.d.	13.27
48	0.108	n.d.	n.d.	277.1	2.0	270.4	0.530	n.d.	13.29
168	0.149	n.d.	n.d.	292.4	1.9	281.2	0.587	n.d.	13.30
				S3					
0.5	0.004	n.d.	n.d.	292.1	1.6	303.4	n.d.	n.d.	13.34
1	0.008	n.d.	n.d.	290.6	1.6	303.3	0.018	n.d.	13.34
2	0.011	n.d.	n.d.	301.0	1.6	303.5	0.023	n.d.	13.34
4	0.019	n.d.	0.02	289.6	1.5	313.4	n.d.	n.d.	13.34
8	0.036	n.d.	0.01	288.9	1.6	313.4	n.d.	n.d.	13.34
16	0.060	n.d.	n.d.	298.7	1.8	303.5	0.533	n.d.	13.34
24	0.088	0.1	0.03	316.5	1.6	302.1	0.266	n.d.	13.32
48	0.121	0.1	0.03	305.4	1.7	313.6	0.622	n.d.	13.34
168	0.166	0.2	0.03	310.7	1.7	302.0	0.598	n.d.	13.32

Continued on next page

Table A2-4 – continued from previous page

age [h]	Al	Ca	Cl	K	Na	OH^-	Si	SO_4	pH
				Qz					
0.5	n.d.	0.1	0.03	288.4	2.0	301.7	0.051	n.d.	13.32
1	n.d.	0.1	0.02	282.4	1.7	301.8	0.043	n.d.	13.32
2	n.d.	0.1	0.03	285.5	1.7	301.8	0.034	n.d.	13.32
4	n.d.	n.d.	0.03	286.5	1.7	301.5	0.032	n.d.	13.32
8	n.d.	n.d.	0.04	287.1	1.7	301.7	0.036	n.d.	13.32
16	n.d.	n.d.	n.d.	281.3	1.7	301.8	n.d.	n.d.	13.32
24	n.d.	n.d.	n.d.	289.9	1.7	290.7	0.004	n.d.	13.30
48	n.d.	n.d.	0.03	275.5	1.5	301.5	n.d.	n.d.	13.32
168	n.d.	n.d.	0.03	272.7	1.3	301.4	n.d.	n.d.	13.32

Table A2-5 - Saturation indices calculated from ion concentrations determined in glass dissolution experiments (Chapter 5).[a]

age [h]	$SiO_{2\ am}$	Tob	$SiO_{2\ am}$	Tob	$SiO_{2\ am}$	Tob	$SiO_{2\ am}$	Tob
	FA_s1		FA_s2		FA_s3		FA_c1	
0.5	−10.40	−13.41	−8.56	−9.08	−10.41	−13.42	−10.40	−13.41
1	−10.41	−13.43	−8.37	−8.64	−10.42	−13.44	−8.42	−8.65
2	−10.42	−13.43	−8.81	−9.44	−10.43	−13.45	−8.19	−8.04
4	−10.41	−13.43	−8.78	−9.60	−10.41	−13.42	−8.31	−8.33
8	−10.40	−13.41	−6.80	−5.17	−10.40	−13.42	−8.27	−8.23
16	−8.25	−8.24	−6.78	−5.13	−8.08	−7.82	−7.77	−7.10
24	−10.46	−13.48	−6.79	−5.15	−10.44	−13.47	−7.95	−7.47
48	−6.72	−5.00	−6.83	−5.22	−7.15	−5.75	−7.74	−7.05
168	−7.64	−6.78	−6.96	−5.46	−7.44	−6.34	−7.10	−5.68
	FA_c2		S1		S2		S3	
0.5	−10.41	−13.42	−10.40	−13.41	−8.40	−8.69	−10.41	−13.42
1	−8.08	−7.84	−8.80	−9.54	−8.30	−8.42	−8.26	−8.28
2	−7.99	−7.63	−8.75	−9.42	−8.21	−8.24	−8.17	−8.05
4	−8.03	−7.70	−10.42	−13.43	−8.15	−8.08	−10.40	−13.41
8	−7.90	−7.39	−10.48	−13.52	−6.87	−5.29	−10.40	−13.41
16	−7.52	−6.54	−7.51	−6.54	−6.75	−5.13	−6.80	−5.14
24	−7.52	−6.53	−7.23	−5.92	−6.77	−5.14	−7.19	0.29
48	−7.25	−5.97	−6.88	0.63	−6.74	−5.08	−6.80	1.40
168	−6.90	−5.30	−6.95	1.24	−6.74	−5.05	−6.88	1.90

[a] $SiO_{2\ am}$ - amorphous SiO_2 used in the calculations as no Ca could be detected in the pore solutions, Tob - Si-rich C-S-H ($C_{0.83}S_{1.0}H_{1.3}$).

Table A2-6 - Multi-component cements Chapter 8: Ion concentrations as measured by ion chromatography, calculated OH^- concentrations and measured pH for pore solutions. Data except pH given in [mmol/l]. n.d. = not detected (either below lower limit of detection or not present).

age [d]	Al	Ca	Cl	K	Na	OH^-	Si	SO_4	pH
				20-10-20-0					
0.04	n.d.	24.8	14.0	86.1	18.9	69.6	0.021	32.6	12.73
0.17	n.d.	23.0	13.1	84.7	19.5	77.8	0.018	31.7	12.78
1	0.004	5.7	6.0	105.4	41.6	108.9	0.027	21.1	12.93
2	0.019	2.0	1.8	126.4	58.2	191.3	0.030	0.7	13.17
7	0.021	0.3	0.9	149.5	80.9	192.8	0.036	0.7	13.17
28	0.066	1.4	1.0	119.8	78.6	214.6	0.075	1.4	13.21
91	0.090	0.5	1.4	128.7	71.1	183.1	0.109	1.6	13.12
182	0.083	0.5	2.5	125.1	73.0	163.2	0.126	2.2	13.08
364	0.191	0.4	1.7	128.6	89.9	204.9	0.107	2.8	13.16
546	0.146	0.6	2.1	120.0	69.3	196.5	0.130	2.7	13.14
728	0.179	0.4	2.3	128.3	81.0	170.9	0.235	3.9	13.11
				20-15-15-0					
0.04	n.d.	24.1	14.1	88.0	18.8	80.7	0.027	27.5	12.80
0.17	n.d.	22.9	13.9	85.5	21.4	87.1	0.026	28.9	12.83
1	0.003	6.5	5.8	102.5	41.2	113.1	0.022	21.9	12.95
2	0.015	2.2	1.8	121.6	56.6	184.2	0.031	0.9	13.16
7	0.026	0.5	0.9	143.3	76.8	207.9	0.037	0.7	13.21
28	0.094	1.3	1.0	118.0	72.1	198.5	0.097	1.3	13.17
91	0.140	0.8	1.3	129.1	69.9	183.0	0.129	1.5	13.12
182	0.166	0.8	2.0	126.9	72.0	163.2	0.151	2.4	13.08
364	0.188	0.5	1.4	124.0	82.4	204.5	0.132	2.0	13.16
546	0.211	0.3	2.1	119.2	68.9	189.0	0.179	2.7	13.12
728	0.245	0.5	2.3	122.5	74.7	164.2	0.166	3.9	13.09
				20-25-5-0					
0.04	n.d.	20.4	14.3	84.8	21.2	83.4	0.028	21.6	12.82
0.17	n.d.	23.6	14.0	87.2	22.4	89.7	0.022	15.8	12.85
1	0.004	5.0	5.4	119.0	48.4	152.4	0.018	22.0	13.04
2	0.021	2.1	2.0	132.4	68.0	212.5	0.029	0.9	13.19
7	0.032	0.5	1.1	147.5	81.4	208.2	0.039	0.8	13.21
28	0.154	1.0	1.0	108.3	72.8	198.2	0.118	1.3	13.17
91	0.283	0.6	1.3	121.3	64.9	169.2	0.192	1.6	13.09
182	0.332	0.8	2.0	130.1	73.8	163.3	0.222	2.2	13.08
364	0.423	0.4	1.5	117.6	67.2	188.8	0.147	1.8	13.12
546	0.413	0.5	2.0	116.7	63.5	181.6	0.225	2.2	13.11
728	0.503	0.4	2.2	124.1	74.4	164.1	0.251	3.0	13.09

Continued on next page

Table A2-6 – continued from previous page

age [d]	Al	Ca	Cl	K	Na	OH^-	Si	SO_4	pH
				20-30-0-0					
0.04	n.d.	21.8	14.7	84.4	20.9	86.3	0.026	16.8	12.83
0.17	n.d.	24.9	14.0	87.5	22.0	89.7	0.029	15.5	12.85
1	n.d.	6.0	5.4	114.4	45.9	146.9	0.015	25.9	13.03
2	0.018	2.5	2.0	131.0	64.8	221.5	0.029	1.0	13.21
7	0.046	0.4	0.8	151.1	83.3	216.4	0.042	0.5	13.22
28	0.321	0.8	0.8	116.1	73.4	198.4	0.136	0.8	13.17
91	0.666	0.5	1.0	126.7	68.7	176.0	0.207	0.9	13.11
182	0.810	0.6	1.3	116.6	65.2	150.6	0.217	1.5	13.04
364	0.911	0.5	1.2	113.9	69.4	188.7	0.223	1.0	13.12
546	0.944	0.6	1.8	117.1	64.9	181.6	0.268	1.5	13.11
728	0.984	0.4	2.1	117.3	69.6	157.5	0.271	2.0	13.08
				20-0-0-30					
0.04	n.d.	26.2	13.2	91.3	16.9	93.3	0.015	32.0	12.83
0.17	n.d.	26.0	13.7	92.3	18.2	100.7	0.006	31.4	12.86
1	n.d.	7.7	5.9	112.3	41.2	131.1	0.020	27.6	12.98
2	0.009	2.2	2.7	118.1	56.1	176.4	0.028	2.4	13.11
7	0.046	1.3	0.8	152.6	78.5	249.7	0.023	0.5	13.25
28	0.097	1.7	0.9	145.2	84.5	229.5	0.046	0.7	13.22
91	0.101	1.4	1.0	128.6	89.7	205.9	0.067	0.6	13.17
182	0.092	1.7	1.5	148.3	88.5	184.0	0.065	1.2	13.12
364	0.103	0.6	1.2	134.4	93.5	221.3	0.032	1.0	13.19
546	0.144	1.0	1.6	128.4	81.6	204.6	0.077	1.1	13.16
728	0.125	0.5	1.7	117.6	82.1	151.8	0.036	1.4	13.06
				30-0-20-0					
0.04	n.d.	26.3	15.3	92.9	17.9	83.3	0.010	31.2	12.78
0.17	n.d.	27.2	15.3	100.3	19.2	97.1	0.008	32.3	12.85
1	n.d.	4.5	6.1	117.7	44.3	158.0	0.018	18.8	13.06
2	0.019	1.7	2.5	126.6	63.4	213.3	0.030	0.9	13.19
7	0.031	0.8	1.2	141.8	71.8	239.9	0.044	1.2	13.24
28	0.042	1.5	1.3	137.0	82.0	199.4	0.054	1.6	13.16
91	0.035	1.2	1.7	122.6	85.4	198.0	0.082	2.1	13.16
182	0.031	2.3	2.4	151.6	91.2	177.4	0.087	2.8	13.11
364	0.062	0.3	1.9	135.2	99.8	221.7	0.081	3.4	13.19
546	0.055	0.7	2.8	122.4	83.5	204.7	0.116	3.1	13.16
728	0.065	0.6	3.1	125.5	94.7	171.2	0.138	3.9	13.11

Continued on next page

Table A2-6 – continued from previous page

age [d]	Al	Ca	Cl	K	Na	OH^-	Si	SO_4	pH
				30-5-15-0					
0.04	n.d.	27.9	16.0	91.8	20.1	97.6	0.029	33.1	12.86
0.17	n.d.	27.6	15.5	95.9	21.2	94.0	0.021	32.4	12.85
1	n.d.	6.9	7.8	108.7	39.0	125.5	0.035	28.5	12.95
2	0.019	1.4	2.4	113.8	59.4	155.4	0.037	0.9	13.04
7	0.026	1.2	1.1	130.1	71.7	247.6	0.038	0.7	13.24
28	0.056	1.3	1.5	118.6	71.1	198.4	0.086	1.2	13.17
91	0.059	1.0	1.8	132.2	76.2	190.5	0.092	2.0	13.14
182	0.086	1.9	2.4	146.1	89.8	177.3	0.122	3.2	13.11
364	0.076	0.7	2.0	124.6	83.4	212.7	0.093	2.8	13.17
546	0.080	0.8	2.5	127.1	81.7	204.8	0.135	3.6	13.16
728	0.099	0.6	3.1	128.6	91.5	171.1	0.128	3.6	13.11
				30-15-5-0					
0.04	n.d.	26.8	16.6	98.3	22.2	108.4	0.021	35.7	12.88
0.17	n.d.	27.7	17.0	102.1	24.1	108.6	0.014	36.0	12.88
1	n.d.	6.6	7.0	115.1	45.7	130.7	0.034	30.5	12.96
2	0.038	1.1	1.1	138.1	78.6	175.5	0.040	0.7	13.09
7	0.013	1.9	2.5	121.9	64.2	238.0	0.031	1.5	13.22
28	0.108	1.2	1.2	115.0	76.3	206.3	0.098	1.5	13.19
91	0.168	1.0	1.6	126.7	71.6	183.1	0.133	1.7	13.12
182	0.372	1.0	2.0	127.2	75.2	164.4	0.155	2.6	13.08
364	0.225	0.5	2.0	118.1	73.3	196.4	0.149	2.3	13.14
546	0.225	0.8	2.3	122.7	71.9	196.6	0.160	2.8	13.14
728	0.221	0.5	3.4	126.9	83.5	170.9	0.214	3.0	13.11

Table A2-7 - Multi-component cements Chapter 8: Effective saturation indices calculated from ion concentrations determined in pore solutions.[a]

age [d]	Jen	Tob	CH	Gp	E	Ms	Mc	Str
				20-10-20-0				
0.04	−0.01	−0.40	0.12	0.01	0.51	0.06	−0.09	−0.80
0.17	−0.03	−0.42	0.11	0.00	0.50	0.05	−0.10	−0.82
1	−0.04	−0.35	0.00	−0.38	0.34	−0.02	−0.10	−0.69
2	−0.06	−0.36	−0.03	−1.37	−0.01	−0.14	−0.04	−0.56
7	−0.22	−0.44	−0.26	−1.83	−0.34	−0.42	−0.24	−0.75
28	−0.01	−0.24	−0.08	−1.33	0.04	−0.08	0.01	−0.36
91	−0.08	−0.23	−0.22	−1.50	−0.09	−0.21	−0.08	−0.39
182	−0.08	−0.22	−0.24	−1.46	−0.09	−0.22	−0.10	−0.40
364	−0.13	−0.27	−0.27	−1.50	−0.08	−0.19	−0.07	−0.34
546	−0.05	−0.19	−0.21	−1.34	0.01	−0.13	−0.03	−0.29
728	−0.07	−0.16	−0.29	−1.44	−0.07	−0.20	−0.09	−0.30
				20-15-15-0				
0.04	0.03	−0.36	0.15	−0.03	0.51	0.07	−0.07	−0.78
0.17	0.01	−0.37	0.13	−0.02	0.50	0.06	−0.08	−0.79
1	−0.06	−0.38	0.01	−0.35	0.34	−0.04	−0.12	−0.75
2	−0.05	−0.35	−0.02	−1.28	0.02	−0.14	−0.05	−0.58
7	−0.17	−0.40	−0.20	−1.70	−0.23	−0.33	−0.17	−0.66
28	0.00	−0.20	−0.10	−1.36	0.05	−0.07	0.03	−0.29
91	−0.03	−0.19	−0.17	−1.45	−0.02	−0.12	−0.01	−0.28
182	−0.01	−0.16	−0.16	−1.33	0.05	−0.08	0.02	−0.23
364	−0.08	−0.22	−0.24	−1.51	−0.06	−0.17	−0.04	−0.29
546	−0.10	−0.19	−0.31	−1.49	−0.09	−0.21	−0.08	−0.29
728	−0.07	−0.19	−0.27	−1.36	0.00	−0.14	−0.04	−0.24
				20-25-5-0				
0.04	0.03	−0.36	0.15	−0.10	0.47	0.05	−0.08	−0.80
0.17	0.04	−0.41	0.22	−0.15	0.48	0.08	−0.04	−0.80
1	−0.08	−0.42	0.01	−0.43	0.32	−0.04	−0.11	−0.74
2	−0.05	−0.37	0.00	−1.32	0.02	−0.12	−0.02	−0.55
7	−0.16	−0.39	−0.20	−1.70	−0.22	−0.32	−0.15	−0.63
28	−0.01	−0.18	−0.15	−1.41	0.02	−0.08	0.03	−0.24
91	−0.02	−0.14	−0.22	−1.46	0.00	−0.10	0.02	−0.17
182	0.02	−0.11	−0.16	−1.36	0.07	−0.03	0.07	−0.11
364	−0.09	−0.20	−0.28	−1.52	−0.04	−0.13	0.00	−0.17
546	−0.04	−0.13	−0.27	−1.45	−0.01	−0.11	0.01	−0.13
728	−0.06	−0.14	−0.29	−1.47	−0.02	−0.13	0.00	−0.14

Continued on next page

Table A2-7 – continued from previous page

age [d]	Jen	Tob	CH	Gp	E	Ms	Mc	Str
				20-30-0-0				
0.04	0.04	−0.38	0.19	−0.14	0.47	0.06	−0.06	−0.79
0.17	0.07	−0.37	0.23	−0.14	0.49	0.09	−0.03	−0.78
1	−0.09	−0.44	0.00	−0.35	0.27	−0.13	−0.21	−0.94
2	−0.04	−0.36	0.02	−1.27	0.05	−0.10	−0.01	−0.55
7	−0.18	−0.40	−0.22	−1.83	−0.27	−0.33	−0.15	−0.60
28	−0.02	−0.17	−0.17	−1.55	0.00	−0.07	0.07	−0.14
91	−0.05	−0.15	−0.25	−1.66	−0.06	−0.10	0.05	−0.08
182	−0.01	−0.12	−0.22	−1.47	0.05	−0.02	0.10	−0.01
364	−0.04	−0.13	−0.26	−1.62	−0.02	−0.07	0.07	−0.02
546	0.00	−0.09	−0.23	−1.50	0.04	−0.03	0.10	0.02
728	−0.05	−0.12	−0.30	−1.53	0.00	−0.08	0.05	−0.02
				20-0-0-30				
0.04	−0.02	−0.45	0.15	0.01	0.53	0.08	−0.07	−0.82
0.17	−0.10	−0.59	0.16	0.01	0.52	0.08	−0.07	−0.90
1	−0.06	−0.40	0.02	−0.28	0.32	−0.10	−0.19	−0.90
2	−0.06	−0.37	−0.03	−1.08	0.07	−0.15	−0.10	−0.67
7	−0.11	−0.42	−0.05	−1.59	−0.07	−0.15	−0.01	−0.51
28	−0.03	−0.32	−0.02	−1.48	0.03	−0.04	0.08	−0.33
91	−0.02	−0.26	−0.06	−1.51	0.00	−0.08	0.05	−0.31
182	0.01	−0.26	−0.01	−1.36	0.08	−0.02	0.08	−0.31
364	−0.16	−0.41	−0.17	−1.61	−0.10	−0.18	−0.04	−0.45
546	−0.04	−0.25	−0.11	−1.46	0.02	−0.08	0.04	−0.28
728	−0.18	−0.40	−0.23	−1.54	−0.09	−0.19	−0.06	−0.43
				30-0-20-0				
0.04	−0.05	−0.51	0.16	0.01	0.53	0.09	−0.06	−0.84
0.17	−0.07	−0.55	0.18	0.01	0.54	0.10	−0.05	−0.86
1	−0.08	−0.42	−0.01	−0.48	0.21	−0.17	−0.23	−0.95
2	−0.08	−0.37	−0.05	−1.37	−0.02	−0.17	−0.06	−0.58
7	−0.10	−0.34	−0.14	−1.49	−0.10	−0.23	−0.10	−0.56
28	−0.02	−0.29	−0.04	−1.29	0.05	−0.09	0.00	−0.44
91	−0.02	−0.23	−0.09	−1.28	0.02	−0.14	−0.05	−0.46
182	0.06	−0.22	0.03	−1.11	0.14	−0.03	0.03	−0.42
364	−0.16	−0.32	−0.27	−1.49	−0.14	−0.28	−0.16	−0.54
546	−0.05	−0.21	−0.19	−1.33	−0.04	−0.19	−0.10	−0.44
728	−0.04	−0.20	−0.19	−1.31	−0.02	−0.18	−0.09	−0.41

Continued on next page

Table A2-7 – continued from previous page

age [d]	Jen	Tob	CH	Gp	E	Ms	Mc	Str
				30-5-15-0				
0.04	0.04	−0.35	0.17	0.02	0.54	0.09	−0.06	−0.77
0.17	0.02	−0.41	0.18	0.01	0.54	0.10	−0.05	−0.80
1	−0.02	−0.31	−0.01	−0.29	0.30	−0.12	−0.22	−0.87
2	−0.08	−0.34	−0.10	−1.38	−0.05	−0.20	−0.10	−0.58
7	−0.08	−0.34	−0.09	−1.49	−0.08	−0.19	−0.07	−0.55
28	−0.01	−0.22	−0.09	−1.36	0.02	−0.11	−0.01	−0.38
91	−0.02	−0.23	−0.12	−1.32	0.02	−0.13	−0.03	−0.40
182	0.07	−0.17	0.00	−1.12	0.18	0.02	0.08	−0.26
364	−0.06	−0.24	−0.17	−1.33	0.00	−0.15	−0.06	−0.40
546	−0.02	−0.18	−0.16	−1.25	0.04	−0.12	−0.04	−0.35
728	−0.05	−0.21	−0.19	−1.33	−0.01	−0.15	−0.06	−0.36
				30-15-5-0				
0.04	0.01	−0.40	0.16	0.02	0.53	0.09	−0.06	−0.80
0.17	−0.02	−0.47	0.18	0.03	0.54	0.10	−0.05	−0.82
1	−0.02	−0.32	0.00	−0.30	0.29	−0.12	−0.21	−0.88
2	−0.08	−0.35	−0.09	−1.55	−0.09	−0.19	−0.05	−0.51
7	−0.06	−0.36	−0.03	−1.21	0.03	−0.15	−0.08	−0.62
28	0.00	−0.20	−0.11	−1.34	0.06	−0.07	0.03	−0.28
91	0.00	−0.17	−0.13	−1.37	0.05	−0.06	0.04	−0.22
182	0.01	−0.15	−0.14	−1.28	0.13	0.01	0.10	−0.10
364	−0.07	−0.20	−0.25	−1.46	−0.04	−0.15	−0.03	−0.25
546	0.00	−0.15	−0.17	−1.29	0.08	−0.05	0.04	−0.18
728	−0.04	−0.15	−0.24	−1.42	−0.02	−0.14	−0.03	−0.24

[a] Jen - Ca-rich C-S-H ($C_{1.67}S_{1.0}H_{2.1}$), Tob - Si-rich C-S-H ($C_{0.83}S_{1.0}H_{1.3}$), CH - portlandite, Gp - gypsum, E - Ettringite, Ms - monosulfoaluminate, Mc - monocarboaluminate, Str - Strätlingite. Al was earliest detectable at 1 d. At earlier ages the Al-concentrations were below the detection limit of 0.003 71 mg/l. For the calculation of effective saturation indices an Al-concentration of 0.001 mg/l was assumed. Sample code corresponds to BFS-FA-LS-Qz.

Table A2-8 - Multi-component cements Chapter 8: Concentrations of various species of sulphur in the pore olutions as detected by ion chromatography. Data exept pH in [mmol/l] unless otherwise stated.[a]

System	age [d]	SO_3^{2-}	SO_4^{2-}	$S_2O_3^{2-}$	S^{2-}	$S_{\{SO_3^{2-}\}}$[b]	$S_{\{SO_4^{2-}\}}$[b]	$S_{\{S_2O_3^{2-}\}}$[b]	$\sum S$[c]	S_{total}[d]	R[e]	Δ_S[f]	pH
20-0-0-30	0.04	<0.12	28.60	1.43	<0.02	<0.12	28.60	2.85	31.59	32.12	98.35	0.53	12.86
20-0-0-30	0.17	<0.12	29.62	1.31	<0.02	<0.12	29.62	2.62	32.38	33.28	97.31	0.89	12.82
20-0-0-30	1	<0.12	29.35	0.13	<0.02	<0.12	29.35	0.27	29.76	29.97	99.29	0.21	12.88
20-0-0-30	2	0.24	1.97	0.04	<0.02	0.24	1.97	0.09	2.31	2.18	105.86	−0.13	13.11
20-0-0-30	7	<0.12	0.47	0.10	<0.02	<0.12	0.47	0.20	0.81	0.72	112.66	−0.09	13.19
20-0-0-30	28	0.22	0.52	0.25	<0.02	0.23	0.52	0.50	1.27	1.12	112.79	−0.14	13.21
20-0-0-30	91	<0.12	0.67	0.46	<0.02	<0.12	0.67	0.93	1.74	1.75	99.47	0.01	13.17
30-0-20-0	0.04	<0.12	28.70	1.59	<0.02	<0.12	28.70	3.17	32.02	32.65	98.06	0.63	12.85
30-0-20-0	0.17	<0.12	29.28	1.32	<0.02	<0.12	29.28	2.64	32.07	33.12	96.82	1.05	12.85
30-0-20-0	1	<0.12	26.60	0.13	<0.02	<0.12	26.60	0.27	27.01	27.91	96.76	0.90	12.91
30-0-20-0	2	0.25	0.91	0.04	<0.02	0.25	0.91	0.07	1.25	1.06	118.02	−0.19	13.12
30-0-20-0	7	0.30	0.75	0.21	<0.02	0.30	0.75	0.41	1.47	1.28	115.33	−0.20	13.19
30-0-20-0	28	0.31	1.27	0.74	<0.02	0.31	1.27	1.48	3.08	3.31	93.11	0.23	13.19
30-0-20-0	91	0.16	1.92	2.02	<0.02	0.16	1.92	4.05	6.15	6.70	91.74	0.55	13.17
20-10-20-0	91	0.19	1.85	1.15	<0.02	0.19	1.85	2.30	4.37	4.40	99.28	0.03	13.12
20-15-15-0	91	0.19	1.71	1.03	<0.02	0.19	1.71	2.07	3.99	4.37	91.25	0.38	13.03
20-25-5-0	91	0.25	1.59	1.27	<0.02	0.25	1.59	2.53	4.39	4.43	99.21	0.03	13.11
20-30-0-0	91	0.30	0.92	0.60	<0.02	0.30	0.92	1.19	2.43	2.28	106.56	−0.15	13.11
30-5-15-0	91	0.17	1.88	1.75	<0.02	0.17	1.88	3.50	5.58	6.21	89.85	0.63	13.12
30-15-5-0	91	0.32	1.60	1.41	<0.02	0.32	1.60	2.82	4.77	5.05	94.36	0.28	13.12

[a] Values indicated by "<" correspond to lower detection limits. Concentrations of corresponding species were too low to be detected.
[b] Elemental sulfur originating from the corresponding species.
[c] Total sulfur calculated as sum of the single sulphur species investigated by ion chromatography.
[d] Investigated by ICP-OES.
[e] Retrieval of S expressed as recovered percentage of $\sum S$ (calculated from the single species) with respect to S_{total}.
[f] Difference between $\sum S$ and S_{total}.

Appendix 3 - Early hydration study - additional data

A3.1 Particle size distribution

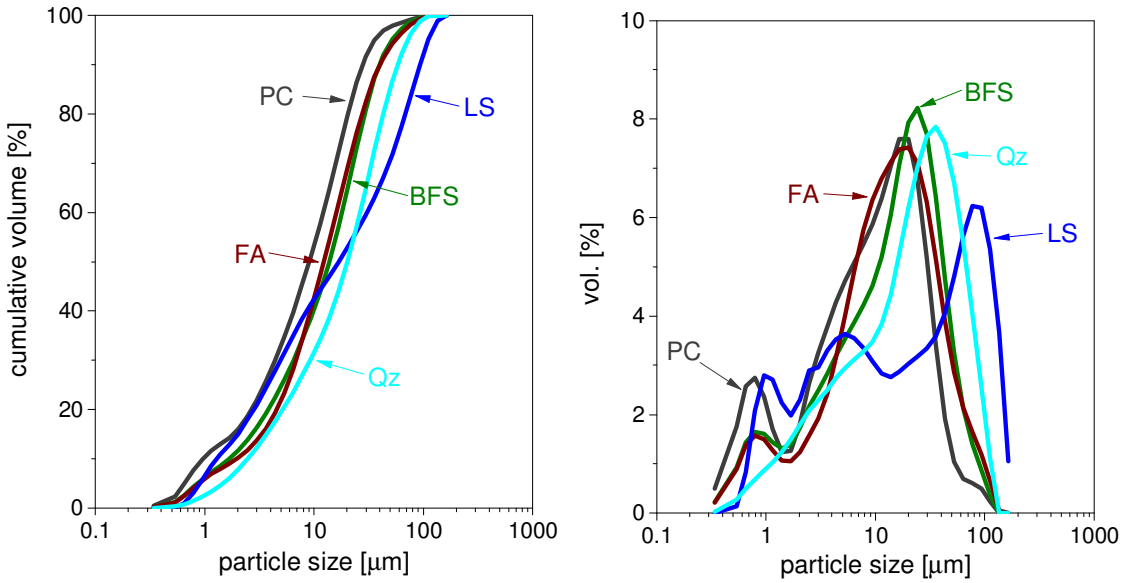

Figure A3-1 - Early hydration study (Chapter 4): Particle size distribution depicted as cumulative volume (left) and relative frequency (right) determined by means of laser diffraction with a 100 mm lens.

A3.2 The effect of limestone and anhydrite on the early hydration of SCM-blended cements

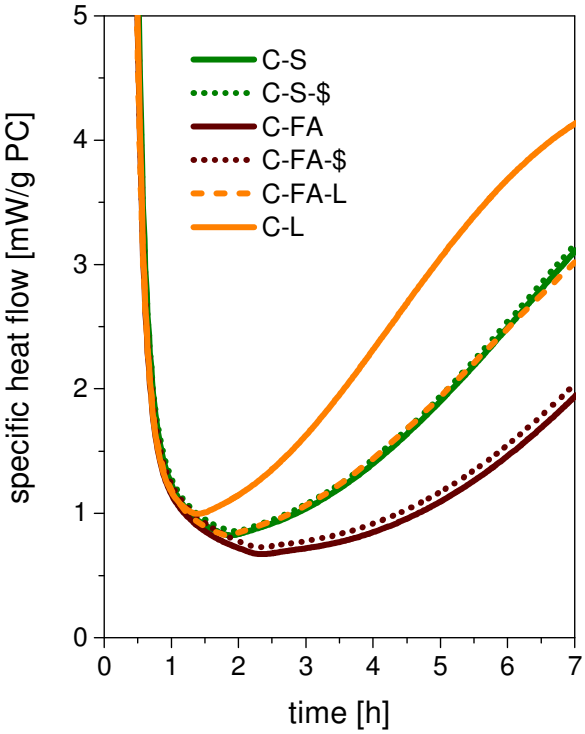

Figure A3-2 - Early hydration study (Chapter 4): Specific heat flow in the first 7 h of hydration for the blast furnace slag blend and the fly ash blend at both sulfate levels along with the blend containing limestone in addition to fly ash. For reasons of comparison the limestone blend is also depicted.

Appendix 4 - Synthetic glasses - additional data

A4.1 Hydrate precipitation in dissolution tests

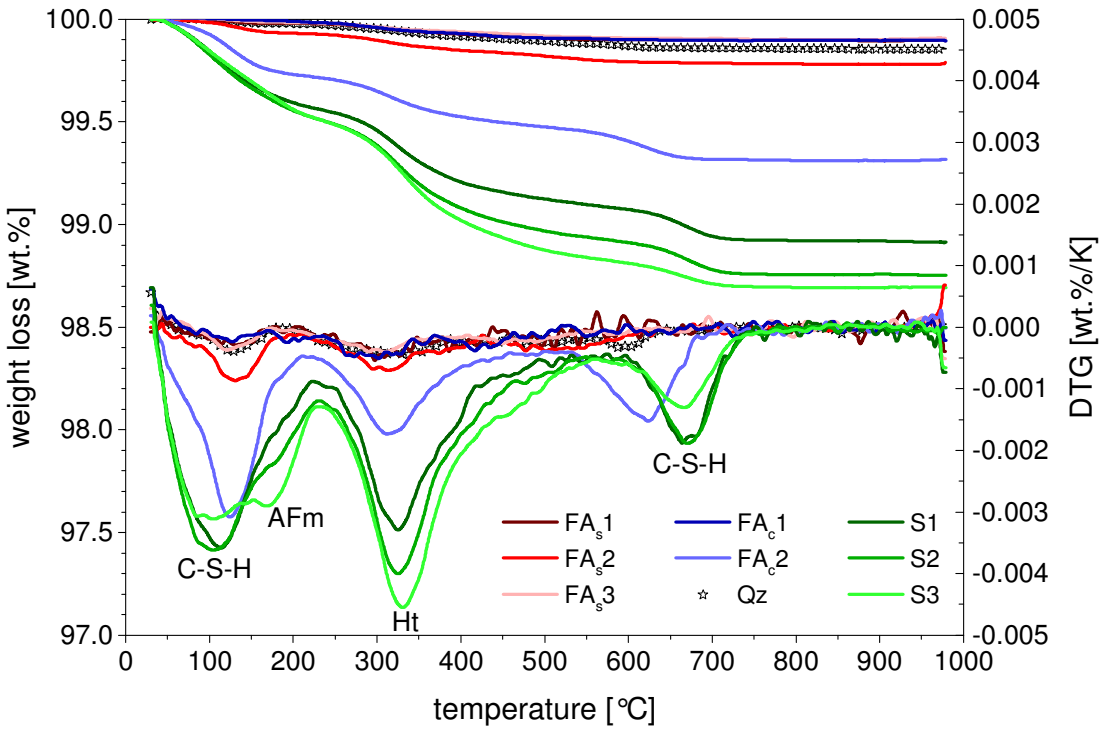

Figure A4-1 - Weight loss curves of residiual glass powder after 168 h of dissolution in 0.3 M KOH-solution as investigated in Chapter 5. AFm - Al_2O_3-Fe_2O_3 (mono), C-S-H - calcium silicate hydrate, Ht - hydrotalcite. DTG = differential thermogravimetry.

Table A4-1 - Total bound water content calculated for residual glass powders after 168 h hours in 0.3 M KOH-solution as investigated in Chapter 5. Data given in [g/100 g dry solids].

	FA$_s$1	FA$_s$2	FA$_s$3	FA$_c$1	FA$_c$2	S1	S2	S3	Qz
BW[a]	0.10	0.20	0.09	0.10	0.55	0.91	1.07	1.17	0.12

[a] The amount of bound water is very low and might also originate from a water-film on the glass surface besides from precipitated hydrates.

A4.2 Al-concentrations in dissolution tests - complete range

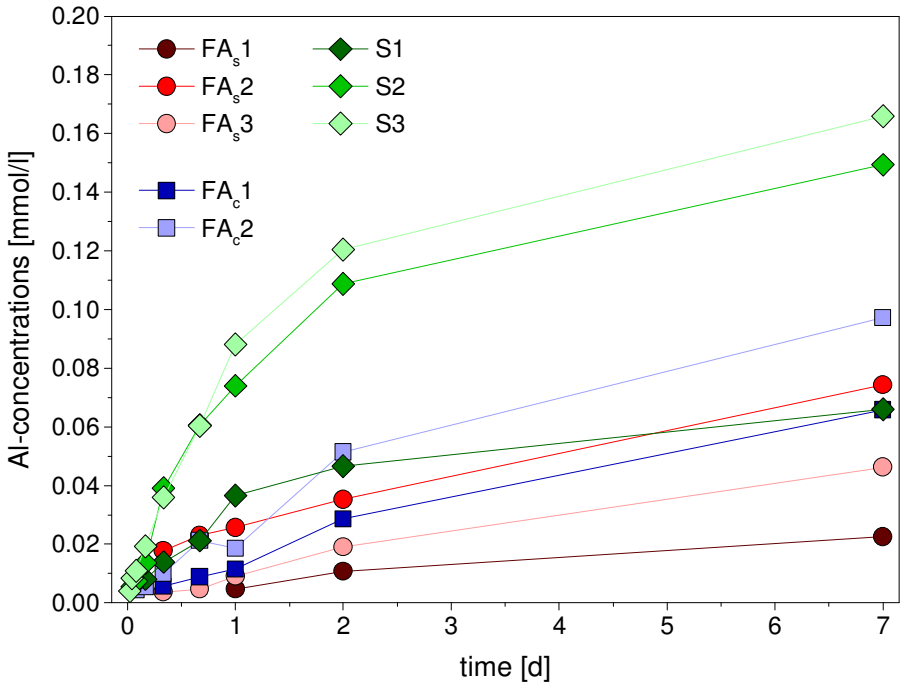

Figure A4-2 - Al concentrations of the dissolution tests as determined by ion chromatography depicted for the whole duration of experiments as investigated in Chapter 5. The relative error is ~10%.

A4.3 Specific heat flow and released heat of glass-blended cements

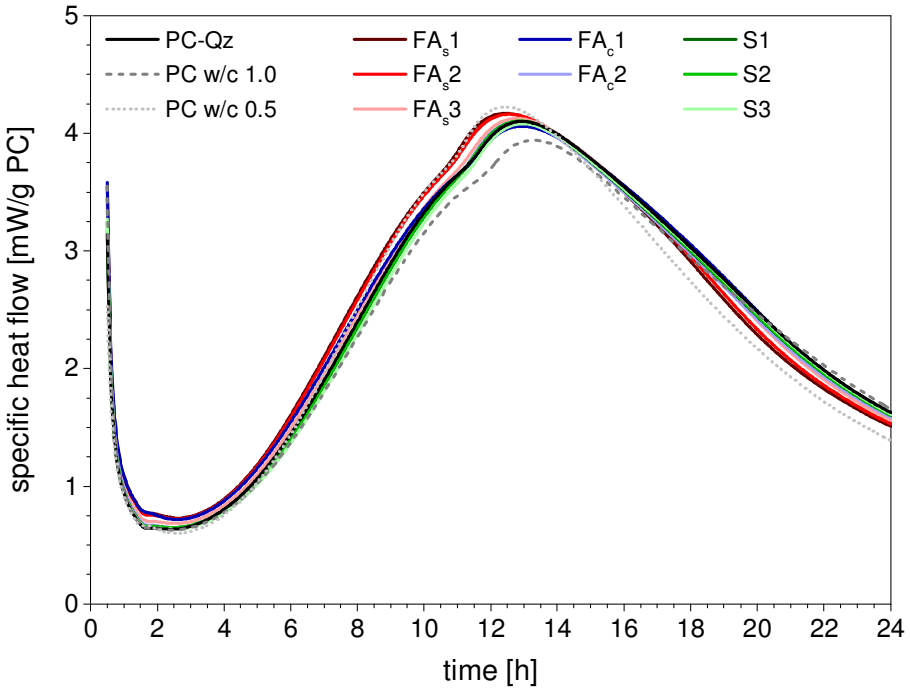

Figure A4-3 - Specific heat flow for glass-blended cements as investigated in Chapter 5. Values are normalized to the mass of PC in the system.

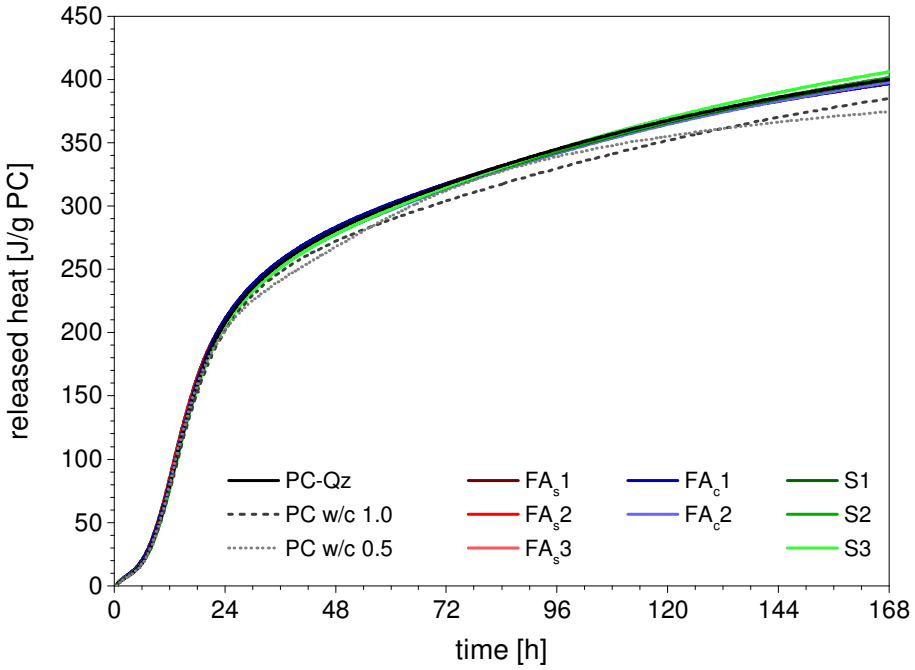

Figure A4-4 - Total released heat for glass-blended cements as investigated in Chapter 5. Values are normalized to the mass of PC in the system.

A4.4 Glass reaction in model systems and blended cements - Bound water/mass balance approach vs. selective dissolution

Table A4-2 - Amount of glass reacted for model systems and blended cements after 91 d of hydration determined by EDTA/NaOH selective dissolution. Data given in [wt.%]. cor = corrected for hydrotalcite as described in 3.3.10.2.

	FA_s1	FA_s2	FA_s3	FA_c1	FA_c2	S1	S2	S3
blended cements	0.18	6.75	3.57	8.83	7.74	12.35	15.89	20.89
blended cements$_{cor}$	0.19	7.01	3.70	9.70	9.04	15.59	19.82	25.75
model systems	5.90	6.78	4.11	7.29	9.89	10.23	8.52	3.62
model systems$_{cor}$	6.15	7.04	4.26	8.02	11.55	12.91	10.63	4.46

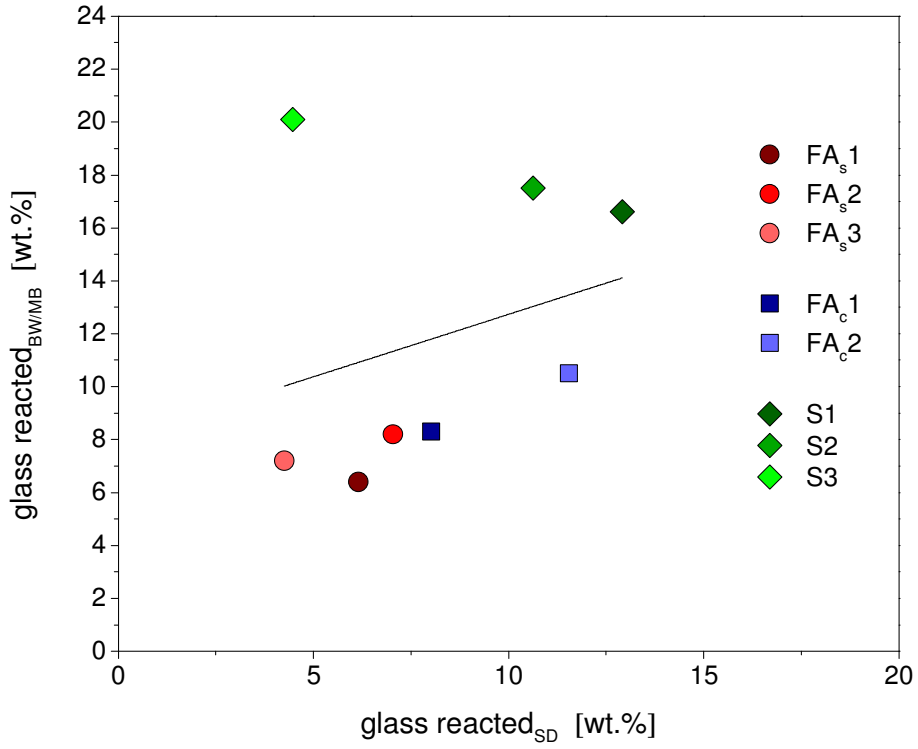

Figure A4-5 - Plot of the calculated amount of glass reacted in the model systems determined by the bound water/mass balance approach vs. EDTA/NaOH selective dissolution. All values for samples hydrated for 91 d. BW/MB = bound water/mass balance approach, SD = selective dissolution.

Appendix 5 - Mix design of model systems: $CaCO_3$ vs. $CaSO_4$

A5.1 Introduction

The pozzolanity tests using model systems as described in detail in 3.2.2 can be applied in order to estimate and compare the reactivity of different SCM. In the model systems portlandite is present in excess and serves as reactant within the pozzolanic reaction. In the mix design small amounts of other reactants can be considered in order to allow the formation of further hydrate phases that are relevant within cement hydration. Small amounts of $CaCO_3$ lead to the formation of monocarbonate and are therefore interesting once the investigated SCM should be included in Portland cement-based composite cements. Substitution of the $CaCO_3$ by SO_3-containig materials (gypsum, bassanite and anhydrite) leads to the formation of ettringite and might be of interest not only because Portland cement-based systems contain these phases as set regulators. Rather, the use of these phases in the pozzolanic tests mimics systems close to supersulfated slags. In this chapter investigations on the influence of $CaCO_3$ and $CaSO_4$ on the reaction of synthetic SCM glasses are presented. While the SO_3-containig model systems are not directly linked to the scope of Chapter 5 (the $CaCO_3$-containing systems are more realistic with respect to Portland cement based system) they were carried out in order to evaluate the bahavior of different mix designs. The results presented in this Appendix might serve as guiding principle for alterations of the model systems with respect not only to Portland cement systems.

A5.2 Materials and methods

Five glasses that were synthesized based on glass compositions as they can be found in blast-furnace slag and Ca-rich fly ash were investigated. Details on the synthesis protocol, the preparation of glass powder and on the characterization of the obtained glasses are given in Chapter 5.1. The model systems contained portlandite in excess, synthetic glass and either $CaCO_3$ or $CaSO_4$ (Table A5-1). All samples were mixed with 0.3 M KOH-solution at a liquid-to-solid ratio of 1.0.

Table A5-1 - Mix design of pozzolanity test samples.

	unit	$C\bar{C}$-systems	$C\bar{S}$-systems
synthetic glass	[g]	55.7	55.7
$Ca(OH)_2$	[g]	38.8	38.8
$CaCO_3$	[g]	5.5	-
$CaSO_4$	[g]	-	5.5
$\sum$ solids	[wt.%]	100.0	100.0
0.3 M KOH solution	[g]	100.0	100.0
deionized H_2O	[g]	1.0	1.0
water/solid	[g/g]	1.0	1.0

Isothermal calorimetry and thermogravimetry coupled with mass balance calculations were used. Detailed information on the methods used and on the sample preparation for the different methods is given in 3.3.

A5.3 Results and discussion

A5.3.1 Kinetics

The recorded specific heat flow curves gained during the isothermal calorimetry experiments are presented in Figure A5-1. The curves for samples containing $CaCO_3$ (Figure A5-1a) are located close to each other for all Si-rich glasses and FA_c1 between 0.75 and 5 µW/g dry mixture. The progression of a uniform reaction can be seen from the linear heat flow. Despite all systems being located in a narrow range successively higher heat flow is present with decrease in SiO_2 content in the glasses. The progression of FA_c2 does not change notably except for somewhat higher heat flow at close to 2 µW/g dry mixture throughout. In contrast to the Si-rich glasses the Ca-rich glasses glasses show clearly higher heat flow and larger differences among themselves with the same characteristics, i.e. higher heat flow with lower SiO_2 in the glass composition. Furthermore a peak is present in these systems. While it is not very pronounced in S1 it becomes more distinct and shifts to earlier times towards S3 where a clear induction and acceleration period can be distinguished. The specific heat flow curves for samples containing $CaSO_4$ are shown in Figure A5-1b. In contrast to the $CaCO_3$ containing samples no peaks dividing the curves in different stages are present. All curves show a slight increase with time and are located at lower values compared to the $CaCO_3$ containing samples. The system with the lowest Si content (FA_c1) shows a hump between 48 h and 168 h which can still be recognized for FA_c2. This hump originates from a reaction between $CaSO_4$ and H_2O (gypsum formation) as can be seen from reference samples that have been measured for comparison (Figure A5-2). While no notable heat flow can be recorded for the $CaCO_3$ containing samples once the calorimeter has reached equilibrium after about 24 h the reference samples containing $CaSO_4$ show an increase in heatflow at about 48 h. This increase is most pronounced for the reference containing $Ca(OH)_2$ and $CaSO_4$ but is also present in the quartz reference. In principle knowledge of this reaction along with the corresponding enthalpies allows correction for gypsum formation. However, this would require quantification of the amount of gypsum formed as a function of time. Corresponding data was not collected in the present study. Another aspect of the formation of gypsum is the kinetic behavior of the glass. A fast reacting SCM would consume $CaSO_4$ before its transformation to gypsum occurs. Accordingly the hump that is present for the fly ash glasses in the $CaSO_4$ containing samples is either not present anymore in the blast-furnace slag systems or is too small to be distinguished.

The calculated released heat of hydration up to 7 d is presented in Figure A5-1c and Figure A5-1d. While both series of samples show similar inherent characteristics the amount of released heat for the same SCM glasses is different. A comparison of total released heat after 168 h for both systems is given in Table A5-2. The difference between the different compositions with respect to the $CaCO_3$ containing samples increases clearly, e.g. decreasing SiO_2 content at simultaneous increase in CaO content in the glasses leads to higher released heat in presence of $CaCO_3$, at least up to 7 d of hydration. This corresponds to the general lower heat of supersulfated slag cements compared to Portland cement based systems [Juenger et al., 2011, Odler, 2000]. Taking into account the contribution of gypsum formation would additionally lower the total released heat for the $CaSO_4$ samples. The reason for the lower heat released for the $CaSO_4$ samples is presently unclear.

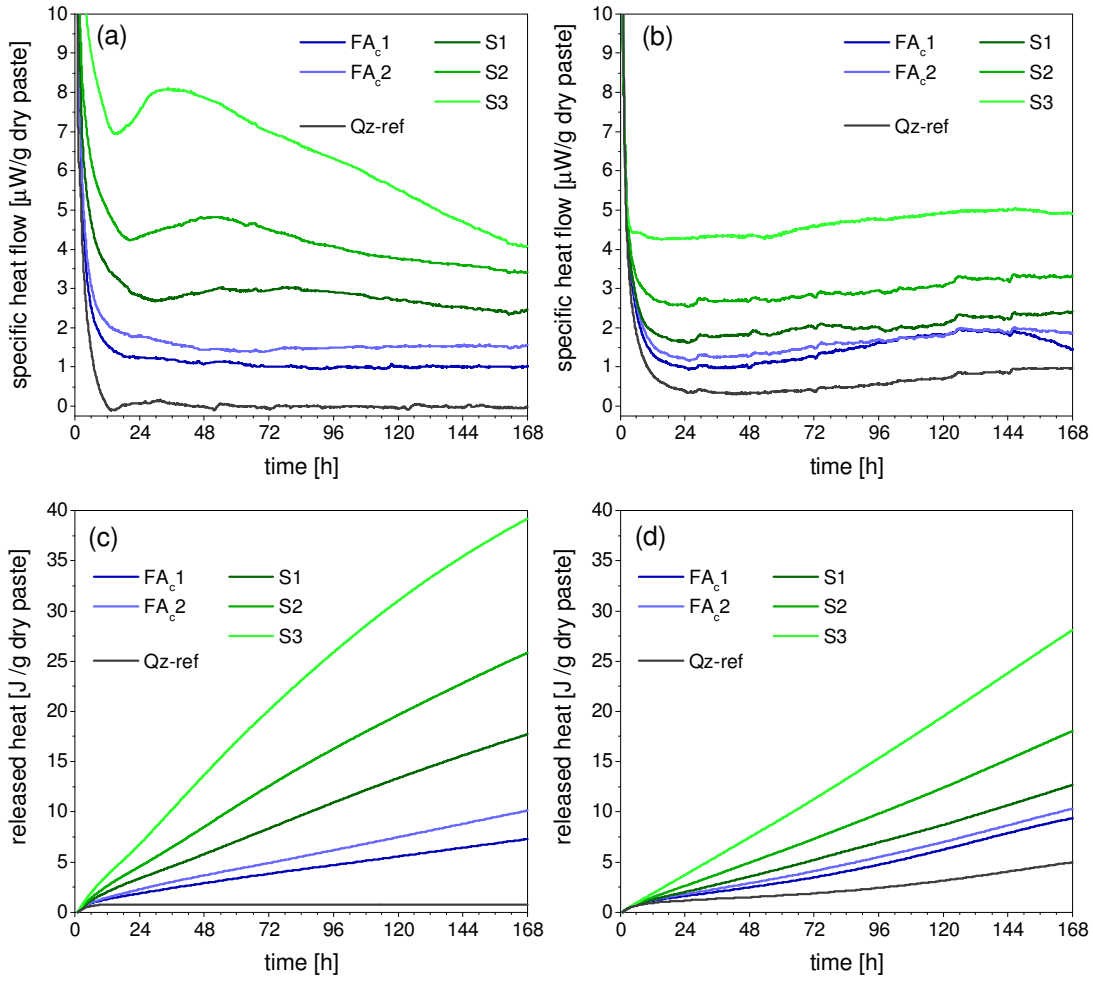

Figure A5-1 - Specific heat flow and released heat for samples containing (a), (c) $CaCO_3$ and (b), (d) $CaSO_4$.

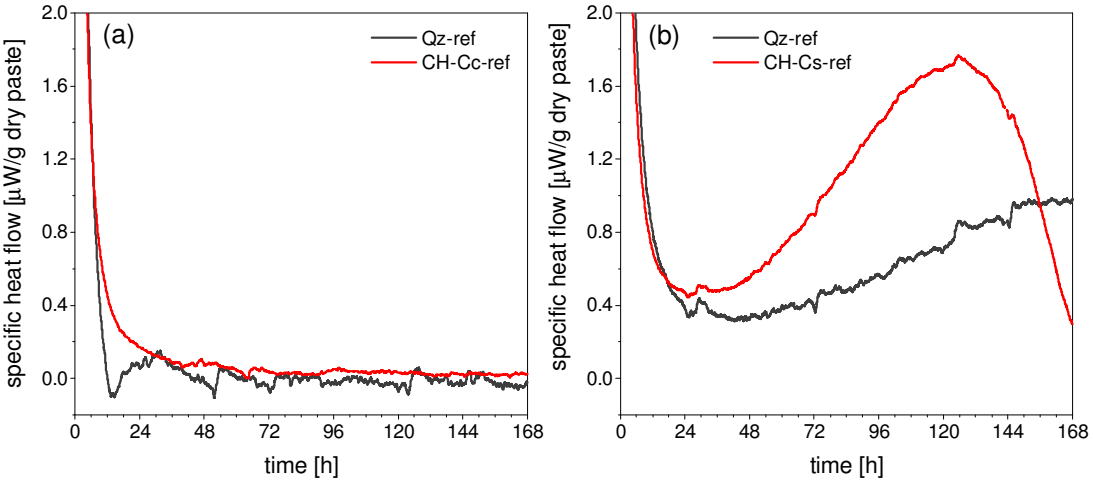

Figure A5-2 - Specific eat flow a for reference mixtures containing quartz and for absence of glass at equal sample size and ratio of (a) $Ca(OH)_2CaCO_3$ or (b) $Ca(OH)_2CaSO_4$. Data recorded for the latter mixtures is normalized to $Ca(OH)_2$ content of the quartz reference (factor 0.44).

Table A5-2 - Comparison of total released heat after 168 h of hydration for samples containing $CaCO_3$ and for samples containing $CaSO_4$. Data given in [J/g dry mixture].

	FA_c1	FA_c2	S1	S2	S3
$CaCO_3$-samples	7.3	10.1	17.7	25.8	39.2
$CaSO_4$-samples	9.4	11.3	12.7	18.1	28.1
Δ [%][a]	0.2	0.0	−0.9	−2.0	−4.3

[a] calculated with respect to $CaCO_3$-samples.

A5.3.2 Bound water and portlandite content

The TGA curves presented in Figure A5-3 show a comparison of hydrate development and portlandite consumption for $CaCO_3$ (Figure A5-3a and Figure A5-3b) and (Figure A5-3c and Figure A5-3d) $CaSO_4$ containing systems. Two representative samples including FA_c1 and S3 are depicted. Hydrates that can be identified are C-S-H, AFm-phases, hydrotalcite and ettringite for $CaSO_4$ containing systems. In case of the $CaCO_3$ containing systems S3 shows somewhat higher portlandite consumption at equal hydration times, regardless of the higher CaO content in the glass itself. In terms of kinetics S3 shows a clear increase of bound water in the region of C-S-H after 2 d while this can be clearly seen for FA_c1 only after 28 d. The weight loss and the peaks in the derivative curve are more pronounced for S3 after 91 d. Apart from the presence of ettringite similar characteristics can be seen from the systems containing $CaSO_4$. The consumption of portlandite is more pronounced for S3 and is higher for both glasses compared to $CaCO_3$ presence. Ettringite/C-S-H is present after 2 d for S3 and after 14 d for FA_c1 while the overall reaction is again faster in case of S3. In case of the latter the weight loss up to 550 °C reveals the formation of clearly more hydrates compared to FA_c1. The formation of gypsum appears in $CaSO_4$ containing systems which is confirmed by the peak at around 150 °C (Figure A5-3c). However, after 91 d this peak is not present anymore which suggests complete gypsum consumption. In case of S3 (Figure A5-3d) only a small hump is present around 150 °C after 2 d and does not increase with time. As indicated by dissolution test and isothermal calorimetry experiments the reaction of S3 proceeds considerably faster than the reaction of FA_c1. As a consequence anhydrite is consumed in the formation of ettringite before a conversion of anhydrite to gypsum can proceed. Summarizing, the TGA curves reveal not only a faster reaction of S3 compared to FA_c1 in equal systems but also an acceleration of the reaction once $CaCO_3$ is replaced by $CaSO_4$ which is in apparent contrast to the findings by calorimetry.

The total bound water content and the portlandite consumption, both calculated from TGA, are presented in Figure A5-4. Bound water for $CaCO_3$ samples is present after 2 d (S1-S3), 7 d (FA_c1) and 28 d (FA_c2). The general progression reveals higher bound water content with increasing CaO content of the glasses. Values for $CaSO_4$ samples are comparable to the $CaCO_3$ samples up to 7 d. At later ages clearly more bound water is present as ettringite is formed (see Figure A5-3c and Figure A5-3d). The principal progression of higher bound water with increasing CaO content in the glasses is present as well. While no bound water is present for the $CaCO_3$ containing quartz reference small amounts are calculated for the $CaSO_4$ containing sample due to the formation of gypsum. The portlandite consumption is presented in Figure A5-4c and Figure A5-4d. The development of portlandite content shows similar characteristics as the bound water content. For $CaSO_4$ containing samples values are lower compared to $CaCO_3$ contain-

ing samples up to 28 d while higher values are present at 91 d. This represents a clear increasing portlandite consumption towards Ca-rich glasses, even as the dissolution of these glasses can provide CaO for a pozzolanic reaction in absence of portlandite. The calculated portlandite consumption for the quartz reference in the $CaCO_3$ system can be related to small inhomogeneities in the samples at different ages as no bound water could be detected which might to some extent also be present for the glass containing samples. However, the overall development of both parameters, bound water and portlandite, reveals a higher amount of glass reacted towards later ages as a function of glass composition, i.e. an increase from Si-rich glasses to Ca-rich glasses.

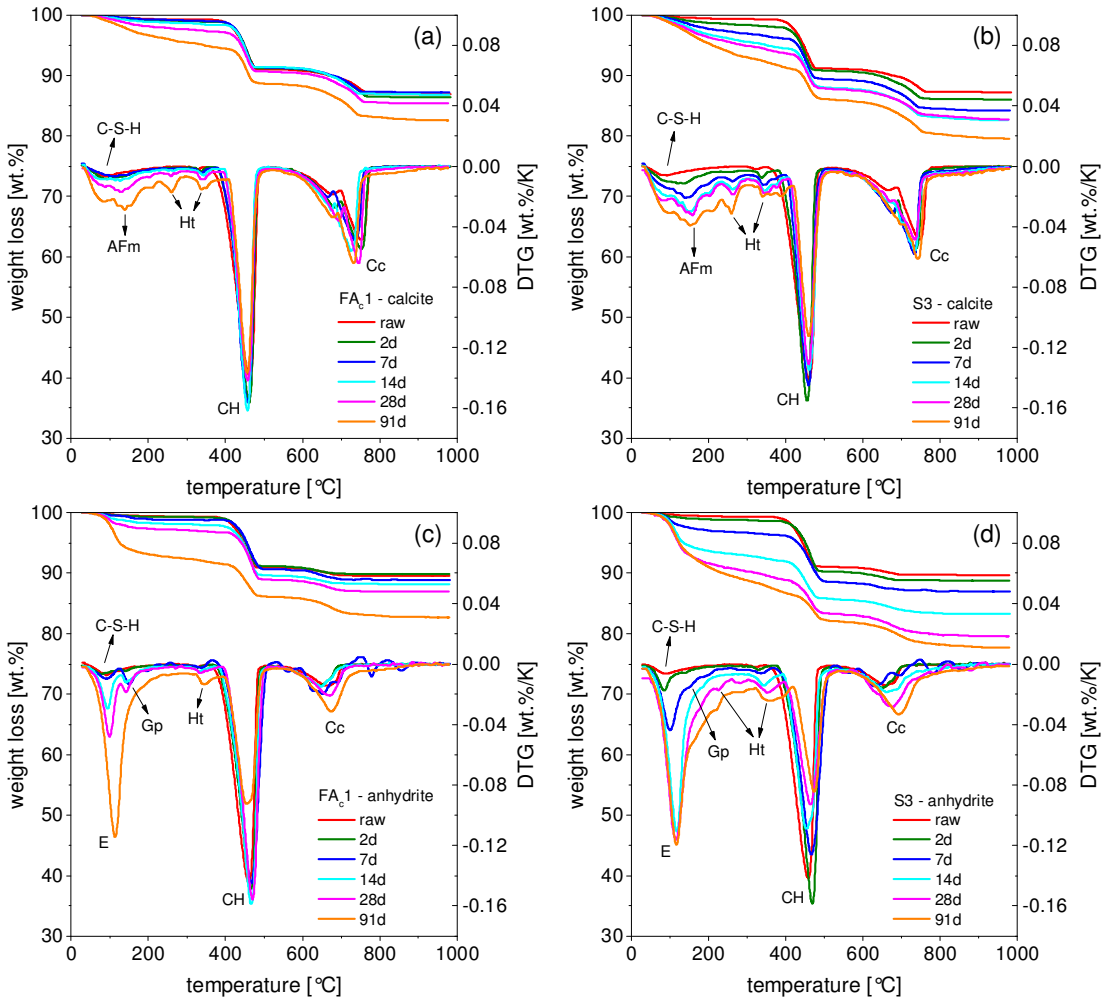

Figure A5-3 - Weight loss and DTG curves for selected pozzolanity test samples containing (a), (b) calcite and (c), (d) anhydrite. Cc - calcite, CH - portlandite, C-S-H - calcium silicate hydrate, E - ettringite, Gp - gypsum, Ht - hydrotalcite.

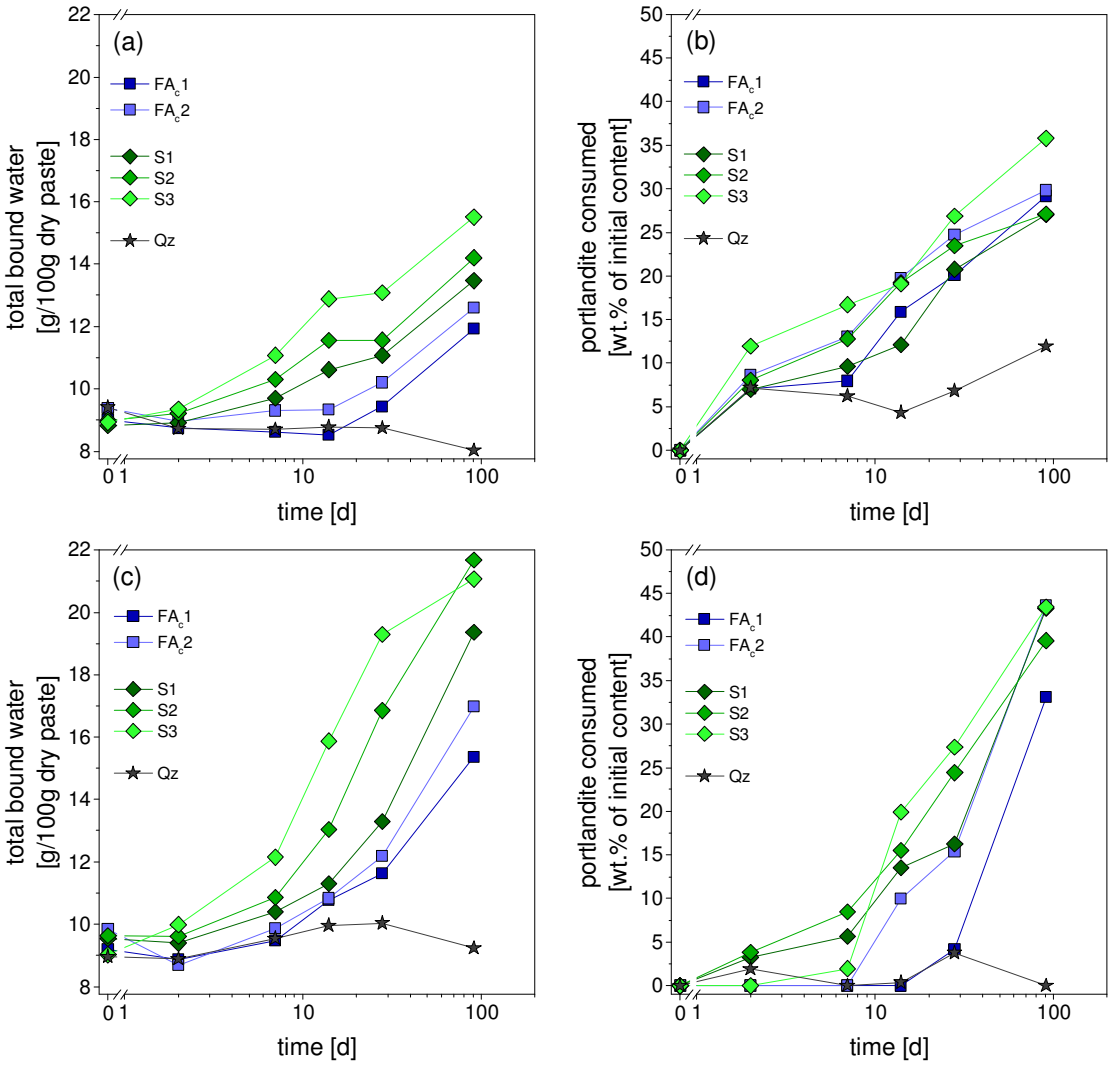

Figure A5-4 - Total bound water content and percentage of portlandite reacted for selected pozzolanity test samples containing (a), (b) calcite and (c), (d) anhydrite.

A5.3.3 Calculation of the degree of glass reaction

The amount of SCM reacted as calculated from the bound water-mass balance approach is presented in Figure A5-5. In good agreement with total released heat after 7 d as calculated from isothermal calorimetry experiments, the blast-furnace slag glasses show higher reactivity in the presence of $CaCO_3$ compared to the presence of $CaSO_4$. While the calculated values are similar at 14 d, $CaSO_4$ leads to clearly higher reaction at later ages. This initial slower reaction in presence of anhydrite seems to be related to the transformation of $CaSO_4$ to $CaSO_4{\cdot}2\,H_2O$. A clearly higher reactivity expressed by means of compressive strength was also reported by [Mehrotra et al., 1982] where supersulfated slag activated by anhydrite showed lower strength values than supersulfated slags activated by gypsum.

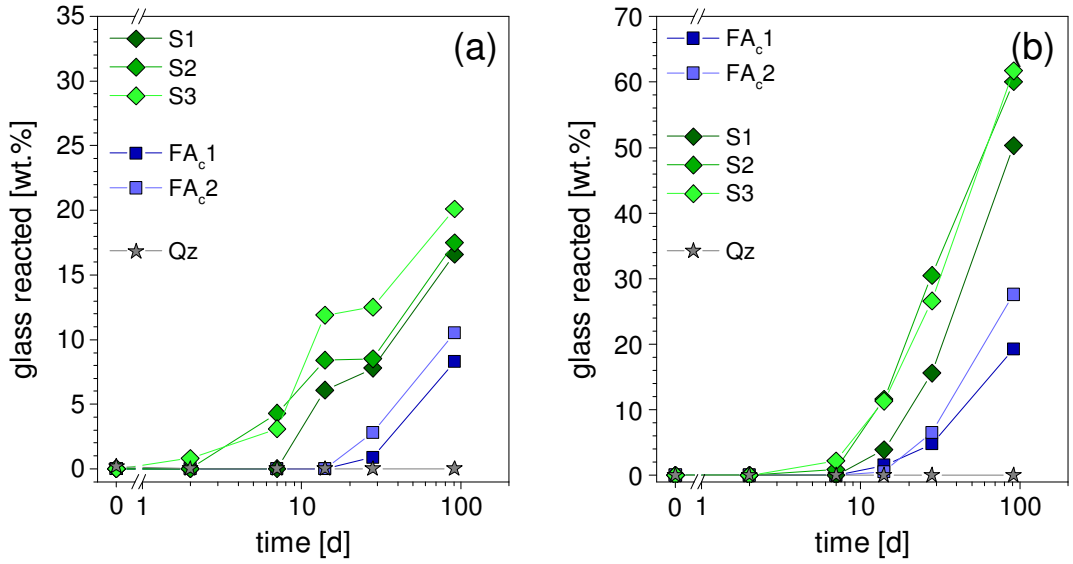

Figure A5-5 - Estimated percentage of reacted glass as a function of time for (a) $CaCO_3$ containing pozzolanity test samples and for (b) $CaSO_4$ containing pozzolanity test samples.

A5.4 Conclusions

(i) Model systems can serve as less complex systems compared to Portland cement blends although they provide similar characteristics. Depending on the mix design and on the actual reactants, especially $CaCO_3$ and $CaSO_4$, different reactivities are to be expected. $CaSO_4$ leads to higher reactivity at 91 d while the reaction before 14 d proceeds slightly slower compared to $CaCO_3$ including systems. This in turn means that the model systems should be designed with respect to the environment in which the investigated SCM will be used, i.e. Portland cement blends or supersulfated or alkali activated binders.

(ii) In terms of $CaSO_4$ containing model systems the use of gypsum should be favored as anhydrite will be transformed to gypsum depending on the reactivity of the SCM. The gypsum formation distorts the results of calorimetric experiments and the calculated bound water.

Appendix 6 - TGA calculations

Table A6-1 - Synthetic glasses (Chapter 5): Bound water[a] and portlandite[b] content as calculated for calcite-containing pozzolanity test samples.

age [d]	$BW_{incl.\ CH}$	$BW_{excl.\ CH}$	CH	$BW_{incl.\ CH}$	$BW_{excl.\ CH}$	CH
		FA_s1			FA_s2	
0	10.13	0.95	37.76	9.92	0.98	36.78
2	9.99	1.16	36.35	9.25	0.96	34.12
7	9.58	0.99	35.30	9.29	1.08	33.75
14	9.58	1.42	33.55	9.76	1.70	33.13
28	10.12	2.25	32.38	9.86	2.57	30.01
91	12.23	5.01	29.69	12.99	6.07	28.46
		FA_s3			FA_c1	
0	9.41	0.88	35.09	9.96	0.95	37.07
2	9.46	1.08	34.46	9.69	1.32	34.46
7	9.63	1.42	33.77	9.58	1.28	34.13
14	9.52	2.01	30.88	9.46	1.88	31.18
28	10.37	3.10	29.89	10.39	3.18	29.62
91	12.39	6.62	23.75	12.88	6.50	26.26
		FA_c2			S1	
0	10.24	0.86	38.58	9.65	0.84	36.26
2	9.82	1.25	35.24	9.76	1.56	33.72
7	10.16	2.01	33.55	10.54	2.57	32.76
14	10.19	2.66	30.95	11.46	3.71	31.87
28	11.07	4.00	29.05	11.91	4.93	28.72
91	13.47	6.89	27.07	14.30	7.87	26.46
		S2			S3	
0	9.87	0.88	36.98	9.80	0.87	36.75
2	10.10	1.83	34.01	10.21	2.34	32.37
7	11.18	3.35	32.23	11.95	4.50	30.61
14	12.42	5.16	29.87	13.75	6.51	29.75
28	12.44	5.56	28.31	13.94	7.41	26.89
91	15.08	8.53	26.94	16.37	10.63	23.60
		Qz				
0	10.39	0.99	38.68			
2	9.71	0.98	35.90			
7	9.68	0.86	36.26			
14	9.77	0.77	37.01			
28	9.73	0.97	36.04			
91	9.02	0.73	34.07			

[a] Bound water calculated in the range of 50 °C and 550 °C.

[b] The portlandite peak typically appears in the range between 370 °C and 500 °C but can shift depending on the actual composition of the system, the sample age and/or the sample preparation. The actual area of the portlandite peak was calculated individually for each measurement.

Table A6-2 - Synthetic glasses (Chapter 5): Bound water[a] and portlandite[b] content as calculated for OPC–glass blends.

age [d]	$BW_{incl.\ CH}$	$BW_{excl.\ CH}$	CH	$BW_{incl.\ CH}$	$BW_{excl.\ CH}$	CH
		FA_s1			FA_s2	
0	0.60	0.55	0.43	0.61	0.55	0.47
2	10.16	9.07	9.19	10.34	9.34	8.88
7	13.37	12.04	11.87	13.32	11.98	12.04
14	14.36	12.94	12.52	14.23	12.62	12.85
28	15.05	13.53	13.66	15.00	13.48	13.78
91	15.95	14.48	13.09	15.72	14.25	12.44
		FA_s3			FA_c1	
0	0.61	0.55	0.46	0.56	0.51	0.42
2	9.99	8.99	8.94	10.02	8.97	9.09
7	13.54	12.18	12.38	13.51	12.09	12.82
14	13.82	12.31	12.37	14.76	13.31	13.12
28	14.65	13.16	13.48	14.94	13.44	13.24
91	15.77	14.51	11.68	15.97	14.56	12.23
		FA_c2			S1	
0	0.69	0.62	0.50	0.68	0.62	0.51
2	10.45	9.23	9.21	9.84	8.64	8.92
7	13.27	11.79	12.55	13.48	12.17	12.17
14	14.24	12.91	12.65	14.80	13.34	12.57
28	15.03	13.57	13.48	15.16	13.69	13.36
91	16.72	15.34	12.04	18.25	16.85	13.13
		S2			S3	
0	0.73	0.66	0.53	0.73	0.67	0.53
2	10.47	9.42	9.09	10.02	9.03	8.77
7	13.63	12.24	12.65	13.73	12.32	12.49
14	14.83	13.38	12.49	15.10	13.78	12.33
28	15.47	14.02	13.03	16.53	15.17	12.97
91	19.41	18.05	12.43	20.89	19.70	12.11
		Qz				
2	10.61	9.48	10.31			
7	12.40	11.01	11.77			
14	13.59	12.09	12.64			
28	14.21	12.65	13.59			
91	15.08	13.59	13.68			

[a] Bound water calculated in the range of 50 °C and 550 °C.

[b] The portlandite peak typically appears in the range between 370 °C and 500 °C but can shift depending on the actual composition of the system, the sample age and/or the sample preparation. The actual area of the portlandite peak was calculated individually for each measurement.

Table A6-3 - Synthetic glasses (Chapter 5): Bound water[a] and portlandite[b] content as calculated for anhydrite-containing pozzolanity test samples.

age [d]	$BW_{incl.\ CH}$	$BW_{excl.\ CH}$	CH	$BW_{incl.\ CH}$	$BW_{excl.\ CH}$	CH
		FA_c1			FA_c2	
0	10.01	0.82	37.78	10.67	0.82	40.50
2	9.69	0.94	36.01	9.50	0.96	35.10
7	10.30	1.28	37.08	10.69	1.66	37.13
14	11.59	2.45	37.59	11.65	2.78	36.47
28	12.45	3.65	36.20	13.00	4.67	34.26
91	16.19	10.04	25.28	17.80	12.24	22.83
		S1			S2	
0	10.39	0.85	39.22	10.50	0.86	39.63
2	10.25	1.02	37.94	10.49	1.22	38.11
7	11.26	2.26	37.01	11.72	2.90	36.26
14	12.16	3.92	33.92	13.90	5.76	33.47
28	14.15	6.17	32.84	17.71	10.43	29.94
91	20.22	14.81	22.24	22.54	16.71	23.95
		S3			Qz	
0	9.85	0.83	37.10	9.83	0.87	36.88
2	10.82	1.62	37.84	9.75	0.95	36.18
7	12.97	4.13	36.37	10.41	1.32	37.39
14	16.69	9.47	29.71	10.83	1.89	36.74
28	20.12	13.57	26.95	10.90	2.27	35.49
91	21.89	16.79	20.98	10.11	1.44	35.65

[a] Bound water calculated in the range of 50 °C and 550 °C.

[b] The portlandite peak typically appears in the range between 370 °C and 500 °C but can shift depending on the actual composition of the system, the sample age and/or the sample preparation. The actual area of the portlandite peak was calculated individually for each measurement.

Table A6-4 - Multi-component cements (Chapter 7): Bound water[a], portlandite[b], $CO_{2\ total}$[c] and calcite[d] as calculated from TGA for blended cements. Sample code: BFS-FA-LS-Qz.

age [d]	$BW_{incl.\ CH}$	$BW_{excl.\ CH}$	CH	$\bar{C}$	$C\bar{C}$
			20-10-20-0		
0	0.76	0.70	0.53	8.59	19.54
0.04	2.20	2.14	0.50	9.18	19.70
0.17	2.81	2.71	0.87	9.16	19.88
1	11.80	10.87	8.67	10.32	19.47
2	16.70	15.43	11.45	10.21	18.65
7	20.50	19.25	12.37	10.99	18.58
28	23.01	21.83	11.79	11.95	18.49
91	23.22	22.14	10.71	11.55	16.81
182	24.95	23.91	10.97	11.87	17.77
364	24.57	23.63	9.23	12.48	16.52
546	23.23	22.24	9.50	12.04	17.00
728	27.26	26.45	9.47	11.46	16.30
			20-15-15-0		
0	0.70	0.64	0.50	6.59	14.51
0.04	2.27	2.21	0.49	6.80	14.24
0.17	2.79	2.69	0.78	7.04	15.10
1	11.21	10.31	8.46	8.75	14.30
2	15.69	14.60	11.14	8.37	14.15
7	20.43	19.19	12.28	8.78	14.42
28	23.31	22.13	12.18	8.73	13.04
91	23.84	22.81	10.50	8.96	12.54
182	24.11	23.12	9.98	10.60	13.18
364	24.40	23.58	8.42	10.60	12.82
546	23.23	22.32	8.67	9.58	12.54
728	26.64	25.71	8.68	9.18	12.36
			20-25-5-0		
0	0.71	0.65	0.51	2.40	5.07
0.04	2.34	2.28	0.46	2.70	5.24
0.17	2.85	2.76	0.70	2.59	5.08
1	11.30	10.39	8.34	4.37	5.09
2	16.05	14.90	10.51	4.49	3.90
7	19.64	18.41	11.84	5.14	4.83
28	22.64	21.46	11.73	4.58	4.38
91	24.03	23.10	9.59	4.84	4.08
182	25.05	24.24	9.24	5.64	4.33
364	[e]				
546	23.37	22.61	7.87	5.13	3.61
728	27.47	26.66	7.95	4.73	3.76

Continued on next page

Table A6-4 – continued from previous page

age [d]	$BW_{incl.\ CH}$	$BW_{excl.\ CH}$	CH	$\bar{C}$	$C\bar{C}$
			20-30-0-0		
0	0.74	0.67	0.54	0.74	1.16
0.04	2.43	2.37	0.45	0.89	1.00
0.17	2.92	2.84	0.68	0.89	1.31
1	11.16	10.27	8.19	2.57	1.27
2	15.12	14.05	10.07	3.01	1.64
7	19.37	18.24	11.44	3.05	0.82
28	22.64	21.48	11.75	2.97	0.55
91	23.12	22.17	9.59	3.20	0.44
182	26.42	25.50	9.85	4.18	0.47
364	25.64	24.81	8.59	3.51	0.44
546	23.31	22.41	8.19	3.53	0.41
728	26.96	26.10	8.39	3.00	1.07
			20-0-0-30		
0	0.81	0.74	0.61	0.28	0.53
0.04	2.17	2.12	0.49	0.37	0.56
0.17	2.64	2.56	0.72	0.41	0.59
1	11.54	10.58	8.65	1.62	1.04
2	16.01	14.86	11.28	1.93	1.22
7	19.20	18.00	12.33	2.23	1.18
28	21.44	20.17	12.39	2.68	0.96
91	23.13	21.89	12.37	3.16	1.04
182	23.58	22.38	11.99	2.64	0.86
364	24.40	23.17	12.27	2.55	0.94
546	24.02	22.91	11.14	2.66	1.03
728	25.30	23.99	12.64	2.51	0.97
			30-0-20-0		
0	0.92	0.84	0.64	8.46	18.79
0.04	2.12	2.06	0.55	8.71	19.08
0.17	2.75	2.65	0.86	9.06	19.60
1	12.13	11.20	9.02	9.91	18.78
2	17.11	15.96	11.43	10.30	18.53
7	20.22	18.98	12.46	10.90	18.37
28	24.40	23.08	13.03	11.08	17.89
91	25.10	23.96	12.26	12.04	17.72
182	25.97	24.85	11.98	11.42	17.36
364	26.33	25.13	12.15	11.42	17.30
546	26.19	24.97	12.21	11.72	17.33
728	27.77	26.54	12.91	10.93	19.29

Continued on next page

Table A6-4 – continued from previous page

age [d]	$BW_{incl.\ CH}$	$BW_{excl.\ CH}$	CH	$\bar{C}$	$C\bar{C}$
			30-5-15-0		
0	0.91	0.84	0.61	6.46	14.40
0.04	2.10	2.04	0.56	6.44	14.29
0.17	3.05	2.95	0.85	6.33	13.42
1	11.96	10.96	8.89	7.84	14.05
2	16.70	15.52	11.30	8.52	14.46
7	20.00	18.84	12.06	8.87	13.38
28	23.51	22.34	12.51	8.99	13.51
91	24.09	22.99	11.75	9.91	12.73
182	25.80	24.71	11.45	9.03	12.64
364	26.69	25.54	11.40	8.89	12.48
546	27.08	25.92	11.48	8.91	12.77
728	27.50	26.44	11.79	8.63	12.56
			30-15-5-0		
0	0.89	0.83	0.54	2.26	4.73
0.04	2.42	2.37	0.41	2.37	4.54
0.17	2.91	2.83	0.67	2.43	4.77
1	11.86	10.92	8.55	3.63	4.93
2	16.05	14.97	10.77	4.00	4.81
7	20.17	18.93	12.01	4.41	4.67
28	24.64	23.47	12.55	4.52	4.26
91	25.11	24.04	11.21	5.47	3.81
182	26.60	25.57	10.25	4.64	3.43
364	26.38	25.37	10.33	4.70	3.38
546	26.00	24.98	10.34	4.57	3.83
728	27.61	26.63	10.03	4.60	3.86

[a] Bound water calculated in the range of 50 °C and 550 °C.
[b] The portlandite peak typically appears in the range between 370 °C and 500 °C but can shift depending on the actual composition of the system, the sample age and/or the sample preparation. The actual area of the portlandite peak was calculated individually for each measurement.
[c] Total CO_2 was calculated in a range between 600 °C and 950 °C.
[d] The peaks of monocarbonate and calcite are overlapped such that the calculated values for calcite can only serve as estimates.
[e] Data missing.

Appendix 7 - X-ray diffractograms

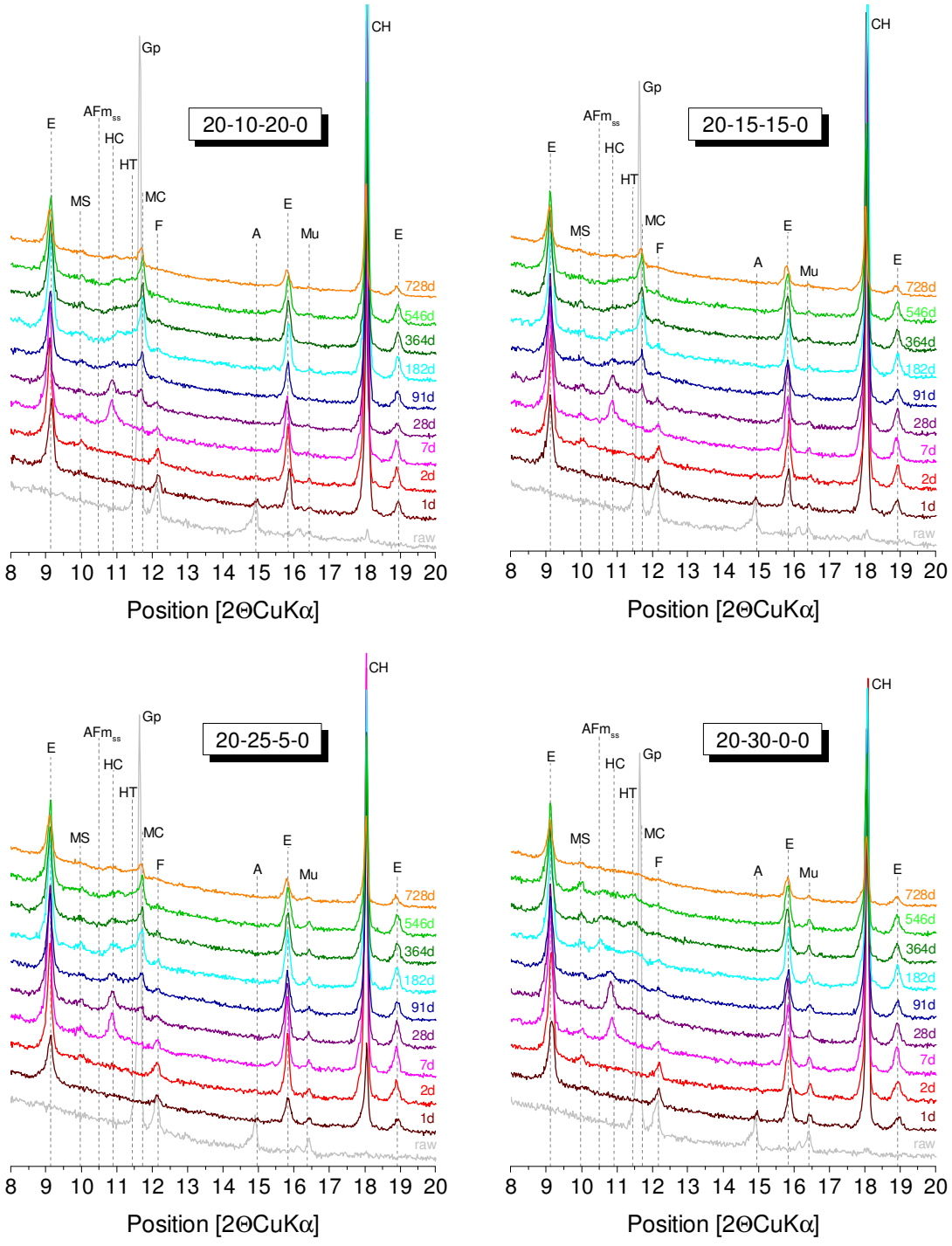

Figure A7-1 - X-ray diffractograms for pastes with a water-to-solid ratio of 0.5 (cf. Chapter 7 and Chapter 8. Note that pastes presented in Chapter 7 were prepared with a slightly lower water-to-solid ration of 0.45). A - alite, AFm_{ss} - solid solution of hemicarbonate and OH^- substituted monosulphate, CH - portlandite, E - ettringite, F - brownmillerite, Gp - gypsum, HC - hemicarbonate, HT - hydrotalcite, MC - monocarbonate, MS - monosulfate, Mu - mullite. Notation: BFS-FA-LS-Qz.

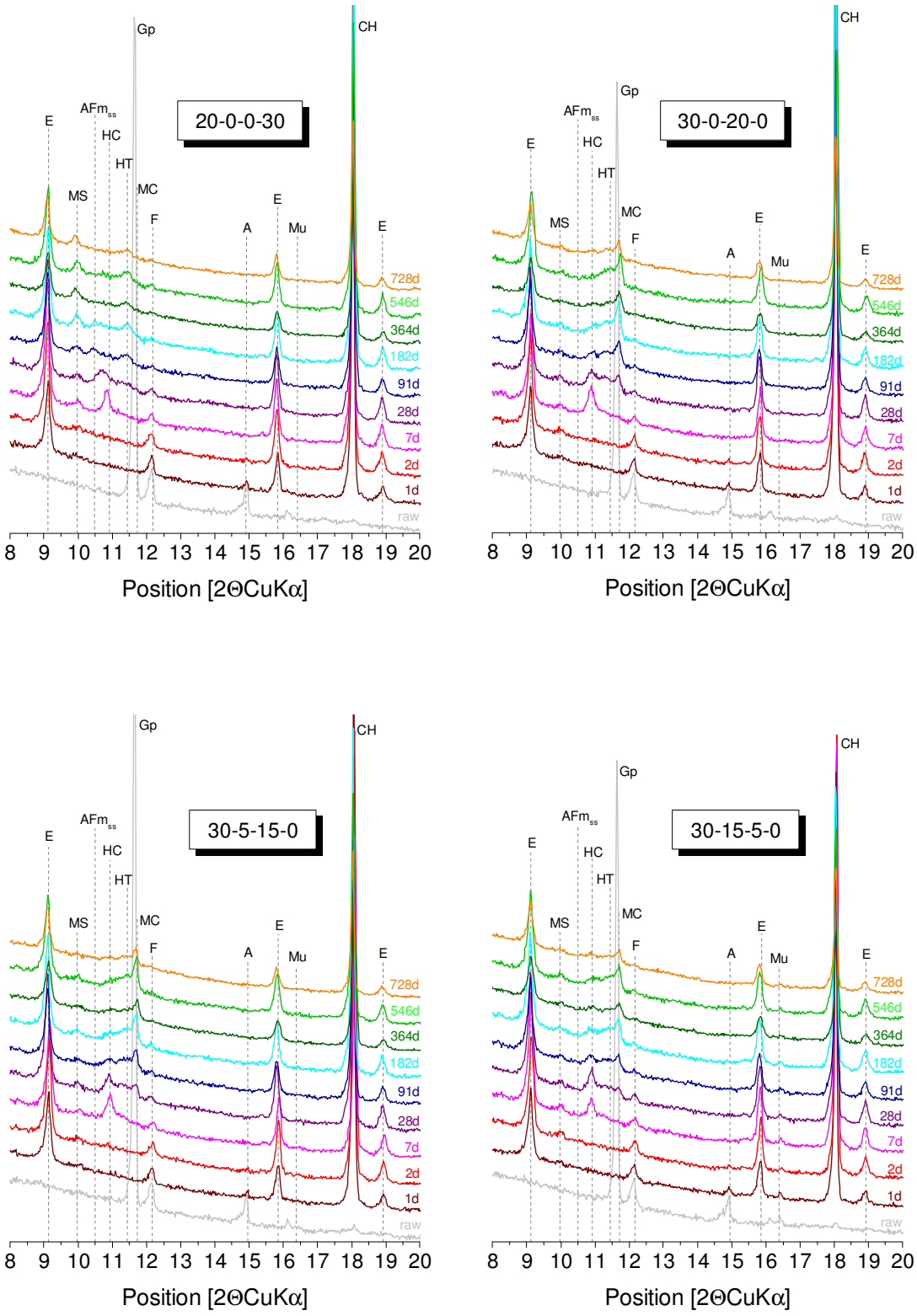

Figure A7-2 - X-ray diffractograms for pastes with a water-to-solid ratio of 0.5 (cf. Chapter 7 and Chapter 8. Note that pastes presented in Chapter 7 were prepared with a slightly lower water-to-solid ration of 0.45). A - alite, AFm_{ss} - solid solution of hemicarbonate and OH^- substituted monosulphate, CH - portlandite, E - ettringite, F - brownmillerite, Gp - gypsum, HC - hemicarbonate, HT - hydrotalcite, MC - monocarbonate, MS - monosulfate, Mu - mullite. Notation: BFS-FA-LS-Qz.

Curriculum Vitae

Name:	Axel Schöler
Date of Birth:	10th January 1980
Nationality:	German

Academic Education

2012–2015	PhD student at the Laboratory for Concrete/Construction Chemistry at the Eidgenössische Materialprüfungsanstalt (Empa), Dübendorf, Switzerland and at the F.A. Finger-Institut für Baustoffkunde at the Bauhaus-Universität Weimar, Germany. Working areas: Hydration of multi-component cements with reduced CO_2-footprint and reactive behaviour of supplementary cementitious materials and glasses
2012	Master's thesis in the field of construction chemistry at the Laboratory for Concrete/Construction Chemistry at the Eidgenössische Materialprüfungsanstalt (Empa), Dübendorf, Switzerland: Hydration of Portland cements blended with supplementary cementitious materials
2010–2012	Degree course *Keramik, Glas und Baustofftechnik*, Technische Universität Bergakademie Freiberg, Germany, Graduation: Master of Engineering (M.Eng.)
2009	Bachelor's thesis in the field of engineering ceramics at CeramTec AG, Marktredwitz, Germany: Development of an aluminium nitride compound suitable for processing by continuous extrusion
2007–2009	Degree course *Werkstofftechnik*, University of Applied Sciences Jena, Germany, Graduation: Bachelor of Engineering (B.Eng.)
2003–2007	Degree course *Werkstoff- und Oberflächentechnik*, University of Applied Sciences Hof, Germany
2002–2003	Degree course *Architektur*, University of Applied Sciences Coburg, Germany

Particular Knowledge

EDP	MS Office, Origin, LaTeX, PANalytical Highscore Plus (XRD/Rietveld), GEM-Selektor (geochemical modeling)
Language skills	German - native language English - fluent in spoken and written (level C1) French - basic knowledge (level A1)

Publications

Journals

A. Schöler, B. Lothenbach, F. Winnefeld, M. Zajac, Hydration of quaternary Portland cement blends containing blast-furnace slag, siliceous fly ash and limestone powder, Cement & Concrete Composites 55 (2015) 374-382.

A. Schöler, F. Winnefeld, M. Ben Haha, B. Lothenbach, The effect of glass composition on the reactivity of synthetic glasses, submitted to Journal of the American Ceramic Society

A. Schöler, B. Lothenbach, F. Winnefeld, M. Ben Haha, M. Zajac, H.-M. Ludwig, Early hydration in SCM-blended Portland cements: A pore solution and isothermal calorimetry study, submitted to Cement and Concrete Research

A. Schöler, B. Lothenbach, F. Winnefeld, M. Ben Haha, Hydration kinetics of quaternary Portland cement blends containing blast-furnace slag, siliceous fly ash and limestone powder, in preparation

Conferences

A. Schöler, B. Lothenbach, F. Winnefeld M. Ben Haha, M. Zajac, Einfluss der chemischen Zusammensetzung der Glasphase von Zementersatzstoffen (SCMs) auf deren Auflösungsverhalten und Reaktivität, 19. IBAUSIL 16. - 18. September 2015, Weimar, Germany, Band 1, 923-930

A. Schöler, B. Lothenbach, F. Winnefeld, M. Zajac, M. Ben Haha, Interactions between supplementary cementitious materials within the hydration of multi-component cements, in Tagung Bauchemie der GDCh-Fachgruppe Bauchermie 6. - 8. Oktober 2014, Kassel, GDCh-Monographie Bd. 48, 9-12

T. Füllmann, T. Witzke, A. Schöler, F. Winnefeld, B. Lothenbach, Quantitative XRD-analysis of hydrated cementitious systems - determination and distinguishing of amorphous phase contents, in Proceedings of the thirty-sixth conference on cement microscopy, Mailand, 13. - 17. April 2014, 318-324

A. Schöler, B. Lothenbach, F. Winnefeld, Effect of supplementary cementitious materials on the early hydration of multi-component cements, Oral presentation, Applications of Isothermal Calorimetry in the Cement Industry 10. - 11. April 2014, TU Berlin Institut für Bauingenieurwesen FG Baustoffe und Bauchemie Berlin

A. Schöler, F. Winnefeld, B. Lothenbach, M. Zajac, Effect of cubic C_3A on the hydration kinetics of Portland fly ash cement, in Tagung Bauchemie der GDCh-Fachgruppe Bauchermie 11. - 12. Oktober 2012, Dübendorf, GDCh-Monographie Bd. 45, 132-137

Other publications

F. Winnefeld, A. Schöler, B. Lothenbach, Sample Preparation, in K.L. Scrivener, R. Snellings, B. Lothenbach, editors. A practical guideline to Microstructural Analysis of Cementitious Materials. Oxford, UK: CRC Press, 2015, ISBN: 978-1498738651

A. Schöler, Hydration of Portland cements blended with supplementary cementitious materials, Master's Thesis, Technische Universität Bergakademie Freiberg, Grin Verlag GmbH, 2012, ISBN: 978-3-656-25856-8

A. Dohn, G. Günthner, A. Schöler, A. Thimm, Stranggepresste Funktionsformkörper aus hochwärmeleitfähiger Keramik, Patent DE102010062342 A1, 9. Juni 2011